



HAL
open science

Neurobiology of central defects and therapeutic exon skipping in a mouse model of Duchenne muscular dystrophy

Amel Saoudi

► **To cite this version:**

Amel Saoudi. Neurobiology of central defects and therapeutic exon skipping in a mouse model of Duchenne muscular dystrophy. Neuroscience. Université Paris-Saclay, 2023. English. NNT : 2023UP-ASL015 . tel-04272462

HAL Id: tel-04272462

<https://theses.hal.science/tel-04272462v1>

Submitted on 6 Nov 2023

HAL is a multi-disciplinary open access archive for the deposit and dissemination of scientific research documents, whether they are published or not. The documents may come from teaching and research institutions in France or abroad, or from public or private research centers.

L'archive ouverte pluridisciplinaire **HAL**, est destinée au dépôt et à la diffusion de documents scientifiques de niveau recherche, publiés ou non, émanant des établissements d'enseignement et de recherche français ou étrangers, des laboratoires publics ou privés.

Neurobiology of central defects and therapeutic exon skipping in a mouse model of Duchenne muscular dystrophy

*Neurobiologie des atteintes centrales et saut d'exon thérapeutique dans
un modèle murin de dystrophie musculaire de Duchenne*

Thèse de doctorat de l'université Paris-Saclay

École doctorale n°568 Signalisation et Réseaux Intégratifs en Biologie (BIOSIGNE)

Spécialité de doctorat : Sciences de la vie et de la santé

Graduate school : Life science and health

Référent : Faculté de Médecine

Thèse préparée dans les unités de recherche **Institut des Neurosciences Paris-Saclay**
(Université Paris-Saclay, CNRS) et **Biothérapies des maladies neuromusculaires**
(Université Paris-Saclay, UVSQ- INSERM), sous la direction de Cyrille VAILLEND, directeur de
recherche, et Aurélie GOYENVALLE directrice de recherche

Thèse soutenue à Paris-Saclay, le 16 mars 2023, par

Amel SAOUDI

Composition du Jury

Membres du jury avec voix délibérative

Micaela GALANTE Professeure d'université, NeuroPSI - UMR9197	Présidente
Maaïke van PUTTEN Assistant professor Leiden University Medical Center	Rapportrice et examinatrice
Rubèn MIRANDA Professor associate Complutense University of Madrid	Rapporteur et examinateur
Stéphanie DAUMAS Professeure d'université, IBPS UMR 8246	Examinatrice

Direction de la thèse

Cyrille VAILLEND Directeur de recherche, NeuroPSI - UMR9197	Directeur de thèse
Aurélien GOYENVALLE Directrice de recherche, UVSQ- INSERM U1179	Directrice de thèse

Table of content

INTRODUCTION	9
I. Duchenne muscular dystrophy	11
1. History.....	11
2. Progressive muscular dystrophy.....	12
3. Non-progressive central alterations	14
A. Intellectual disability	14
B. Cognitive profile.....	15
C. Sensory disorders.....	16
D. Psychosocial and neurobehavioral functioning.....	17
4. DMD gene, products, and mutations	20
A. <i>DMD</i> gene.....	20
B. Dystrophin proteins	21
C. <i>DMD</i> gene mutations	32
D. Genotype-phenotype relationship	33
II. DMD animal models	38
1. The <i>mdx</i> mouse model.....	39
A. Muscular dystrophy phenotype.....	40
B. Emotional phenotype: behavioral parameters and brain circuits.....	42
C. Synaptic plasticity and memory.....	44
2. The <i>mdx52</i> mouse model.....	48
III. Therapeutic approaches for DMD	49
1. Pharmacological approaches.....	49
A. Glucocorticoids	49
B. Stop codon readthrough	50
C. Utrophin overexpression.....	51

2. Cell therapies.....	52
3. Gene therapy	53
A. Gene replacement therapy	53
1. Viral vectors	53
2. Micro-dystrophin	55
B. Gene editing therapy (CRISPR/Cas9)	56
IV. Exon skipping strategies.....	57
1. Splicing mechanisms.....	57
2. Therapeutic exon skipping.....	58
3. Therapeutic application of the exon skipping approach in DMD.....	60
A. Different types of ASOs used for DMD.....	61
B. AAV-mediated exon skipping for DMD.....	64
4. Therapeutic application of exon-skipping to treat the CNS in DMD.....	66
A. AAV-mediated exon-skipping in the CNS.....	66
B. ASO-mediated exon skipping in the CNS	67
Research objectives	71
RESULTS	75
I. Behavioral phenotyping	77
II. Optimization of ASO-based therapeutic exon skipping in the CNS.....	101
III. Therapeutic rescue of the <i>mdx52</i> behavioral deficits.....	123
DISCUSSION	143
CONCLUSION & PERSPECTIVES.....	161
REFFERECNES	163
ANNEXES	193

INTRODUCTION

I. Duchenne muscular dystrophy

1. History

Duchenne muscular dystrophy (DMD) was largely described in 1861 by Guillaume Duchenne de Boulogne (Duchenne, 1861). Dr. Duchenne first associated the disease with a mental disorder as patients exhibited verbal language disturbance and lower intelligence. He then evidenced and characterized the muscular dystrophy in 1868 and described muscle degeneration and high fibrosis in patients' biopsies. He established diagnostic criteria based on these anatomical changes and electrical muscle stimulation (Duchenne, 1868). Even though DMD was named in reference to Dr. Duchenne, he was not the first to describe the muscular symptoms. Indeed, in 1847 Dr. W.J. Little reported the case of two boys exhibiting Duchenne muscular dystrophy symptoms. Notably, Dr. Little was the first to practice tenotomy, a surgery aiming to prevent severe contractures, which is still used nowadays for myopathies. In 1851, the Dr. Edward Meyron at the Royal Medical and Chirurgical Society congress exposed the case of eight boys from three families. In 1864, Dr. E. Meyron identified a pattern of expression for the pathology, as it was exclusively found in young-boy patients with maternal antecedents. Later confirmed by the neurologist Dr. Willian Gowers, who reported the higher frequency of DMD familial cases with mother antecedents than isolated cases. In 1879, Dr. Gowers described how young DMD boys rise from the floor as follows: “from a supine or sitting position, a child will first roll prone, extending their arms and legs far apart. With most of the trunk weight resting on the extended arms, they push the body backward to shift the weight of the trunk over the extended legs. To extend the hip, the child places their hands onto the knees and walks the arms up the thighs until upright” (Gowers, 1879). This clinical description is now known as Gower’s sign (Figure 1).

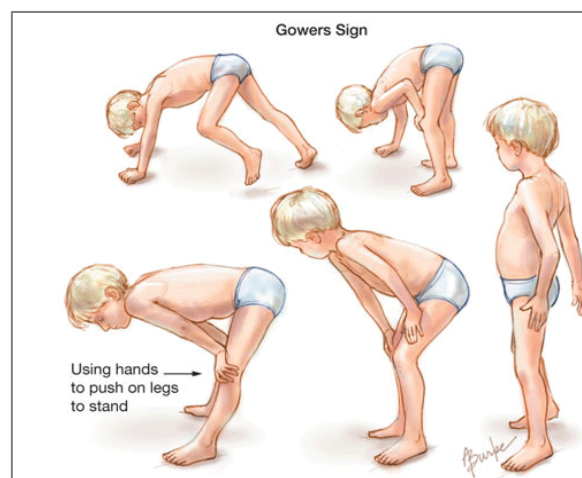


Figure 1: Gower’s Signs. Schematic view of a child with Duchenne muscular dystrophy (Asadi et al., 2017)

2. Progressive muscular dystrophy

Duchenne muscular dystrophy (DMD) is a recessive X-linked neuromuscular syndrome that affects one out of 5000 male births (Mah et al., 2014), characterized by a total loss of the dystrophin protein's expression. Muscle weakness and wasting progressively affect DMD patients (Figure 2). The onset of DMD muscular symptoms occurs in early childhood between 3 and 5 years old, and some of the most noticeable early signs include mildly delayed walking, difficulty to climb stairs, a waddling gait, frequent falls (Mercuri et al., 2019), and Gower's sign (Figure 1). As the disease progresses, the weakness hitting the lower limbs progressively affects the back leading to sclerosis and ambulation loss; early DMD teens by 12 years of age become wheelchair dependent (Mercuri et al., 2019). At this point, the histological analysis of muscle biopsies in DMD patients revealed calf muscle hypertrophy associated with typical hyper-fibrosis and muscle fiber hypotrophy, inflammation cells infiltration, and necrosis (see Figure 3). This muscle degeneration leads to a generally significant increase of blood creatine kinase (CK), with levels reaching 20,000 to 50,000 U/L while physiological levels are around 80 to 250 U/L. Indeed, creatine kinase is released in the serum following membrane loss of integrity and altered permeability in the muscle fibers, which is used as a biomarker for DMD diagnosis as well as in muscle degenerating pathologies. CK levels progressively lower as the muscular mass loss increases with age. Between 15 and 20 years of age, cardio-respiratory insufficiency leads to the need for a ventilator assistance. With optimal care and advances in the therapeutic field, most patients with DMD live until their late 20's and in some cases reach the late 30's. Diaphragm and cardiac muscle affection are the last but often, the most severe damages responsible for respiratory failure as well as impaired heart pump flexibility and efficiency, which are the major causes of patient mortality (Duan et al., 2021; Mercuri et al., 2019).

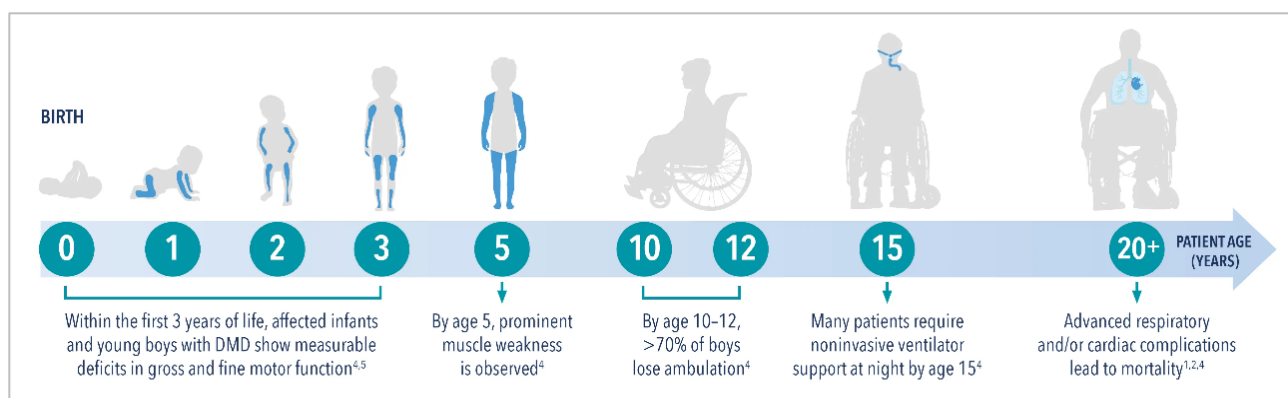


Figure 2. Duchenne muscular dystrophy progress throughout the lifespan. Schematic representation of age-related clinical signs in DMD patients (Neurology live website)

A milder form of muscular dystrophy, known as Becker muscular dystrophy (BMD), affects around 1 out of 20,000 boys. This milder form of dystrophy is diagnosed around the age of 12, although some patients remain asymptomatic until adulthood. Becker's myopathy presents a strong clinical heterogeneity; this can range from locomotor incapacity in young adolescents to other milder clinical signs such as simple muscle pain associated with cramps. The constant signs in a large proportion of BMD patients are elevated serum creatine kinase levels and early calf muscle hypertrophy. In some BMD patients cardiomyopathy similar to that found in DMD happens to be observed over time (Emery, 1993). BMD individuals with the most severe clinical signs die between the ages of 40 and 50, while life expectancy is almost normal for patients with milder forms. In contrast with DMD patients, dystrophin protein expression is detected in BMD patients. They mainly present the expression of shorter dystrophins, deleted in the internal region but functional, while dystrophin is undetectable in DMD patients.

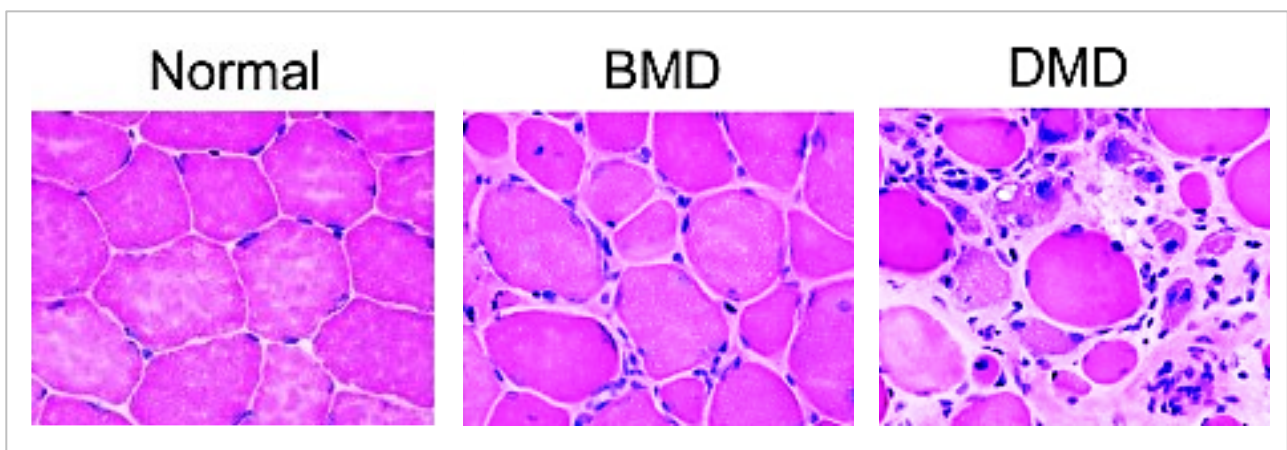


Figure 3. Cross-sectional muscle histology: Hematoxylin and eosin (HE) staining (McGreevy et al., 2015)

In the last decades, the underlying cellular and molecular mechanisms involved in muscular dystrophy led to the emergence of therapeutic approaches efficient to rescue the muscular dystrophy, which were somewhat aimed to at least reduce the DMD phenotype to a milder BMD-like phenotype (Duan, 2018a; Bizot et al., 2020). However, the understanding of the neurological component in DMD, and thus the therapeutic approaches targeting brain, is so far less well extended. Indeed, despite the early description of certain central alterations by Dr. Duchenne already in 1868, a large controversy surrounded the central alterations in DMD and thus limited the advances.

3. Non-progressive central alterations

Neurological alterations in DMD appear a few months after birth before the first muscular symptoms (van Dommelen et al., 2020). Little has been reported about cognitive abilities in the first years of life, even though young DMD children have a specific profile of neurological disturbances. Below the age of two years, cognitive, motor, and emotional aspects are strictly intertwined, and these are difficult to distinguish (Pane et al., 2013). While a few studies have focused on specific aspects of neurodevelopment, such as locomotor (Smith et al., 1991) or language milestones (Cyrulnik et al., 2007), others have used neurodevelopmental scales, but the cohorts were relatively small or included older children up to age of six years (Cyrulnik et al., 2008; Smith et al., 1990). However, early central symptoms are known and thus can be considered for early diagnosis of the pathology.

In fact, the muscular dystrophy being the cause of the death, therapeutic studies first aimed to target the muscular dystrophy and increase the lifespan. As it is now well advanced, DMD patients with an encouraging muscular rescue show more visible central alterations and encounter difficulties to be fully independent. Many central alterations found in DMD patients are related to delayed language acquisition, memory deficits, intellectual disability, anxiety, and social difficulties which impact their development and hinder adults' autonomy despite muscular rescue (Hinton et al., 2000, 2006; Taylor et al., 2010; Ricotti et al., 2016b). A better understanding and the identification of these symptoms could constitute an early diagnostic biomarker for a treatment that could eventually prevent the emergence of these deficits in parallel with dystrophy management.

A. Intellectual disability

Full-scale intelligence quotients (IQ) of children with DMD have a Gaussian distribution analogous to that of the population standard, with overall lower values, the average full-scale IQ of DMD patients being around 80 (Dubowitz, 1979). A meta-analytical review involving 32 studies that included a total of 1231 patients (1224 DMD patients, 7 patients with Becker muscular dystrophy (BMD) over a period of forty years, was able to establish an IQ average of overall at 80.2 (verbal IQ at 80.4, performance IQ at 85.4). This mean full-scale IQ is of a value of -1 standard deviation compared to that of the standard population, with a Gaussian distribution whose curve presented a translation to the left of about twenty points. More than 20% of this study's population had an IQ of less than 70 (Cotton et al., 2001) corresponding to intellectual disability (ID). Moreover, within the

DMD population, the IQ is found to vary leading to the identification of subgroups with a more or less affected IQ. It should be noted, that this variation in IQ scores in DMD patients was shown to be relatively stable during the lifespan, confirming that the central deficits are independent from the muscular dystrophy evolution (Billard et al., 1992). Certain studies even suggested an amelioration of IQ scores in patients aged 20 years and older (Prosser et al., 1969; Miller et al., 1985). Recent studies in mouse models of DMD showed that central aspect in DMD may worsen with age (Bucher et al., 2019; Bagdatlioglu et al., 2020), suggesting that increasing lifespan of DMD patients may come along with increased central alterations.

B. Cognitive profile

IQ scores do not provide a fully detailed report of cognitive functioning. Indeed, learning and memory performance, as well as attention processing are found to be altered in DMD even in patients with IQs in the normal range (Billard et al., 1992). Bresolin et al. studied 50 DMD patients and detected non-specific verbal expression disorders and short-term memory deficits (Bresolin et al., 1994). Hinton et al. studied 80 boys with DMD but IQs above 70 and showed that they poorly performed on tests requiring attention to complex verbal information, all had a diminished verbal span, difficulties in story recall and verbal comprehension, and exhibited verbal working memory deficits (Hinton et al., 2000). Poor academic achievement was also reported on 26 boys with DMD by Hinton's group. Children with DMD showed physical disabilities and poorer verbal memory spans. In this study, a linear regression analysis revealed that executive function, and physical disability did not contribute substantially to academic performance, whereas performance on verbal span did. Authors concluded that DMD boys presented a selective developmental aberration in verbal span that has wide-ranging consequences on learning skills (Hinton et al., 2004). Mento and colleagues conducted a study involving a cohort of 14 DMD boys. The reported results indicate consistent deficits in planning and inhibition in children with DMD (Mento et al., 2011). They also found alterations in phonological abilities, as well as in praxis concluding that those with DMD may exhibit a broader deficit in higher-order cognitive processing capabilities. The authors pointed that the limited verbal span hypothesis (Hinton et al., 2004) is insufficient to account for the range of deficits reported in the literature. Wicksell et al. focused on a neuropsychological assessment conducted to study cognition, with emphasis on memory, information processing/learning ability, and executive functions in 20 boys with DMD. They underlined difficulties on the achievement of the executive functions, which are involved in all the strategies for developing tasks appropriate to obtain a goal (planning, inhibition,

and control of impulses, process of active search in memory, flexibility of thought and action). These authors also underlined the preservation of visual-spatial and auditory-verbal functions (Wicksell et al., 2004). Donders and Taneja, in a cohort of 22 DMD patients, demonstrated that memory deficits strongly manifest in a delayed recall of both verbal and non-verbal information. They suggest that this memory deficit concerns a brain circuit involving the cerebellum, the hippocampus, and the neo-associative cortex, regions where dystrophin transcripts are richly expressed (Donders and Taneja, 2009). The cerebral cortex, specifically prefrontal regions are implicated in higher-order processing and executive functions (Spencer-Smith and Anderson, 2009). Further, the cerebellum is also activated during the completion of tasks that assess executive functioning. Anatomically, neuronal projections exist between the cerebellum and prefrontal regions (Kelly and Strick, 2003) that are implicated in executive function. This suggests that the cerebellum may play a pivotal role in the neural network underlying executive functions (Snow et al., 2013 for review).

Altogether, these studies indicate cognitive impairments, emphasizing the working memory deficits, learning difficulties, and academic achievement problems found in all DMD patients.

The cognitive profile of BMD boys appears less homogeneous and less affected than DMD, with a normally distributed IQ with a mean of 95.6 that did not differ significantly from the population mean. Still, males with Becker muscular dystrophy have a high incidence of learning difficulties and low academic achievement. Moreover, part of these BMD patients also exhibit ID and ASD (Young et al., 2008).

C. Sensory disorders

So far, the main sensory alterations reported in DMD are visual alterations involving retinal neurotransmission, as recently reviewed by our group (Barboni et al., 2022). A classic feature of DMD is reduced or nearly abolished scotopic full-field flash electroretinogram (ERG) b-wave, the positive ERG component. This has been confirmed by several groups in the past decades in patients (Pillers et al., 1993; Girlanda et al., 1997; Pascual Pascual et al., 1998; Cibis and Fitzgerald, 2001; Ricotti et al., 2016a). Barboni and colleagues reported a significant amplitude reduction in ERGs of DMD patients, also in the mesopic condition (low-light intensity). In addition, contrast sensitivity was found significantly lower in the DMD patients (Barboni et al., 2013). Moreover, the same group evidenced in DMD patients a dysfunction of red and green cones dependent perception (Barboni et al., 2016). They recently showed a significant reduction in the dark-adapted b-wave amplitude

correlated with dark-adapted rod sensitivity in DMD patients (Barboni et al., 2021). These visual alterations are not leading to any major impairment of visual perception. However, severe cases of retinal alterations have been reported in DMD patients including proliferative retinopathy (Fagan et al., 2012; Hahn et al., 2013; Park et al., 2019; Kecik et al., 2021). The cases report showed that retinopathies, with severely impaired visual acuity, appeared associated with advanced stage of the disease. This suggested that it may result from hypoperfusion and hypoxia in the retina due to the cardiopulmonary failure in advanced stages. Moreover, cataracts cases are more frequently found increased in DMD population and the glucocorticoid therapy for DMD presents a risk factor of developing cataract (Rice et al., 2018).

Other sensory processing problems may explain certain behaviors reported in DMD boys. Some parents of DMD boys reported that their children present increased sensitivity to tactile stimulations, either human or particular textile touch. Others report that their sons are aversive regarding certain tastes, consistencies, and textures. In some cases, parents reported that their children are reticent to “messy play” or have difficulties tolerating noisy environments. Other children are reported hyporeactive and may be nonresponsive to discussions or may seek out stimulation through excessive activity or by smelling or chewing on objects. These behavioral specificities are similar to those described in attention deficits hyperactivity disorder (ADHD), obsessive-compulsive disorder (OCD), as well as Autism spectrum disorders (Poysky, 2007).

D. Psychosocial and neurobehavioral functioning

It is now documented that certain neuropsychiatric disorders are more prevalent in DMD patients than in the general population, such as for ASD (21%), hyperactivity (24%), attention disorder (44%) and internalizing problems including anxiety (24%) (Hendriksen and Vles, 2008; Hinton et al., 2009; Snow et al., 2013; Ricotti et al., 2016b; Colombo et al., 2017). Among neurobehavioral psychiatric alterations found to be common between DMD and ASD, altered social behavior including poor facial and emotional affect recognition have been reported (Hinton et al., 2007, 2006). Limited ability to initiate and maintain peer relationships was found to be more frequent in children with neuromuscular disorders (Yude et al., 1998).

Many studies examining neurobehavioral functioning in DMD have used the Child Behavior Checklist (CBCL (Achenbach, 1991). CBCL is a checklist that consists of a two-part survey filled out by parents of DMD children and adolescents.

The first part explores the social competences. In their first study, involving 26 DMD boys, Hinton et al. reported high ratings on the CBCL reflecting some of the psychosocial aspects of the illness (Hinton et al., 2004). This was later confirmed in a larger study with parental rating, in which 181 DMD boys compared to unaffected siblings exhibited significantly more problems on the Social Problem behavior scale (Hinton et al., 2006). Furthermore, Donders and Taneja reported that, even after controlling for IQ scores, boys with DMD rated more poorly on the Social Problems and the Social Withdrawal scales than their unaffected siblings. In this latter study, data from an additional parental assessment also indicated that children with DMD experienced more difficulties than siblings in initiating social interactions and in responding to changes in the social environment (Donders and Taneja, 2009).

The second part of the CBCL investigates children and adolescents behavioral and emotional problems based on two broad scales, to detect internalizing problems (i.e. anxiety, depressive behaviors, and over-controlled) and externalizing behavioral problems (i.e. emotional dysregulations, aggressiveness, and under-controlled). In one study of DMD patients, anxiety features were defined as symptoms consistent with apprehension, fear, worry, or uncertainty resulting from anticipation of a threatening situation, which results in significant impairment of physical and psychological functioning (Darmahkasih et al., 2020). Emotional and behavioral dysregulations were also described as significant changes in controlling mood or behavior that impact daily functioning. This encompasses the following parent-reported concerns: Increased emotional dysregulation, behavioral outbursts, aggressiveness, anger problems, mood variations. Ricotti et al. studied a cohort of 87 DMD patients and found that emotional and behavioral problems (internalizing and externalizing) were highly prevalent (24% and 15% respectively). Moreover, in light of the multitude of neurodevelopmental, emotional, and behavioral problems observed in this population, they identified a high prevalence of clustering of DMD with psychiatric symptoms (Ricotti et al., 2016b). Colombo et al. described a cohort of 47 DMD patients assessed using a CBCL scale that exhibited higher mean score in the Internalizing Problems scale, together with the Anxious/Depressed Problems and externalizing problems with aggressive behaviors (Colombo et al., 2017).

In their study, Hinton and Fee investigated the resilience of DMD boys and evidenced the social and familial environment influence on the CBCL scale rating. In this study, 84% of DMD children, although living with a disabling and fatal disease were considered at low risk for psychosocial aspects. The authors demonstrated the importance of parent adjustment and social support, defined as the number and quality of interactions, in the resilience process, and confirm that the child's intellectual level is independent of his psychosocial profile (Fee and Hinton, 2011). Others also found many alterations related to physical abilities and social relationships in DMD patients, but above all, they highlighted the essential role of the parents and environment for patients to become resilient. This emphasizes that the social environment involvement and family support may help to improve the quality of life of DMD children by softening the central alterations (Lue et al., 2017; Uttley et al., 2018). The importance of this support, essential for the quality of life of patients, however, biases the studies. It is difficult to precisely determine whether emotional disorders are specific, i.e. linked to the loss of dystrophin in the brain, or societal, therefore dependent on family, environmental or disability-related factors.

4. DMD gene, products, and mutations

A. *DMD* gene

The pattern of expression of the pathology, as it exclusively affects young DMD boys with maternal antecedents, was a major clue for the discovery of the *DMD* gene and its location on the short arm of the X chromosome, precisely at the Xp21 locus (Jacobs et al., 1981; Davies et al., 1983; Monaco et al., 1985) and was fully sequenced in 1988 (Koenig et al., 1988). *DMD* gene size reaches 2.4 Mb, constituting 0.1% of the human genome (Lander et al., 2001). It is so far the largest gene identified. However, 99% of the gene consists of introns, and the 14 kb mRNA contains 79 exons (Figure 4). The use of probes made it possible to determine deletions in the *DMD* gene in about 50% of patients (den Dunnen et al., 1987; Koenig et al., 1987). Interestingly, the *DMD* gene was also found to be involved in Becker muscular dystrophy (BMD) (Kingston et al., 1984) and the same type of deletions were found later in BMD patients (Den Dunnen et al., 1989).

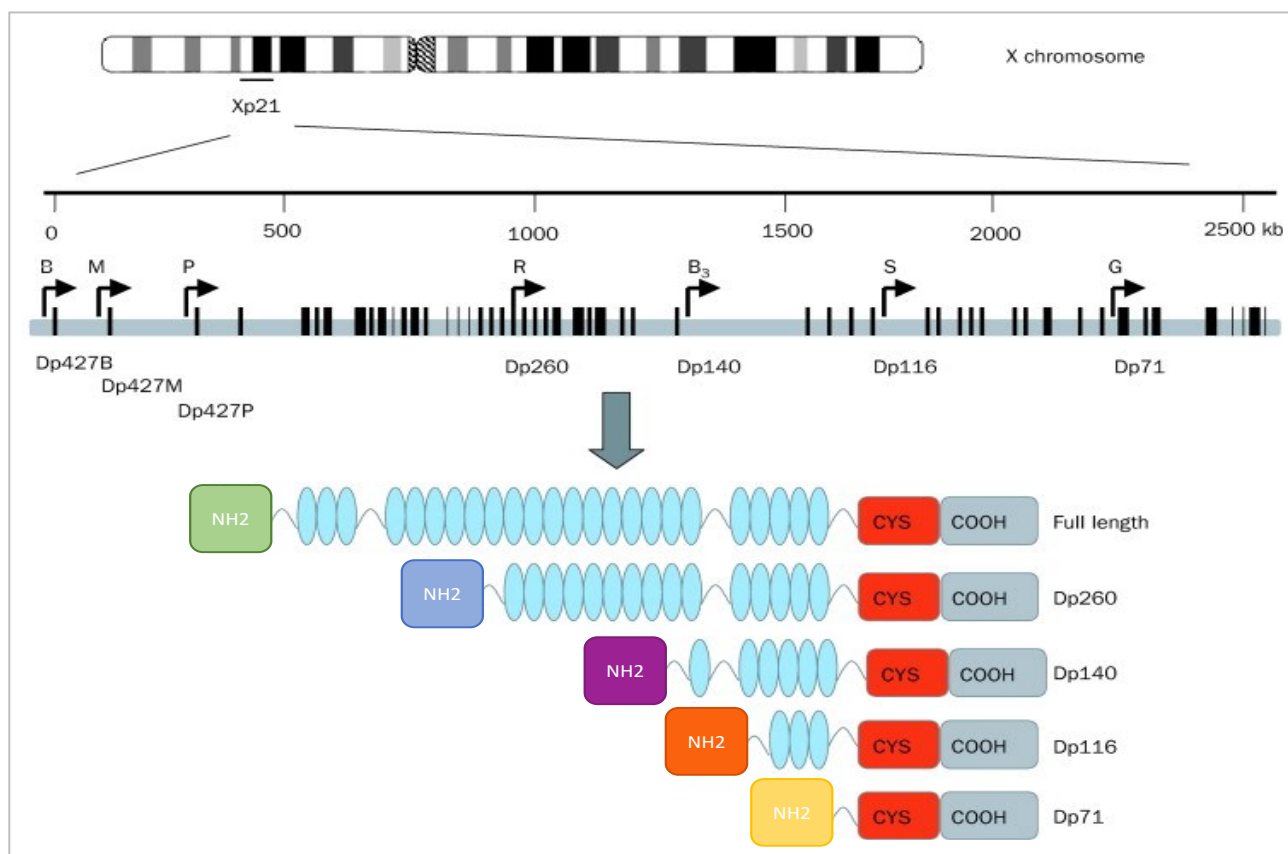


Figure 4. Genomic organization of the *DMD* gene, located in Xp21. The black vertical lines represent the 79 exons of the dystrophin (DMD) gene. The arrows indicate the various promoters: brain (B), muscle (M), and Purkinje (P), R : Dp260 (retinal), B₃: Dp140 (brain3), S: Dp116 (Schwann cells), and G: Dp71 (general). Adapted from (Muntoni et al., 2003)

B. Dystrophin proteins

The *DMD* gene contains 7 internal and independent promoters that control the expression of different dystrophin-gene products, known as dystrophin proteins (Dp), in a tissue and/or cell-specific manner (Figure 4). The distinct dystrophins thus differ by their molecular weight, their tissue and cellular distribution, and their roles. Yet, have the common property of being associated with scaffolds of transmembrane and cytosolic proteins involved in the clustering of various membrane ion channels and receptors (Hoffman et al., 1987).

1) Dp427 “Full-length dystrophin”

The full-length dystrophin protein (Dp) is composed of 3,685 amino acids with a molecular mass of 427 kDa (Koenig et al., 1988).

It is a membrane-associated protein made up of four distinct domains (Figure 5):

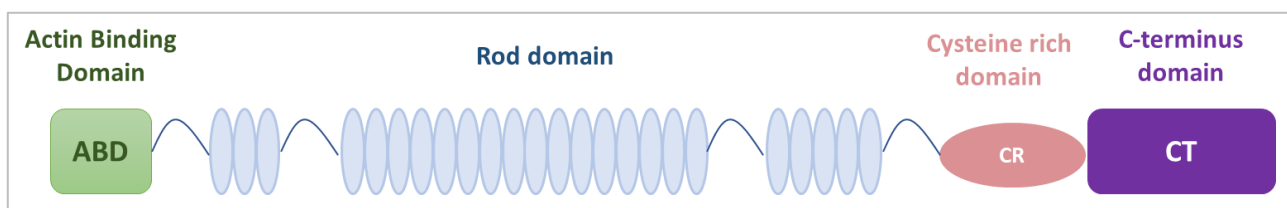


Figure 5. Full-length dystrophin (Dp427) schematic representation

- The N-Terminal domain (green) is made up of approximately 240 amino acids and contains two Actin binding sites (Koenig and Kunkel, 1990).
- The rod domain (light blue) is made up of 2840 amino acids divided into 24 spectrin-like repetitions of around 109 amino acids each (Koenig and Kunkel, 1990). This domain also contains the four hinges regions (curvy blue lines) which are rich in proline residues, giving the dystrophin protein its flexibility.
- The cysteine-rich domain (light pink) extends from amino acids 3361 to 3685. It has 15 cysteines, two potential calcium fixing sites (EF1 and EF2), and a zinc-finger domain (Koenig et al., 1988).
- The C-Terminal domain consists of the last 325 amino acids and contains the binding sites for dystrobrevins and syntrophins (Koenig et al., 1988). This part enables plasma membrane association through protein-protein interactions with integral membrane proteins (sarcoglycan, dystroglycan, syntrophin, and dystrobrevin complexes) that are assembled in the dystrophin-glycoprotein complex (DGC) (Figure 6).

Dp427 expression is regulated by three different promoters within the *DMD* gene leading to three full-length dystrophins expressed in distinct tissues and cell types:

- Dp427**m** (**m**uscle) is historically the first dystrophin discovered (Arahata et al., 1988). It is expressed at the membrane level of cardiac muscle, smooth and skeletal muscle fibers (Byers et al., 1991).
- Dp427**c** (**c**ortical), discovered by (Nudel et al., 1989), is expressed in cortical neurons and in pyramidal neurons of the hippocampus. It is the first central dystrophin identified and characterized in the CNS (Chelly et al., 1990; Lidov et al., 1990).
- Dp427**p** (**P**urkinje), discovered by (Górecki et al., 1992), is mainly expressed in the Purkinje cells layer (PCL) of the cerebellum (Holder et al., 1996).

Dystrophins are associated with a glycoprotein complex (DGC) formed of at least ten partners encoded by autosomal genes, including transmembrane and extracellular proteins (dystroglycan complex) and cytosolic proteins (syntrophins, dystrobrevins). This complex provides both a link between the actin cytoskeleton and the basal lamina / extracellular matrix, as well as interactions with cytosolic signaling proteins playing a role in cellular communication. Thus, the DGC acts as a transmembrane signaling complex (Rando, 2001; Petrof, 2002) and also interacts with membrane proteins (channels, receptors), providing a molecular bridge connecting the interior of the cell to the extracellular matrix (ECM) (Figure 6 A). The DGC was initially identified in association with Dp427 in muscle cells, where Dp427m interacts with actin via its N-terminal domain, and with several proteins *via* its cysteine-rich domain (CR) and its C-terminal domain. There are three protein sub-complexes associated with dystrophin: the dystroglycan complex, the sarcoglycan-sarcospan complex and the dystrobrevin-syntrophin complex (Blake et al., 2002). The DGC is thought to protect muscle from mechanical damage and maintains physiological Ca²⁺ handling in fibers. In DMD, loss of Dp427m causes partial disassociation of the DGC at the sarcolemma, entry of calcium ions, with consequent metabolic alterations and activation of calcium-dependent calpain proteases and phospholipase A2. Ultimately, this leads to muscle necrosis resulting in inflammation, and depletion of stem cell reserves through repeated cycles of muscle damage and regeneration (Turner et al., 1988; Ervasti et al., 1990; Millay et al., 2008).

In BMD patients, partially deleted dystrophins are still able to bind the proteins of the complex, provided that the mutation does not affect the C-terminal domain. Thus, in most BMD cases, it is

possible to detect the expression of DGC proteins at the muscle fiber membrane, although sometimes at lower levels (Matsumura et al., 1993; Matsumura and Campbell, 1994).

DGC is now also considered as a scaffold for proteins involved in membrane stabilization and transmembrane signaling of several cell types in the CNS, but also as a cell-signaling contributor *via* the multiple proteins associated or interacting with one of its components. The multiplicity of brain dystrophins embrace their expression in distinct structures and cell types. This diversity result in variability of DGC components, including dystrophins. Thus, distinct DGC complexes are formed and perform different functions (Waite et al., 2009; García-Cruz et al., 2022). Central Dp427 (c and p) is present in inhibitory synapses of neurons, along the plasma membrane and proximal dendrites, where it colocalizes with a subset of gamma-aminobutyric acid A (GABA_A) receptors (GABA_ARs) (Brüning et al., 2002). It is found in all cortical areas (parietal, pyriform, cingulate), in layers CA1–3 of the hippocampus, in neurons of the amygdala and in Purkinje cells of the cerebellum (Nudel et al., 1989; Górecki et al., 1992; Lidov et al., 1993; Sekiguchi et al., 2009). A low expression of Dp427 has also been shown in the spinal cord (De Stefano et al., 1997; Masaki et al., 2001). It is assumed to be absent (or under detectable levels) in the striatum, thalamus, and hypothalamus (Knuesel et al., 1999; Lidov et al., 1993). In the central inhibitory synapses, the Dp427-associated DGC ensures a link between the actin cytoskeleton, membrane proteins of the post-synaptic membrane and the pre-synaptic membrane *via* neurexin- α (Figure 6 B).

1. The dystroglycan complex

The dystroglycan complex consists of α -dystroglycan and β -dystroglycan. α -Dystroglycan is an extracellular glycoprotein, receptor for laminin in muscle (Figure 6 A) and neurexin (Figure 6 B) in the CNS. β -dystroglycan is a transmembrane glycoprotein that interacts directly with Dp427 whether in muscle or in CNS. Dystroglycans are ubiquitously expressed. Loss of dystroglycans in animal models appears lethal, showing the importance of dystroglycans for early embryonic development, particularly for the correct positioning of laminin and collagen IV in the ECM (Williamson et al., 1997).

2. The sarcoglycan-sarcospan complex

The sarcoglycan and sarcospan complex is composed of α -, β -, γ - and δ -sarcoglycans as well as sarcospan in muscle tissue (Crosbie et al., 1999; Blake et al., 2002). Sarcoglycans are transmembrane glycoproteins interacting with β -dystroglycan in muscle cells (Boulay et al., 2015). On the other hand,

in the CNS, other sarcoglycan isoforms are expressed (ϵ and ζ – sarcoglycans) (Wheeler et al., 2002; Waite et al., 2009; García-Cruz et al., 2022).

3. The dystrobrevin-syntrophin complex

Dystrobrevins are proteins part of the dystrophin superfamily as they share strong homology with the cysteine-rich (CR) and carboxy-terminal (CT) of dystrophins domains. Dystrobrevins and dystrophins interact with another family of proteins: the syntrophins. The latter also interact with different membrane associated proteins in a cell and tissue dependent manner. There are several isoforms of dystrobrevins: α -dystrobrevin is found in the muscles but also in astrocytes in the brain. The β -dystrobrevin is found in the pyramidal neurons of the hippocampus and cortex as well as the Purkinje cells of the cerebellum (Blake et al., 1999). Similarly, there are five syntrophin isoforms: α -, β 1-, β 2-, γ 1-, and γ 2-syntrophins. The α and β 1 forms are strongly expressed in skeletal muscles while α , β 2 and γ 1 forms are predominantly expressed in the CNS. The γ 1 form seems to play an important role in the neurons of the hippocampus, cortex, and cerebellum (Alessi et al., 2006). These different syntrophins interact with other important proteins such as nNOS, PSD95, Kir4.1, AQP4 and neuroligins (Brenman et al., 1996; Adams et al., 2001; Hogan et al., 2001; Connors et al., 2004; Alessi et al., 2006). Neuroligins are synaptic adhesion proteins located postsynaptically and interact with the presynaptic proteins neuexins thus forming a trans-synaptic cell adhesion complex. There are at least 4 neuroligins, neuroligin 1 is present in glutamatergic synapses and neuroligin 2 is associated with Dp427 in GABAergic inhibitory synapses.

In hippocampal and cerebellar GABAergic synapses, the Dp427-associated DGC may play a major role for the regulation of GABA-A receptors ($GABA_A$ Rs) clustering and the molecular composition of these receptors in the synaptic and extra synaptic domains (Knuesel et al., 1999; Fritschy et al., 2003; Zarrouki et al., 2022a). Accordingly, the loss of brain Dp427 leads to a marked reduction in $GABA_A$ -receptor clustering, which affects central inhibition and synaptic plasticity (Vaillend and Billard, 2002; Brünig et al., 2002; Vaillend et al., 2004; Kueh et al., 2008; Sekiguchi et al., 2009; Dallérac et al., 2011; Kueh et al., 2011; Krasowska et al., 2014; Fuenzalida et al., 2016; Pereira da Silva et al., 2018; Wu et al., 2022). If Dp427 is important for proper $GABA_A$ Rs clustering at synapses, a determinant contribution of dystroglycan for receptor localization has also been advocated. Lack of DG determines reduction of $GABA_A$ Rs and of other postsynaptic proteins, such as neuroligin2 and S-SCAM, in cerebellar Purkinje cells, with consequent severe GABAergic denervation and motor learning disability (Briatore et al., 2020). A central role of the DG complex

and of α -DG glycosylation in regulating GABAergic transmission and homeostatic synaptic plasticity has been also reported in hippocampal neurons (Früh et al., 2016; Pribiag et al., 2014). The dystrobrevins are also involved in the clustering of GABA_ARs in cerebellar Purkinje cells. The β -Dystrobrevin, predominant isoform in cerebellar neurons, co-localizes with inhibitory postsynaptic clusters at the soma and dendrites of Purkinje cells. The association of β -dystrobrevin with GABA_ARs is dependent on dystrophin and vice versa. Similarly to dystrophin, the loss of both β - and α - dystrobrevin disrupts GABA_AR clustering in Purkinje cells (Blake et al., 1999; Grady et al., 2006). A mutation affecting the neuroligin family has been shown to be associated with fragile X syndrome as well as autism (Durand et al., 2007; Yamakawa et al., 2007). Besides the GABAergic synapses abnormalities these syndromes also share phenotypic similarities with DMD including intellectual disability and disturbed psychosocial and neurobehavioral functioning.

DMD is a neurodevelopmental disorder (NDD), and the absence of Dp427 during brain development stages may explain some of the non-progressive deficits typically associated with DMD. Indeed, homeostatic mechanisms at the synaptic and circuit levels are crucial for fine-tuning the network excitability across space and time. The highly dynamic GABAergic system has pivotal roles in modulating the activity and plasticity of neural networks during development and adulthood (Tang et al., 2021). Clinical research on NDDs further support the excitation–inhibition (E/I) imbalance hypothesis.

Multiple other NDD have distinct etiologies but display partially overlapping clinical features, including E/I imbalance through GABAergic malfunctioning with intellectual disabilities as well as cognitive impairments such as Rett syndrome (Banerjee et al., 2016; Zhang et al., 2014), Down syndrome (Kleschevnikov et al., 2012) and Fragile X syndrome (Centonze et al., 2008; Liu et al., 2018) as well as ASD (Rubenstein and Merzenich, 2003). These findings highlight the central role of GABAergic system in intellectual disabilities and ASD, disease found to be highly prevalent in DMD.

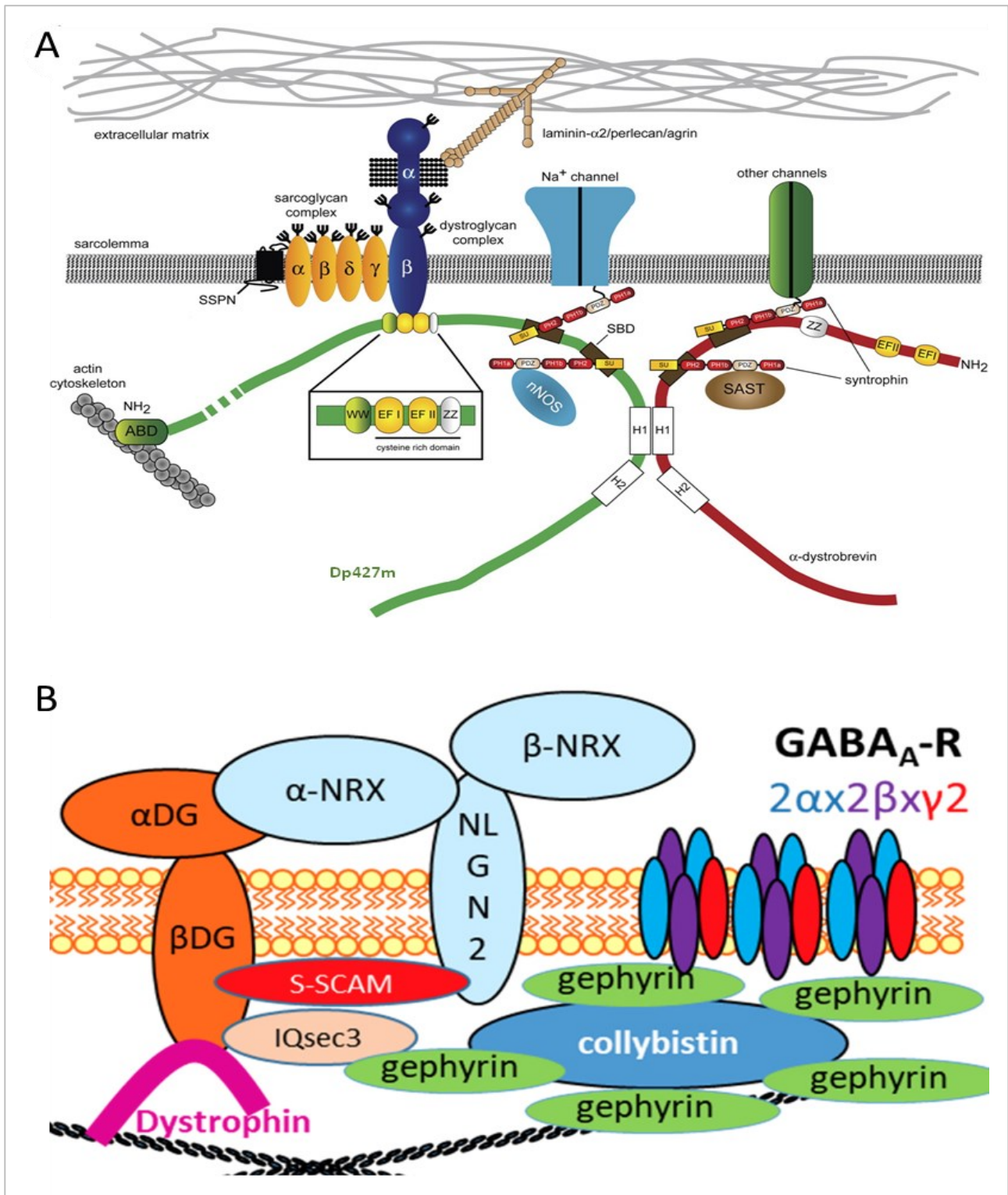


Figure 6. Dystrophin-associated glycoprotein complex. (A) In the muscle. DGC (α , β , δ and γ dystroglycans) interacts with membrane proteins (channels) connecting the interior of the cell to the extra cellular matrix *via* the laminin. From (Waite et al., 2009). **(B) In the brain.** In central inhibitory synapses, the DGC (α and β dystroglycans) interacts with ECM proteins (neurexin) and postsynaptic scaffolding proteins (Neuroigin-2, S-SCAM, IQsec3) involved in the regulation of GABA_AR clustering, while their anchoring to the membrane is insured by the gephyrins (Zarrouki et al., 2022a)

2) Dp260

Dp260 was identified by Pillers et al. in 1993, unexpectedly when their study focused on the role of Dp427 in the retina. Its promoter is located in intron 29 (D'Souza et al., 1995). It has a molecular weight of 260 kDa and is considered to be the specific form of the retina, expressed in photoreceptors in the outer plexiform layer of the retina (Wersinger et al., 2011). Patients with a mutation causing the loss of Dp260 have an alteration in the β wave of the electroretinogram associated with a slightly invalidating "night blindness" phenotype and a deficit in color perception (Pillers et al., 1993; Fitzgerald et al., 1994; Costa et al., 2007; Barboni et al., 2013, 2016). In the retina, the photoreceptor DGC (Figure 7) has Dp260 and/or Dp427 as the central component. These dystrophins are associated with the transmembrane dystroglycan complex, which binds the extracellular retinal matrix-like protein Pikachurin, which in turn interacts with the membrane receptor GPR179 at bipolar cell dendrites (Omori et al., 2012; Orlandi et al., 2018). The photoreceptor DGC may therefore be considered a part of the bridge that connects photoreceptors to bipolar cells (Barboni et al., 2022).

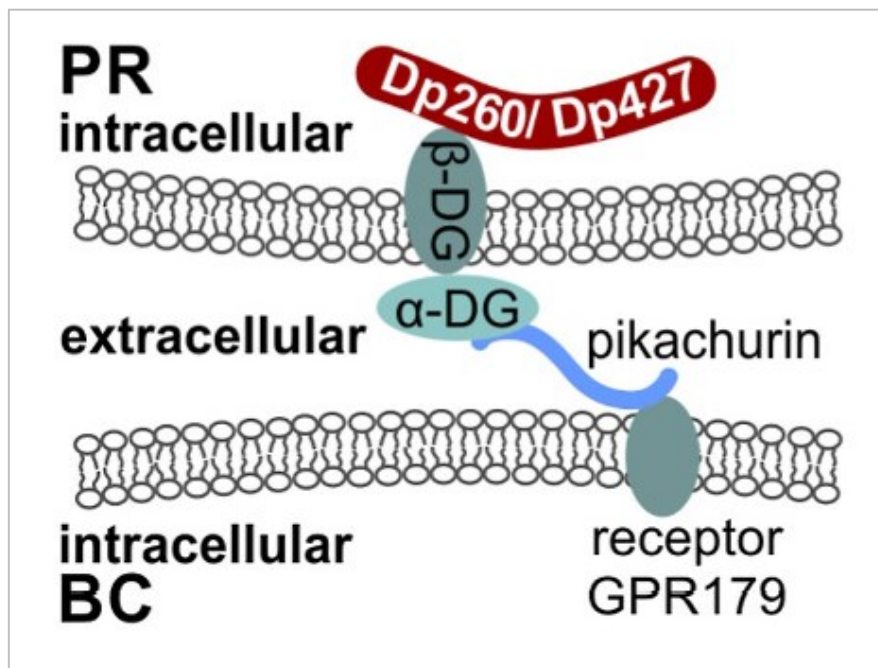


Figure 7. Dystrophin-associated glycoprotein complex in the retina (Barboni et al., 2022)

3) Dp140

The Dp140 promoter is located in intron 44 and produces a 7.4 kb transcript. However, as its initiation codon is located in exon 51 the protein is 140 kDa long. Dp140 is more highly expressed in the human fetal brain than in the adult brain (Lidov et al., 1995; Morris et al., 1995; Doorenweerd et al., 2017) which suggests an involvement in brain formation, perhaps in neuronal proliferation or migration (Hildyard et al., 2020; Romo-Yáñez et al., 2020). Recent studies also suggested its possible presence in the gliovascular system (Caudal et al., 2020; Belmaati Cherkaoui et al., 2021). Dp140 mRNA was recently detected in neuron, astrocyte and in all oligodendrocyte-related cells (García-Cruz et al., 2022). Oligodendrocytes are known to play a major role in the myelination of neuronal axons (Aranmolate et al., 2017). Physical interactions with the vascular endothelium are required for the migration of their precursors (Tsai et al., 2016). Structurally, Dp140 retains the last two hinges, 5 spectrin-like repeats, the cysteine-rich domain, and the C-terminal domain, which theoretically allows it to interact with DGC. So far, its cellular expression and role remains to be characterized. In his studies, Lidov raises the possibility that Dp140 loss in addition to Dp427 loss might be responsible for the increased incidence of cognitive impairment in patients (Lidov et al., 1995; Lidov and Kunkel, 1997). It was later confirmed by clinical genotype-phenotype studies (Desguerre et al., 2009; Taylor et al., 2010; Ricotti et al., 2016b; Colombo et al., 2017). A recent MRI study revealed structural network abnormalities in DMD patients lacking Dp140, providing a possible clue for Dp140 precise role on cognitive deficits severity (Preethish-Kumar et al., 2022).

4) Dp116

Byers, et al. showed that a shorter form of dystrophin of 116 kDa, thus named Dp116, derived from a 5.6 kb transcript, is expressed specifically in the Schwann cells of peripheral nerves (Byers et al., 1993) and in the brain during embryonic development (Blake et al., 1995; García-Cruz et al., 2022). The promoter is located 850 base pairs upstream of exon 56 (inside intron 55), Dp116 lacks the actin-binding domain, suggesting a different function from dystrophin (Blake et al., 1995).

5) Dp71

Nudel et al. (1989) first identified a short dystrophin of 71 kDa in the brain. The Dp71 promoter is located in intron 62, which is then spliced with exon 63, resulting in a 6.5 kb transcript (Bar et al., 1990; Lederfein et al., 1992). Dp71 is expressed ubiquitously except in adult skeletal muscle (Hugnot et al., 1992; Tokarz et al., 1998). A low expression of Dp71 is detected in the embryonic brain but it is mainly expressed postnatally and in adult brain astrocytes and Müller glial cells of the retina (Górecki and Barnard, 1995; Sarig et al., 1999; Acosta et al., 2004). Dp71 does not have any repeated spectrin-like domain, only the cysteine-rich domain and the C-terminal domain. Therefore, Dp71 is able to interact with DGC *via* its carboxy-terminal part (Figure 8), it is however known that the DGC complex formed with Dp71 is different from the DGC formed with Dp427 (Blake et al., 1999).

It presents strong expression at the glio-vascular interface, precisely in the astrocytic end-feet, where it is associated to potassium channels Kir4.1 and aquaporin 4 (AQP4) and contribute to their regulation (Belmaati Cherkaoui et al., 2021). These findings suggest a role in the blood-brain barrier, which is compromised in case of downregulation or knock-out of Dp71 (Nico et al., 2003, 2004). Likewise, the loss of Dp71 also alters the blood-retinal barrier (Vacca et al., 2016). Dp71 deficiency has also been associated with an impaired clustering of AQP4 channels and a delayed edema onset possibly due to impaired assembly of a DGC complex containing α -syntrophin (Vajda et al., 2002; Waite et al., 2009). Indeed, AQP4 channels can associate *via* its carboxyl-terminus region to α -syntrophin (Neely et al., 2001). Similarly, a direct association between the DGC and the K⁺ channels has been suggested *via* the carboxyl-terminal of the Kir4.1 channels binding to α -syntrophin (Connors et al., 2004). Daoud et al. showed in 2009 that, beyond its glial expression, Dp71 also colocalizes with key proteins of glutamatergic excitatory synapses, such as NMDA and AMPA receptors (Daoud et al., 2009b).

Dp71-deficiency leads to altered synapse density in the adult brain, several electrophysiological abnormalities, including reduced synaptic plasticity and enhanced field excitatory post-synaptic potentials (EPSPs). This results in augmented glutamatergic neurotransmission in CA1 region of the hippocampus and in the prefrontal cortex, the cerebellar synapses formed by climbing fibers (CFs) onto Purkinje neurons, but not at those formed by parallel fibers in the cerebellum (Daoud et al., 2009b; Helleringer et al., 2018; Chaussonot et al., 2019). These data raise the possibility that loss of Dp71 may alter glutamatergic neurotransmission contributing to the cognitive dysfunction in patients

with DMD. Indeed, as Dp71 is the most expressed dystrophin in the brain (Jung et al., 1993; Lederfein et al., 1992; Tadayoni et al., 2012), many studies investigated the involvement of its loss on intellectual disability in DMD patients (Bar et al., 1990; Daoud et al., 2009a). Others showed that the cognitive processes that depend on prefrontal cortex integrity are affected in Dp71-null mice, such as cognitive flexibility and sensitivity of spatial working memory (Chausseot et al., 2019). Cerebellum-dependent processing of the procedural components of spatial learning is also altered (Helleringer et al., 2018).

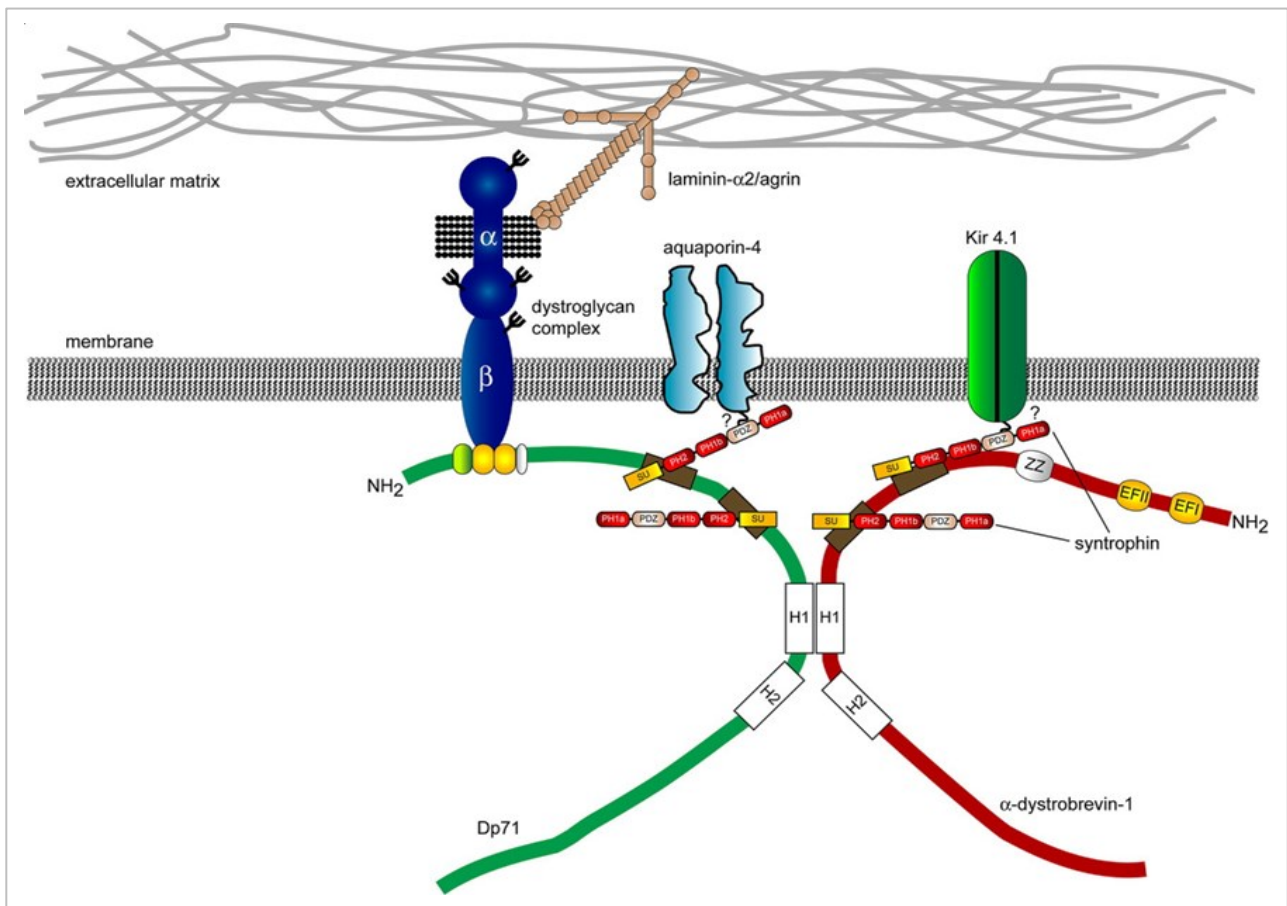


Figure 8. Dystrophin-associated glycoprotein complex in glia and astrocyte end-feet (Waite et al., 2009)

6) Dp40

Resulting from the cleavage of Dp71, Dp40 ends at exon 70 due to an alternative polyadenylation signal (3'UTR) that is derived from the intron 70 sequence. Therefore, Dp40 is not expressed from a specific internal promoter and its mRNA is 2.2 kb (Tinsley et al., 1993). Consisting of 341 amino acids, Dp40 is currently the smallest *DMD* gene product known. Dp40 is unique because, unlike other dystrophins, it lacks the carboxy-terminal part common to the other dystrophins. Dp40 contains the β -dystroglycan binding site, but not the binding sites for syntrophin and dystrobrevin (Tinsley et al., 1993). Given that detection antibodies often target the carboxyterminal part, Dp40 has been relatively difficult to detect and localize precisely. In 2012, Tozawa et al. developed a specific antibody against Dp40 that showed an expression timing pattern similar to that of Dp71, since both are expressed from a common promoter; thus, Dp40 expression is also observed in early developmental stages (García-Cruz et al., 2022). Few studies have reported Dp40 involvement in synaptic functions (Tozawa et al., 2012; Fujimoto et al., 2014), however, its specific role remain so far poorly understood and needs to be further studied.

C. *DMD* gene mutations

The *DMD* gene is the largest gene identified and spans more than 2.4 Mb, about 1.5% of the X chromosome. The rate of mutations in the coding sequence of the *DMD* gene is 1.10^{-4} per generation (Blake et al., 2002), which is higher compared to the estimated average of 1.10^{-5} to 1.10^{-6} for human genes in general. The *DMD* gene is very complex and different types of mutations can affect its expression (Figure 9).

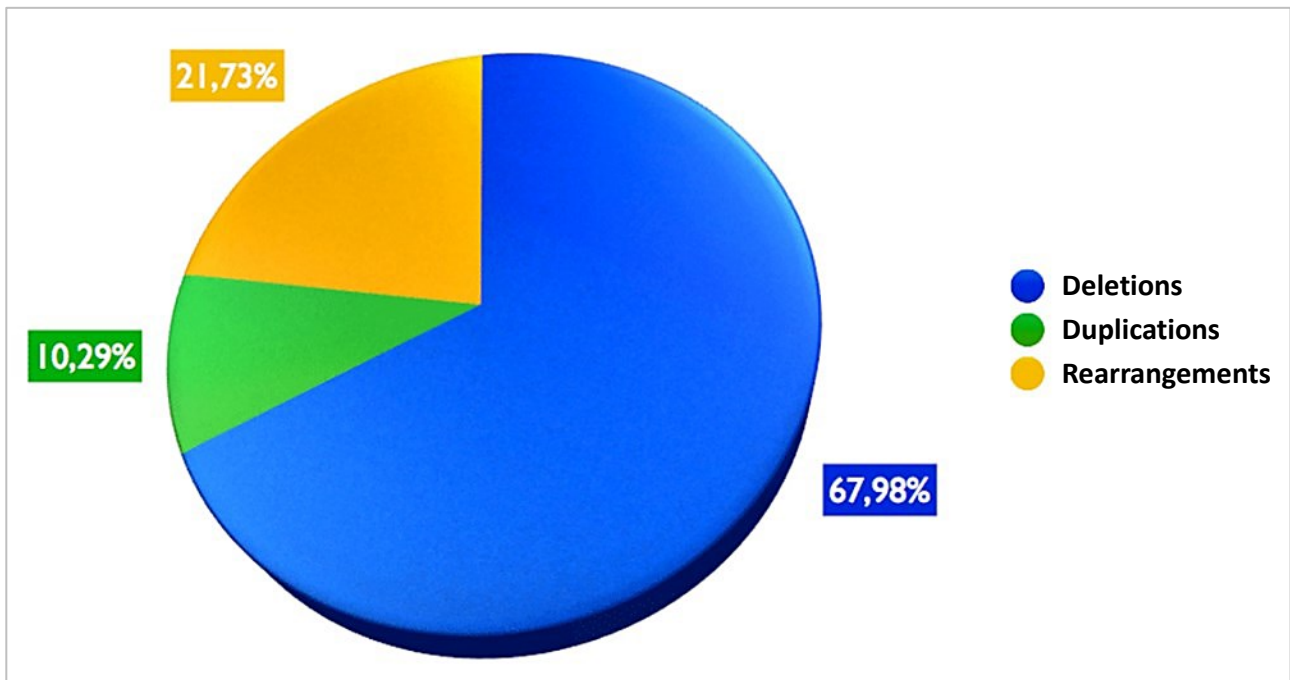


Figure 9. Mutations distribution in *DMD* (France UMD/BMD database)

The most common changes in dystrophin are intragenic deletions, which account for approximately 65% of dystrophin mutations (Koenig et al., 1989). Deletions and, more rarely, duplications can happen almost anywhere in the *DMD* gene. However, there are two deletion hotspots, i.e. where mutations are most likely to occur, a minor one between exons 2-19 and a major one between exons 45-55 (Oudet et al., 1992; Nobile et al., 1995).

Deletions are found in about 60-65% of patients with *DMD* and *BMD*, and the frequency of duplications may range from 5% to 15% (Abbs and Bobrow, 1992). The remaining cases are thought to be caused by a combination of small mutations (most commonly point mutations resulting in nonsense or frame-shift mutations), pure intronic deletions, or exonic insertion of repetitive sequences (Roberts et al., 1994; Ferlini et al., 1998).

At the genomic level, the most frequent breakpoints are found in the largest introns, namely introns 2 and 7 for the minor hotspot region, and intron 44 for the major hotspot region. This grouping of deletions in two main regions represents a main advantage for the diagnosis, since 98% of DMD/BMD deletions can be exposed by the multiplex PCR technique on only 19 exons (Beggs et al., 1990).

The severity of the dystrophic phenotype, in DMD or the milder BMD form, depends not so much on the extent of the deletion (and the same applies for duplication) but on whether or not it disrupts the reading frame (Monaco et al., 1988). Indeed, very different deletions by their size or location within the gene can give rise to a very similar phenotype. Mutations that maintain the reading frame (in-frame) generally result in truncated but partly functional dystrophin and are associated with the BMD phenotype. In patients with DMD, deletions and duplications disrupt the reading frame (frameshift) giving rise to the appearance of a premature STOP codon and thus a truncated and non-functional dystrophin.

D. Genotype-phenotype relationship

Genotype–phenotype correlation studies have provided unique perspectives on DMD pathogenesis. Studies in patients with BMD have corroborated basic research findings on the relationship between dystrophin structure and function. For example, patients with BMD who lack the actin binding domain (ABD) or spectrin-like repeats (R16/R17) often have a more severe disease than patients with BMD who have other variants. Notably, altered R16/17 domain may lead to the loss of Dp140 expression (Aartsma-Rus et al., 2006; Bello et al., 2016). Genotype–phenotype correlation studies have also implicated regions of dystrophin that are important for cardiac disease (Wasala et al., 2018) and central alterations (Ricotti et al., 2016b). The DMD cognitive profiles diversity, however, seem to rely on larger factors than the full-length dystrophin structure itself. Indeed, in the last decades, many studies have been questioning the origin and puzzling out this variability. The multiple dystrophins expressed in the CNS, their specific structures, various cell types expression, associated DGC, and thus, functions in the brain constitute a main factor of this large heterogeneity of central alterations found in DMD population.

The evolution of technologies and the improvement of molecular biology during that period allowed a real improvement in the genotyping of patients and therefore allowed to elaborate more conclusive hypothesis on cognitive impairments heterogeneity.

In 1992, Billard et al., conducted a controlled neuropsychological study including 24 DMD patients matched with 7 spinal muscular atrophy (SMA) patients aged 12-16 years. They aimed to investigate the contribution of the muscular dystrophy on the central alterations. The study included evaluations of IQ, verbal skills (fluency, confrontation naming and syntax comprehension) and memory abilities. The results indicate significantly altered cognitive skills only in the DMD group, demonstrating that the central phenotype in DMD is independent from the muscular dystrophy. Their study already brought to evidence a genetic relationship with the central phenotype (Billard et al., 1992). Later on, Hinton et al. investigated working memory and IQ, by including pairs of DMD boys and their unaffected siblings, not only as controls for performance but also to consider external bias of multiple background factors (both genetic and environmental). Replicating and confirming the cognitive deficits in DMD boys, they still had a large intragroup variability (Hinton et al., 2001).

During a whole decade, different studies emerged with the hypothesis of a correlation between mutations profiles in the *DMD* gene and central alterations. Den Dunnen et al. showed that a unique loss of the full-length dystrophin correlated with normal intellectual capabilities (den Dunnen et al., 1991). Rapaport et al. noted an apparent association between intellectual disability and the deletion of exon 52 which affects the expression of shorter brain dystrophin (Dp140) (Rapaport et al., 1991). In the following years, Roberts et al., Lenk et al., and Tuffery et al., identified a subpopulation of DMD patients with intellectual disability and carrying point mutations affecting the distal part of the *DMD* gene (Roberts et al., 1992; Lenk et al., 1993; Tuffery et al., 1995). These pioneering studies suggested that this part of the gene is involved in the genesis of intellectual disability, thus, supporting the hypothesis of correlated central alterations and mutation profiles of DMD patients. This hypothesis is all the more credible since the Dp140 promoter is located in exon 44 and its start codon in exon 51, while the Dp71 promoter is located between exons 62 and 63.

Bardoni et al. demonstrated the impact of Dp140 loss on central functions. Indeed, patients with mutations disturbing the normal expression of Dp140 had more severe cognitive deficits than patients only lacking Dp427 (Bardoni et al., 2000).

The same year, Moizard et al. showed that patients carrying distal mutations leading to the loss of all brain dystrophins, including Dp71, exhibit severe intellectual disability (IQ <50) (Moizard et al., 2000). These studies further supported and confirmed the important role of short brain dystrophins, namely, Dp140 and Dp71, and the incidence of their loss on the severity of the cognitive deficits in DMD patients (Figure 10).

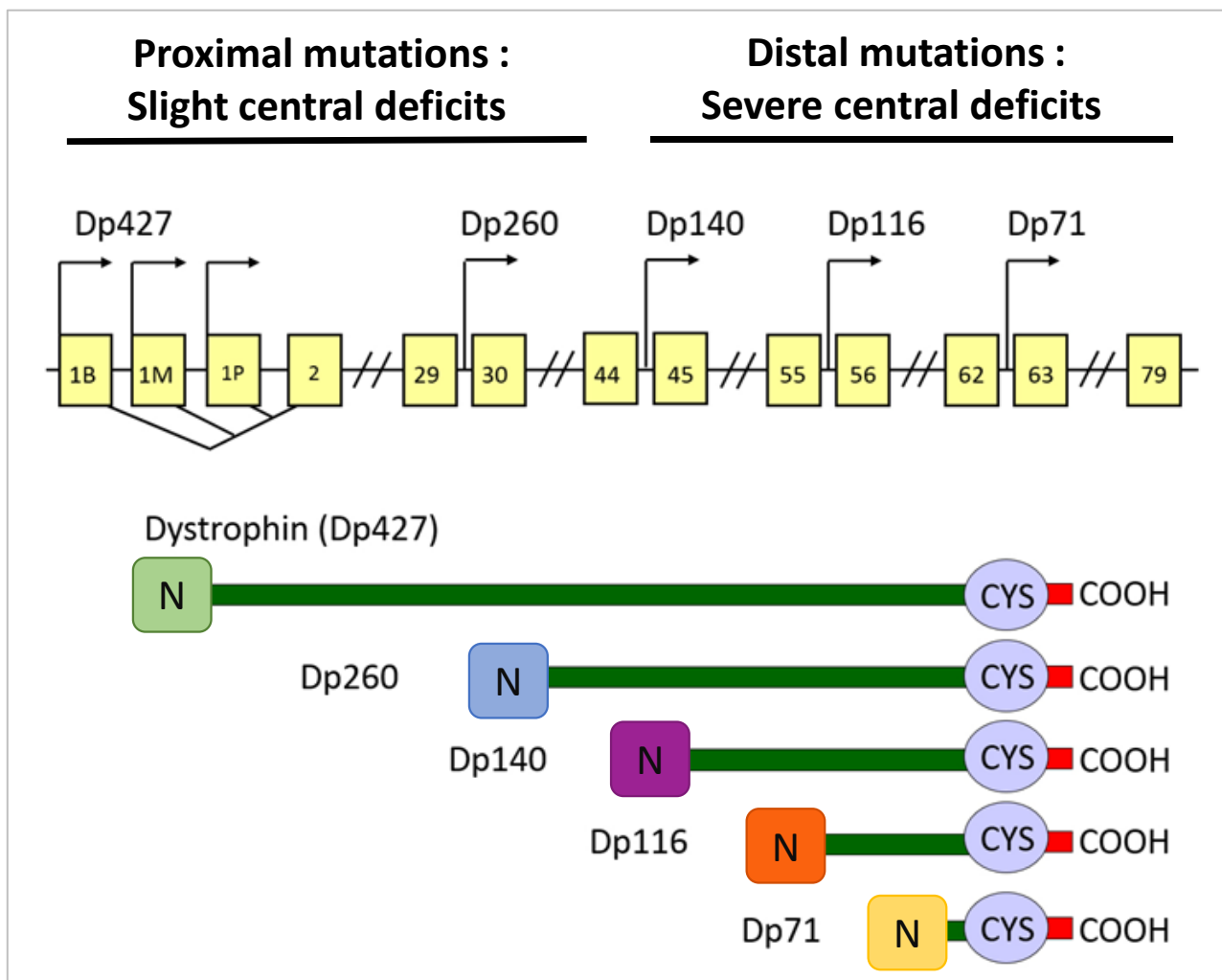


Figure 10. Genotype-phenotype correlation: Mutation position and dystrophins loss. (Vaillend et al., 2019)

This part of the DMD literature will wait until the end of the next decade to be enriched. In 2009, was published the first fully detailed clinical study encompassing 10 years of investigations and follow up of DMD patients. The study was a specific report on the clinical heterogeneity, and precisely defining four sub-phenotypes making it possible to establish predictive criteria for the evolution of the disease. The motor phenotype (classified from "poor" to "very poor") is independent of the location of the mutation (all DMD patients lacking Dp427), while in contrast, the cognitive phenotype (classified "normal" to "very poor") is correlated with the nature of the mutation profile and thus the lacking dystrophins (Desguerre et al., 2009). The study of Daoud et al. focused on the impact of an

additional Dp71 loss, compared to patients lacking all dystrophins except Dp71. They report that patients with mutations affecting Dp71 present systematically an intellectual disability, whereas those in whom all the dystrophins are mutated, with the exception of Dp71, present a more variable cognitive status (Daoud et al., 2009a), in line with the study of Desguerre et al. They suggested that mutations affecting Dp427 do not always lead to cognitive impairment and that the loss of Dp140 would be a susceptibility factor for intellectual disability.

In 2010, Taylor and colleagues further demonstrated a correlation between the mutation position, and thus the brain dystrophins lost, and the IQ scores (Figure 11). Their study demonstrated the impact of a cumulative loss of several brain dystrophins on the severity of the intellectual disability (Taylor et al., 2010).

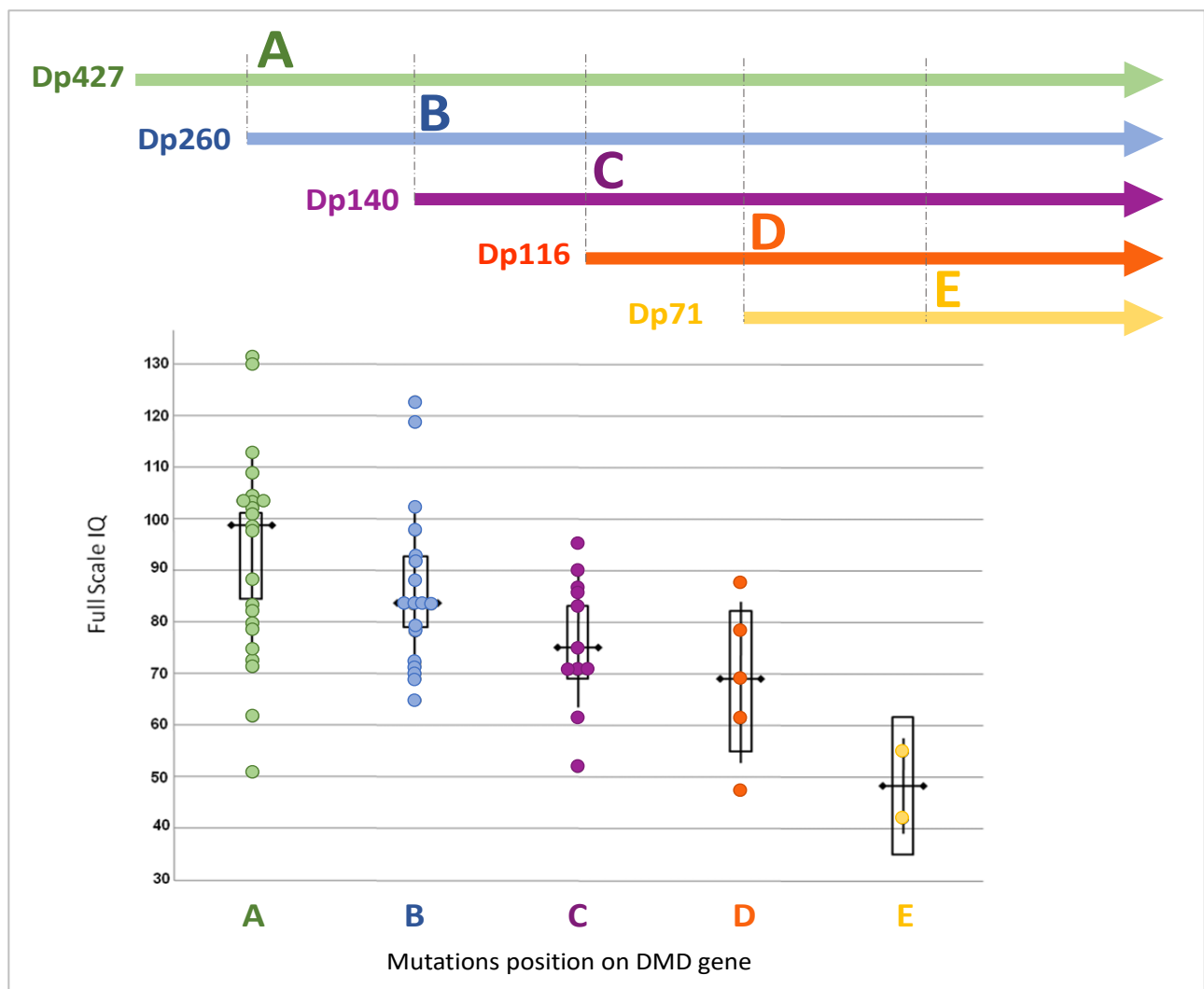


Figure 11. Specific correlation between mutation position in DMD gene, the cumulative loss of brain dystrophins and IQ scores upon DMD population. Adapted from (Taylor et al., 2010)

Another study focusing on the neurocognitive profile of DMD patients confirmed the genotype-phenotype relationship regarding intellectual disability. Specifically, they noted that patients with mutations in the distal part of the gene show greater deficits in verbal tasks of short and long-term memory, visual memory, visuospatial organization, sequence analysis and possibly in working memory tasks. Patients with a mutations in the proximal part of the gene, on the other hand, express difficulties in social judgment and critical understanding of sentences, deficits also observed in autistic patients, as well as in visual attention tasks (D'Angelo et al., 2011).

The findings on heterogeneity and its correlation with mutation profiles were confirmed in multiple studies supporting that severe deficits are associated with the cumulative loss of brain dystrophins (Rasic et al., 2014; Ricotti et al., 2016b; Colombo et al., 2017; Naidoo and Anthony, 2020). Certain studies further suggest that there is a high prevalence of clusters of symptoms among DMD patients. Patients with mutations downstream of exon 30 appear to be at increased risk of developing comorbid neurodevelopmental, behavioral, and emotional difficulties compared to those whose mutation only affect the full-length Dp427. This was notably illustrated by Ricotti et al., who suggested the term “DMD neuropsychiatric syndrome” to describe the clustering of neuropsychiatric symptoms in DMD (Ricotti et al., 2016b; Darmahkasih et al., 2020).

The reliable achievement of mutation detection and comprehensive analysis of expression profiles of the distinct cerebral dystrophin in patient cohorts is essential for diagnosis, prognosis, and the development of suitable therapeutic approaches. The fine combinations of clinical, cognitive, molecular and protein data analysis in large cohort studies will allow the emergence of consistent genotype-phenotype relationships that converge with animal model studies investigating at the cellular and molecular level the contribution of distinct brain dystrophins to the cognitive and behavioral deficits (Vaillend et al., 2004; Daoud et al., 2009b; Chausseot et al., 2015; Miranda et al., 2015; Vaillend and Chausseot, 2017).

II. DMD animal models

The availability of multiple animal models for DMD plays a pivotal role in studying and better understanding DMD pathology. It is unlikely that animal models can fully recapitulate the DMD neuropsychiatric syndrome, although alterations in learning and behavior are apparent. Despite differences in some pathological hallmarks compared to humans, animal models have provided important insights about mechanisms involved in maintaining cognitive function through molecular and cellular engagement in nervous system and into causal gene relationships of disease pathogenesis (Durbeej and Campbell, 2002; Wells, 2018; van Putten et al., 2020).

Currently, there are two types of animal models of DMD: those with a spontaneous or chemically induced mutation in the DMD gene, and those that have been artificially generated by genetic engineering (i.e. in which the mutation has been specifically chosen). Nearly 60 animal models of DMD exist, and the list continues to grow. They equally include non-mammalian models such as the *C. elegans* worm, *Drosophila* or zebrafish and mammals such as mice, cats, dogs, and more recently rats or pigs (McGreevy et al., 2015). Among these DMD models, canine models have been widely used.

Canine models of Duchenne muscular dystrophy have been described for more than 50 years in the literature and ~20 different breeds are involved. The golden retriever muscular dystrophy dogs (GRMD) model is the first and the most widely used DMD canine model. It was initially identified by De Lahunta and colleagues and then characterized by Cooper and Kornegay (Valentine et al., 1986; Cooper et al., 1988; Kornegay et al., 1988; Hoffman and Gorospe, 1991). The mutation in the DMD gene was located in the splice acceptor site of exon 7 at intron 6. This splice mutation induces an elimination of exon 7 in the mature messenger and consequently a distribution of the open reading frame, causing a stop codon in exon 8 (Sharp et al., 1992). Muscle weakness in these dogs becomes evident around 2 months of age and their lifespan is significantly reduced (Valentine et al., 1990). Subsequent molecular, histological, and clinical studies validated GRMD dogs as a reliable model for human DMD (Valentine et al., 1992; Lanfossi et al., 1999; Cozzi et al., 2001; Nguyen et al., 2002). Their muscular phenotype is very close to that of humans, making it a good study model for therapies aimed at restoring the expression of dystrophin in the muscle. In addition, the dog's immune responses present similarities to humans and the large size of this animal makes it possible to better understand the effects of a treatment on a large individual. Otherwise, another canine model, the Dystrophin-Deficient Cavalier King Charles Spaniels (CKCS), replicates similar mutation profiles of patients are

of interest for preclinical studies (Walmsley et al., 2010). However, studies of central alterations in the DMD dogs are scarce (Crawford et al., 2022). This unique behavioral study is the first to address the cognitive phenotype in DE50-MD dogs lacking full-length dystrophin (Dp427). The study reported central alterations including deficits in attention, problem solving and exploration of novel objects. The genotype-phenotype correlations cannot be addressed in canine model due to a lack of models with distinct mutations.

Because of the well-established behavioral paradigms and the large genetic modifications possible as well as the low cost and easy access, mouse models are much widely used both for the study of the functional role of dystrophins, the associated cognitive deficits as well as the development of new therapies. The main DMD mouse models, their mutations and thus the dystrophins they lack are reported below (Figure 12).

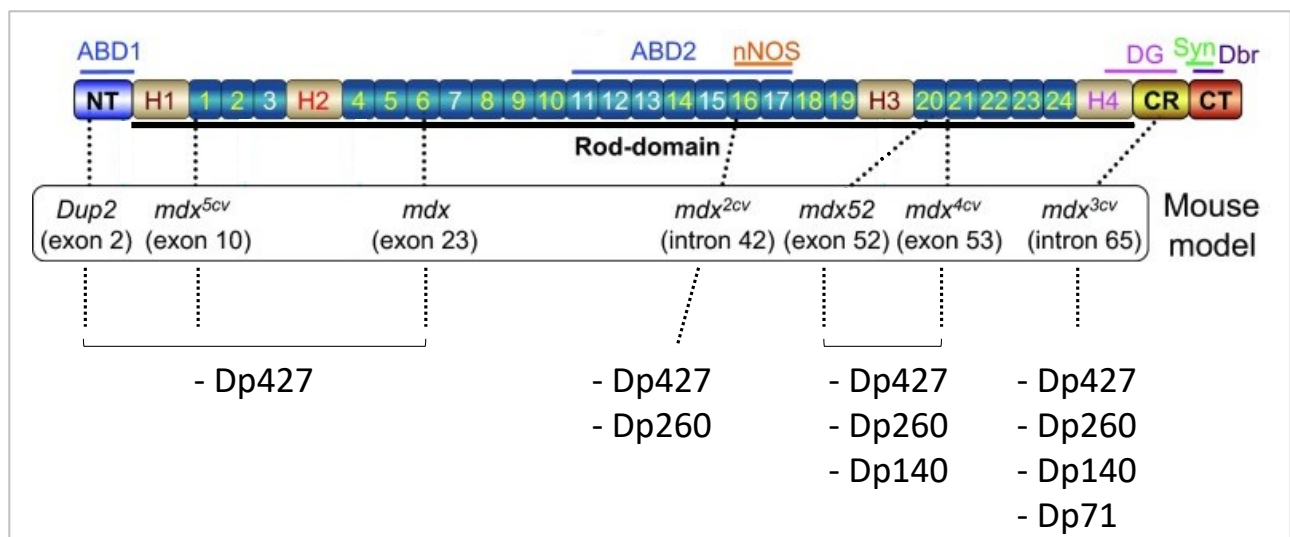


Figure 12. DMD mouse models. Adapted from (McGreevy et al., 2015)

1. The *mdx* mouse model

The most widely used animal model for DMD research is the *mdx* mouse. It was discovered in the early 1980s in a colony of C57BL/10ScSn mice due to elevated serum creatine kinase (CK) and histological evidence of myopathy (Bulfield et al., 1984). The mutation in the *mdx* mouse is a nonsense point mutation in exon 23 that aborts full-length dystrophin expression (Figure 12) (Sicinski et al., 1989).

A. Muscular dystrophy phenotype

Despite being deficient in dystrophin, *mdx* mice have minimal clinical symptoms and their lifespan is only reduced by ~25% (Chamberlain et al., 2007; Li et al., 2009). In contrast, the lifespan of individuals with DMD is reduced by ~75%. Skeletal muscle disease in *mdx* mice has several distinctive phases. In the first 2 weeks, *mdx* muscle is indistinguishable from that of normal mice. Between 3 to 6 weeks, necrosis begins to set in place. Subsequently, by 26 weeks, 80-90% of muscle fibers exhibit one or more non-peripheral nuclei, as a result of at least one degeneration-regeneration cycle. This plateau is maintained (in the presence of continued degeneration), from 26 weeks to 104 weeks. Limb muscles of *mdx* mice often become hypertrophic during this phase. This degeneration-regeneration cycles are persistent and stable during this period explaining the slowly progressive phenotype of *mdx* mice (Stedman et al., 1991).

Severe dystrophic phenotypes, such as muscle wasting, scoliosis, and heart failure, do not occur until mice are 15 months old or older (Pastoret and Seville, 1995; Lynch et al., 2001; Bostick et al., 2008, 2009; Hakim et al., 2011). A significant proportion of aged *mdx* mice also develops spontaneous sarcoma (Chamberlain et al., 2007; Schmidt et al., 2011; Wang et al., 2014).

Young adult *mdx* mice have normal spontaneous locomotor activity under certain experimental conditions (Vaillend et al., 1995; Vaillend and Chaussonot, 2017), yet, Rafael et al. also showed that the *mdx* mouse display increased fatigability (Rafael et al., 2000). Moreover, Grady et al. showed abnormal motor behavior, both in a grip test for muscle strength, which is reduced by about 30%, but also in a test of motor coordination using a rotarod. The rotarod is a cylinder that can turn on itself, at constant speed or with progressive acceleration. While *mdx* mice maintain their balance at constant speed, they cannot perform as well as wild-type control mice when the speed is gradually increased, reflecting their impaired muscle strength and/or a deficit in cerebellar-dependent motor coordination (Grady et al., 2006).

It should be noted that a few dystrophin positive fibers can be found in the muscles of DMD patients as well as in animal models of the disease, in particular *mdx* mice and GRMD dogs (Hoffman et al., 1990; Burrow et al., 1991). These fibers are called revertant fibers (RFs) and have been further studied in *mdx* mice. These fibers are often detected in the form of small clusters and represent less than 1% of the total number of fibers, although their number tends to increase with age in *mdx* mice (Figure 13) (Lu et al., 2000).

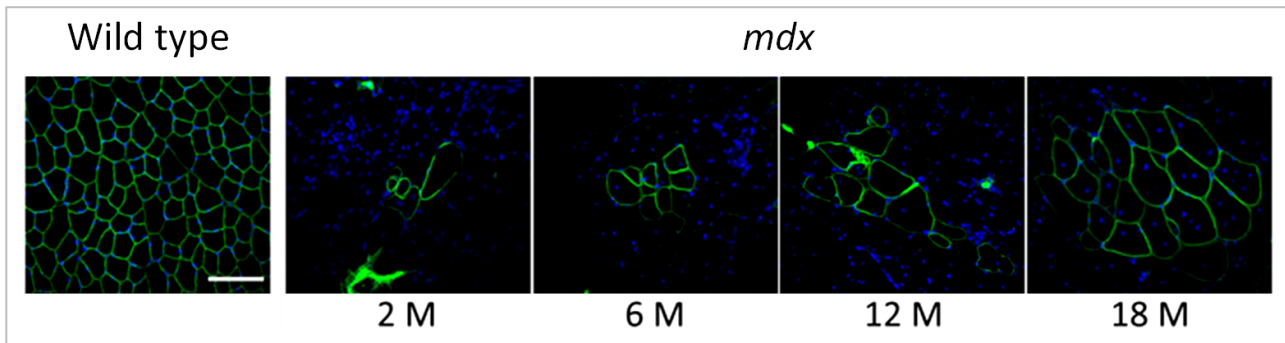


Figure 13. Dystrophin-positive revertant fibers with central nuclei of WT and *mdx* at ages of 2, 6, 12, and 18 months (Echigoya et al., 2013)

Revertant fibers' dystrophins are likely functional as the same fibers also express membrane-localized proteins of the DGC. A few reports have investigated mechanisms and clinical significance of RFs. Hoffman et al showed that the number of revertant fibers in *mdx* muscles increases after X-irradiations (Hoffman et al., 1990). Wilton et al examined DMD gene transcripts around the mutated exon 23 in *mdx* mice and revealed several alternatively processed transcript species with skipping of additional exons neighboring the mutated exon 23 (Wilton et al., 1997). Interestingly, these shortened transcripts were also present in normal adult and embryonic mouse muscle tissues. These studies overall, based mainly on cluster and clonal assumption, concluded that somatic mutations, specifically genomic deletion, are the most likely mechanism for the restoration of reading frames in DMD. Variation in signal intensity also led Nicholson et al. to propose a modified hypothesis that strong positive revertant dystrophin signals might be a result of somatic mutations whereas weak dystrophin signals could be a result of exon splicing (Nicholson et al., 1993). These studies indicated that revertant fibers most likely result from random epigenetic events that skip exon(s) flanking the mutated exon, leading to the restoration of the reading frame. Some of these events establish themselves as relatively permanent skipping patterns, a mechanism similar to multiple transcript species established in various cell types (Lu, 2021).

Despite being often criticized for its late myopathy onset and weak muscular phenotype, the *mdx* mouse remains a model of choice as it mimics the common feature of all DMD patients, namely, the loss of dystrophin Dp427. Concerning behavioral studies that aimed at assessing brain and cognitive alterations, which frequently involve at least some motor demand, delayed myopathy progression is an advantage as it will not interfere with the assessment.

B. Emotional phenotype: behavioral parameters and brain circuits

The most robust and typical phenotype in *mdx* mice is their increased emotional reactivity in response to mild stress, such as restraint-induced stress. This unconditioned defensive phenotype depends on the fear circuits (Figure 14) that involves, among other structures, the amygdala. This brain structure normally express Dp427 in the GABAergic inhibitory synapses.

Manual restraint is a method aimed at hindering movements of the mouse and it consists of grabbing the skin of the back preventing the mobility of the four paws and the head. Done well, the restraint is only intended to immobilize the mouse and is not painful. It may induce some stress in animals, which, once released in their home cage, may show a defensive response expressed as fighting, escape seeking or freezing (Cannon, 1915). In the *mdx* mouse, however, the typical response is immobility; it is called "freezing response" and is defined by a lasting tonic immobilization of the animal body apart from the movements related to the breathing. Sekiguchi et al. showed that the freezing response of *mdx* mice is dramatically high during the minutes following restraint. Moreover, they showed an age-related aggravation of the phenotype as it reaches a plateau by 3-4 months of age (Sekiguchi et al., 2009). This was further confirmed and completed by Vaillend and Chausseot in their study, demonstrating that this enhanced fearfulness induces long-lasting motor inhibition, suggesting that neurobehavioral dysfunctions significantly influence motor outcome measures in this model (Vaillend and Chausseot, 2017). This phenotype has been attributed to a dysfunction of the fear circuit, as supported by altered GABAergic inhibitory responses to norepinephrine inputs to pyramidal neurons of the basolateral amygdala in Dp427-deficient *mdx* mice (Sekiguchi et al., 2009).

The anxiety-related responses are also emotional behaviors involving the amygdala, as well as hippocampus and prefrontal cortex (Figure 14). Consequently, the anxiety traits have been investigated in *mdx* mice, yet a certain variability has been reported among laboratories (Vaillend et al., 1995; Sekiguchi et al., 2009; Manning et al., 2014; Vaillend and Chausseot, 2017). Manning and colleagues reported behavioral indices of enhanced anxiety in *mdx* mice, observed in free exploration of open field (OF) test. Indeed, the avoidance of the center of the arena is regarded as a measure of anxiety (Manning et al., 2014). This phenotype was later confirmed by others (Vaillend and Chausseot, 2017). Besides, anxiety was tested in other dedicated paradigms such as the light dark choice test (LD) and the elevated plus maze (EPM). In the LD test the animals are given the choice between a brightly lit box and a dark box. The anxiety measure is based on the avoidance of the anxious stimuli namely the brightly lit compartment. Vaillend and colleagues did not bring to

evidence a clear phenotype as they found similar behavioral responses between *mdx* mice and WT (Vaillend et al., 1995). Yet, a recent study of the same group reported that *mdx* mice avoided the lit compartment significantly more than the controls (Vaillend and Chaussonot, 2017). Thus, the anxious phenotype is found to be variable. Further, *mdx* mice were also submitted to the EPM test. In this paradigm, the animals are given the choice to freely explore a plus shaped maze with two enclosed arms and two open arms. The open arms are more exposed to the light and the void, as the maze is elevated from the floor. The anxiety results from the threat induced by void in the elevated open arms and is then reflected by the time spent in the open arms. Different studies reported normal behavior in this test (Sekiguchi et al., 2009; Vaillend and Chaussonot, 2017). The cause of such differences observed among distinct anxiety tests remains unclear. Together, these reports suggested that changes in anxiety are borderline in *mdx* mice.

For more than a century after the original discovery that temporal lobe structures govern emotional behaviors (Brown and Sharpey-Schafer, 1888), our understanding of the neural substrates of anxiety was largely restricted to insights gleaned through lesion and inactivation studies. While this important early work led to the identification of key loci controlling anxiety, notably including the amygdala (Baso Lateral Amygdala: BLA, Central Amygdala: CeA), the bed nucleus of the stria terminalis (BNST), the ventral hippocampus (vHPC) and the prefrontal cortex (PFC), progress in dissecting the contributions of regional microcircuits to this emotional state was limited.

Innovative approaches in animal research, especially targeted manipulations of neurons based on projection target or genetic identity via optogenetics, have opened these questions for causal testing and accelerated the pace of discovery. The resulting paradigm shift in anxiety research has expanded the focus to broader circuit-level interactions in emotional processing (Figure14).

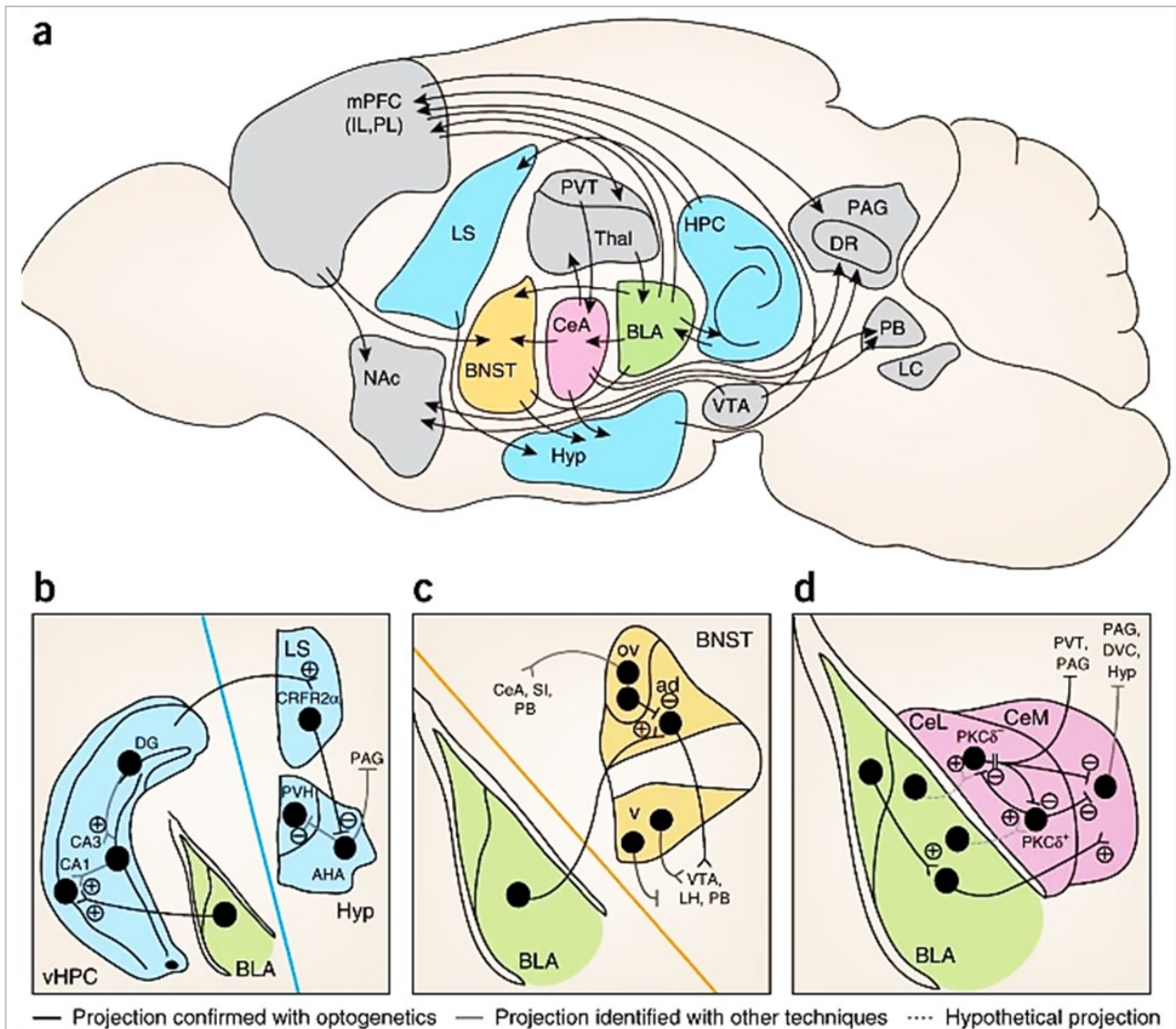


Figure 14. Neural basis of emotional circuits of fear and anxiety (Calhoun and Tye, 2015)

C. Synaptic plasticity and memory

The *mdx* mouse exhibits no deficits in the Morris water maze, which evaluates hippocampus-dependent spatial learning and memory (Sesay et al., 1996) or in a radial maze spatial discrimination task (Chausseot et al., 2015; Vaillend et al., 1998). However, retention deficits at long delays have been reported in spontaneous alteration and bar-pressing tasks (Vaillend et al., 1995) and impairments of memory consolidation in both spatial and non-spatial learning tasks (Vaillend et al., 2004). These deficits could be explained by a more fragile memory after partial learning, with the consequence of specific long-term memory deficits that could partly depend on a dysfunction of the consolidation and/or recall processes involving the hippocampus.

The mechanisms underlying these deficits might be due to alteration of the neuronal function, carried by a synaptic dysfunction associated with a loss of the Dp427. Indeed, Vaillend et al. showed an abnormal increase in synaptic plasticity (i.e., long-term potentiation: LTP) in the CA1 layer of the hippocampus of *mdx* mice, likely related to deficient inhibitory processes. They later specified that this increase in LTP can last for several hours (Vaillend et al., 2004) and that it is correlated with ultrastructural modifications of synapses (Miranda et al., 2009, 2011, 2016). Since these forms of plasticity have been associated with memory consolidation processes, it is currently assumed that there is a link between memory deficits and these alterations in synaptic plasticity in *mdx* mice.

The exacerbation of the unconditioned defensive fear responses in *mdx* suggested that this model might also exhibits deficits in amygdala-dependent aversive tasks involving emotional memory. A study of Muntoni and colleagues, had shown a long-term memory deficit in a passive avoidance task (Muntoni et al., 1991). Later, Sekiguchi et al. performed a Pavlovian context-associated fear conditioning task on *mdx* mice , based on association between an electric shock and an experimental context. The study revealed a stronger freezing response in *mdx* than in wild-type mice, underlying a strong conditioned defensive response to the experimental context (Sekiguchi et al., 2009). However, Perronnet et al. (2012) found a transient deficit of recall during the first seconds of re-exposure to the experimental context, supporting a long-term memory deficit. However, the averaged amount of freezing during the 5-min recall session was comparable between *mdx* and WT mice. This variable expression of contextual fear between laboratories suggests that it may depend on the basal level of stress of the mice, perhaps due to discrepancies in animal care procedures. Further, *mdx* mice were also tested in an auditory-cued fear conditioning, a Pavlovian associative task. This task is based on the association between non-aversive stimulus (an auditory tone as conditioning stimulus: CS) and an electric foot shock (conditioned stimulus: US). During learning, the CS (auditory tone) predicts the delivery of the US (shock). Freezing in response to the tone then reflects learning of the CS-US association. Surprisingly, *mdx* mice, which usually show strong stress reactivity expressed as unconditioned freezing, display reduced freezing in response to the CS in this task, which indicates a cognitive deficit in this task involving fear memory. These performances were replicated several times in *mdx* mice. Their phenotype was consistently characterized by delayed acquisition and retention of the task, but *mdx* mice could finally perform in a comparable manner to their wild-type littermates after repetition of stimulus presentation (Chausseot et al., 2015; Vaillend and Chausseot,

2017). Notably, the cued associative fear learning is an amygdala-dependent task particularly consolidation processes involving the basolateral amygdala (BLA) (Figure 15).

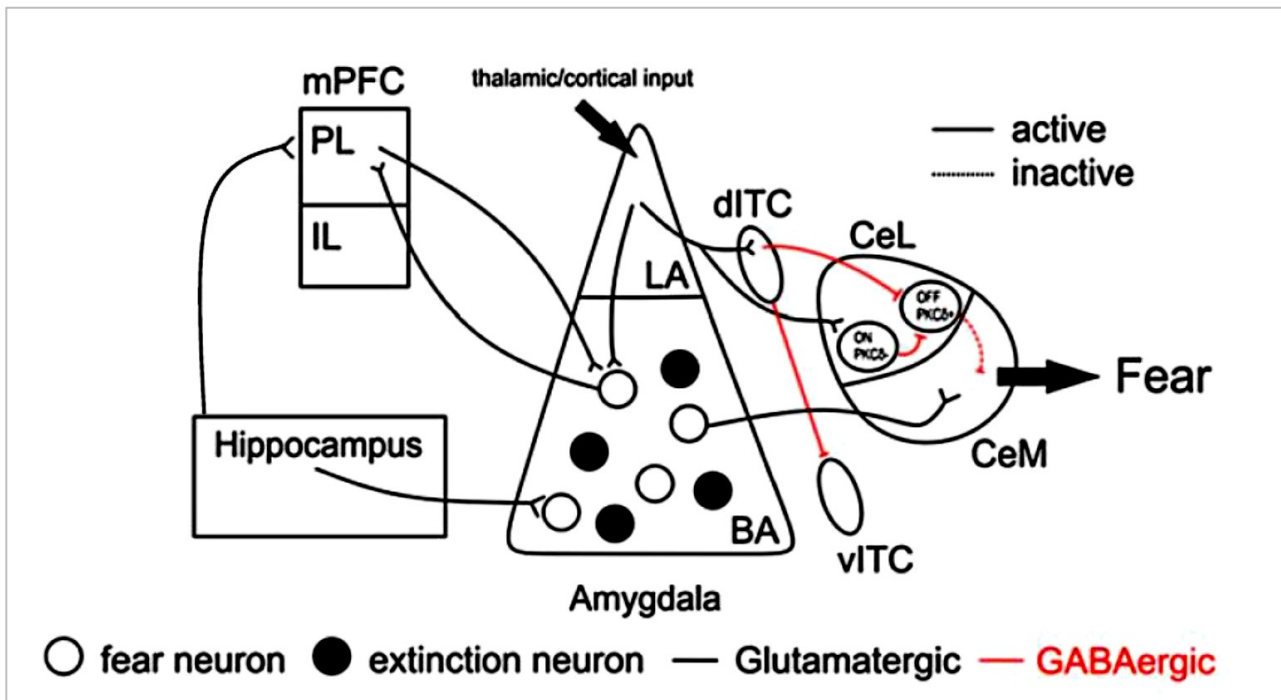


Figure 15. Functionality of the fear circuit during associative fear learning. Information from the auditory (CS) (thalamo-cortical input) and from the aversive (US) (not shown) converges on the LA neurons. The behavioral expression of fear (\rightarrow Fear) is set up through the activation of the fear cells (white) of the BA and the disinhibition of the central nucleus. This regulation of activity is controlled by the PL and the hippocampus. **mPFC**: Medial Prefrontal Cortex; **PL**: Prelimbic; **IL**: Infralimbic; **vITC/dITC**: intercalated cells (ventral/dorsal); **LA**: lateral nucleus of the amygdala; **BA**: basal nucleus of the amygdala; **CeL/CeM**: central nucleus of the amygdala (Lateral/Median) (Singewald et al., 2015)

Altogether, these studies emphasize the central role of dystrophin (Dp427) in the emotional circuits, although, the molecular mechanisms underlying the behavioral disturbances in *mdx* mice are still unclear. Brain Dp427 is normally expressed in postsynaptic densities of GABAergic inhibitory synapses of neurons. Its loss is thought to induced molecular and physiological changes in synapses and compensatory phenomena in the density of interneurons (Del Tongo et al., 2009) and/or of inhibitory synapses (Miranda et al., 2009), which may contribute to the altered synaptic plasticity and memory deficits in this model (Knuesel et al., 1999; Grady et al., 2006; Miranda et al., 2009; Sekiguchi et al., 2009; Vaillend et al., 2010; Krasowska et al., 2014). Dp427 is thought to be a key element of the molecular scaffold involved in the mechanisms that regulate the clustering and/or properties of postsynaptic GABA_A receptors in inhibitory synapses (Fritschy et al., 2012). The loss

of Dp427 would therefore lead to a reduction in GABAergic inhibition and a consequent and abnormal increase in the plasticity of glutamatergic synapses (Vaillend and Billard, 2002; Miranda et al., 2009; Sekiguchi et al., 2009; Fuenzalida et al., 2016). A drastic decrease in the number of GABA_A receptor α subunits (30-70% decrease depending on the study) has been reported in the various brain structures that normally express Dp427, namely the amygdala, hippocampus, and cerebellum. However, since the total amount of GABA_A receptors does not decrease significantly, it is believed that Dp427 is not required for anchoring these receptors (which rather requires gephyrin) but is rather involved in stabilizing them as large clusters at the postsynaptic membrane. The loss of dystrophin leads to changes in the molecular composition of GABA-A receptors and possibly to lateral diffusion of unstable receptors to extrasynaptic domains (Kueh et al., 2011; Vaillend and Chaussonot, 2017; Zarrouki et al., 2022a).

Overall, the original *mdx* mouse model remains so far, the most studied DMD mouse model. Four chemical variant (cv) strains of the original *mdx* were reported (Figure 12) (Chapman et al., 1989). These mice were generated by chemical mutagenesis on the C57BL/6 background and named *mdx*^{2cv}, *mdx*^{3cv}, *mdx*^{4cv} and *mdx*^{5cv}. Each of these strains carries a different point mutation (Cox et al., 1993; Im et al., 1996). Although the overall clinical presentation of these mice differs very little from that of *mdx* mice, each line has unique features. Specifically, *mdx*^{3cv} mice, which have altered expression of all the dystrophin-gene products, still express ~5% of a near-full-length dystrophin protein (Cox et al., 1993; Li et al., 2008). *Mdx*^{5cv} mice have a more severe skeletal muscle phenotype as compared to *mdx* mice, even though both models only lack Dp427, which has been attributed to differences due to their genetic background (Beastrom et al., 2011). In addition to these four strains, several dystrophin-deficient transgenic lines have been generated (Aigner et al., 2009). Among which the *dmd*-null mice generated with a Cre-loxP mediated deletion of the entire *Dmd* gene and thus do not express any of the *Dmd* gene products. This model displays severe muscular hypertrophy and dystrophy, behavioral abnormality and male sterility (Kudoh et al., 2005).

Various DMD mouse model lacking only full-length (Dp427) (Sekiguchi et al., 2009; Miranda et al., 2015; Vaillend and Chaussonot, 2017) or the smallest (Dp71) (Daoud et al., 2009a; Vacca et al., 2016; Belmaati Cherkaoui et al., 2021) have been studied over the years. However, no existing mouse model replicate the sole loss of Dp140, a short brain dystrophin, which absence seems involved in the aggravation of central alterations severity. This significantly slows down the understanding of its central localization, cellular role, and precise involvement in the neurobiology of DMD central alterations. However, two mouse models, *mdx4cv* and *mdx52*, show a cumulative loss of Dp427 and

Dp140, that recapitulates the genetic alterations found in about 60% of DMD patients. The *mdx52* model is described in the next section.

2. The *Mdx52* mouse

This transgenic mouse lacking multiple dystrophins (Figure 12), has been generated by gene targeting (Araki et al., 1997). The *Mdx52* mouse lacking both Dp427 and Dp140, thus expressing only Dp71, provides an interesting alternative to investigate the specific role of Dp140. Comparative analysis may shed more light about the specific role of Dp140 since the role of Dp427 and Dp71 have already been investigated.

Moreover, it carries a deletion located in a “hotspot” region of the *Dmd* gene (deletion of exon 52) and this replicates a widely spread mutation profile, associated to severe central deficits found in DMD patients (63%) (Bérout et al., 2007). This model is also of great interest for preclinical studies aiming at developing therapeutic approaches for central deficits in DMD. Indeed, recent studies demonstrated that therapeutic strategies were able to restore muscle Dp427 expression and motor functions in the *mdx52* mouse (Aoki et al., 2010; Aupy et al., 2020). Therefore, it is important to determine the behavioral profile and neurobiological bases of the central deficits of *mdx52* mice to identify the relevant outcome measures for using this model in preclinical studies. Nevertheless, a current challenge is to rescue both Dp427 and Dp140. Comparative studies between Dp427 and Dp427+Dp140 rescue might also help to better understand the specific role of Dp140. The *mdx52* mouse model also lacks Dp260 in the retina and is thus an adequate model to access the therapeutic potential of its rescue.

Animal models have greatly enriched our understanding of the biological function of dystrophin and the pathology of DMD, providing excellent platforms for investigating the efficacy and toxicity of experimental therapies.

III. Therapeutic approaches for DMD

There are significant unmet needs for DMD treatments, especially for central alterations, as the standard of care is principally limited to motor, cardiac and respiratory symptoms relief based on pharmacological approach that can only induce an improvement of the phenotype. Other therapeutic strategies aim to correct the origin of the pathology, slow the progression of the disease, and thus increase the life expectancy of DMD patients, which currently rarely exceeds the 40's despite improved standard of care (Saito et al., 2017).

Throughout this chapter, the current treatment and therapeutic approaches for DMD will be reviewed.

1. Pharmacological approaches

A. Glucocorticoids

As early as 1974 it was demonstrated that glucocorticoids have a beneficial effect on DMD patients. They thus were the first form of therapy implemented since the 1980s and are still part of the international standards of current care (Drachman et al., 1974; Bushby et al., 2010a, 2010b). Corticosteroids, which comprise a class of steroid hormones, bind to the glucocorticoid receptor, which regulates many pathways involved in immune response and metabolism (Beato et al., 1995). Among the most widely used glucocorticoids are Prednisolone and Deflazacort, whose effectiveness in terms of improving muscle strength has been demonstrated many times. Taking prednisolone makes it possible to prolong the ambulatory capacity of patients, to stabilize lung function by improving the strength of the respiratory muscles, to reduce scoliosis and slow down the progressive decline of heart muscle. Their anti-inflammatory and immunosuppressive potential limit the infiltration of mononuclear cells into the muscle during necrosis and are in part responsible for the improvement observed in patients (Yilmaz et al., 2004; Arpan et al., 2014; Morrison-Nozik et al., 2015; Heier et al., 2019). Glucocorticoids can also play a role on calcium homeostasis, stabilization of muscle fiber membrane and increased myogenesis (Muntoni et al., 2002). Many studies indicate that an influx of calcium allowed by microlesions in the muscle membrane participate in the induction of necrosis crisis. Although the use of these corticosteroids is now widespread, their mechanism of action is not fully understood, probably due to their broad spectrum of action. Though widely prescribed, corticosteroids are controversial because of their common adverse effects on body mass,

bone integrity, sleep quality, mood swings and long-term memory in DMD patients (Poysky, 2007; Snow et al., 2013; Jeronimo et al., 2016; Birnkrant et al., 2018). Patients cite ‘side effects’ and ‘not enough benefit’ as their primary reasons to stop corticosteroids (Cowen et al., 2019).

B. Stop codon readthrough

Ataluren (Translarna™, previously known as PTC124) is an oral small molecule, developed by PTC Therapeutics, targeting nonsense mutations only, which occur in 10– 15% of patients with DMD (nonsense mutation Duchenne Muscular Dystrophy, nmDMD). This molecule hampers the recognition of premature termination codons (PTCs) during translation by ribosomes (read-through approach), thus partially restoring a limited amount of full-length functional dystrophin protein (Politano, 2021).

When administered in *mdx* mice, treatment with PTC124 restored dystrophin production in all skeletal muscles examined, including the diaphragm, and cardiac muscle. The dystrophin levels were found to be 20-25% of those of WT mouse muscles, and partially restored force generation and resistance against eccentric exercise, suggesting that PTC124 was able to reduce muscle fragility (“Molecule of the month. Ataluren,” 2010). PTC-treated *mdx* mice also exhibited increased levels of sarcoglycans, consistent with stabilization of the dystrophin-associated proteins. The rescue of skeletal muscle was observed within 2 to 8 weeks of exposure. Readthrough by PTC124 was selective and specific to disease-causing premature termination, without evidence of changes in the ribosomal readthrough of normal stop codons. These encouraging results led to the initiation of clinical studies in humans (Hirawat et al., 2007; Finkel et al., 2013; Bushby et al., 2014). Hirawat et al. assessed safety and tolerability of PTC124 in a Phase 1 study enrolling 62 healthy adult volunteers and concluded that the drug was well tolerated, except for mild headaches, dizziness, and gastrointestinal discomfort at high dose (Hirawat et al., 2007).

In 2014, Bushby et al. published the results of a randomized, double-blind, placebo-controlled study enrolling 174 DMD patients ≥ 2 years with nm-dystrophinopathy who received orally, 3 times daily, ataluren 40 mg/kg/day (n = 57); ataluren 80 mg/kg/day (n = 60); or placebo (n = 57) for 48 weeks. The primary endpoint was a change in 6-Minute Walk Distance (6MWD) at Week 48. Ataluren was generally well tolerated. Unexpectedly, both the primary and secondary endpoints (timed function tests) favored ataluren versus placebo, at the lower dosage and not at the higher dosage. As a consequence, the European Medicines Agency (EMA) granted ataluren with conditional approval for

the treatment of ambulant patients aged 5 years and older with Duchenne muscular dystrophy resulting from a nonsense mutation in the DMD gene (Finkel et al., 2013; Bushby et al., 2014). Clinical trials are currently assessing the long-term efficacy and tolerance of Translarna. Based on these results, the EMA will decide whether to grant Translarna a final Marketing Authorization (MA).

C. Utrophin overexpression

Utrophin is a paralog protein of dystrophin with no less than 70% homology. Utrophin is mostly embryonic in the muscles and is replaced by dystrophin after development. However, it has been shown that in the absence of dystrophin, the expression of utrophin is increased in order to compensate for the missing dystrophin, both in *mdx* mice and DMD patients (Dowling et al., 2002). One of the therapeutic avenues explored was to induce an overexpression of utrophin via pharmacological agents such as Ezutromide or even butyrate associated with L-arginine. The overexpression of utrophin via pharmacological agents allows in *mdx* mice an increase in muscle strength as well as an improvement in muscle resistance to fatigability (Tinsley et al., 2011).

In view of these promising preclinical results, several molecules have been developed to overexpress utrophin. Ezutromid, which demonstrated satisfactory results in *mdx* mice, was tested in a phase 1 clinical trial in healthy volunteers and demonstrated good tolerability (Tinsley et al., 2015). A clinical trial in DMD patients was subsequently conducted to confirm the efficacy of the molecule (Summit Therapeutics, NTC02858362). Ezutromide was shown to be well tolerated in DMD patients and allowed a reduction in circulating CK (Ricotti et al., 2016c), however it did not meet the primary Endpoint and its development was discontinued in 2018.

This therapeutic approach was also evaluated in the CNS of *mdx* mouse. The overexpression of utrophin via arginine-butyrate allowed an overexpression of utrophin in the CNS, however this overexpression did not correct the behavioral deficits due to the absence of cerebral Dp427 and no benefit could be demonstrated (Perronnet et al., 2012).

2. Cell therapies

Cell therapy approaches aim to provide new cells to patients to compensate for their deteriorated cells in the targeted tissue. Cells can be from a donor or from the patient himself. Both approaches have advantages and disadvantages. While cells from the donor are mutation free, an immune reaction is a risk. Autologous cells have lower risk of causing an immune reaction; however, the cells need to be restored for dystrophin expression prior to reinjection.

Based on promising results in animal models (Partridge et al., 1989), cell therapies for DMD initially focused on local intramuscular injections of myoblasts derived from healthy donors to re-introduce dystrophin expression in muscles of DMD patients (Mendell et al., 1995; Skuk et al., 2006). Unfortunately myoblast transfer strategies have thus far failed to produce adequate therapeutic effects, due in part to issues of poor survivability, limited migration from the injection site and immune rejection of transplanted cells (Fan et al., 1996; Skuk et al., 2006, 2011). Expectations have been further tempered by challenges in expanding sufficient numbers of myogenic stem/progenitor cells in culture while preserving their ability to self-renew and efficiently engraft *in vivo* (Montarras et al., 2005). However, these early observations helped identifying hurdles that needed to be overcome to improve treatment outcomes. Bone marrow-derived stem cells as well as muscle blood vessel-associated cells such as pericytes and mesoangioblasts (MABs) were shown capable of contributing to muscle regeneration, albeit with lesser efficiency than traditional myogenic stem/progenitor cells (Péault et al., 2007; Farini et al., 2009). Promising cell candidates eventually emerged, including MABs for which phase 1/2 clinical trials relying on transplantations of MABs derived from healthy HLA-matched donors are in progress (EudraCT no. 2011-000176-33). The next goal was to generate MABs from a dystrophic patient, correct the genetic mutation during cell expansion in culture, then transplant the corrected cells back into the patient (Tedesco et al., 2012). Induced pluripotent stem (iPS) cells have recently gained attention in re-programming strategies aimed at “manufacturing” ideal cell candidates that fulfill many of the identified needs for successful stem cell therapies of DMD. These iPS cells can be induced to a pluripotent, stem cell state by addition of several combinations of transcription factors important during early embryonic development (Tedesco et al., 2012). iPS cells harbor virtually limitless expansion potential during which dystrophin vectors can be re-introduced to correct or bypass the genetic mutation (Seto et al., 2012; Konieczny et al., 2013). Corrected iPS cells can subsequently be directed towards adopting myogenic fates using various techniques, such as gene-transfer of myogenic determination factors, and serve as a patient specific cell source for autologous transplantation. Successful re-programming of iPS cells into

stem/progenitor cells capable of myogenic differentiation has been reported (Darabi et al., 2011; Tanaka et al., 2013).

In summary, cell replacement holds an interesting potential for treatment of neuromuscular disorders including DMD yet with major limitations. Challenges are the limited number of cells available, low migration ability of the cells, tumor formation due to mis-differentiation, and immune responses against donor cells. Moreover, cell therapy seems particularly difficult to set up for CNS treatment; the rate of neuronal regeneration being very limited postnatally, such therapy would have a limited impact.

3. Gene therapy

Once the *DMD* gene was identified as the origin of the disease, the investigation field of gene therapy emerged in order to compensate the loss of dystrophin. Gene therapy methods are being developed to either replace the defective *DMD* gene or edit the mutated gene.

A. Gene replacement therapy

The efficient transduction of targeted tissues by the genetic material needed for the gene therapy remains one of the main limiting factors for developing a gene therapy that can provide therapeutic benefit in DMD. This aspect of the gene therapy approach is one of the most studied, and many tools have been evaluated to determine the best way to deliver a dystrophin expression cassette. The main challenge for *DMD* gene therapy results from the very large size of the *DMD* gene.

1. Viral vectors

Replacement of the defective *DMD* gene with a synthetic substitute using delivery vehicles such as viral vectors is a promising approach for safe, long-term therapy. A significant advantage of gene replacement technologies is that they should be applicable to all patients, regardless of their underlying genetic mutation. Regarding the different gene therapies used for DMD, three types of viral vectors are mainly used: lentiviruses, adenoviruses and AAV vectors (adeno-associated virus), as each owns specific advantages and limitations (Figure 16).




 LENTIVIRUS	 ADENOVIRUS	 ADENO ASSOCIATED VIRUS
<p>Advantages</p> <ul style="list-style-type: none"> • Long term gene expression • Transduce dividing and non-dividing cells • High packaging capacity <p>Disadvantages</p> <ul style="list-style-type: none"> • Potential risk of insertional oncogenesis 	<p>Advantages</p> <ul style="list-style-type: none"> • High packaging capacity • High efficiency rate of host cell infection • Low genotoxicity <p>Disadvantages</p> <ul style="list-style-type: none"> • Highly immunogenic 	<p>Advantages</p> <ul style="list-style-type: none"> • Several serotypes – several specific tropisms • Low immunogenicity • Non insertional • Long term gene expression <p>Disadvantages</p> <ul style="list-style-type: none"> • Low packaging capacity

Figure 16. Types of viral vectors used in gene therapy: advantages and limitations (Imbert et al., 2017)

Among the numerous vehicles that have been tested for gene therapy approach, vectors derived from adeno-associated virus (AAV) are the most widely used in therapies for DMD. AAV is a small, non-pathogenic parvovirus that contains a 4.7 kb single stranded DNA genome. Generation of AAV vectors involves removing all viral genes and replacing them with the gene of interest. Advantages of using AAV-based vectors are that they can be produced at high titers on an industrial scale (Wright, 2008) and can stably persist for years. Of the many known serotypes, AAV6, 8 and 9 exhibit a high tropism for striated muscles, which is ideal for lessening off-target events in the treatment of muscular dystrophies (Schultz and Chamberlain, 2008; Zincarelli et al., 2008). Moreover, when administered intravenously, AAVs 9, rh.10, rh.8, and rh.43 can penetrate the blood–brain barrier and drive gene expression throughout the central nervous system (Foust et al., 2009; Zhang et al., 2011). The strongest and most widespread neuronal transduction is observed with AAV serotypes 1, 9, and rh.10 (Burger et al., 2004; Cearley and Wolfe, 2006; Klein et al., 2008). Also, tropism differs among AAV serotypes following ocular administration via subretinal injection, which is generally an efficient method for outer retina transduction. AAVs 1, 2, 5, 7, 8, and 9 transduce cells of the retinal pigmented epithelium and photoreceptors (Acland et al., 2005; Lei et al., 2009; Vandenberghe et al., 2013), while AAV2-7m8, ShH10 can specifically transduce Müller cells (Klimczak et al., 2009).

The AAV vectors are mostly non-integrative and remain in the form of episomes in the target cell. Therefore it is more suitable for quiescent target cells like differentiated muscle cells and neurons. However, AAV induces humoral immune response which restrict the treatment to a single injection; therefore, high efficacy and a high titer are required to have an effect. A significant limitation of AAV vectors is that they can carry only a limited size of genetic material, ~4.7 kb whereas the mDp427 dystrophin is encoded by an ~11.4 kb cDNA. Yet, some studies demonstrated the applicability of this approach for the short central dystrophin Dp71 (Vacca et al., 2016; Barboni et al., 2020). However,

for Dp427 to accommodate this minimal carrying capacity of AAV vectors, a common strategy is to insert a miniaturized but highly functional copy of the *DMD* gene into the vector known as the ‘microdystrophin’ (Ramos and Chamberlain, 2015).

2. Micro-dystrophin

Evidenced in patients with BMD, internally deleted dystrophins can be partly functional. Based on these observations, ‘microdystrophin’ constructs have been generated. Microdystrophin constructs lack all but the most crucial domains (the N-terminal ABD, 4–5 spectrin-like repeats, 2–3 hinge regions and the CR domain). The cDNA for these micro-dystrophins fits in AAV vectors and the expression of these microdystrophin constructs was shown to improve pathology in mouse and dog models of DMD (Duan, 2018a).

Clinical trials evaluating the systemic delivery of different versions of microdystrophins using different serotypes of AAV vectors at high doses ($1-3 \times 10^{14}$ vectors/kg) are ongoing (Duan, 2018b). Preliminary results from these studies have confirmed microdystrophin expression in the majority of muscle fibers (>80%) in muscle biopsies at levels of over 60% (Verhaart and Aartsma-Rus, 2019; Mendell et al., 2020), although it is not yet clear whether treatment will ameliorate disease progression. However, severe adverse events have been observed in a subset of patients, including transient renal failure (likely due to an innate immune response) and transient elevation of liver enzymes (likely due to a cellular immune response to the vector) (Duan, 2018a; Mendell et al., 2020). Notably, all treated patients included in these studies were pre-screened to rule out a pre-existing humoral immune response to the viral capsid used and all patients were pre-treated with high doses of steroids to suppress an immune response to the virus. Additionally, AAV administration induces an anti-AAV capsid-neutralizing antibody, which precludes retreatment. Strategies to counter this antibody response, such as plasmapheresis, alternative AAV serotype and immune-modulating drugs, are being explored.

Right now, gene therapy for DMD has made substantial progress. However, sizable safety concerns remain prevalent, despite great efficiency in promoting protein production. The full effectiveness of this strategy for DMD patients remains to be seen.

B. Gene editing therapy (CRISPR/Cas9)

Genome editing is the ultimate gene therapy approach aiming to correct a genetic defect on a permanent genomic basis. Several methods to edit the *DMD* gene were studied, all working in a similar fashion. In particular, CRISPR/Cas9 systems, which are specific, efficient, and versatile genome editing technologies that belong to a class of programmable nucleases, have revolutionized basic science research. These nucleases determine specific changes in regions of interest in the genome by inducing targeted double-strand breaks (DSBs) on specific genomic regions, thus triggering the DNA repair systems. These breaks are then repaired by the DNA repair systems. In dividing cells, error-free repair can occur via homologous recombination, thus providing a possibility to correct mutations. By contrast, in non-dividing cells, the error-prone, non-homologous end-joining system is used. As the most affected tissues in DMD are post-mitotic, the focus on genome editing therapy for DMD has been on using non-homologous end joining. Guide RNAs are designed such that they can restore the reading frame. This can be achieved in multiple ways through: deleting an exon, abolishing a splice site such that the exon is not included in the mRNA, or reframing an exon (Cox et al., 2015; Wang et al., 2020).

Proof-of-concept of this approach has been achieved, confirming that genome editing can restore dystrophin production in DMD cells and animal models (Nelson et al., 2017; Chemello et al., 2020). Some studies further demonstrated efficient editing of muscle stem cells using AAV9 in the *mdx* mouse model (Nance et al., 2019; Kwon et al., 2020). Genome editing is a mutation-specific approach because different exons need to be deleted for different mutations.

There are however challenges related to CRISPR/Cas9 clinical application; off-target mutagenesis effects and genotoxicity, delivery, and immune responses to the AAV vectors and gene-editing platforms represent frequent concerns, still unaddressed (Lee and Kim, 2019). In addition, an ethical barrier limits these strategies: modifications affecting the DNA are very sensitive from an ethical point of view because it aims at modifying the human genome.

CRISPR/Cas9 genome-editing technology shows remarkable pre-clinical potential for being translated into the clinic, yet only one therapeutic tool have reached the clinical trial stage so far (CRD-TMH-001). This recent n-of-1 clinical trial aimed to intravenously administer CRISPR-based therapy. However, the patient passed away in November 2022 and the circumstances of this death are currently unknown.

IV. Exon skipping strategies

Studies demonstrated that typical out-of-frame mutations are found in DMD patients while in-frame mutations in BMD patients and that these BMD patients express internally truncated functional dystrophin. In parallel, in revertant fibers, it was shown that the splicing mechanism could lead to spontaneous skipping of one or multiple exons, thus reframing out of frame mutations. Inspired by these findings, the concept of exon skipping therapy emerged for DMD treatment. This strategy, aimed at attenuating the severe DMD phenotype into a milder BMD-like phenotype, is based on the modulation of mRNA splicing to restore the reading frame and induce the synthesis of an internally truncated but functional dystrophin.

1. Splicing mechanisms

Splicing of precursor mRNAs (pre-mRNA) is an important step during eukaryotic gene expression. The identification of the actual splice sites and the proper removal of introns are essential for the production of the desired mature mRNA isoforms and their encoded proteins. The genomes of all eukaryotes contain introns, but their number, size, and distribution vary considerably between species (Deutsch and Long, 1999). The correct identification and removal of introns by the splicing machinery is a central, conserved step during gene expression in all eukaryotes (Wang and Cooper, 2007; Anna and Monika, 2018). The splicing machinery, also called the spliceosome is a large RNA–protein complex consisting of five small nuclear ribonucleoproteins (snRNPs), which occur and function individually (U1 and U2), in heterodimers (U4/U6), and heterotrimers (U4/U6.U5) (Wahl et al., 2009; Shi, 2017; Wilkinson et al., 2020). During splicing, the spliceosome follows a strict assembly and rearrangement choreography and each snRNP and splicing factor assumes a specific function and/or position within the spliceosome (Figure 17 A). These snRNAs are complementary with specific sequences found on the different introns and exons of the pre-mRNA. A major step in splicing is the recognition by the spliceosome of target sequences that are splicing consensus sequences. There are 3 types of consensus sequences: the donor site (= 5' splice site = 5'ss), the branch point (BP) and the acceptor site (= 3' splice site = 3'ss).

Furthermore, the non-continuous exon–intron structure of eukaryotic genes allows the formation of alternative mRNA isoforms. During this process the exons of a pre-mRNA are assembled in different ways; for example, by skipping one or several exons or using alternative splice sites (Lee and Rio, 2015). Alternative splicing is regulated by interactions of RNA-binding proteins (RBPs) and splicing

factors with sequences in the pre-mRNA, and by base-pairing between complementary RNA sequences: exonic splicing enhancer (ESE) and exonic splicing silencer (ESS) (Figure 17 B).

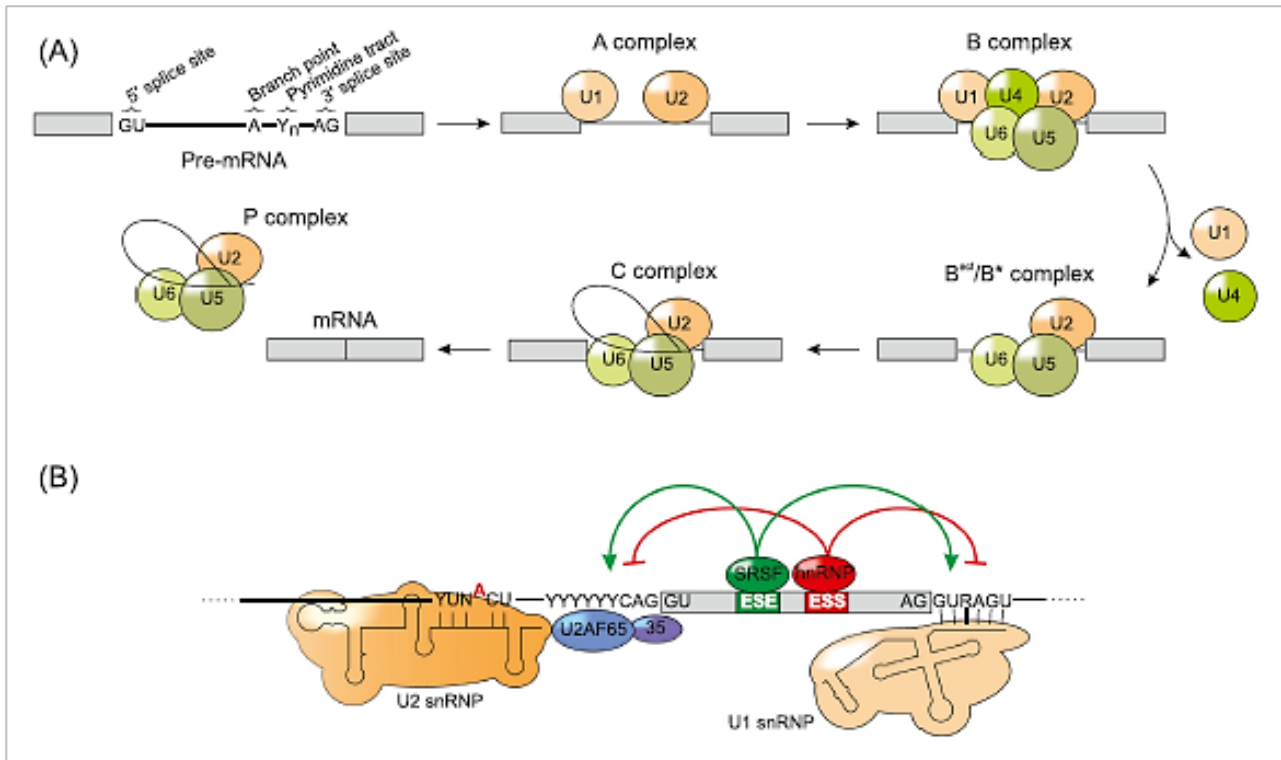


Figure 17. Splicing mechanisms (A) and its regulation (B) (Gehring and Roignant, 2021)

2. Therapeutic exon skipping

In order to interfere with the splicing process, sequences of antisense oligoribonucleotides (ASOs) were designed to specifically hybridize to the mRNA through a Watson–Crick base pairing. These sequences aim to mask the important splicing signals, such as the consensus sites or the exonic splicing sequences, to omit a specific exon inclusion (“exon skipping”) in the mRNA (Ferlini et al., 2021).

ASOs are synthetic single-stranded nucleotide sequences and their potential as antisense molecules was discovered by Zamecnik and Stephenson (Zamecnik and Stephenson, 1978). Oligonucleotides generally consist of 15 to 30 nucleotides which are complementary to the mRNA of the gene of interest, hence their name “antisense” (Kurreck, 2003; Griepenburg et al., 2015). Since the first application of ASOs, this technology has been hugely developed and the technique has rapidly

evolved. In particular, thanks to the progress made in terms of chemical modifications, which have considerably broadened the possible fields of application. While the first unmodified phosphodiester (PO) types of ASO were rapidly degraded in the bloodstream, various modifications were gradually introduced into their backbone/chemical structure to increase their stability and affinity for RNA (Wickstrom, 1986).

One of the first changes was the replacement of the oxygen atom of the PO₄ phosphate group with a sulfur atom, thus creating phosphorothioate (or thiophosphate) (PS) bonds. This substitution not only improved the endogenous resistance of ASOs to nucleases, but also offered a significant advantage in terms of pharmacokinetics. Indeed, ASO-PS (phosphorothioate-like ASO) exhibit increased affinity for many proteins (Crooke et al., 2017; Gaus et al., 2019) which facilitates their cellular distribution and uptake compared to their phosphodiester counterparts. However, PS-like modifications are also known to cause adverse effects due to their affinity for certain plasma proteins, sometimes giving ASO-PS an undesirable toxicological profile (Iannitti et al., 2014). In order to improve their resistance to nucleases and their affinity for the targeted mRNAs, second-generation ASOs were then developed, with the introduction of chemical modifications at the 2' position of the ribose, such as 2'O-methyl (2'OMe) and 2'O-methoxyethyl (2'MOE) (Goyenvallé et al., 2016), or by substantial changes in the structure of the sugar, leading to a wide variety of molecules, such as morpholinos (or PMO for phosphoroamidate morpholino oligomer) (Summerton and Weller, 1997).

The search for alternative ASO chemistries has led to the identification of bicyclo-(bc)-DNA which has been introduced as the first member of the class of conformationally constrained DNA analogues in 1993 (Tarköy and Leumann, 1993). Tricyclo-(tc)-DNA were designed in the late nineties as a conformationally constrained DNA analogue (Steffens and Leumann, 1997, 1999), being thus a second-generation analogue of bicyclo-(bc)-DNA. Other constrained oligonucleotides such as LNA for locked nucleic acid (Hagedorn et al., 2018) and cEt for 2'-4'-constrained ethyl (Seth et al., 2008) were further identified (Figure 18).

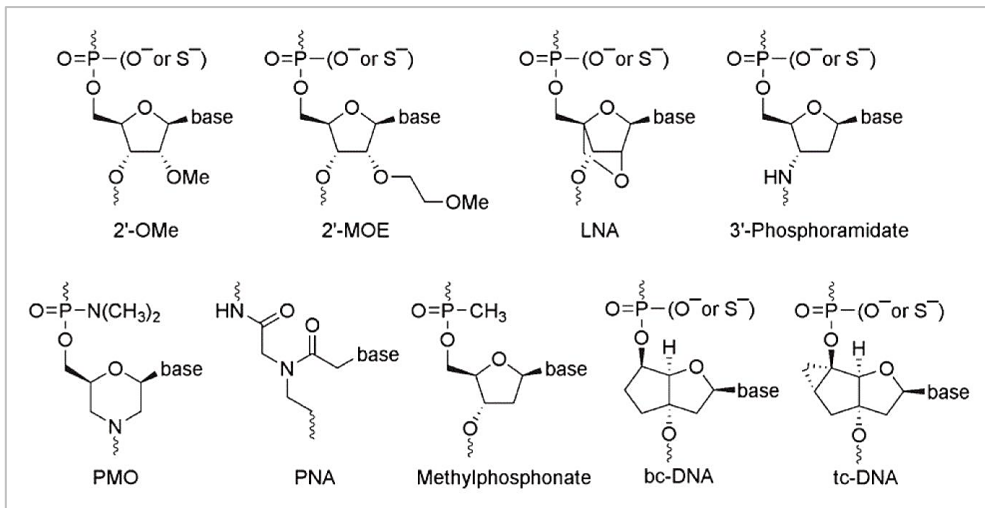


Figure 18. Chemical structures of a selection of oligonucleotide (Goyenville et al., 2016)

3. Therapeutic application of the exon skipping approach in DMD

ASO-mediated exon-skipping is theoretically applicable to ~83% of all DMD patients. According to literature review, the skipping of exons 51, 45, 53, and 44 has the major applicability per mutation, covering 19.1%, 11.8%, 11.4% and 8.8% of the deletions, respectively (Aartsma-Rus et al., 2009). The exon skipping therapy is a mutation-specific approach that aims to rescue the expression of an internally truncated but still functional dystrophin protein. In fact, skipping the same exon can rescue different mutation profiles; for example, the deletion of exons 47–50, 48–50, 49–50 and 52 can be restored by exon 51 skipping (Figure 19).

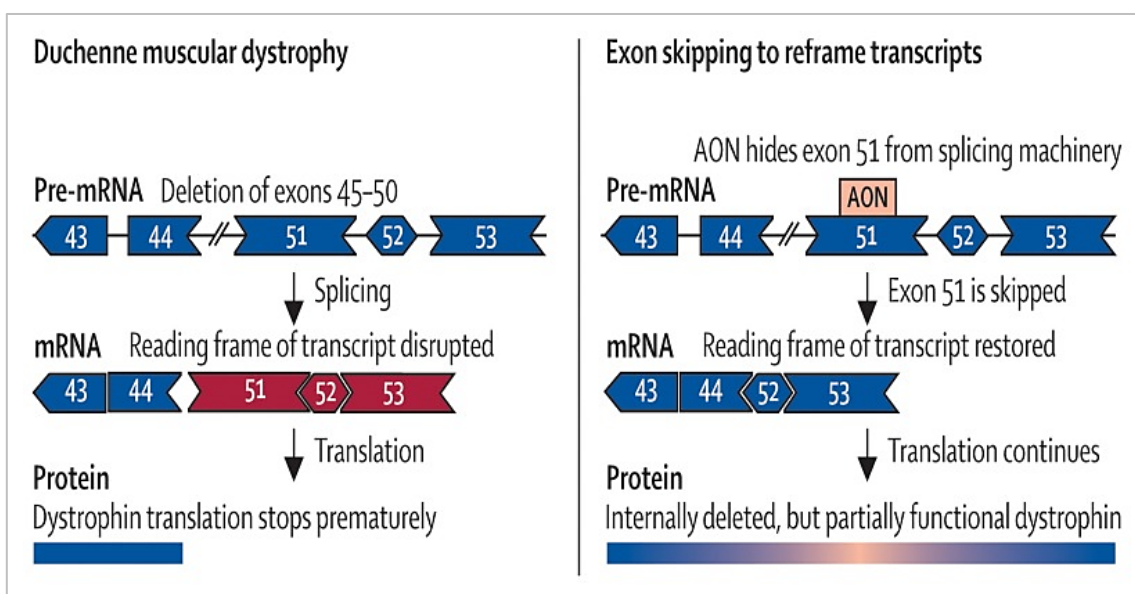


Figure 19. ASO-mediated exon 51 skipping to reframe DMD transcripts (Aartsma-Rus and Ommen, 2009)

A. Different types of ASOs used for DMD

Several ASO chemistries have been investigated to achieve exon skipping for DMD. In this section, I will focus on the two major ones that were clinically tested and the tcDNA-ASO that were developed in my host laboratory.

2'-O-Methyl-PS RNA

This charged ASO was first studied in *mdx* mice, in which the intramuscular injection of a 2'OMe-PS allowing exon 23 skipping was reported to induce restoration of dystrophin in a large number of muscle fibers. In addition, chronic administration enhances dystrophin restoration without inducing any immune response (Lu et al., 2003). The same group subsequently investigated the systemic injections of 2'OMe-PS in *mdx* mice, which led to dystrophin restoration in a large number of skeletal muscles, but no dystrophin restoration was observed in the heart. Notably, 2'OMe-PS did not cause any tissue toxicity during the 3 weeks of treatment (Lu et al., 2005). In another study, higher doses of 2'OMe-PS were administered subcutaneously to *mdx* and dKO utrophin/dystrophin mice for 6 months treatment period. This study showed that 2'OMe-PS is well tolerated over the long term, and that it allows a reexpression of approximately 2 to 3% of dystrophin in the treated mice.

In parallel, a 20-mer 2'OMe-PS ASO targeting exon 51, named Drisapersen, was developed and shown to restore significant levels of dystrophin in mouse models of DMD following systemic treatment. Based on these encouraging preclinical data, intramuscular injections of drisapersen were evaluated in DMD patients eligible for exon 51 skipping (van Deutekom et al., 2007). The treatment was well tolerated and confirmed the proof of principle of the ASO-mediated exon-skipping approach for DMD since some dystrophin expression was detected, supporting the development of further clinical investigations. Results evaluating the systemic administration were reported (Goemans et al., 2011) and led to further studies from the same group. Subcutaneous treatment delivery showed no improvement in ambulatory state plus multiple adverse effects (Goemans et al., 2016, 2018). The inability to meet the primary end point together with the significant adverse effects (injection-site reactions and renal issues) led to the rejection of the application for drisapersen by the US Food and drugs Administration (FDA).

Phosphorodiamidate Morpholino Oligomer (PMO)

PMO are very stable and neutrally charged ASO, conferring an ideal safety profile to PMO molecules. Evaluation of PMO-mediated therapeutic exon skipping in *mdx* mice, dKO utrophin/dystrophin, *mdx52* and dystrophic dogs, showed dystrophin restoration in skeletal muscle associated with improved muscle function. In addition, the toxicological profile of PMOs appeared safe with high doses and no adverse effects. Yet, PMOs exhibited low cellular uptake with high renal clearance, which requires high doses to reach a therapeutic effect (Moulton and Moulton, 2010; Järver et al., 2014; Miyatake et al., 2018).

Following these preclinical studies, the UK MDEX consortium conducted a phase I/II trial with a 30-mer PMO targeting exon 51, named Eteplirsen, in seven patients. Intramuscular injection of eteplirsen was well tolerated by all patients and intensity of dystrophin staining increased to 42% of normal levels in dystrophin-positive fibers of patients treated with the higher dose (Kinali et al., 2009).

While intramuscular injection was a valuable proof-of-concept, the main challenge in DMD is to target cardiac and respiratory muscles, therefore systemic delivery was next assessed by Sarepta (Cirak et al., 2011). Adverse events were generally mild to moderate and a dose-dependent significant increase in dystrophin expression was observed. Following these encouraging results, phase II studies with higher doses resulted in increased dystrophin production in all patients following at least 24 weeks of treatment depending on the age-related disease progression (Mendell et al., 2013, 2016). Based on detection of dystrophin protein (although minor) and the absence of adverse events, eteplirsen was approved by the FDA in 2016, under the accelerated approval pathway, despite no measures of muscle function. Although its approval was shrouded in controversy, eteplirsen became the first approved drug for DMD in the USA, as well as the first approved splice switching ASO (Aartsma-Rus and Goemans, 2019). Later the European Medicines Agency (EMA) gave a negative report for this treatment (Aartsma-Rus and Goemans, 2019) testifying that the current benefit-risk balance was not positive since the efficacy was not sufficiently demonstrated.

Despite this setback in Europe, Sarepta continued the clinical development of their PMO-ASOs, notably targeting exons 45 and 53. Based on positive results from phase I/II clinical trials (Frank et al., 2020; Wagner et al., 2021), golodirsen and casimersen were granted accelerated approval in the USA in 2019 and 2021 for the treatment of DMD patients amenable to exon 53 skipping and exon 45 skipping respectively.

An additional PMO-ASO targeting exon 53 and developed by the Japanese company NS-pharma was also approved by the FDA in August 2020 (Clemens et al., 2022).

Tricyclo-DNA (tc-DNA)

The main issue with first and second generations of ASOs (2'OMe and PMO) was the very poor tissue delivery and uptake. Alternative chemistries such as tc-DNA, a constrained analog of DNA, were therefore specifically developed to overcome this limitation.

The constrained structure of tc-DNA decreases the flexibility of the ribose, which favors hybridization in the form of duplexes. This is characterized by more stable hybridization, as tc-DNAs have an increased melting temperature of 1.2°C per nucleotide in a tc-DNA/DNA duplex and an increase of 2.4°C per nucleotide in a tc-DNA /RNA complex (Renneberg and Leumann, 2002). This property of strong hybridization with RNA allows a reduction of their length to 13-15 nt long (Relizani et al., 2017), in contrast with 2'OMePS or PMO which are generally 20 to 30 nt-long. In addition to their high resistance to nucleases, tc-DNA show increased hydrophobicity and the possibility to form nanoparticles improving their biodistribution in tissues (Ezzat et al., 2015).

A major preclinical study in *mdx* mice assessed the efficacy of intravenous injection for 12 weeks of a tcDNA targeting exon 23. The treatment allowed the restoration of mDp427 up to 40% in many muscles, including the heart and the diaphragm. Protein restoration was 5 times greater than that observed at equivalent dose of 2'OMe and PMO and was associated with muscle, respiratory and cardiac improvement (Goyenvalle et al., 2015).

In the scope of improving their biodistribution, further modifications of tc-DNA were investigated based on the hypothesis that fatty-acid conjugation could facilitate tc-DNA transport across the continuous capillary endothelium in the skeletal and cardiac muscle through improved binding of the conjugated-tcDNA to serum albumin (Chappell et al., 2020). A preclinical study in *mdx* mice treated with tc-DNA conjugated to a palmitic acid demonstrated enhanced potency in skeletal and cardiac muscles, which allowed a significant reduction of the administered dose. Also, functional improvement in dystrophic mice and the safety profile following a long-term treatment with these conjugated compounds as well as the persistence of the treatment efficacy after a recovery period was reported (Relizani et al., 2022). These encouraging preclinical results demonstrated a promising therapeutic potential of tc-DNA, which will be soon evaluated in DMD patients in a phase I/II clinical trial (H1 2023, SQY Therapeutics).

B. AAV-mediated exon skipping for DMD

In order to increase stability, sustain the effect of ASOs, and thus avoid the need for a recurrent (potentially lifelong) administration, it has been proposed to shuttle antisense sequences in adeno-associated viruses recombinant vectors (AAV). For this, the antisense sequences have been inserted into an optimized U7snRNA (U7 small-nuclear RNA). U7snRNA is a small non-coding nuclear RNA that is naturally involved in the processing of histone pre-mRNAs. To make it a splicing modulation tool, the histone downstream element (HDE) of U7snRNA is replaced by an antisense sequence of interest. Thanks to this inclusion in the U7snRNA, and its vectorization, the antisense sequence is directly addressed and expressed in the nucleus, continuously under the control of the natural promoter of the U7snRNA (Figure 20).

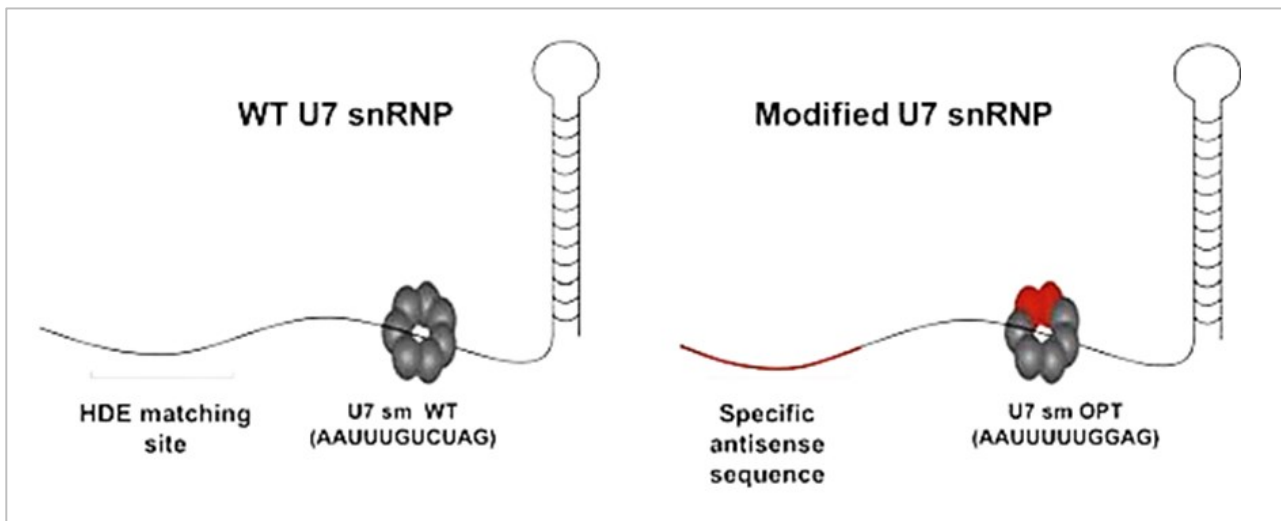


Figure 20. U7snRNA system modification (Imbert et al., 2017)

Preclinical studies were performed in mouse models of DMD (Goyenvalle et al., 2004, 2012). In *mdx* mice, intramuscular injection of an AAV2/1 containing U7dtex23 allowed a restoration of muscle Dp427 up to 40 to 80% of the WT level (Goyenvalle et al., 2004). Later, a study on the double Knock-Out (dKO) dystrophin/utrophin mouse model, showed that AAV9sc-U7dtex23 systemic treatment restores up to 40 and 90% of dystrophin in different muscles, particularly in the cardiac muscle, associated increased life expectancy (Goyenvalle et al., 2012). Later, AAV9-U7 targeting exon 51 showed a strong efficacy in *mdx52* mice, reaching up to 20-25% of mDp427 rescue in different tissues along with functional restoration (Aupy et al., 2020)

The AAV-mediated exon skipping therapeutic approach was also evaluated in the GRMD dog model, carrying a point mutation in the splice site of the intron 6 – exon 7 junction, inducing the exclusion of exon 7 therefore leading to the reading frame shift. This mutation is eligible to exon skipping but requires the exclusion of two exons (6 and 8) from the mature mRNA to restore the open reading frame. For this purpose, two modified U7 snRNAs were created targeting exons 6 and 8 respectively (multiple exon skipping) and inserted into the same AAV vector in order to restore the reading frame. Following intramuscular injections, 60% restoration of mDp427 has been shown, accompanied by improvement of muscle strength in treated GRMD dogs (Vulin et al., 2012). Another study in GRMD dogs, using AAV8 serotype, also showed a strong restoration of muscle Dp427 following systemic injections in these dogs (Le Guiner et al., 2014). Overall, these experiments demonstrated the good tolerability of this treatment in GRMD dogs, offering hope for a future clinical trial.

A phase I/II clinical trial (NCT04240314) for exon 2 skipping was undertaken in DMD patients presenting with a duplication of this exon. Exon duplications account for 11% of mutations affecting the DMD gene, and exon 2 duplication is the most common in patients (Wein et al., 2014). Exon skipping targeting duplications aims to restore a complete and therefore fully functional dystrophin, which has a significant advantage over quasi-dystrophins resulting from the removal of internal exon(s) to correct the frame reading or nonsense mutations. The preliminary results of this phase I/II study were presented at the 25th congress of the World Muscle Society (WMS) in October 2020 (Waldrop et al., 2020). The results revealed, in the treated patients, a decrease of respectively 95% and 81 % of serum creatine kinase levels (typically high in patients with DMD) at three months post-injection, and a respective reexpression of 5.8% and 1.4% of dystrophin. By 4 months post-treatment, a biopsy showed that 99% of the participant's muscle fibers produced full-length dystrophin, at levels 70% of normal amounts confirming the therapeutic potential of this vectorized approach.

However, the advantages of the AAV-U7 also need to be tempered. Indeed, ASOs vectorization in AAV prevents any reinjection due to the immune reactivity generated against the AAV vector (Lorain et al., 2008). This is to be noted because in long-term studies, progressive loss of AAV genomes has been reported and therefore a reduction of the U7 over time in muscle fibers leading to a progressive decrease in dystrophin expression. This loss is all the greater in animal models with severe muscle damage close to humans (Vulin et al., 2012; Le Hir et al., 2013).

4. Therapeutic application of exon-skipping to treat the CNS in DMD

In DMD, the cardiac and respiratory deficiencies are the major causes of death, thus logically the main therapeutic research focused on the muscular pathology, in order to alleviate the severity of the phenotype in particular in heart and diaphragm.

The rescue of mDp427 at significant levels may lead to an increased lifespan of DMD patients. Thus, the central deficits may become even more visible and significantly hinder the quality of life requiring a management.

The complexity of central treatment in DMD is due to the multiplicity of central dystrophins but also to the presence of the blood brain barrier (BBB). Indeed, unlike muscles, the brain is hermetically bounded by the BBB that drastically limits the treatment delivery, which is a challenge for the development of therapeutic management.

In the next section, we will review the work that has been done in an attempt to address the central alterations in DMD mouse models.

A. AAV-mediated exon-skipping in the CNS

The AAV-U7 system, which had demonstrated particularly promising results to restore the expression of Dp427 in the muscles of *mdx* mice was also evaluated in the CNS of *mdx* mice by my host laboratories. Indeed, the rationale of skipping exon 23 to restore expression of Dp427 also applies to the centrally expressed Dp427.

In a first study, the AAV2/1-U7 carrying the antisense sequences targeting exon 23 in order to induce its exclusion and rescue cDp427 was administered locally using intra-hippocampal injection. The single intra-hippocampal injection of AAV2/1-U7 rescued substantial levels of brain dystrophin expression (15–25%) in the hippocampus of *mdx* mice that lasted for months (Vaillend et al., 2010). The immunohistochemistry confirmed the correct localization of the restored cerebral Dp427 in the inhibitory synapses of the hippocampus. Moreover, dystrophin was properly colocalized with the GABA_A receptors at the membrane level of pyramidal neurons, around the soma as well as in the dendritic regions.

Surprisingly, this partial rescue of brain Dp427 expression was sufficient to achieve a total recovery of GABA_A receptor clustering. Indeed, the size and the number of clusters were normalized by the

treatment. This demonstrated the possibility of reaching the therapeutic threshold in the brain using this approach, and of restoring molecular synaptic defects of *mdx* mice in the mature brain. A year later, a follow-up study showed that two months after a single intrahippocampal injection, 25% of Dp427 rescue reverses the abnormally enhanced LTP phenotype at CA3–CA1 synapses of *mdx* mice (Dallérac et al., 2011).

Together, these studies showed that AAV-U7-mediated exon skipping in the brain can restore Dp427 expression and despite partial internal truncation, this Dp427 appears functional. Indeed, it restored the synaptic dysfunctions in *mdx* mice, without overt toxic effects.

This paved the way for vectorized antisense therapy for DMD central and cognitive defects rescue. In fact, these findings established proof of principle for the efficacy of post-natal rescue of dystrophin. However, AAV treatment showed few limitations, the diffusion following intra-hippocampal injection was restricted to approximately 1 mm perimeter around the injection site. Hence, to better characterize the potential of Dp427 rescue, in different structures and its functionality, other approaches need to be investigated and compared.

Indeed, Dp427 is expressed in hippocampal and cortical pyramidal neurons, but also in the cerebellum, which are two distant structures. Considering that AAV treatment is limited to a single injection due to immune reactivity, multiple or repeated injections to different regions is not an option. Yet, alternative routes of administration and/or different serotypes of AAV are needed to transduce larger territory and widely rescue central dystrophin. For example, intracerebroventricular (ICV) injections allow a direct delivery to the cerebrospinal fluid (CSF). The CSF circulates in the CNS and reaches all the brain structures. Thus, ICV injection represents an interesting route for brain dystrophins rescue.

A possible alternative to AAV treatment is the non-vectorized ASOs, which are non-immunogenic and may present a better biodistribution in the CNS.

B. ASO-mediated exon skipping in the CNS

PMO

In 2009, Sekiguchi et al used a PMO-ASO targeting exon 23 to restore cerebral Dp427 in *mdx* mice. The delivery route chosen was intracerebroventricular (ICV) injection (Sekiguchi et al., 2009), which directly delivers the ASO to the lateral ventricles and allows the molecule to circulate all over the

brain via the cerebrospinal fluid. *Mdx* mice received a total of 1 mg of PMO *via* ICV infusion using an osmotic infusion pump that persistently delivered the ASO for 1 week. The treatment resulted in approximately 25% of cerebral dystrophin restored 35 and 50 days after infusion. Restoration of dystrophin was shown to be effective in several distant brain structures, thus demonstrating that PMO was well distributed in the brain after ICV administration. This restoration was accompanied by a substantial reduction of stress-induced unconditioned fear responses in *mdx* mice, confirming the important major role of brain Dp427 in the control of amygdala-dependent emotional behaviors. The analysis of the kinetics of restoration of brain Dp427 revealed that the protein was not yet expressed 3-4 weeks after injection and was no longer present 12 weeks after injection. Moreover, the normalization of fear responses was only found to be significant when dystrophin was re-expressed during this therapeutic window, i.e. 5 to 7 weeks after the ICV. This specific therapeutic window of dystrophin (re)expression mediated by ASO administration is likely a critical factor in the success of DMD central therapy.

Tc-DNA

One of the most interesting properties of tc-DNA is their unique ability to cross the BBB. Indeed, the study assessing the systemic treatment efficacy of tc-DNA in *mdx* mice also demonstrated this unique ability (Goyenvalle et al., 2015). Tc-DNA were compared to other ASOs (2'OMe and PMO) and emerged as the only ASO capable of crossing the BBB. Exon 23 skipping was quantified by qPCR and revealed levels between 2 to 6% depending on the different brain structures. Moreover, Dp427 rescue was detected and correctly localized in these structures including the hippocampus, cortex, and cerebellum. Remarkably, the low levels of dystrophin rescued appeared sufficient to significantly reduce the enhanced fear response in systemically treated *mdx* mice (Figure 21).

These findings highlighted not only the unique capacity of tc-DNA to cross the BBB which represents a large advantage for DMD, but also the possibility to rescue post-natally some emotional features associated to the lack of dystrophin in the brain. Since DMD is a neuromuscular syndrome with both muscular and central alterations, a single molecule such as tc-DNA-ASO may be able to rescue both aspects of the pathology, which represents a major turning point in the therapeutic management and the quality-of-life improvement for DMD patients.

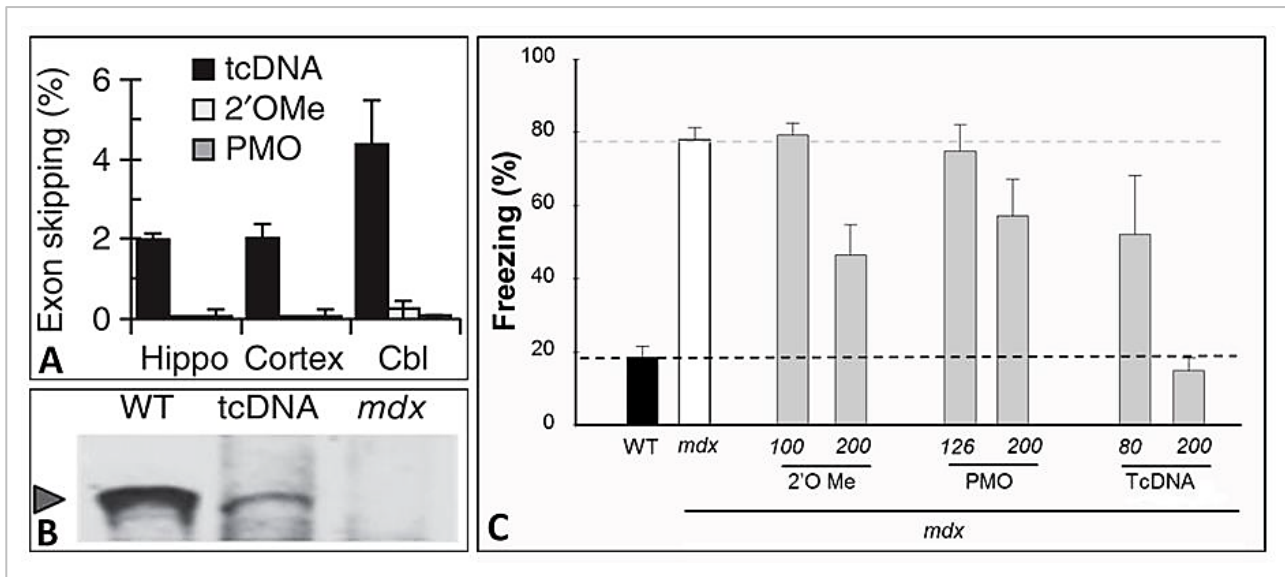


Figure 21. Central rescue of Dp427 following systemic treatment with tc-DNA: Restoration of cerebral.

(A) Quantification by qPCR of the skipped *Dmd* mRNA in the hippocampus (hippo), cortex and cerebellum (Cbl) for different ASOs (tcDNA, 2'OMe and PMO). (B) Quantification by western blot of Dp427 in the cerebellum of WT, tcDNA treated *mdx* mice and control *mdx* mice. (C) The unconditioned fear response induced by restraint expressed as a percentage of tonic immobility (freezing) over 5 minutes at different doses (80, 100, 125, 200) of the different ASOs (Goyenvalle et al., 2015)

These studies also raised the need to perform further work, in particular to better understand how much dystrophin rescue is required but also whether other central deficits such as memory could be restored.

So far, the centrally treated *mdx* mice exhibited restored unconditioned fear response, associated with exon 23 skipping in several brain structures and about 25% of Dp427 rescue. However, beyond emotional reactivity, other central deficits in this model were also investigated, such as memory performance.

Indeed, a recent study from our teams (Zarrouki et al., 2022b), assessed the therapeutic potential of tc-DNA targeting the exon 23 injected *via* a single ICV delivery. The results first showed that 5 weeks following the tc-DNA injection, brain dystrophin expression was rescued up to 10-30% of wild-type levels, which significantly reduced the abnormal unconditioned fear responses in *mdx* mice in a dose-dependent manner, as previously reported (Goyenvalle et al., 2015). Exon skipping efficiency, tc-DNA-ASO biodistribution, and protein expression were homogeneously rescued. Also, they

demonstrated a proper synaptic-like expression of Dystrophin in brain structures including the hippocampus and the amygdala.

The authors further assessed the efficacy of a maximum feasible dose of 400µg at 6-7 weeks post-injection on different memory performances. *Mdx* mice normally display poor long-term recognition memory and impaired fear learning and fear memory in a cued associative task.

The partial restoration of Dp427 in the CNS of tcDNA-treated *mdx* mice fully compensated the long-term recognition memory deficit normally shown by this model. However, the treatment was insufficient to fully overcome the learning and memory deficits during cued fear conditioning task. The authors hypothesized that this could be due to an insufficient amount of rescued Dp427, particularly in the amygdala. They also suggested that these particular deficits may not be fully reversible (i.e. rescued by postnatal treatment).

So far, much less is known about the role of the shorter brain dystrophins and whether the dysfunctions due to their loss can be rescued by postnatal re-expression. In particular, the regional and cellular localization of Dp140 is still unknown. According to genotype-phenotype studies, its loss exacerbates the severity of the central phenotypes, hence the importance of further investigations. Moreover, very few studies investigated therapeutic approaches targeting ‘hot spot’ mutations, though they are associated with severe central phenotype. The development of such therapies may greatly contribute to improve the quality of life of a large group of DMD patients. The *mdx52* mouse, which lacks both Dp427 and Dp140, appears as a relevant model to address these issues.

Research objectives

The central alterations resulting from the loss of brain dystrophins in DMD are getting increased interest. Indeed, thanks to advances in the therapeutic management of muscular dystrophy, the lifespan of DMD patients has expanded, and the neurological aspect of the pathology has become a significant hinder for a proper quality of life.

The understanding of the neurobiology of DMD central alterations is essential to adapt the therapeutic management. Central deficits are found to be variable among DMD patients and this is correlated with the mutation profile. In fact, a large proportion of DMD patients carries a mutation in a ‘hot spot’ region (63%). These distally located mutations lead to the loss of multiple brain dystrophins and result in a severe neurological phenotype. In the first part of my thesis work, the objective was to characterize the behavioral phenotype of the *mdx52* mouse model, that results from the cumulative loss of 3 central dystrophins (Dp427+Dp260+Dp140). The aim was to validate it as a reliable model for preclinical studies. I started by addressing putative visual alterations due to the absence of these three dystrophins in the retina (**Annex 1, Publication 1**). The nature, specificity and severity of the behavioral deficits resulting from the absence of Dp427 and Dp140 in the brain were then addressed. We focused on the emotional phenotype, namely the anxiety and fear related behaviors that are also expressed in patients (**Publication 2**). Because these phenotypes were well characterized in the original Dp427-deficient *mdx* mouse model, our work in the *mdx52* mice provides a key comparative study to better understand the genotype-phenotype relationships. As part of a collaborative work within the European funded project BIND (Brain Involvement In Dystrophinopathies), other deficits were further investigated. Among which, I investigated spatial and non-spatial memory performance (**Publication 3, manuscript in preparation**).

As mentioned in the introduction, exon skipping therapy presents a great therapeutic potential for DMD treatment, and a majority of DMD patients are eligible for exon skipping therapies (80%). Multiple ASOs have been developed for the management of the muscular dystrophy treatment. In the second part of my thesis project, we aimed to investigate the impact of postnatal restoration of dystrophins on central deficits in the *mdx52*, using exon skipping approaches. We first determined the optimal conditions for the local delivery of ASO therapies to the CNS. As part of a collaborative work, various ASOs chemistries were compared. In particular, we compared the tcDNA chemistry developed by my teams to the PMO chemistry that has previously showed efficient exon skipping in *mdx* mice following a local intracerebroventricular (ICV) delivery (Sekiguchi et al., 2009). As mentioned in the introduction, PMO targeting exon 51 was the first approved ASO for the treatment

of DMD in the US in 2016 (Syed, 2016). Because the mutation carried by *mdx52* model is eligible for exon 51 skipping, we thus compared the efficacy of tcDNA to that of PMO targeting exon 51 for the central treatment of DMD using local (ICV) delivery. As ICV administration is an invasive delivery method we also wanted to assess the efficacy of both ASOs via intrathecal (IT) injections. IT is a less invasive yet direct delivery route to the CNS that holds a translational potential. Indeed, IT delivery is already successfully used in the clinic for the administration of ASO in other neuromuscular disease such as SMA (Finkel et al., 2016). This work therefore aimed at establishing the most appropriate delivery route for each ASO to reach its maximal efficacy (**Publication 4**).

As mentioned above, the deletion of exon 52 (mutation carried by the *mdx52* mouse) is eligible to exon 51 skipping. However, while the promoter of Dp140 lies in intron 44, its first methionine initiation codon is located in exon 51 (Lidov et al., 1995). Thus, skipping exon 51 results in the elimination of Dp140 start codon and Dp140 cannot be expressed. An alternative approach is the exon 53 skipping, that would preserve the exon 51 and allow the rescue of both Dp427 and Dp140. Comparative studies of the sole rescue of Dp427 and both Dp427 and Dp140 would allow to further elucidate the role of brain dystrophins. In the third part of this work, we investigated the impact of sole Dp427 restoration on central alterations in the *mdx52* model. For that purpose, *mdx52* mice were treated with the tcDNA-Ex51 via ICV delivery. We first determined the optimal therapeutic window following the administration of tcDNA and then assessed emotional reactivity and memory through a behavioral test battery within this therapeutic window. The molecular rescue was analyzed by measuring exon 51 skipping levels and Dp427 protein re-expression in different brain regions involved in the emotional circuitry. We also evaluated the putative contribution of peripheral (muscular) factors to this behavioral deficits by comparing and combining peripheral and central treatments (**Publication 5**).

Publications

Barboni, M. T. S., Liber, A. M. P., Joachimsthaler, A., **Saoudi, A.**, Goyenvalle, A., Rendon, A., Roger, J. E., Ventura, D. F., Kremers, J., & Vaillend, C. (2021). Altered visual processing in the *mdx52* mouse model of Duchenne muscular dystrophy. *Neurobiology of disease*, 152, 105288. <https://doi.org/10.1016/j.nbd.2021.105288>

Saoudi A., Zarrouki F, Sebr   C, Isabelle C, Goyenvalle A, Vaillend C. (2021). Emotional behavior and brain anatomy of the *mdx52* mouse model of Duchenne muscular dystrophy. *Dis Model Mech.*;14(9):dmm049028. doi:10.1242/dmm.049028

Mitsogiannis M. D*, **Saoudi A***, Zarrouki F, Fergus C, Stojek E, Talavera S, Kelly V.P, Goyenvalle A, Montanaro F, Muntoni F, Sokolowska E, Vaillend C. Impact of distinct dystrophin-gene mutations and genetic background on behavioral outcome measures in DMD mouse models. *In preparation*.

Saoudi A., Fergus C., Gileadi T., Montanaro, F., Morgan, J. E., Kelly, V. P., Tensorer, T., Garcia, L., Vaillend, C., Muntoni, F., & Goyenvalle, A. (2023). Investigating the Impact of Delivery Routes for Exon Skipping Therapies in the CNS of DMD Mouse Models. *Cells*, 12(6), 908. doi:10.3390/cells12060908

Saoudi A., Barberat S, Le Coz O, Vacca O, Doisy Caquant M, Tensorer T, Sliwinski E, Garcia L, Muntoni F, Vaillend C and Goyenvalle A. (2023). Partial restoration of brain dystrophin by tricyclo-DNA antisense oligonucleotides alleviates emotional deficits in *mdx52* mice. *Molecular Therapy - Nucleic Acids Vol. 32p173–188. Published online*.

Saoudi A., Goyenvalle A. (2021) Les approches th  rapeutiques de modulation de l'  pissage - Avanc  es et perspectives [RNA splicing modulation : Therapeutic progress and perspectives]. *Med Sci (Paris)* ;37(6-7):625-631. doi:10.1051/medsci/2021091

RESULTS

- I -

Behavioral phenotyping of *mdx52* mouse model

I.1. Impact of Dp427 and Dp260 loss on retinal physiology and vision

A detailed description of functional electroretinogram (ERG) changes in the *mdx52* mouse retina, and the impact of these alterations of retinal physiology on visual behavior was recently published by our group (Publication 1. Annex I.1). I contributed to this study by analyzing the quantitative optomotor response (OMR) to achromatic sinusoidal gratings. The test consists of real time video tracking and measurements of compensatory head movements in freely moving mice (optomotor reflex) and was performed using an OMR recording setup. Each mouse was placed on a platform (5 cm in diameter) in the center of four computer-controlled LC Displays monitors (Kretschmer et al., 2013, 2015). Visual stimuli were a range of sinusoidally-modulated luminance gratings generated by four LCD screens randomly presented each for 60s with constant rotation in either clockwise or counterclockwise direction (Figure 22).

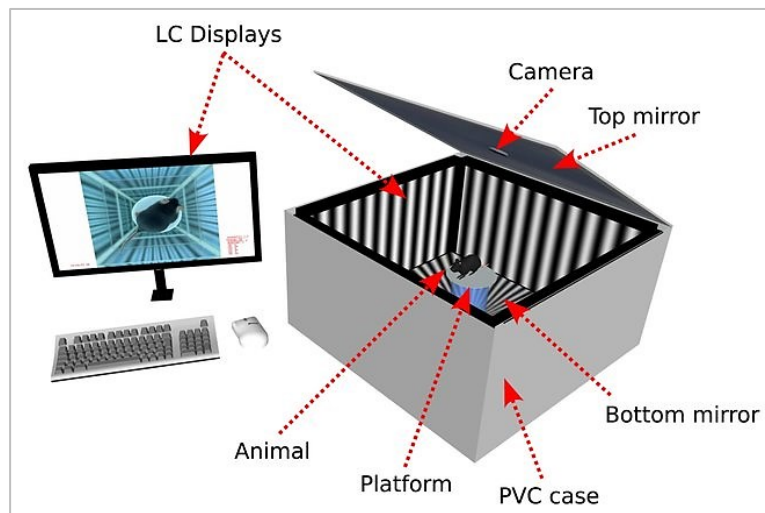


Figure 22. Overview of the setup (Kretschmer et al., 2013)

Groups of *mdx52* mice aged 3-4 months and their WT littermates were tested. The measurements were completed in three trials for each animal, which we had previously validated as an optimal number of replicates to reduce the variability of individual's scores. OMRs were recorded using two different Michelson contrasts and different spatial frequencies (presented in random order) in two distinct cohorts of mice: 100% contrast ($n = 8$ mice per genotype) or 50% contrast ($n = 10$ *mdx52* and 8 WT littermates). At 100% contrast, OMRs were recorded in response to sinusoidal gratings at 12 spatial frequencies between 0.0125 and 0.5 cycles per degree (cpd). At 50% contrast, sinusoidal gratings were presented at 10 different spatial frequencies between 0.0125 and 0.4 cpd.

The number of head movements recorded at a speed range from 2 to 14 degrees per second in the same direction as the stimulus (nCorrect) and in the opposite direction (nUncorrect) were used to calculate the OMR indices ($n_{\text{Correct}} / n_{\text{Uncorrect}}$) at each spatial frequency.

The analysis showed that at 100% contrast mean OMR indices were comparable between the genotypes while at 50% contrast they were significantly reduced in *mdx52* mice compared to WT (Figure 23).

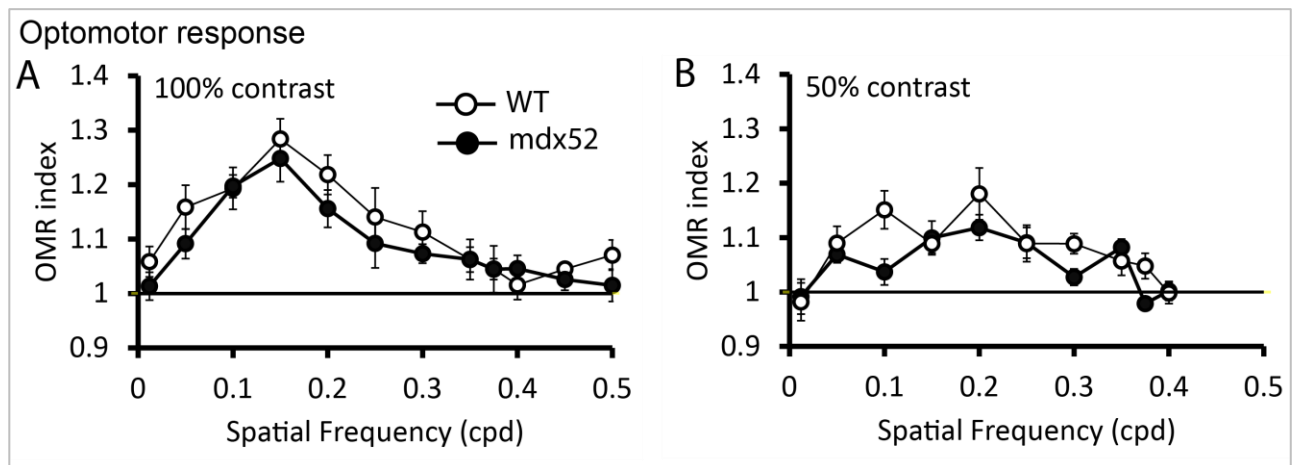


Figure 23: Optomotor response (OMR). The mean OMR indices (\pm SEM) are plotted as a function of spatial frequency for each genotype and the baseline (1; horizontal line) represents unspecific head movements and no response to the stimulus. OMR at 100% (A) and 50% (B) contrast in WT littermate mice (open symbols, n=8) and in *mdx52* mice (filled symbols, n=8 for 100% and n=10 for 50%)

This OMR results combined with the ERG in this study evidence that visual alterations found in *mdx52* mouse well mimics those reported in patients. This study evidenced *mdx52* as a relevant model to appraise the roles of several retinal dystrophins and for retinal preclinical studies related to DMD retinopathy.

I.2. Impact of the loss of brain Dp427 and Dp140 on cognitive and behavioral processes

Mdx52 DMD mouse model emerges as a critical model for Duchenne muscular dystrophy as it holds a mutation in position the most frequently found in patients (60%). The behavioral phenotype and central deficits associated to this mutation had not been described so far. The characterization of this mouse model could step further the knowledge of the genotype-phenotype relationships in DMD and establish the *mdx52* as a reliable model that mimics at least some of the patient's neurological deficits and thus makes a promising preclinical model for the development of central treatment for DMD central deficits.

Material and methods: In order to characterize the *mdx52* mouse, C. Vaillend and C. Sébrier first studied the macroscopic anatomy of the *mdx52* brain using MRI imaging and histological staining. I then performed the behavioral testing, in which two-month-old *mdx52* mice and their C57BL/6 wild-type littermates were included in a comparative behavioral study to the classic *mdx* mouse model and their own C57BL/10 wild-type littermates. This work focused on the emotional reactivity that is found to be slightly altered in the *mdx* model. The anxiety was tested using an elevated plus maze apparatus, followed by a light-dark choice test and an open field exploration tested in two levels of anxiogenic conditions. A distinct group of *mdx52* and WT mice was submitted to unconditioned fear testing and conditioned Pavlovian fear learning and memory.

Results: No gross anatomical differences were found in the brain of *mdx52* mice as compared to the wild-type mice. A severe emotional disturbance was found in *mdx52* mice as compared to the classic Dp427-deficient *mdx* model. Enhanced anxiety, exacerbated unconditioned fear response and impaired fear learning and memory were found in *mdx52* mice.

Conclusion: The behavioral profile of the *mdx52* DMD mouse model reminds the emotional reactivity found in patients carrying a similar mutation profile, meaning that the *mdx52* model is a relevant model for future therapeutic preclinical studies. Moreover, this mouse model opens to deeper investigations for better understanding of the roles of central dystrophins.

Publication 2

Published in **Disease Models and Mechanisms**, 2021

© 2021. Published by The Company of Biologists Ltd | Disease Models & Mechanisms (2021) 14, dmm049028. doi:10.1242/dmm.049028



RESEARCH ARTICLE

Emotional behavior and brain anatomy of the *mdx52* mouse model of Duchenne muscular dystrophy

Amel Saoudi^{1,2}, Faouzi Zarrouki¹, Catherine Sebré³, Charlotte Izabelle¹, Aurélie Goyenvallé² and Cyrille Vaillend^{1,*}

ABSTRACT

The exon-52-deleted *mdx52* mouse is a critical model of Duchenne muscular dystrophy (DMD), as it features a deletion in a hotspot region of the *DMD* gene, frequently mutated in patients. Deletion of exon 52 impedes expression of several brain dystrophins (Dp427, Dp260 and Dp140), thus providing a key model for studying the cognitive impairment associated with DMD and testing rescuing strategies. Here, using *in vivo* magnetic resonance imaging and neurohistology, we found no gross brain abnormalities in *mdx52* mice, suggesting that the neural dysfunctions in this model are likely at the level of brain cellular functionalities. Then, we investigated emotional behavior and fear learning performance of *mdx52* mice compared to *mdx* mice that only lack Dp427 to focus on behavioral phenotypes that could be used in future comparative preclinical studies. *mdx52* mice displayed enhanced anxiety and a severe impairment in learning an amygdala-dependent Pavlovian association. These replicable behavioral outcome measures are reminiscent of the internalizing problems reported in a quarter of DMD patients, and will be useful for preclinical estimation of the efficacy of treatments targeting brain dysfunctions in DMD.

KEY WORDS: Duchenne muscular dystrophy, Brain dystrophins, DMD mouse model, Fear conditioning, Anxiety, Intellectual disability

INTRODUCTION

X-linked Duchenne muscular dystrophy (DMD) is a recessive neuromuscular syndrome that affects one out of 3500 to 5000 male births. Besides the well-characterized muscular dystrophy, DMD is frequently associated with non-progressive cognitive deficits and comorbid behavioral and neuropsychiatric disturbances (Colombo et al., 2017; Hinton et al., 2009; Ricotti et al., 2016). DMD occurs as a result of mutations in the *DMD* gene, composed of 79 exons with multiple independent internal promoters that control the expression of different dystrophin-gene products, known as dystrophin proteins (Dp), in a tissue and/or cell-specific manner. The distinct dystrophins thus differ by their molecular weight, their tissue and cellular distribution, and their roles, but have the common

property of being associated with scaffolds of transmembrane and cytosolic proteins involved in the clustering of various membrane ion channels and receptors. The full-length dystrophin Dp427 (427 kDa) is expressed in both muscle and the central nervous system (CNS), Dp260 (260 kDa) is only detected in the retina, and Dp140 (140 kDa) and Dp71 (71 kDa) are detected in the brain. Therefore, the position of a mutation or deletion within the *DMD* gene may lead to the loss of different brain dystrophins (Hoffman et al., 1987), hence complex phenotype-genotype relationships and various degrees of cognitive and behavioral disturbances. Proximal mutations that selectively affect the expression of Dp427 are associated with mild central alterations, whereas distal mutations causing a cumulative loss of Dp427 and loss of one or both of the shorter brain dystrophins Dp140 and Dp71 are frequently linked to severe cognitive deficits and lower IQ scores (intellectual disability) (Daoud et al., 2009a; Felisari et al., 2000; Lorusso et al., 2013; Ricotti et al., 2016; Taylor et al., 2010).

Structure-function and functional studies of different mouse models of DMD may provide an essential contribution to our understanding of the affected brain mechanisms depending on the position of the mutation and loss of different dystrophins. The original Dp427-deficient *mdx* mouse model of DMD features a nonsense mutation in exon 23 of the gene, leading to the loss of both muscle and brain Dp427. The *mdx* mouse has been extensively studied, and it was shown that the loss of brain Dp427 alters brain GABAergic inhibition, and is associated with emotional disturbances and mild cognitive deficits (Knuesel et al., 1999; Vaillend et al., 1995, 2004; Vaillend and Chaussonot, 2017a). The loss of brain Dp427 appears to particularly alter the functionality of the neuronal network involved in the processing of fear responses, as demonstrated in *mdx* mice by the presence of drastically enhanced fearfulness in response to mild stress and delayed fear learning and memory (Goyenvallé et al., 2015; Razzoli et al., 2020; Sekiguchi et al., 2009; Vaillend and Chaussonot, 2017). In contrast, the selective loss of Dp71 in mice does not induce muscular dystrophy (Sarig et al., 1999) but alters critical molecular mechanisms involved in excitatory synapse and astrocyte functions (Belmaati Cherkaoui et al., 2020; Daoud et al., 2009b), which results in a different profile of behavioral disturbances, including deficits in spatial learning, working memory and cognitive flexibility (Chaussonot et al., 2019; Hellinger et al., 2018). However, so far, there has been very limited behavioral studies of mouse models with distal mutations leading to cumulative loss of several dystrophins (Vaillend et al., 1998; Vaillend and Ungerer, 1999). In particular, no behavioral studies have been conducted in mice featuring a mutation in the 'hotspot' central region of the *Dmd* gene, which is frequently mutated in DMD patients (63%) and leads to a cumulative loss of Dp427 and Dp140, despite its association with more severe cognitive impairments (Ricotti et al., 2016; Felisari et al., 2000; Beroud et al., 2007; Daoud

¹Université Paris-Saclay, CNRS, Institut des Neurosciences Paris Saclay, 91190, Gif-sur-Yvette, France. ²Université Paris-Saclay, UVSQ, Inserm, END-ICAP, 78000 Versailles, France. ³Université Paris-Saclay, CEA, CNRS, Inserm, BioMaps, Service Hospitalier Frédéric Joliot, 4 place du général Leclerc, 91401 Orsay, France.

*Author for correspondence (cyrille.vaillend@universite-paris-saclay.fr)

© C.I., 0000-0001-5723-3129; C.V., 0000-0002-8783-8185

This is an Open Access article distributed under the terms of the Creative Commons Attribution License (<https://creativecommons.org/licenses/by/4.0/>), which permits unrestricted use, distribution and reproduction in any medium provided that the original work is properly attributed.

Handling Editor: Steven J. Clapcote
Received 22 March 2021; Accepted 30 July 2021

et al., 2009a; Taylor et al., 2010; Lorusso et al., 2013; Colombo et al., 2017).

A mouse model with a deletion in exon 52 of the *Dmd* gene, the *mdx52* mouse (Araki et al., 1997), is an interesting model for preclinical studies addressing both muscular and CNS dysfunctions, as it is deficient in both Dp427 and Dp140. Although *mdx52* mice display clear and typical muscular dysfunctions, their behavioral disturbances need to be characterized. The *mdx52* mice are expected to display at least comparable cognitive and behavioral deficits as the ones observed in the original *mdx* mouse lacking Dp427. However, the impact of the additional loss of Dp140 in *mdx52* mice is unknown and might influence the severity and/or nature of the central deficits. The cellular function of Dp140 is largely unknown (Lidov et al., 1995) but its higher expression in fetal brain compared to adult brain (Morris et al., 1995) suggests that its loss might affect fetal brain formation and development. Importantly, it has been shown that exon-skipping strategies based on intracerebral or systemic administration of antisense sequences are efficient at skipping exon 23 to restore the reading frame and partially re-express Dp427 in the brain of *mdx* mice, thereby improving GABAergic functions, synaptic plasticity and behavioral fear responses in this model (Dallérac et al., 2011; Goyenvalle et al., 2015; Vaillend et al., 2010). Recent studies demonstrated that the *mdx52* mouse is also eligible for exon-skipping strategies using systemic administration of naked or vectorized antisense sequences to skip exon 51, with therapeutic potential to restore muscle Dp427 expression and motor functions (Aoki et al., 2010; Aupy et al., 2020). Therefore, it is important to determine the behavioral profile and neurobiological bases of central deficits of *mdx52* mice to identify the relevant outcome measures for using this model in preclinical studies.

In the present study, we have undertaken a behavioral characterization of the *mdx52* mouse compared to the original *mdx* mice and respective wild-type littermate controls in order to estimate the presence and severity of the deficits, with a focus on the main phenotypes previously described and used in preclinical studies in the original *mdx* mouse. We also performed a first characterization of brain anatomy, to determine whether Dp140 loss induced gross malformations that were not detected in previous studies of the *mdx* mouse, by means of macroscopic volumetric measures using *in vivo* magnetic resonance imaging (MRI) and analysis of brain architectural organization using histological staining of brain sections. We show that *mdx52* mice display emotional disturbances and a deficit in fear learning that are more severe than in the original *mdx* mouse lacking only Dp427. No gross brain abnormalities were detected in *mdx52* mice, indicating that specific cellular and physiological dysfunctions should be further investigated to determine the neural basis of brain dysfunctions in this new model of DMD.

RESULTS

Neuroanatomical analyses

The lack of exon 52 in the *Dmd* gene in *mdx52* mice results in the lost expression of several dystrophins proteins in the CNS, i.e. Dp427, Dp260 and Dp140, whereas expression of the shorter Dp71 product is preserved, as previously shown by western blot analyses of retinal and brain samples in the original biochemical characterization of this mouse model (Araki et al., 1997). Using immunofluorescence and confocal image analyses of hippocampal and cerebellar cryosections, we confirmed that *mdx52* mice lack the full-length brain dystrophin (Dp427), which normally shows punctate immunoreactive signals in wild-type mice due to its

expression in brain inhibitory synapses (Fig. S1A). We also confirmed the preserved expression of Dp71, typically detected along the walls of blood vessels in both wild-type and *mdx52* mice (Fig. S1B), due to its main expression at the membrane of perivascular astrocyte endfeet forming the blood-brain barrier (Belmaati Cherkaoui et al., 2020).

We then explored brain neuroanatomy to determine whether the loss of brain dystrophins induced major neurodevelopmental macroscopic brain changes, in particular because Dp140 normally shows highest expression levels in the developing brain compared to the adult brain (Morris et al., 1995). The selection of regions of interest (ROI) was not only driven by functional hypothesis, as putative developmental alterations may affect any region normally expressing Dp427 and Dp140. Hence, we first selected structures showing sufficient contrast to reliably delineate volumes from MRI images on the basis of the mouse brain atlas. The *in vivo* MRI volumetric measurements showed little inter-individual variations within genotypes (Fig. 1A; $n=11$ wild type and 14 *mdx52* mice). The total brain volume was comparable between genotypes [*mdx52*, 521.89 ± 4.86 mm³; wild type, 526.75 ± 4.97 mm³; genotype effect, $F(1,23)=0.47$, $P>0.49$]. Volumes of the 12 studied brain structures (Table 1) were also comparable between genotypes, whether we analyzed raw mean volumes [genotype \times structure interaction, $F(11,253)=0.45$, $P>0.9$] or relative volumes following normalization to the volume of the whole brain [$F(11,253)=0.81$, $P>0.6$].

The absence of gross macroscopic changes was confirmed by comparing the lengths of the main cerebral arteries forming the Willis circle (Fig. 1B), as estimated by angiography [genotype effect, $F(1,16)=0.56$, $P>0.45$; genotype \times distance interaction, $F(2,32)=0.86$, $P>0.42$]. Moreover, T2 maps analyses (Fig. 1C) were undertaken in four main regions: we discriminated the primary sensory cortex and the piriform cortex, a prominent cortical area of the rodent brain, important as a main recipient of olfactory inputs and for its widespread projections to forebrain structures, such as the amygdala and the thalamus. We also analyzed the hippocampus, a major structure involved in cognitive functions, and the thalamus, which has extensive connections to the cerebral cortex and midbrain, and plays a major role in relaying motor and sensory signals between subcortical, cerebellar and cortical areas. The T2 maps analyses did not reveal any overall effect of genotype [$F(1,18)=0.78$, $P>0.38$] in the four selected regions [genotype \times region interaction: $F(3,54)=1.15$, $P>0.33$], suggesting an absence of major alterations of white-matter tissue microstructure.

To further explore general brain architecture and cellular organization, we processed fixed forebrain and cerebellar sections for Nissl staining and histological evaluation. The general appearance and organization of forebrain structures (Fig. 2A), ventricles and fiber tracts (corpus callosum and anterior commissure), as well as of cerebellar lobules and glia limitans (Fig. 2B), were comparable between the genotypes. The brain of *mdx52* mice was properly divided into two hemispheres and the cellular lamination of cortex, hippocampus and cerebellum appeared unaffected at both low (Fig. 2A,B) and high (Fig. 2C-E) magnifications, with no sign of dysplastic cerebral cortex or heterotopic or ectopic cells. In all, there was no overt sign of gross structural malformations or migration defects as reported in some developmental disorders associated with intellectual disability, as for instance in mouse models of congenital muscular dystrophies that hold a deletion of the transmembrane component of dystrophin-associated complex dystroglycan (Satz et al., 2010; Vaillend et al., 2008).

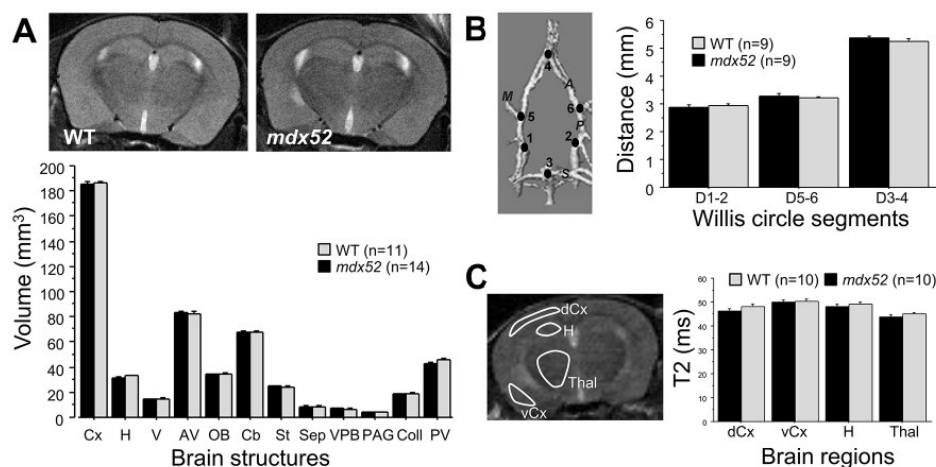


Fig. 1. *In vivo* MRI structural analyses. (A) Top images are representative MRI coronal sections and the histogram below shows the volumes (mm^3) of the analyzed brain structures, as defined in Table 1. MRI volumetric analyses are shown in the histogram for wild-type (WT, grey bars) and *mdx52* mice (black bars). (B) Angiographic estimation of the length of the main cerebral arteries. The three-dimensional image shows the medial (M), anterior (A), posterior (P) and superior (S) arteries, and the six points defined around the Willis circle used to quantify distances (D) between the points (in mm) D1 and D2, D5 and D6, and D3 and D4 in the histogram (right). (C) T2 maps generated at Bregma -1 mm in four brain regions shown in the sample MRI coronal image on the left: dorsal (primary sensory) and ventral (piriform) cortex layers (dCx and vCx, respectively), hippocampus (H) and thalamic nuclei (Thal). T2 quantifications are shown in the histogram (right). Data are mean \pm s.e.m. Statistics undertaken with two-way ANOVA for repeated measures were all insignificant ($P > 0.05$).

Behavioral study

Exploration and emotional reactivity

Spontaneous locomotor activity was analyzed during exploration of an open field arena for 25 min and compared in *mdx* and *mdx52* mouse models and their respective wild-type littermates (Fig. 3A-E).

The Kruskal–Wallis global analysis revealed significant differences among the four groups for all parameters, and two-group comparisons were further analyzed using post-hoc Dunn's tests. No statistical differences were detected between the two control lines (C57BL/10 and C57BL/6) for main locomotor activity parameters (Fig. 3A-C), reflecting that spontaneous locomotor activity was globally comparable in the two genetic backgrounds. However, we preferred to rigorously compare each mouse model to its wild-type littermate group. No significant differences were detected between *mdx* mice and their wild-type littermates for the mean distance traveled (horizontal activity, Fig. 3A) and vertical activity (Fig. 3B), but the running speed was lower in *mdx* mice (Fig. 3C). In contrast, the *mdx52* mice showed significant reductions for both the distance run and running speed compared to their wild-

type littermates, as well as to the *mdx* mice. The large and significant reductions in horizontal activity selectively detected in *mdx52* mice compared to their wild-type littermates suggest that the deletion of exon 52 has a greater impact on locomotion than the original *mdx* mutation.

To evaluate anxiety-related behavioral responses, we analyzed the relative time spent and distance run in the center zone of the open field arena in two different contexts. For the first group of mice described above, open field exploration was undertaken in the presence of sawdust and low illumination, which corresponded to a low-anxiogenic condition. The relative time spent and distance run in the center zone of the open field arena were expressed as a percentage of total time and distance to avoid biased conclusions due to the differences in general activity among groups (Fig. 3D,E). For the time spent in the center, there was a main group effect [$F(3,47) = 4.078$; $P = 0.012$], and post-hoc analyses revealed a significant difference between the two wild-type backgrounds ($P = 0.04$), as the C57BL/6 mice spent more time in the central area compared to the C57BL/10 line. There was no statistical difference between *mdx* and *mdx52* mice with this parameter. Comparisons of

Table 1. Brain regions of interest in the MRI volumetric study

ROI	Abbreviation	Included structures
Olfactory bulbs	OB	Olfactory bulbs
Ventricles	V	Ventricles
Cortex area	Cx	Cortex, amygdala nuclei and corpus callosum
Striatum area	St	Striatum
Hippocampus	H	Hippocampal formation
Septal area	Sep	Accumbens, septal, parabrachial and cuneiform nu.
VPB area	VPB	Preoptic and ventral pallidum nu., bed nu. of stria terminalis, substantia innominata
PAG area	PAG	Periaqueductal gray
Anterior ventral parts	AV	Thalamus and hypothalamus nu., and ventral nu. anterior to cerebellum coordinates
Posterior ventral parts	PV	Ventral nu. from cerebellum presence in sections
Cerebellum	Cb	Cerebellum
Colliculus area	Coll	Sup. and inf. colliculus, anterior pretectal nu.

The list of included structures and nuclei are provided for each delineated region. Abbreviations are also used in Fig. 1. nu., nucleus; sup., superior; inf., inferior.

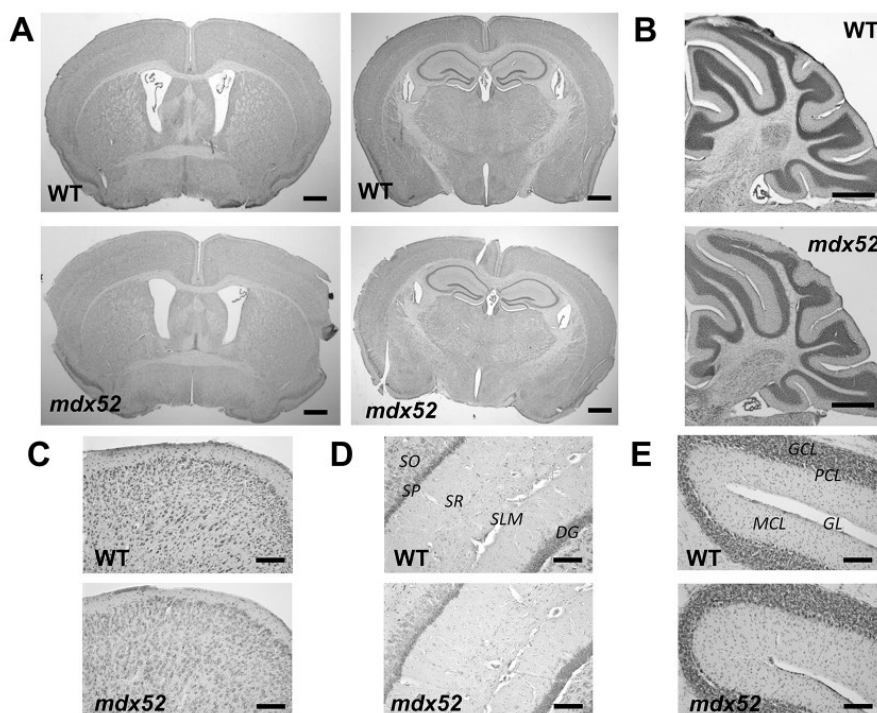


Fig. 2. Brain histology. (A) Sample light micrographs of Nissl-stained coronal forebrain sections taken at Bregma 0.14 (left) and Bregma -1.7 (right). (B) Sample light micrographs of Nissl-stained sagittal sections (lateral, 0.84 mm), including the cerebellum. (C-E) Images taken at higher magnification to show the general organization of neuronal layers in dorsal cortex (C), dorsal hippocampus (D) and cerebellar lobules (E). DG, dentate gyrus; GCL, granular cell layer; GL, glia limitans; MCL, molecular cell layer; PCL, Purkinje cell layer; SLM, stratum lacunosum moleculare; SO, stratum oriens; SP, stratum pyramidale; SR, stratum radiatum. Scale bars: 500 μm (A,B); 200 μm (C-E).

each mutant group with its respective wild-type littermate control group showed that the percentage of time spent in the center zone by bins of 300 s was equivalent between *mdx* and wild-type littermates (genotype effect, $P > 0.44$), and not significantly different between *mdx52* and wild-type littermates ($P = 0.054$). However, there were significant differences for the percentage of distance traveled in the center for 25 min (Fig. S2A,B) between *mdx52* mice and their wild-type littermates [$F(1,20) = 4.773$; $P = 0.041$], but not between *mdx* and wild type [$F(1,27) = 0.5487$; $P > 0.4$].

To better estimate anxiety during open field exploration, we then tested new groups of mice in a more anxiogenic context, i.e. in the same open field without sawdust and with a higher illumination (100 lx instead of 50 lx). In this condition, the total distance traveled and vertical activity were comparable among groups, whereas reduced running speed was selectively detected in *mdx52* mice compared to their wild-type littermates (Fig. S2C-E). The percentage of time spent in the center zone by bins of 300 s is shown in Fig. 3F,G. Here, the mean difference between the two wild-type lines was not significant ($P = 0.09$), but the different time courses were associated with significant differences at specific time points (300, 900 and 1500 s, each $P < 0.02$). For *mdx* mice the percentage of time spent in the center zone in this more anxiogenic condition was significantly reduced compared to their wild-type littermates, selectively during the first 5 min of the test [genotype effect, $F(1,23) = 2.898$, $P > 0.1$; time \times genotype effect, $F(4, 92) = 2.856$, $P < 0.03$; Fig. 3F]. In contrast, in *mdx52* mice, the

percentage of time in the center zone was reduced compared to their wild-type littermates during the entire testing period [genotype effect, $F(1,27) = 7.923$, $P = 0.009$; time \times genotype effect, $F(4, 108) = 0.173$, $P > 0.9$; Fig. 3G]. Although both *mdx* and *mdx52* mice showed a tendency for a reduced percentage of distance traveled compared to their respective wild-type littermates, the difference was only significant for *mdx52* mice (Fig. 3H), and comparisons of the distance traveled by bins of 300 s confirmed these conclusions (Fig. S2F,G). Overall, this suggested a transient effect of this anxiogenic context in *mdx* mice, and a persistent effect in *mdx52* mice.

The first groups of mice submitted to the low-anxiogenic open field test (Fig. 3A-E) were also tested in two additional anxiety tests: the light-dark choice and elevated plus-maze tests. The light/dark choice, illustrated in Fig. 4A (left panel), is based on the choice given to the mice to stay in a secure dark compartment or to explore an anxiogenic (brightly lit) compartment characterized by a gradient of illumination from the trap door (50 lx) to the end of the compartment (600 lx). As shown in Fig. 4B-D, both mutants display longer latencies and fewer visits compared to their respective wild-type littermates. However, for the latency, only *mdx52* mice displayed a significant difference compared to their wild-type littermates ($P < 0.01$), and for the number of entries into the lit compartment the significance was stronger in *mdx52* ($P < 0.001$) than in *mdx* mice ($P < 0.05$). Moreover, only *mdx52* mice spent significantly less time in the lit compartment ($P < 0.001$). The mean duration of visits (total

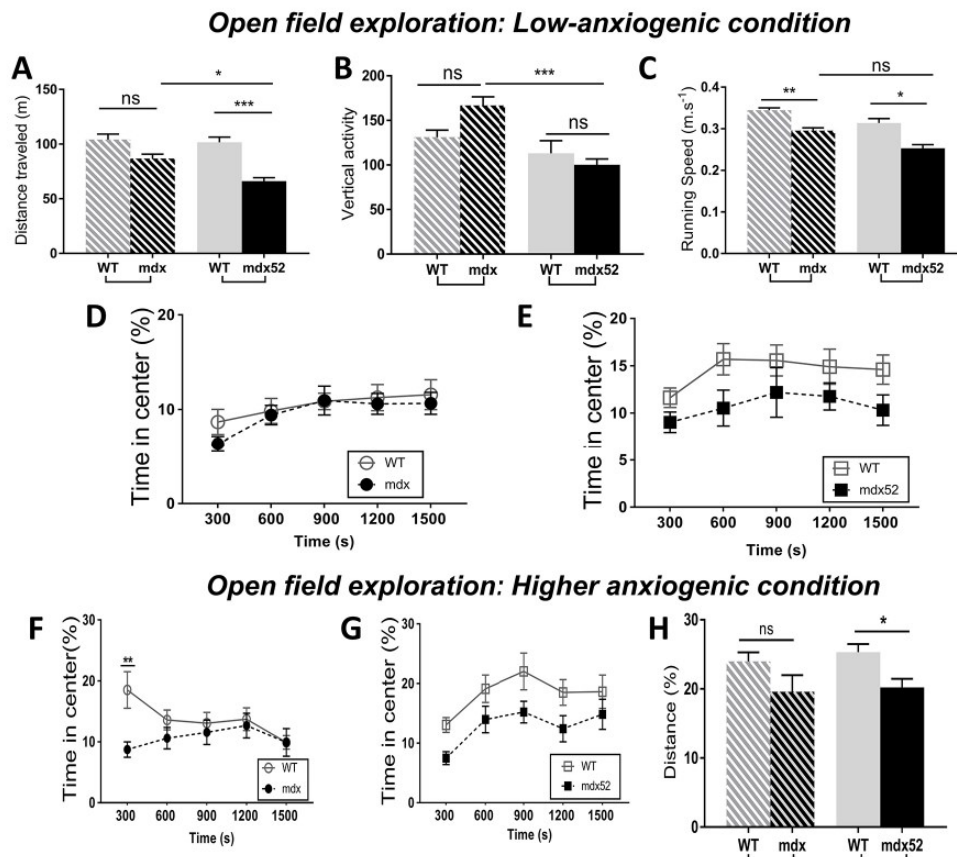


Fig. 3. Exploration of an open field. (A–E) Exploration during 25 min in a low-anxiogenic condition in 2-month-old *mdx* ($n=15$) mice and their wild-type (WT) littermates ($n=14$), and in *mdx52* mice ($n=12$) and their wild-type littermates ($n=9$). (A) Locomotor activity expressed as the total distance traveled (m). (B) Vertical activity defined by the number of rearings/leanings. (C) Mean running speed ($m \cdot s^{-1}$). (D, E) Anxiety-related behavioral responses: percentage of time spent in the center zone of the arena expressed by bins of 300 s in *mdx* and wild-type mice (D) and in *mdx52* and wild-type mice (E). (F–H) Exploration of an open field in a more anxiogenic context using distinct cohorts of mice of the same age (*Mdx*, $n=12$ and their wild-type littermates, $n=13$; *Mdx52*, $n=15$ and their wild-type littermates, $n=14$). Plots show the percentage of time spent in the center zone of the arena by bins of 300 s in *mdx* and wild-type littermates (F), and in *mdx52* mice and wild-type littermates (G). (H) Percentage distance traveled in the center area during the whole session in the four groups of mice. Data are mean \pm s.e.m. *** $P < 0.001$; ** $P < 0.01$; * $P < 0.05$; ns, not significant (four-group comparisons using a Kruskal–Wallis test followed by two-group post-hoc comparisons with Dunn’s test). Time courses by 5-min bins analyzed using two-way ANOVA for repeated measures.

time spent in the lit compartment normalized to the number of visits) was comparable between each group of mouse models and their wild-type littermates (Fig. S3A), indicating no main hypoactivity in the DMD mouse models in this test. To further estimate the level of anxiety in this test, we analyzed the number of entries and time spent in the brightest part of the lit compartment, considered more anxiogenic due to its high illumination (600 lx). We used the virtual line dividing the lit compartment in its middle (broken line in Fig. 4A) to quantify the number of line crossings and the time spent beyond the line (in the brightest part of the lit compartment). These parameters were comparable between *mdx* and wild-type mice (Fig. 4E,F). In contrast, *mdx52* mice showed a significantly reduced number of entries and time spent in this highly lit part (anxiogenic) compared to their wild-type littermates, which further supported the conclusion that *mdx52* mice display more anxiety-like responses compared to *mdx* mice.

In the elevated plus-maze test, anxiety results from the threat induced by the void in the elevated open arms. In this test, the total

number of visits to all arms was reduced in *mdx52* mice compared to their wild-type controls ($P < 0.001$), which was not observed in *mdx* mice (Fig. S3B). As shown in Fig. 4G,H, the percentage of the number of entries and the percentage of time spent in open arms were largely and significantly reduced in *mdx52* mice ($P < 0.001$). All groups performed a comparable number of protected head dips (Fig. 4I), i.e. head dips towards the void while their body is still inside a closed arm. In contrast, only *mdx52* mice showed a reduced number of unprotected head dips (head dips towards the void while being within an open arm; Fig. 4I). However, the number of head dips once normalized to the percentage of time spent in the respective arms showed no more differences between *mdx52* and wild type (Fig. S3C), indicating that the reduced number of unprotected head dips in *mdx52* mice simply reflected their shorter time spent in the more anxiogenic open arms. Overall, the three tests converge towards higher levels of anxiety in *mdx52* mice compared to *mdx* mice and wild-type controls.

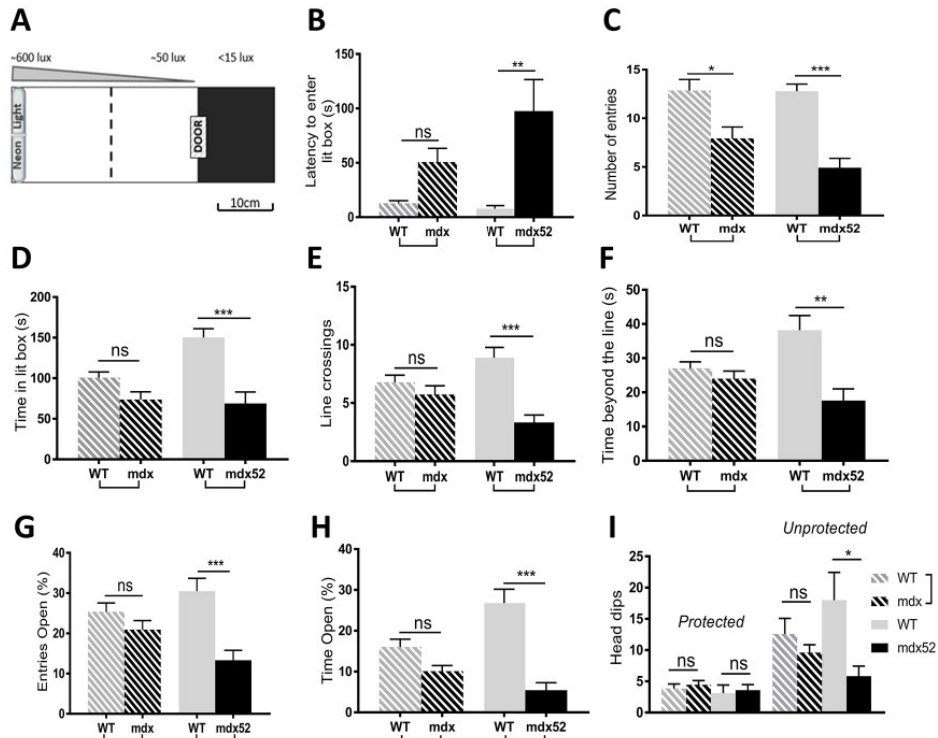


Fig. 4. Anxiety in light-dark choice and elevated plus-maze tests. Both tests were performed in the same 2-month-old groups of *mdx* mice ($n=15$) and their wild-type (WT) littermates ($n=14$), and in *mdx52* mice ($n=12$) and their wild-type littermates ($n=9$). (A-F) Light-dark choice test. (A) Schematic representation of the light/dark test apparatus (top view) composed of a dark box (15×15 cm), in which each mouse was first introduced, and a lit box (40×15 cm). The two compartments were connected by a sliding door. The lit box was separated in half by a virtual line (dotted line) to analyze behavior in the first and second parts of this box, which had different light intensities; the light intensity gradient is shown above the drawing. The end part of the lit box (600 lx) was considered to be more anxiogenic than the first part near the door (50 lx). Parameters were measured for 5 min. (B) Latency of the first entry into the lit box (s). (C) The number of entries in the lit box. (D) Time spent in the lit box. (E) Number of crossings of the virtual line. (F) Time spent beyond the virtual line, i.e. in the most anxiogenic part of the apparatus. (G-I) Elevated plus-maze. Behavioral parameters were analyzed for 5 min. (G) Number of entries in open arms, expressed as percentage of total number of arm entries. (H) Percentage time spent in open arms. (I) Number of head dips made in closed arms (protected) and in open arms (unprotected). Data are mean \pm s.e.m. *** $P < 0.001$; ** $P < 0.01$; * $P < 0.05$; ns, not significant (Kruskal–Wallis test followed by Dunn's test).

Unconditioned and conditioned fear responses

We first studied the stress-induced freezing response, an innate antipredator fear-related behavior, characterized by a complete tonic immobilization of the mouse, except for respiration. It is expressed as the percentage of time spent in tonic immobility (percentage of freezing) during a 5-min period following a brief (15 s) manual scruff restraint, which is considered to be a measure of unconditioned fearfulness. This manual restraint did not result in any observable fear response in the wild-type mice (mean percentage of time spent immobile, $< 20\%$). In contrast, the scruff restraint induced a large quantity of freezing in both *mdx* and *mdx52* mice ($> 80\%$) during the 5 min that followed the stress; Fig. 5A). Even if *mdx* mice in this experiment were younger (4 months old) than *mdx52* mice (7 months old), it has previously been demonstrated that freezing amounts in *mdx* mice reach plateau values at 3 months (Sekiguchi et al., 2009; Vaillend and Chaussonot, 2017). The present results show that, at the adult age, *mdx52* mice display amounts of freezing comparable to that of *mdx* mice.

We then investigated fear learning and memory using auditory-cued fear conditioning, which involves the learning of an aversive

cue–outcome association. This test reliably showed delayed acquisition and retention deficits in the original *mdx* mice in many experimental replicates in previous studies (Chaussonot et al., 2015; Vaillend and Chaussonot, 2017a). Therefore, we studied the conditioned fear response only in *mdx52* mice compared to their wild-type littermates, using an identical protocol and experimental conditions (Fig. 5B–E).

Acquisition of fear conditioning (fear learning) was significantly impaired in *mdx52* mice (Fig. 5B), as reflected by a strongly reduced amount of freezing displayed by *mdx52* mice compared to wild type in response to presentation of the conditioned stimuli (CS, tone) [genotype effect, $F(1,32)=8.612$, $P < 0.007$; genotype \times trial interaction, $F(4128)=5.989$, $P < 0.001$]. In contrast, the freezing displayed during the intertrial intervals (ITIs) between presentations of the successive pairs of conditioned (CS)–unconditioned (US) stimuli (i.e. after shock delivery) was comparable in the two genotypes [genotype effect, $F(1,34)=0.6248$; $P > 0.4$; genotype \times trial interaction, $F(4136)=1.509$, $P > 0.2$; not shown], indicating that *mdx52* mice expressed similar fear responses as wild-type mice following delivery of the US (electric footshock).

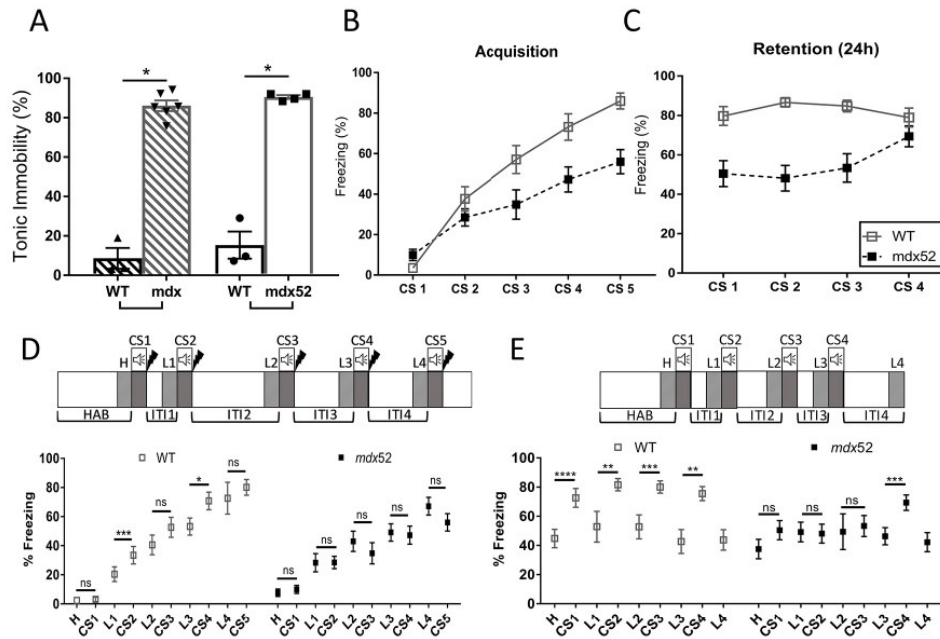


Fig. 5. Fear-related tonic immobility. (A) Unconditioned fear expressed as the percentage of time spent in tonic immobility (% freezing) during a 5-min period following a brief scruff restraint (15 s). This was compared in 4-month-old *mdx* mice ($n=6$) and their wild-type (WT) littermates ($n=3$), and in 7-month-old *mdx52* mice ($n=4$) and their wild-type littermates ($n=3$). Symbols show individual scores. Statistical significance was determined using a Kruskal–Wallis test followed by Dunn’s test. (B–E) Auditory-cued fear conditioning. Fear learning (B, conditioning session) and fear memory (C, retention session) were assessed in adult (3–4 months) *mdx52* mice ($n=18$) and wild-type littermate mice ($n=16$). Learning performance was expressed as the percentage of time spent freezing during presentation of the conditioned stimulus (tone, 30 s), repeated five times during acquisition (CS 1–5; each was an 80 dB tone lasting 30 s, followed by a footshock) and repeated four times (CS1–4) during the retention session performed 24 h later in a new context (fear memory). Genotype differences were significant in both sessions (genotype effects and genotype \times trial interactions; two-way ANOVA for repeated measures). (D,E) Detailed analyses of the changes in freezing induced by the CS presentations during acquisition (D) and retention (E) sessions. Diagrams show the experimental sequences: habituation (HAB), successive tone presentations (CS, loud-speaker symbol), shock delivery (lightning symbol) and ITIs of various durations. Freezing during the last 30 s of habituation (H) and last 30 s of ITIs (L1–L4) (hatched areas) were each statistically compared to each following 30-s CS presentation (gray areas) using paired *t*-tests. Plots below show the freezing (%) during each analyzed period in both genotypes (as indicated) and significance of paired comparisons are shown. Data are mean \pm s.e.m. * $P<0.05$; ** $P<0.01$; *** $P<0.001$; $P<0.001$; ns, not significant.

Moreover, fine examination of recordings showed that CS presentation did not induce other types of fear-related escape behaviors in *mdx52* mice (jumps and rearing against walls), indicating that the reduced freezing reflected a more rapid recovery of ambulation compared to wild-type mice, but not a change in fear expression. The selective reduction of freezing during the CS presentation in *mdx52* mice therefore suggests a specific deficit in learning the predictive value of the CS. Twenty-four hours later (retention session, Fig. 5C), the *mdx52* mice also exhibited reduced quantities of freezing during the four presentations of the CS alone (not followed by electric footshocks) [genotype effect, $F(1,32)=21.57$, $P<0.0001$; time \times genotype interaction, $F(3, 96)=4.493$, $P<0.006$], suggesting a performance deficit in the recall of fear memory. However, the amount of freezing displayed by both *mdx52* and wild-type mice during this session was not significantly different from their performance at the end of the acquisition session (i.e. during presentation of CS5 during fear learning) [CS5-learning versus CS1-memory; genotype effect, $F(1,34)=11.52$, $P<0.01$; trial effect, $F(1,34)=1.52$, $P>0.2$; genotype \times trial interaction, $F(1,34)=0.03424$, $P>0.8$; not shown]. This suggests that the deficit displayed by *mdx52* mice 24 h post-acquisition rather reflects their reduced initial level of learning.

To further detail associative learning performance during the cued fear conditioning, we used paired *t*-tests to compare the amount of freezing during the last 30 s of the habituation period of 2 min and/or the last 30 s of each ITI (L1 to L4) to the following presentations of CS1 to CS5 (30 s duration each). This allowed us to visualize and analyze the changes in freezing specifically induced by the presentation of each 30-s CS, compared to the freezing expressed during the 30 s preceding its presentation (Fig. 5D,E). During the acquisition session (Fig. 5D), the wild-type mice showed clear increases in freezing during CS presentation compared to ‘baseline’ freezing recorded during the preceding 30 s periods (L1–L3), which was statistically significant for CS2 and CS4, until they reached maximal performance of $\sim 80\%$ of freezing in response to CS5. In marked contrast, there was no increase in freezing in *mdx52* mice upon presentations of the CS during the whole session, suggesting a deficit in learning the CS-US association. The retention session (Fig. 5E), during which CS were presented without any following electric footshock, largely confirmed this conclusion; the wild-type mice systematically displayed an increase in freezing during each CS presentation (CS1–4) compared to the baseline freezing levels preceding CS presentation (all changes were significant), thus attesting solid memory retention of the conditioned CS-US association. In contrast, the *mdx52* mice did

not show significant increases in freezing following CS presentations, except during the last CS presentation (CS4). This performance deficit during the retention session likely reflected the initial level of performance of *mdx52* mice, as they showed comparable freezing levels at the end of acquisition and at the start of the retention sessions.

DISCUSSION

Neuropsychological studies have given greater consideration to the contribution of a central component in the genesis of emotional and neuropsychiatric disturbances in neuromuscular diseases (Colombo et al., 2017; Ricotti et al., 2016). Therefore, investigating the *mdx52* mouse model is important to further understand how the cumulative loss of brain dystrophins impact brain functions. In the present study, we provide the first behavioral investigation of *mdx52* mice lacking brain Dp427 and Dp140, which evidences an exacerbation of anxiety responses and a different pattern of impairment of conditioned fear compared to the original *mdx* model that only lacks Dp427. Moreover, our macroscopic study of brain morphology and architectural organization suggests that alterations related to the cumulative loss of Dp427 and Dp140 likely depend on putative cellular dysfunction rather than major developmental malformation. The behavioral and cognitive deficits that we characterized here are not exhaustive but already confirm the potential of this mouse model for preclinical use, as behavioral tests can easily be implemented as functional outcome measures when evaluating new treatments targeting the CNS.

Absence of overt gross brain abnormalities

Macroscopic brain abnormalities, such as ventricular enlargement and cortical atrophy in line with grey and white-matter alterations and/or changes in brain metabolism and perfusion, have been reported in some DMD patients, with an apparently higher prevalence when distal mutations affect expression of several dystrophins, particularly Dp140 (Septien et al., 1991; Anderson et al., 2002; Lee et al., 2002; Doorenweerd et al., 2014, 2017). However, brain autopsies and imaging studies still have not led to consistent results, and a possible link between the loss of specific dystrophins and gross and/or ultrastructural brain abnormalities remains uncertain. Structural MRI was also used in DMD mouse models lacking Dp427, which evidenced that Dp427 loss is not associated with major brain volumetric changes (Kogelman et al., 2018; Miranda et al., 2009), which further supported the hypothesis that developmental changes may be due to the loss of other brain dystrophins. In the present study, we addressed this question using *in vivo* MRI and neurohistological analyses in the *mdx52* mouse lacking Dp427 and Dp140. However, *mdx52* mice did not show any overt changes in the whole brain volume or in the volume of several brain structures involved in cognitive functions. Nevertheless, subtle changes in small structures and/or nuclei have been detected in Dp427-deficient *mdx* mice (Kogelman et al., 2018), as well as progressive alterations with aging in longitudinal studies (Bagdatlioglu et al., 2020), which could be further studied in *mdx52* mice in future imaging studies. We cannot exclude that alterations occurring during fetal brain development may have been compensated in the postnatal period, but the present data do not favor major and lasting macroscopic brain malformations in this model.

Dp140 is more highly expressed in the human fetal brain than in the adult brain (Doorenweerd et al., 2017; Lidov et al., 1995; Morris et al., 1995), which suggests it is involved in brain formation, perhaps in neuronal proliferation or migration (Hildyard et al., 2020;

Romo-Yáñez et al., 2020). Moreover, the loss of distinct dystrophins reduces the expression of the membrane-spanning core protein of the dystrophin-associated complex, dystroglycan (Kameya et al., 1997; Culligan et al., 2001; Daoud et al., 2009b; Benabdesselam et al., 2012; Belmaati Cherkaoui et al., 2020). Dystroglycan has been implicated in basement membrane formation, cell migration and corticogenesis (Paprocka et al., 2021), as defective glycosylation of the extracellular component of the dystroglycan subcomplex results in defects of the glia limitans and cortical plate disorganization, with overmigration of neurons into the arachnoid space in the Walker-Warburg, Fukuyama congenital muscular dystrophy and muscle-eye-brain syndromes associated with intellectual disability (Godfrey et al., 2007; Guimaraes and Dahmouh, 2020). Although it remains unknown whether dystroglycan interacts with specific dystrophins or utrophin paralogues during fetal brain development, genetic loss of dystroglycan recapitulates the brain abnormalities observed in these congenital muscular dystrophies called dystroglycanopathies (Satz et al., 2010). However, we found no sign of cortical disorganization or modification of the architecture of hippocampus and cerebellum in *mdx52* mice, suggesting that these processes do not require Dp427 and Dp140, or have been compensated by interaction with other brain dystrophins or utrophins.

Overall, the results of this first neuroanatomical study show that the loss of Dp427 and Dp140 is not associated with gross brain abnormalities, similar to what was observed in the original *mdx* mouse that only lacks Dp427. This suggests that the neural dysfunctions resulting from the cumulative loss of these two dystrophins rather take place at the level of brain cellular functionalities. Dp427 has been implicated in GABAergic inhibition and blood-brain barrier functions due to its expression in central inhibitory synapses and vascular smooth muscles, respectively (Belmaati Cherkaoui et al., 2020; Fritschy et al., 2012; Nico et al., 2003). In contrast, the localization and function of Dp140 remain largely unknown. Co-expression networks generated from transcriptomic analyses of human brains suggest putative roles for Dp140 in generic transcription pathways, neuronal differentiation and axonal and dendritic development (Doorenweerd et al., 2017), and experimental studies in animal models revealed expression in vascular and/or glial elements (Caudal et al., 2020; Lidov et al., 1995) and oligodendrocytes (Aranmolate et al., 2017). Oligodendrocytes play a major role in the myelination of neuronal axons, and physical interactions with the vascular endothelium are required for the migration of their precursors (Tsai et al., 2016), which further emphasizes the need for future studies addressing the possible roles of Dp140 in structure connectivity and/or the vascular system.

Severe disturbances in amygdala-dependent behaviors and associative learning

One of the main challenges for preclinical research aimed at rescuing brain-related dysfunction in DMD is to identify robust behavioral phenotypes in a mouse model with translational value for the clinical condition. The *mdx52* mouse models a frequent genetic profile corresponding to ~60% of DMD patients (Beroud et al., 2007), which has been primarily associated with emotional behavioral disturbances and cognitive dysfunction (Ricotti et al., 2016). Previous work in *mdx* mice (Sekiguchi et al., 2009; Vailland and Chaussonot, 2017) has shown that a mild stress, induced by a short (15 s) scruff restraint, results in an exacerbated unconditioned fear response characterized by potent and sustained tonic

immobility (>80% of a 5-min time period spent freezing). Here, we found comparable levels of freezing in *mdx* and *mdx52* mice, confirming that this measure of enhanced fearfulness is a reliable outcome measure to evaluate the impact of Dp427 restoration in preclinical studies. This phenotype has been attributed to a dysfunction of the fear circuit, as supported by altered GABAergic inhibitory responses to norepinephrine inputs to pyramidal neurons of the basolateral amygdala in Dp427-deficient *mdx* mice (Sekiguchi et al., 2009).

In this study, we further investigated amygdala-dependent behaviors and learning performance in *mdx* and *mdx52* mice. In the original *mdx* mouse, the presence of anxiety-related responses has been reported, yet the variability among laboratories and the lack of phenotype in the elevated plus-maze test suggested that the changes in anxiety are borderline in *mdx* mice (Manning et al., 2014; Sekiguchi et al., 2009; Vaillend and Chaussonot, 2017). Our present results confirmed this conclusion for *mdx* mice, but further revealed that *mdx52* mice display clearer and significant behavioral changes in all behavioral parameters reflecting anxiety during exploration of the light/dark box, elevated plus maze and open field. It has been reported that muscle wasting may be more severe when mutations affecting expression of muscle Dp427 are expressed in a C57BL/6 background compared with the original C57BL/10 background (Beastrom et al., 2011). Although this may potentially constitute a confounding factor in behavioral analyses, we previously showed in *mdx* mice that reactivity to stress influences locomotor activity, which is otherwise unaltered in unstressed animals (Vaillend and Chaussonot, 2017). In the present study, measures of anxiety were robust in tests with low motor demand, and we normalized anxiety-related parameters to the locomotor activity of an individual to further minimize putative influence of motor factors in our analyses. Besides, the genetic background may also influence brain and behavioral functions (Mortazavi et al., 2021 preprint), which cannot be ruled out without direct comparisons with controls in the same background. Some behavioral parameters were comparable between control mice of the two genetic backgrounds but some others were statistically different, and we therefore preferred to rigorously compare the mutant mice to their respective littermate controls. The significant differences between *mdx52* mice and their littermate controls compared to the non-significant differences between *mdx* mice and their littermate controls suggest that emotional reactivity may be more affected in *mdx52* than in *mdx* mice. This is also in line with the significant deficit shown by *mdx52* mice in the elevated plus maze, which was not observed in *mdx* mice in the present study, as well as in previous reports (Sekiguchi et al., 2009; Vaillend and Chaussonot, 2017). So far, in the present study, we cannot claim a definitive conclusion regarding the severity of the behavioral changes potentially linked to the mutation profile, yet our data show that there are important emotional disturbances in *mdx52* mice that represent robust outcome measures that can be used to evaluate treatment efficacy in future preclinical studies.

Fear conditioning performance was replicated several times by our group in identical experimental conditions in *mdx* mice: the phenotype of this model lacking only Dp427 was consistently characterized by delayed acquisition and retention of the task, but *mdx* mice could finally perform in a comparable manner to their wild-type littermates after repetition of stimulus presentation (Chaussonot et al., 2015; Vaillend and Chaussonot, 2017). In marked contrast, we found here that *mdx52* mice were more severely impaired as they failed to improve their learning performance to reach wild-type performance level and consistently displayed

reduced fear responses when auditory CS were presented. However, *mdx52* mice showed similar levels of fear responses as wild-type mice following electric shock delivery during the intervals between CS presentations, indicating that the difference cannot be simply explained by a reduced sensitivity to electric shocks or different expression of fear responses.

To further analyze the cognitive component of fear responses in this task, we compared equivalent time periods just preceding or following CS presentation. Strikingly, this analysis revealed that CS presentation elicited significant increases in fear levels in wild-type mice but not in *mdx52* mice. This was particularly clear during the retention session when no electric shocks were delivered, as the freezing increases observed in wild-type mice were selectively induced in response to CS. In this aversive cue-outcome Pavlovian associative learning, the CS is expected to elicit a specific fear response if animals learn that the CS predicts the delivery of the US (electric footshock). Therefore, our results demonstrate that the performance of *mdx52* mice likely results from the formation of inappropriate or weaker fear associations. This strongly supports a key role for the amygdala in this phenotype, as integrity of this structure is required for fear conditioning (Phillips and LeDoux, 1992). The exact amygdala nuclei and processes remain to be specified. The loss of Dp427 in *mdx* mice likely alters the correct processing of norepinephrine inputs by the basolateral amygdala (BLA) (Sekiguchi et al., 2009). However, the severe phenotype observed here in *mdx52* mice suggests that additional mechanisms involved in the association of fear with a predictive auditory stimulus are affected due to the additional loss of Dp140. This might include alteration of sensory inputs processing, impairment of CS-US association by neurons of the lateral amygdala, altered specificity of the activation of BLA fear neurons by the lateral amygdala and/or impaired plasticity of BLA networks (Herry et al., 2008; Janak and Tye, 2015; Wallace and Rosen, 2001). Although learning the CS-US association was clearly impaired in *mdx52* mice, their reduced performance during the retention session 24 h later does not imply that long-term memory processes, such as consolidation, extinction, reconsolidation and recall processes were impaired. Indeed, the performance of *mdx52* mice during retention was comparable to their level of performance at the end of the acquisition. Hence, it is likely that the retention deficit in *mdx52* mice simply reflected their reduced initial level of learning.

Several animal species with genetic alterations of the *DMD* gene also display strong fear-related behavioral disturbances and enhanced stress reactivity (Frésard et al., 2012; Nonneman et al., 2012; Mori et al., 2015). Moreover, several studies and reports of parents' rating have revealed internalizing problems, including anxiety in Duchenne and Becker muscular dystrophies, which likely contribute to and/or enhance maladaptive social behaviors and neuropsychiatric disturbances (Poysky and Behavior in DMD Study Group, 2007; Young et al., 2008; Snow et al., 2013). According to a recent study of genotype-phenotype relationships (Ricotti et al., 2016), clinical levels of emotional problems are not dependent on the genotype or presence of intellectual disability, and affect a quarter of DMD patients, which represents a high prevalence and supports the face validity of the *mdx52* mouse model characterized by strong emotional and fear-related phenotypes.

In conclusion, in *mdx52* mice lacking Dp427 and Dp140, the disturbances in emotional behavior (anxiety and unconditioned fear) and impairment in learning a Pavlovian CS-US association during fear conditioning appear more severe than in mice lacking Dp427 only. This is in line with the presence of emotional internalizing and externalizing problems, and cognitive deficits in

patients with a comparable genetic profile. The behavioral deficits reported in this mouse model confirm that a focus should be placed on the roles of amygdala and brain fear circuit in emotional behaviors, and learning in the context of the central defects associated with DMD. As *mdx52* mice do not display more overt gross brain abnormalities compared to the Dp427-deficient *mdx* mouse, the neural basis of the behavioral and cognitive deficits in this model lacking Dp427 and Dp140 can likely be found at the level of cellular functionalities. Future studies will detail the nature of the deficits and the underlying neurobiological mechanisms resulting from the cumulative loss of these two brain dystrophins. Previous preclinical studies in *mdx* mice revealed that exon-skipping strategies have the potential to alleviate emotional disturbances following treatment at adulthood. The present work provides relevant, robust and translational behavioral readouts to determine the efficacy of such treatments in the *mdx52* mouse model, which recapitulates the most frequent genetic condition associated with brain defects in DMD.

MATERIALS AND METHODS

Animals

Exon 52-deleted X chromosome-linked muscular dystrophy mice (*mdx52* mice) were produced by replacement of exon 52 of the *Dmd* gene by the neomycin resistance gene, thereby eliminating expression of Dp427, Dp260 and Dp140 dystrophins but preserving expression of Dp116 (in peripheral nerves) and Dp71 (in brain and retina) (Araki et al., 1997). The mouse line was backcrossed with the C57BL/6J strain for more than eight generations. Breeders were generously provided by Dr. Jun Tanihata and Dr. Shin'ichi Takeda (National Center of Neurology and Psychiatry, Tokyo, Japan). Heterozygous females were crossed with C57BL/6JRj male mice to generate *mdx52* and littermate control (wild type) males in the animal facility of Neuro-PSI at the Université Paris-Saclay in Orsay (France). The C57BL/10ScSn-Dmd^{mdx52}/J (*mdx52*) and C57BL/10ScSn lines were originally purchased from Charles River Laboratories, and the breeding of heterozygous *mdx* females with C57BL/10ScSn males generated the *mdx* male mice and wild-type littermates used in this study. All genotypes were determined by PCR analysis of tail DNA. Animal care and all experimental procedures complied with the European Communities Council Directive (CEE 86/609/EEC), EU Directive 2010/63/EU, the French National Committee (87/848) and the ethics committee (Paris Centre et Sud, N°59).

Experimental groups

Only the cages containing mice of both genotypes were selected for experiments. Siblings were kept in groups (two to five per cage) under a 12-h light-dark cycle (light on at 7 am) with food and water *ad libitum*. Behavioral testing was performed blind to the genotype. Mice used for brain imaging, histology and histochemistry were adult males (3-5 months old). For the behavioral study, male mice of the four genotypes (*mdx* and their wild-type littermates, and *mdx52* mice and their wild-type littermates) were tested for exploration and anxiety at the age of 2 months by being successively submitted to three behavioral tests with intervals of 24 h between tests, in the following order: elevated plus maze, light/dark choice test and open field activity. Restraint-induced unconditioned fear was tested in distinct groups of *mdx* and wild-type littermate mice (4 months old), and *mdx52* and wild-type littermates (7 months old). Independent groups of naive mice aged ~2 months were submitted to a second open field session in a more anxiogenic context. A distinct group of *mdx52* and wild-type littermate mice aged 3-4 months were submitted to the auditory-cued fear conditioning.

Detection of dystrophins by immunofluorescence

Sagittal sections (30 μ m) were cut at -12°C in a cryostat from fresh-frozen dissected brains. Sections were collected on SuperFrost glass slides (Roth, France) and stored at -80°C . For immunocytochemistry, slides were thawed for 1 min at room temperature, immersed in acetone/methanol (1:1) for 5 min at

-20°C , washed three times in 0.1 PBS and incubated in a blocking solution for 45 min [10% normal goat serum (NGS), 0.3% Triton X-100 and 1% bovine serum albumin (BSA)]. Slides were then incubated overnight at 4°C with the following primary antibodies: 5G5 (dilution, neat), a monoclonal antibody directed against the N-terminal part of full-length (Dp427) dystrophin, and the polyclonal H4 antibody (1:800) directed against the C-terminal part of dystrophins and recognizing Dp71 (generous gifts from D. Mornet, INSERM Esprit 25, Université de Montpellier, UFR de Médecine, Montpellier, France). Incubation with primary antibody was followed by washes and incubation with goat anti-mouse IgG or anti-rabbit IgG secondary antibodies conjugated to Cy3 (1:500; Jackson ImmunoResearch, USA, 111-165-003) in PBS (0.1 M) with 5% NGS and 1% BSA for 1 h at room temperature. Cover slips were applied to slides using a mounting medium containing DAPI (Fluoromount-G, Clinisciences, France). No staining was observed in sections processed from control samples from both genotypes when primary antibody was omitted. A laser scanning confocal microscope LSM 700 (Zeiss, France) was used to sequentially collect Cy3 immunoreactivity at 555 nm and DAPI staining at 405 nm. Stacks of 7-15 confocal images and mosaic images (1024 \times 1024 pixels, 16 bits) were imported using an EC Plan-Neofluar 40 \times 1.30 Oil M27 at a resolution of 156 nm/pixel and processed with ImageJ (National Institutes of Health, USA) using a maximum intensity projection of all the z-stack images. All images were randomly taken at the same exposure times and equivalent stereotaxic coordinates.

Histology and light microscopy

Brains were collected and fixed in a 4% paraformaldehyde fixative solution in 0.1 M phosphate buffer (pH 7.3-7.4) cryoprotected in 30% sucrose and then quickly frozen in 2-methylbutane (Roth, Karlsruhe, Germany) cooled with dry ice to -40°C . Coronal serial sections (30 μ m) were collected and stored at -80°C . Nissl stain was performed with thionin and photographed at 1.253 \times with a Sony DFW-X700 digital camera (Sony, Tokyo, Japan) coupled to an Olympus BX60 light microscope (Olympus, Hamburg, Germany).

In vivo magnetic resonance imaging

Male mice aged 3 months (11 wild-type and 14 *mdx52* mice) were imaged under isoflurane anesthesia (induction 2%; flow rate 1.8-1.2% in 100% compressed air) controlled on the basis of respiratory parameters. The body temperature was maintained at 37°C using a heated mattress. MRI measurements were taken using a 7T horizontal bore magnet (Oxford, UK) driven by Paravision 6.0.1 (Bruker, Wissembourg, France) and equipped with a 300 mT/m actively shielded gradient device (internal diameter, 90 mm, Bruker). For MRI examination, the head of each animal was introduced in a 'bird-cage' 1-H coil (internal diameter, 20 mm). After positioning and shimming processes, we performed axial and sagittal anatomic T2-weighted 2D-TurboRARE (rapid acquisition with refocusing echoes) [AXIAL, TR/TE eff=4250/39 ms (repetition time/effective echo time); 8 averages; rare factor=8; 20 \times 20 mm field of view (FOV); 256 \times 256 matrix; 34 slices, 450 μ m thickness with 50 μ m slice gap; voxel size=78 \times 78 \times 500 μm^3 ; SAGITTAL, TR/TE eff=2550/32.6 ms; rare factor=8; lipid removal; ten averages; 20 \times 15 mm FOV; 256 \times 192 matrix; 24 slices, 450 μ m thickness with 50 μ m slice gap; voxel size=78 \times 78 \times 500 μm^3] and an angiography [TOF-3D-FLASH sequence (time of flight-fast low angle shot MRI) with TR/Te=14/2.6 ms; excitation pulse angle 20 $^{\circ}$; 20 \times 20 \times 15 mm FOV; 256 \times 256 \times 96 matrix; voxel size=78 mm 3]. T2 maps were additionally generated using multi-spin-multi-echo sequence (Tr=2200 ms; 14 echoes time, each 9 ms, first echo time 9 ms; 18 \times 15 mm FOV; 108 \times 96 matrix; pixel size=167 \times 156 μm ; seven slices of 800 μ m thickness; 250 μ m slice gap; one coronal 6-mm saturation slice; time scan 111 s). The total time spent by the mouse in the magnet never exceeded 44 min. After each experiment, mice were recovered from anesthesia and returned to their home cages with free access to food and water.

Areas and volumes were estimated in both the coronal and sagittal MRI planes using AMIRA software (TGS Inc., San Diego, CA, USA). Analyses were performed as described previously (Sebric et al., 2008) with some modifications: the mouse brain atlas and reference database (Ma et al., 2005;

Paxinos and Franklin, 2001) were used as initial guides and the brain was first subdivided into 12 main ROI (Table 1).

Brain volumes were determined by boundary tracing of cross-sectional areas and extracted by multiplying areas by section thickness. Boundary tracing was performed twice by two independent experimenters. MRI angiographic measurements were analyzed by measuring distances between six points defined around the Willis circle (Janniczky and Hallgrímsson, 2011). Brain T2 maps were generated using PV6.0.1 software (Bruker). Calibration was performed using the signal measured in the tongue muscles at the Bregma level. Intensities for different echo time were measured at Bregma -1 mm and T2 was calculated ($R^2 > 99\%$ for exponential) following delineation of 4 ROI, including dorsal (dCx) and ventral (vCx) cortical layers corresponding to primary sensory and piriform cortices, respectively, and hippocampus (H) and thalamic nuclei (Thal).

Behavioral study

Elevated plus maze

The maze had two facing arms enclosed with high walls (closed arms, 20×8×25 cm), two open arms without walls (20×8 cm) and a central area (8×8 cm) forming a plus sign situated above a vertical stand to elevate the maze 65 cm above the floor. Illumination was 150 lx in the open and 30 lx in closed arms. Mice were individually placed at the center of the maze with the head facing a closed arm. The number of entries and time spent in open or closed arms were recorded for 5 min. Head dipping over the sides of open arms were counted and classified as protected head dips when the rest of the body of the mouse remained in a closed arm, and as unprotected head dips when the whole body of the mouse was located in an open arm.

Light-dark choice

The apparatus had 20-cm-high Plexiglas walls and consisted of a black and dark compartment (15×15 cm; illumination <15 lx) connected by a trap door (6×6 cm) to a brightly lit white compartment (40×15 cm). Bright illumination was provided by a light source placed at the end of the white compartment, opposite from the trap door in order to create an illumination gradient (50 lx close to the trap door to 600 lx close to the light). Each mouse was placed in the dark compartment for 10 s. The trap door was then opened and the mouse was allowed to freely explore the whole apparatus for 5 min. Step through latency, number of entries and total time spent in the lit compartment were manually scored by the experimenter.

Open field activity

The test box was a square open field (50×50×50 cm) with black walls and a floor covered with sawdust. Experiments were undertaken under constant room temperature (22–23°C) and homogeneous dim illumination (50 lx). Each mouse was released near the wall and video tracked for 25 min using ANY-maze software (Stoelting, USA). Recorded XY positions were used to generate tracking plots of the exploration paths and to calculate the distance traveled, speed and time spent in distinct zones of the box, i.e. in the whole apparatus and in a central area (30 cm×30 cm, 10 cm from walls), referred to as the center zone. The percentage of time spent and distance traveled in the center zone were used as relative measures of anxiety. The number of rearings and leanings, referred to as vertical activity, were counted manually by the experimenter from saved videos.

In a second experiment with distinct groups of mice, the conditions were modified to increase the anxiogenic context of the test: testing was performed in a higher homogeneous illumination (100 lx instead of 50 lx) and each mouse was released in the center of the white floor of the box, which did not contain sawdust. The floor was cleaned with water then ethanol before each mouse.

Restraint-induced unconditioned fear

The mouse was restrained by grasping the scruff and back skin between thumb and index fingers, while securing the tail between the third and little fingers and tilting the animal upside down in order that the ventral part of its body faced the experimenter. After 15 s, the mouse was released to a novel cage (24×19 cm, with 12-cm-high walls) containing clean sawdust and was then video tracked for 5 min under dim illumination (60 lx) using ANY-maze software (Stoelting, USA). Unconditioned fear responses induced by

this short acute stress were characterized by periods of tonic immobility (freezing) and quantified during a 5-min recording period. Complete immobilization of the mouse, except for respiration, was regarded as a freezing response (Paylor et al., 2001). The percentage of time spent freezing was calculated for group comparisons.

Auditory-cued fear conditioning

The conditioning procedure was carried out using the StartFear system (Panlab S.L., Barcelona, Spain) in the same conditions used previously in our studies of *mdx* mice (Vaillend and Chaussonot, 2017). The conditioning chamber (25×25×25 cm) had three black methacrylate walls, a transparent front door, a grid floor connected to a shock scrambler to deliver US and a speaker mounted on the ceiling to deliver audible tones as CS. The conditioning chamber rested on a high sensitivity weight transducer system to generate an analogical signal reflecting the movement of the animal. The chamber was confined in a ventilated soundproof enclosure (67×53×55 cm) on an anti-vibration table with a surrounding 60-dB white noise. Interchangeable floors and walls (i.e. plain floor and white walls) were used to analyze the retention of cued fear in a novel context. On the first day (acquisition), a 2-min baseline period was recorded before delivery of five CS-US pairs [tone (CS), 80 dB, 10 kHz, 30 s; footshocks (US), each at 0.4 mA for 2 s] with variable and pseudo-randomly distributed intervals between pairs of stimuli (60, 120 and 180 s). On the next day (retention), the session started with the mouse being placed in a different context for 2 min (baseline) before the delivery of four CS (80 dB, 10 kHz, 30 s) separated by intervals of variable durations (60, 90 and 120 s). The movement of the animal was sampled at 50 Hz for quantitative analysis (FREEZING software, Panlab S.L.). Freezing was analyzed during the delivery of the CS (periods of 30 s) to specifically reflect associative learning performance (Chaussonot et al., 2015). *mdx52* mice and their wild-type littermates were gently handled every day for a week before being submitted to tasks, in order to avoid any stress before testing.

Statistics

Data are presented as mean±s.e.m. Two-tailed statistics were performed using GraphPad Prism7 (San Diego, California, USA). Repeated measures in the MRI and behavioral studies were analyzed using two-way ANOVA with genotype as the between-group factor and temporal variables (brain structure for MRI, and time or trial in behavioral studies). Analyses of performance in cued fear conditioning with ANOVA were followed by detailed comparisons of specific intervals within groups using paired *t*-tests. Four-group comparisons (*mdx* and their wild-type littermates, and *mdx52* and their wild-type littermates) in anxiety tests were analyzed using non-parametric Kruskal–Wallis tests followed by two-group post-hoc comparisons with Dunn's test.

Acknowledgements

We thank Dr. Jun Tanihata and Dr. Shin'ichi Takeda from the National Center of Neurology and Psychiatry (Tokyo, Japan) for kindly providing the *mdx52* breeder mice, and the Zootechnic platform of our institute for mouse breeding, care and genotyping.

Competing interests

The authors declare no competing or financial interests.

Author contributions

Conceptualization: C.V.; Methodology: C.S., C.V.; Validation: C.V.; Formal analysis: A.S., F.Z., C.S., C.I.; Investigation: A.S., F.Z., C.S., C.I.; Resources: C.V.; Data curation: A.S., F.Z., C.S., C.V.; Writing - original draft: A.S.; Writing - review & editing: C.S., A.G., C.V.; Visualization: A.S., C.I., C.V.; Supervision: C.V.; Project administration: C.V.; Funding acquisition: A.G., C.V.

Funding

This work was supported by the Centre National de la Recherche Scientifique; the Université Paris-Saclay; the Association Monégasque contre les Myopathies (to C.V.); and PhD fellowships from the Ministère de l'Enseignement Supérieur et de la Recherche (to A.S. and F.Z.) We also gratefully acknowledge support to C.V. and A.G. from the European Union Horizon 2020 Framework Programme research and innovation program 'Brain Involvement in Dystrophinopathies' (grant agreement, 847826).

References

- Anderson, J. L., Head, S. I., Rae, C. and Morley, J. W. (2002). Brain function in Duchenne muscular dystrophy. *Brain J. Neurol.* **125**, 4-13. doi:10.1093/brain/awf012
- Aoki, Y., Nakamura, A., Yokota, T., Saito, T., Okazawa, H., Nagata, T. and Takeda, S. (2010). In-frame dystrophin following exon 51-skipping improves muscle pathology and function in the exon 52-deficient *mdx* mouse. *Mol. Ther.* **18**, 1995-2005. doi:10.1038/mt.2010.186
- Araki, E., Nakamura, K., Nakao, K., Kameya, S., Kobayashi, O., Nonaka, I., Kobayashi, T. and Katsuki, M. (1997). Targeted disruption of exon 52 in the mouse dystrophin gene induced muscle degeneration similar to that observed in Duchenne muscular dystrophy. *Biochem. Biophys. Res. Commun.* **238**, 492-497. doi:10.1006/bbrc.1997.7328
- Aranmolate, A., Tse, N. and Colognato, H. (2017). Myelination is delayed during postnatal brain development in the *mdx* mouse model of Duchenne muscular dystrophy. *BMC Neurosci.* **18**, 63. doi:10.1186/s12868-017-0381-0
- Aupy, P., Zarrouki, F., Sandro, Q., Gastaldi, C., Buclez, P.-O., Mamchaoui, K., Garcia, L., Vaillend, C. and Goyenvalle, A. (2020). Long-term efficacy of AAV9-U7snRNA-mediated exon 51 skipping in *mdx52* mice. *Mol. Ther. Methods Clin. Dev.* **17**, 1037-1047. doi:10.1016/j.omtm.2020.04.025
- Bagdatlioglu, E., Porcari, P., Greally, E., Blamire, A. M. and Straub, V. W. (2020). Cognitive impairment appears progressive in the *mdx* mouse. *Neuromuscul. Disord.* **30**, 368-388. doi:10.1016/j.nmd.2020.02.018
- Beastrom, N., Lu, H., Macke, A., Canan, B. D., Johnson, E. K., Penton, C. M., Kaspar, B. K., Rodino-Klapac, L. R., Zhou, L., Janssen, P. M. L. et al. (2011). *mdx^{0cv}* mice manifest more severe muscle dysfunction and diaphragm force deficits than do *mdx* mice. *Am. J. Pathol.* **179**, 2464-2474. doi:10.1016/j.ajpath.2011.07.009
- Belmaati Cherkaoui, M., Vacca, O., Izabelle, C., Boulay, A.-C., Boulogne, C., Gillet, C., Bamier, J.-V., Rendon, A., Cohen-Salmon, M. and Vaillend, C. (2020). Dp71 contribution to the molecular scaffold anchoring aquaporin-4 channels in brain macroglial cells. *Glia* **69**, 954-970. doi:10.1002/glia.23941
- Benabdellam, R., Dorbani-Mamine, L., Benmessaoud-Mesbah, O., Rendon, A., Mhaouty-Kodja, S. and Hardin-Pouzet, H. (2012). Dp71 gene disruption alters the composition of the dystrophin-associated protein complex and neuronal nitric oxide synthase expression in the hypothalamic supraoptic and paraventricular nuclei. *J. Endocrinol.* **213**, 239-249. doi:10.1530/JOE-12-0066
- Beroud, C., Tuffery-Giraud, S., Matsuo, M., Hamroun, D., Humbertclaude, V., Monnier, N., Moizard, M. P., Voelckel, M. A., Calemard, L. M., Boisseau, P. et al. (2007). Multiexon skipping leading to an artificial DMD protein lacking amino acids from exons 45 through 55 could rescue up to 63% of patients with Duchenne muscular dystrophy. *Hum. Mutat.* **28**, 196-202. doi:10.1002/humu.20428
- Caudal, D., Francois, V., Lafoux, A., Ledevin, M., Anegon, I., Le Guiner, C., Larcher, T. and Huchet, C. (2020). Characterization of brain dystrophins absence and impact in dystrophin-deficient *Dmd^{mdx}* rat model. *PLoS ONE* **15**, e0230083. doi:10.1371/journal.pone.0230083
- Chaussonot, R., Amar, M., Fossier, P. and Vaillend, C. (2019). Dp71-dystrophin deficiency alters prefrontal cortex excitation-inhibition balance and executive functions. *Mol. Neurobiol.* **56**, 2670-2684. doi:10.1007/s12035-018-1259-6
- Chaussonot, R., Edeline, J.-M., Le Bec, B., El Massioui, N., Laroche, S. and Vaillend, C. (2015). Cognitive dysfunction in the dystrophin-deficient mouse model of Duchenne muscular dystrophy: A reappraisal from sensory to executive processes. *Neurobiol. Learn. Mem.* **124**, 111-122. doi:10.1016/j.nlm.2015.07.006
- Colombo, P., Nobile, M., Tesse, A., Civati, F., Gandossini, S., Mani, E., Molteni, M., Bresolin, N. and D'Angelo, G. (2017). Assessing mental health in boys with Duchenne muscular dystrophy: Emotional, behavioural and neurodevelopmental profile in an Italian clinical sample. *Eur. J. Paediatr. Neurol. EJPN Off. J. Eur. Paediatr. Neurol. Soc.* **21**, 639-647. doi:10.1016/j.ejpn.2017.02.007
- Culligan, K., Glover, L., Dowling, P. and Ohlendieck, K. (2001). Brain dystrophin-glycoprotein complex: persistent expression of beta-dystroglycan, impaired oligomerization of Dp71 and up-regulation of utrophins in animal models of muscular dystrophy. *BMC Cell Biol.* **2**, 2. doi:10.1186/1471-2121-2-2
- Dallérac, G., Perronet, C., Chagneau, C., Leblanc-Veyrac, P., Samson-Desvignes, N., Peltekian, E., Danos, O., Garcia, L., Laroche, S., Billard, J.-M. et al. (2011). Rescue of a dystrophin-like protein by exon skipping normalizes synaptic plasticity in the hippocampus of the *mdx* mouse. *Neurobiol. Dis.* **43**, 635-641. doi:10.1016/j.nbd.2011.05.012
- Daoud, F., Angeard, N., Demerre, B., Martie, I., Benyaou, R., Leturcq, F., Cossée, M., Deburgrave, N., Saillour, Y., Tuffery, S. et al. (2009a). Analysis of Dp71 contribution in the severity of mental retardation through comparison of Duchenne and Becker patients differing by mutation consequences on Dp71 expression. *Hum. Mol. Genet.* **18**, 3779-3794. doi:10.1093/hmg/ddp320
- Daoud, F., Candelario-Martinez, A., Billard, J.-M., Avital, A., Khelfaoui, M., Rozenvald, Y., Guegan, M., Momet, D., Jaillard, D., Nudel, U. et al. (2009b). Role of mental retardation-associated dystrophin-gene product Dp71 in excitatory synapse organization, synaptic plasticity and behavioral functions. *PLoS ONE* **4**, e6574. doi:10.1371/journal.pone.0006574
- Doorenweerd, N., Mahfouz, A., van Putten, M., Kaliyaperumal, R., T' Hoen, P. A. C., Hendriksen, J. G. M., Aartsma-Rus, A. M., Verschuuren, J. J. G. M., Niks, E. H., Reinders, M. J. T. et al. (2017). Timing and localization of human dystrophin isoform expression provide insights into the cognitive phenotype of Duchenne muscular dystrophy. *Sci. Rep.* **7**, 12575. doi:10.1038/s41598-017-12981-5
- Doorenweerd, N., Straathof, C. S., Dumas, E. M., Spitali, P., Ginjaar, I. B., Wokke, B. H., Schrans, D. G., van den Bergen, J. C., van Zwet, E. W., Webb, A. et al. (2014). Reduced cerebral gray matter and altered white matter in boys with Duchenne muscular dystrophy. *Ann. Neurol.* **76**, 403-411. doi:10.1002/ana.24222
- Felisari, G., Martinelli Boneschi, F., Bardoni, A., Sironi, M., Comi, G. P., Robotti, M., Turconi, A. C., Lai, M., Corrao, G. and Bresolin, N. (2000). Loss of Dp140 dystrophin isoform and intellectual impairment in Duchenne dystrophy. *Neurology* **55**, 559-564. doi:10.1212/WNL.55.4.559
- Frésard, L., Leroux, S., Dehais, P., Servin, B., Gilbert, H., Bouchez, O., Klopp, C., Cabau, C., Vignoles, F., Feve, K. et al. (2012). Fine mapping of complex traits in non-model species: using next generation sequencing and advanced intercross lines in Japanese quail. *BMC Genomics* **13**, 551. doi:10.1186/1471-2164-13-551
- Fritschy, J.-M., Panzanelli, P. and Tyagarajan, S. K. (2012). Molecular and functional heterogeneity of GABAergic synapses. *Cell. Mol. Life Sci. CMLS* **69**, 2485-2499. doi:10.1007/s00018-012-0926-4
- Godfrey, C., Clement, E., Mein, R., Brockington, M., Smith, J., Talim, B., Straub, V., Robb, S., Quinlivan, R., Feng, L. et al. (2007). Refining genotype-phenotype correlations in muscular dystrophies with defective glycosylation of dystroglycan. *Brain* **130**, 2725-2735. doi:10.1093/brain/awm212
- Goyenvalle, A., Griffith, G., Babbs, A., Andaloussi, S. E., Ezzat, K., Avril, A., Dugovic, B., Chaussonot, R., Ferry, A., Voit, T. et al. (2015). Functional correction in mouse models of muscular dystrophy using exon-skipping tricyclonol oligomers. *Nat. Med.* **21**, 270-275. doi:10.1038/nm.3765
- Guimaraes, C. V. A. and Dahmouh, H. M. (2020). Imaging phenotype correlation with molecular and molecular pathway defects in malformations of cortical development. *Pediatr. Radiol.* **50**, 1974-1987. doi:10.1007/s00247-020-04674-5
- Helleringer, R., Verger, D. L., Li, X., Izabelle, C., Chaussonot, R., Belmaati-Cherkaoui, M., Dammak, R., Decottignies, P., Daniel, H., Galante, M. et al. (2018). Cerebellar synapse properties and cerebellum-dependent motor and non-motor performance in Dp71-null mice. *Dis. Model. Mech.* **11**, dmm033258. doi:10.1242/dmm.033258
- Herry, C., Ciocchi, S., Senn, V., Demmou, L., Müller, C. and Lüthi, A. (2008). Switching on and off fear by distinct neuronal circuits. *Nature* **454**, 600-606. doi:10.1038/nature07166
- Hildyard, J. C. W., Crawford, A. H., Rawson, F., Riddell, D. O., Harron, R. C. M. and Piercy, R. J. (2020). Single-transcript multiplex *in situ* hybridisation reveals unique patterns of dystrophin isoform expression in the developing mammalian embryo. *Wellcome Open Res.* **5**, 76. doi:10.12688/wellcomeopenres.15762.1
- Hinton, V. J., Cyrułnik, S. E., Fee, R. J., Batchelder, A., Kiefel, J. M., Goldstein, E. M., Kaufmann, P. and De Vivo, D. C. (2009). Association of autistic spectrum disorders with dystrophinopathies. *Pediatr. Neurol.* **41**, 339-346. doi:10.1016/j.pediatrneurol.2009.05.011
- Hoffman, E. P., Brown, R. H., Jr and Kunkel, L. M. (1987). Dystrophin: the protein product of the Duchenne muscular dystrophy locus. *Cell* **51**, 919-928. doi:10.1016/0092-8674(87)90579-4
- Jamniczky, H. A. and Hallgrímsson, B. (2011). Modularity in the skull and cranial vasculature of laboratory mice: implications for the evolution of complex phenotypes. *Evol. Dev.* **13**, 28-37. doi:10.1111/j.1525-142X.2010.00453.x
- Janak, P. H. and Tye, K. M. (2015). From circuits to behaviour in the amygdala. *Nature* **517**, 284-292. doi:10.1038/nature14188
- Kameya, S., Araki, E., Katsuki, M., Mizota, A., Adachi, E., Nakahara, K., Nonaka, I., Sakuragi, S., Takeda, S. and Nabeshima, Y. (1997). Dp260 disrupted mice revealed prolonged implicit time of the b-wave in ERG and loss of accumulation of beta-dystroglycan in the outer plexiform layer of the retina. *Hum. Mol. Genet.* **6**, 2195-2203. doi:10.1093/hmg/6.13.2195
- Knuesel, I., Mastrocola, M., Zuellig, R. A., Bornhauser, B., Schaub, M. C. and Fritschy, J. M. (1999). Short communication: altered synaptic clustering of GABA_A receptors in mice lacking dystrophin (*mdx* mice). *Eur. J. Neurosci.* **11**, 4457-4462. doi:10.1046/j.1460-9568.1999.00887.x
- Kogelman, B., Khmelinskii, A., Verhaart, I., van Vliet, L., Bink, D. I., Aartsma-Rus, A., van Putten, M. and van der Weerd, L. (2018). Influence of full-length dystrophin on brain volumes in mouse models of Duchenne muscular dystrophy. *PLoS ONE* **13**, e0194636. doi:10.1371/journal.pone.0194636
- Lee, J. S., Pfund, Z., Juhász, C., Behen, M. E., Muzik, O., Chugani, D. C., Nigro, M. A. and Chugani, H. T. (2002). Altered regional brain glucose metabolism in Duchenne muscular dystrophy: a pet study. *Muscle Nerve* **26**, 506-512. doi:10.1002/mus.10238
- Lidov, H. G., Selig, S. and Kunkel, L. M. (1995). Dp140: a novel 140 kDa CNS transcript from the dystrophin locus. *Hum. Mol. Genet.* **4**, 329-335. doi:10.1093/hmg/4.3.329
- Lorusso, M. L., Civati, F., Molteni, M., Turconi, A. C., Bresolin, N. and D'Angelo, M. G. (2013). Specific profiles of neurocognitive and reading functions in a sample of 42 Italian boys with Duchenne Muscular Dystrophy. *Child Neuropsychol. J. Norm. Abnorm. Dev. Child. Adolesc.* **19**, 350-369. doi:10.1080/09297049.2012.660912

- Ma, Y., Hof, P. R., Grant, S. C., Blackband, S. J., Bennett, R., Slatest, L., McGuigan, M. D. and Benveniste, H. (2005). A three-dimensional digital atlas database of the adult C57BL/6J mouse brain by magnetic resonance microscopy. *Neuroscience* **135**, 1203-1215. doi:10.1016/j.neuroscience.2005.07.014
- Manning, J., Kulbida, R., Rai, P., Jensen, L., Bouma, J., Singh, S. P., O'Malley, D. and Yilmazer-Hanke, D. (2014). Amitriptyline is efficacious in ameliorating muscle inflammation and depressive symptoms in the *mdx* mouse model of Duchenne muscular dystrophy. *Exp. Physiol.* **99**, 1370-1386. doi:10.1113/expphysiol.2014.079475
- Miranda, R., Sébrié, C., Degrouard, J., Gillet, B., Jaillard, D., Laroche, S. and Vaillend, C. (2009). Reorganization of inhibitory synapses and increased PSD length of perforated excitatory synapses in hippocampal area CA1 of dystrophin-deficient *mdx* mice. *Cereb. Cortex N. Y. N.* **19**, 876-888. doi:10.1093/cercor/bhn135
- Mori, T., Yanagisawa, Y., Kitani, Y., Sugiyama, M., Kishida, O. and Nishimura, K. (2015). Gene expression profiles in *Rana pirica* tadpoles following exposure to a predation threat. *BMC Genomics* **16**, 258. doi:10.1186/s12864-015-1389-4
- Morris, G. E., Simmons, C. and Nguyen, T. M. (1995). Apo-dystrophins (Dp140 and Dp71) and dystrophin splicing isoforms in developing brain. *Biochem. Biophys. Res. Commun.* **215**, 361-367. doi:10.1006/bbrc.1995.2474
- Mortazavi, M., Ren, Y., Saini, S., Antaki, D., St. Pierre, C., Williams, A., Sohni, A., Wilkinson, M., Gymrek, M., Sebat, J. et al. (2021). Polymorphic SNPs, short tandem repeats and structural variants are responsible for differential gene expression across C57BL/6 and C57BL/10 substrains. *bioRxiv*, 2020.03.16.993683.
- Nico, B., Frigeri, A., Nicchia, G. P., Corsi, P., Ribatti, D., Quondamatteo, F., Herken, R., Girolamo, F., Marzullo, A., Svelto, M. et al. (2003). Severe alterations of endothelial and glial cells in the blood-brain barrier of dystrophic *mdx* mice. *Glia* **42**, 235-251. doi:10.1002/glia.10216
- Nonneman, D. J., Brown-Brandt, T., Jones, S. A., Wiedmann, R. T. and Rohrer, G. A. (2012). A defect in dystrophin causes a novel porcine stress syndrome. *BMC Genomics* **13**, 233. doi:10.1186/1471-2164-13-233
- Paprocka, J., Jezela-Stanek, A., Tytki-Szymańska, A. and Grunewald, S. (2021). Congenital disorders of glycosylation from a neurological perspective. *Brain Sci.* **11**, 88. doi:10.3390/brainsci11010088
- Paxinos, G. and Franklin, K. B. J. (2001). *The Mouse Brain in Stereotaxic Coordinates*, Compact, 2nd edn. San Diego: Academic Press.
- Paylor, R., Zhao, Y., Libbey, M., Westphal, H. and Crawley, J. N. (2001). Learning impairments and motor dysfunctions in adult *Lhx5*-deficient mice displaying hippocampal disorganization. *Physiol. Behav.* **73**, 781-792. doi:10.1016/S0031-9384(01)00515-7
- Phillips, R. G. and LeDoux, J. E. (1992). Differential contribution of amygdala and hippocampus to cued and contextual fear conditioning. *Behav. Neurosci.* **106**, 274-285. doi:10.1037/0735-7044.106.2.274
- Poysky, J., Behavior in DMD Study Group. (2007). Behavior patterns in Duchenne muscular dystrophy: report on the Parent Project Muscular Dystrophy behavior workshop 8-9 of December 2006, Philadelphia, USA. *Neuromuscul. Disord.* **17**, 986-994. doi:10.1016/j.nmd.2007.06.465
- Razzoli, M., Lindsay, A., Law, M. L., Chamberlain, C. M., Southern, W. M., Berg, M., Osborn, J., Engeland, W. C., Metzger, J. M., Ervasti, J. M. et al. (2020). Social stress is lethal in the *mdx* model of Duchenne muscular dystrophy. *EBioMedicine* **55**, 102700. doi:10.1016/j.ebiom.2020.102700
- Ricotti, V., Mandy, W. P. L., Scoto, M., Pane, M., Deconinck, N., Messina, S., Mercuri, E., Skuse, D. H. and Muntoni, F. (2016). Neurodevelopmental, emotional, and behavioural problems in Duchenne muscular dystrophy in relation to underlying dystrophin gene mutations. *Dev. Med. Child Neurol.* **58**, 77-84. doi:10.1111/dmcn.12922
- Romo-Yáñez, J., Rodríguez-Martínez, G., Aragón, J., Siqueiros-Márquez, L., Herrera-Salazar, A., Velasco, I. and Montañez, C. (2020). Characterization of the expression of dystrophins and dystrophin-associated proteins during embryonic neural stem/progenitor cell differentiation. *Neurosci. Lett.* **736**, 135247. doi:10.1016/j.neulet.2020.135247
- Sarig, R., Mezger-Lallemand, V., Gitelman, I., Davis, C., Fuchs, O., Yaffe, D. and Nudel, U. (1999). Targeted inactivation of Dp71, the major non-muscle product of the DMD gene: differential activity of the Dp71 promoter during development. *Hum. Mol. Genet.* **8**, 1-10. doi:10.1093/hmg/8.1.1
- Satz, J. S., Ostendorf, A. P., Hou, S., Turner, A., Kusano, H., Lee, J. C., Turk, R., Nguyen, H., Ross-Barta, S. E., Westra, S. et al. (2010). Distinct functions of glial and neuronal dystroglycan in the developing and adult mouse brain. *J. Neurosci.* **30**, 14560-14572. doi:10.1523/JNEUROSCI.3247-10.2010
- Sebrié, C., Chabert, C., Ledru, A., Guedj, F., Po, C., Smith, D. J., Rubin, E., Rivals, I., Beloeil, J.-C., Gillet, B. et al. (2008). Increased dosage of DYRK1A and brain volumetric alterations in a YAC model of partial trisomy 21. *Anat. Rec. Hoboken NJ* **2007**, 254-262. doi:10.1002/ar.20640
- Sekiguchi, M., Zushida, K., Yoshida, M., Maekawa, M., Kamichi, S., Sahara, Y., Yuasa, S., Takeda, S. and Wada, K. (2009). A deficit of brain dystrophin impairs specific amygdala GABAergic transmission and enhances defensive behaviour in mice. *Brain* **132**, 124-135. doi:10.1093/brain/awn253
- Septien, L., Gras, P., Borsotti, J. P., Giroud, M., Nivelon, J. L. and Dumas, R. (1991). [Mental development in Duchenne muscular dystrophy. Correlation of data of the brain scanner]. *Pediatrics* **46**, 817-819.
- Snow, W. M., Anderson, J. E. and Jakobson, L. S. (2013). Neuropsychological and neurobehavioral functioning in Duchenne muscular dystrophy: a review. *Neurosci. Biobehav. Rev.* **37**, 743-752. doi:10.1016/j.neubiorev.2013.03.016
- Taylor, P. J., Betts, G. A., Maroulis, S., Gilissen, C., Pedersen, R. L., Mowat, D. R., Johnston, H. M. and Buckley, M. F. (2010). Dystrophin gene mutation location and the risk of cognitive impairment in Duchenne muscular dystrophy. *PLoS ONE* **5**, e8803. doi:10.1371/journal.pone.0008803
- Tsai, H.-H., Niu, J., Munji, R., Davalos, D., Chang, J., Zhang, H., Tien, A.-C., Kuo, C. J., Chan, J. R., Daneman, R. et al. (2016). Oligodendrocyte precursors migrate along vasculature in the developing nervous system. *Science* **351**, 379-384. doi:10.1126/science.aad3839
- Vaillend, C., Billard, J. M., Claudepierre, T., Rendon, A., Dutar, P. and Ungerer, A. (1998). Spatial discrimination learning and CA1 hippocampal synaptic plasticity in *mdx* and *mdx*^{3cv} mice lacking dystrophin gene products. *Neuroscience* **86**, 53-66. doi:10.1016/S0306-4522(98)00023-2
- Vaillend, C., Billard, J.-M. and Laroche, S. (2004). Impaired long-term spatial and recognition memory and enhanced CA1 hippocampal LTP in the dystrophin-deficient *Dmd*^{mdx} mouse. *Neurobiol. Dis.* **17**, 10-20. doi:10.1016/j.nbd.2004.05.004
- Vaillend, C. and Chaussonot, R. (2017). Relationships linking emotional, motor, cognitive and GABAergic dysfunctions in dystrophin-deficient *mdx* mice. *Hum. Mol. Genet.* **26**, 1041-1055.
- Vaillend, C., Perronet, C., Ros, C., Gruszczynski, C., Goyenvalle, A., Laroche, S., Danos, O., Garcia, L. and Peltekian, E. (2010). Rescue of a dystrophin-like protein by exon skipping *in vivo* restores GABAA-receptor clustering in the hippocampus of the *mdx* mouse. *Mol. Ther.* **18**, 1683-1688. doi:10.1038/mt.2010.134
- Vaillend, C., Poirier, R. and Laroche, S. (2008). Genes, plasticity and mental retardation. *Behav. Brain Res.* **192**, 88-105. doi:10.1016/j.bbr.2008.01.009
- Vaillend, C., Rendon, A., Misslin, R. and Ungerer, A. (1995). Influence of dystrophin-gene mutation on *mdx* mouse behavior. I. Retention deficits at long delays in spontaneous alternation and bar-pressing tasks. *Behav. Genet.* **25**, 569-579. doi:10.1007/BF02327580
- Vaillend, C. and Ungerer, A. (1999). Behavioral characterization of *mdx*^{3cv} mice deficient in C-terminal dystrophins. *Neuromuscul. Disord.* **9**, 296-304. doi:10.1016/S0960-8966(99)00029-2
- Wallace, K. J. and Rosen, J. B. (2001). Neurotoxic lesions of the lateral nucleus of the amygdala decrease conditioned fear but not unconditioned fear of a predator odor: comparison with electrolytic lesions. *J. Neurosci.* **21**, 3619-3627. doi:10.1523/JNEUROSCI.21-10-03619.2001
- Young, H. K., Barton, B. A., Waisbren, S., Portales Dale, L., Ryan, M. M., Webster, R. I. and North, K. N. (2008). Cognitive and psychological profile of males with Becker muscular dystrophy. *J. Child Neurol.* **23**, 155-162. doi:10.1177/0883073807307975

I.3. Impact of the genetic background on cognitive and behavioral processes

Research studies evidenced differences in the severity of muscular dystrophy in DMD associated to the genetic background. The severity of the central deficits are reported to be associated with the loss of multiple brain dystrophins. Yet, less is known about the impact of the genetic background. The original Dp427 deficient-*mdx* mouse model was generated in a C57BL/10 background and its phenotype has been largely characterized and described (Vaillend et al., 1995, 2004; Vaillend and Chaussonot, 2017; Engelbeen et al., 2021).

We addressed the behavioral deficits of the *mdx5^{cv}* mouse model also lacking Dp427 but generated on C57BL/6 genetic background. The behavioral phenotype of *mdx5^{cv}* was compared to the *mdx52* mouse that was generated on the same genetic background ([Publication 3, in preparation](#)). The aim of this study was two-fold: (1) to determine the involvement of the genetic background on different mutations in DMD mouse models (by evaluating phenotype differences in *mdx5^{cv}* compared to the phenotype previously reported in the original *mdx* mouse, and (2) to compare the impact of a unique loss of Dp427 (*mdx5^{cv}*) with loss of Dp427+Dp140 (*mdx52*) on emotional reactivity, learning and memory processes. The phenotyping addressed a wide range of behavioral tests previously characterized in the *mdx* model. In the scope of the BIND consortium project, this work was conducted in collaboration with Transpharmation Ireland Ltd. Laboratory and Dr. Mitsogiannis M. and I equally contributed to this work. I do not present the totality of the study here but focus on the experiments I have performed and that will be included in the paper in preparation.

Among the behavioral testing, I first assessed the anxiety of *mdx5^{cv}* mouse model using the elevated plus maze, the light-dark choice test and the Open Field exploration. Furthermore, different memory processes were tested in the *mdx52* model. Spatial memory was assessed in a delayed alternation task in a T-maze, at various delays to assess both short and long-term memories (1h-6h and 24h). The spatial and non-spatial recognition memories were tested using various protocols of object recognition (recognition of object location versus novel object).

Emotional reactivity

A group of 2-month-old *mdx5^{cv}* (n=10) and their WT littermates (n=15) were submitted to a similar battery of tests that was used for *mdx* and *mdx52* model characterization. At first, the free exploration of an Open field during 30 minutes was analyzed. The avoidance of the center part of the arena constitutes the expression of the anxious behavior. [Figure 24 A](#) shows the percent of distance and time spent in the center of the OF and *mdx5^{cv}* mice behaved similarly to their WT littermates. The

changes in emotional reactivity could not be detected in this test. To better estimate the anxious phenotype, the same groups of *mdx5cv* and their WT littermates were next submitted to two additional anxiety tests: the light-dark choice (LDC) and elevated plus-maze (EPM) tests. LDC is based on the choice given to the mice to stay in a secure dark compartment or to explore an anxiogenic (brightly lit) compartment characterized by a gradient of illumination from the trap door (50 lx) to the end of the compartment (600 lx). The anxious phenotype is expressed by the percent of time spent and the number of entries in the lit box. As shown in [figures 24 B](#), *mdx5cv* exhibited increased anxious phenotype as they entered less in the lit box and once in, spent significantly less time as compared to their WT littermates. In the EPM test, anxiety results from the threat induced by the void in the elevated open arms. The percent time and entries in the open arms was significantly lower in the *mdx5cv* group ([Figure 24 C](#)). Overall, the anxiety phenotype of *mdx5cv* appeared affected and more defined than the borderline phenotype of the *mdx* model (Vaillend and Chaussonot, 2017). Yet, the phenotype is less severe than in *mdx52* mice (Saoudi et al., 2021).

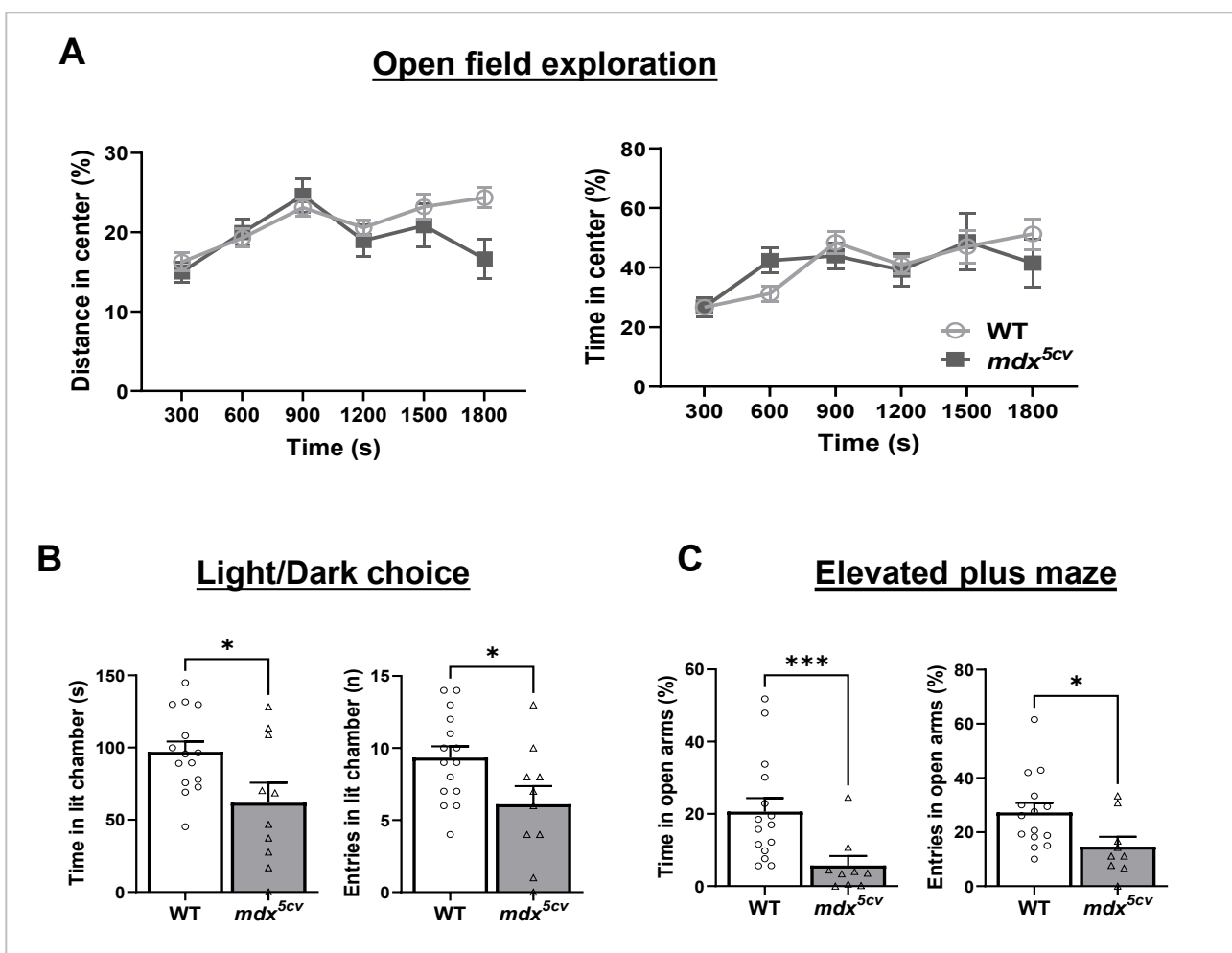


Figure 24. Emotional related behaviors . (A) Free exploration of an open field during 25 min in 2-month-old *mdx5cv*. Percent of distance and time spent in the center of the arena expressed per bins of 5 minutes. (B) Light/Dark choice test.

The time spent in the lit box and the number of entries. (C) Elevated plus maze test. Percent of time and percent of entries in the open arms. Data are mean± SEM. ***P<0.001; **P<0.01; *P<0.05.

Spatial recognition memory

A group of 3-4 months-old *mdx52* (n=18) and their WT littermates (n=21) have been submitted to a T-maze alternation task. In a first 2-trial session (Acquisition), mice were forced to explore one of the two lateral arms of a T maze. Spatial recognition memory was evaluated by the percent of mice alternating their arm choice during a retention session after a variable delay (1h, 6h and 24h) (Figure 25 A). The latency to choose an arm at the retention session was significantly increased for *mdx52* mice as compared to the WT (Figure 25 B). This supports the enhanced emotional reactivity of the *mdx52* model. Further, the recognition memory was reflected by a significant alternation rate compared to chance level (50% alt.) at all delays. No differences were found between genotypes reflecting no deficit in this task (Figure 25 C). In contrast, *mdx* mice have previously been reported to exhibit impaired retention at 24h delay (Vaillend et al., 1995).

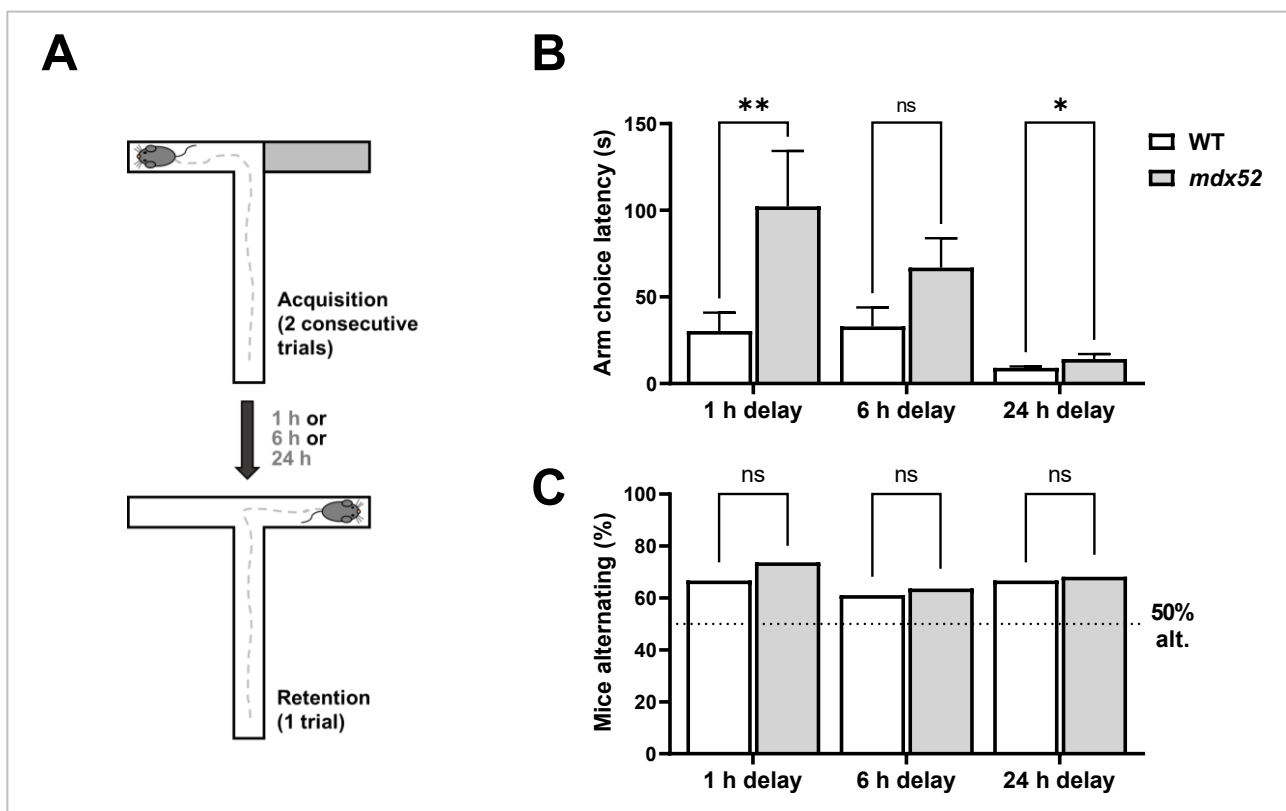


Figure 25. Spatial memory. (A) Schematic representation of the testing protocol. (B) Latency to choose an arm during the retention session. (C) The percent of mice alternating arms during the retention session.

Spatial and non-spatial recognition memory

Object recognition memory, which is impaired in *mdx* mice at a 24h retention delay (Vaillend et al., 2004), was assessed in *mdx52* (n=13) and WT littermate (n=17) mice at 3 months old. At first, we used a similar protocol as for *mdx*, i.e. a set of 2 different objects (Figure 26 A). The animals underwent a habituation period of 1 week and were then submitted to two different objects during an acquisition session. The recognition memory with a novel object was assessed 10' and 24h later expressed as a recognition index (Figure 26 B). The recognition index appeared similar to chance level (about 50% exploration of each objects) at 10' and 24h delays, reflecting no recognition memory even in the WT group. This result suggested that this protocol may not be appropriate for mice with a C57BL/6 genetic background. We thus adapted the protocol using a more simple set of two identical objects during the acquisition (Figure 26 C). The recognition index of both genotypes appeared significantly different from chance level at 10' and 24h delays (Figure 26 D). No differences were found between *mdx52* and WT reflecting no deficits of short- and long-term recognition memory. The impaired long-term memory of *mdx* mice was not replicated in this test.

Following the previously used 1-week habituation the animals were agitated and frequently climbed on the objects. Also, they exhibited increased jumping against the walls of the arena which reflects increased frustration. Consequently, they were not interested in the task which compromised the testing. We further adapted the protocol, by shortening the habituation that precedes the test to a single day. We submitted another group of *mdx52* (n=14) and their WT littermates (n=14) to an alternative protocol involving recognition memory of a set of 3 different objects during the acquisition session. The recognition memory was assessed 24h later, first by replacing one object with a novel one (Figure 26 E). The recognition index of WT was significantly different from chance level (33% for 3 objects) while *mdx52* failed to reach it (Figure 26 F). Yet, no difference was found between *mdx52* and WT reflecting a slightly impaired phenotype. The same protocol allows to address spatial object recognition memory, by moving an object at the retention session (Figure 26 G). The recognition index was significantly different from chance level (33%) and similar for both genotypes (Figure 26 H). In line with the T-maze results, the spatial object recognition memory did not appear impaired in *mdx52* model.

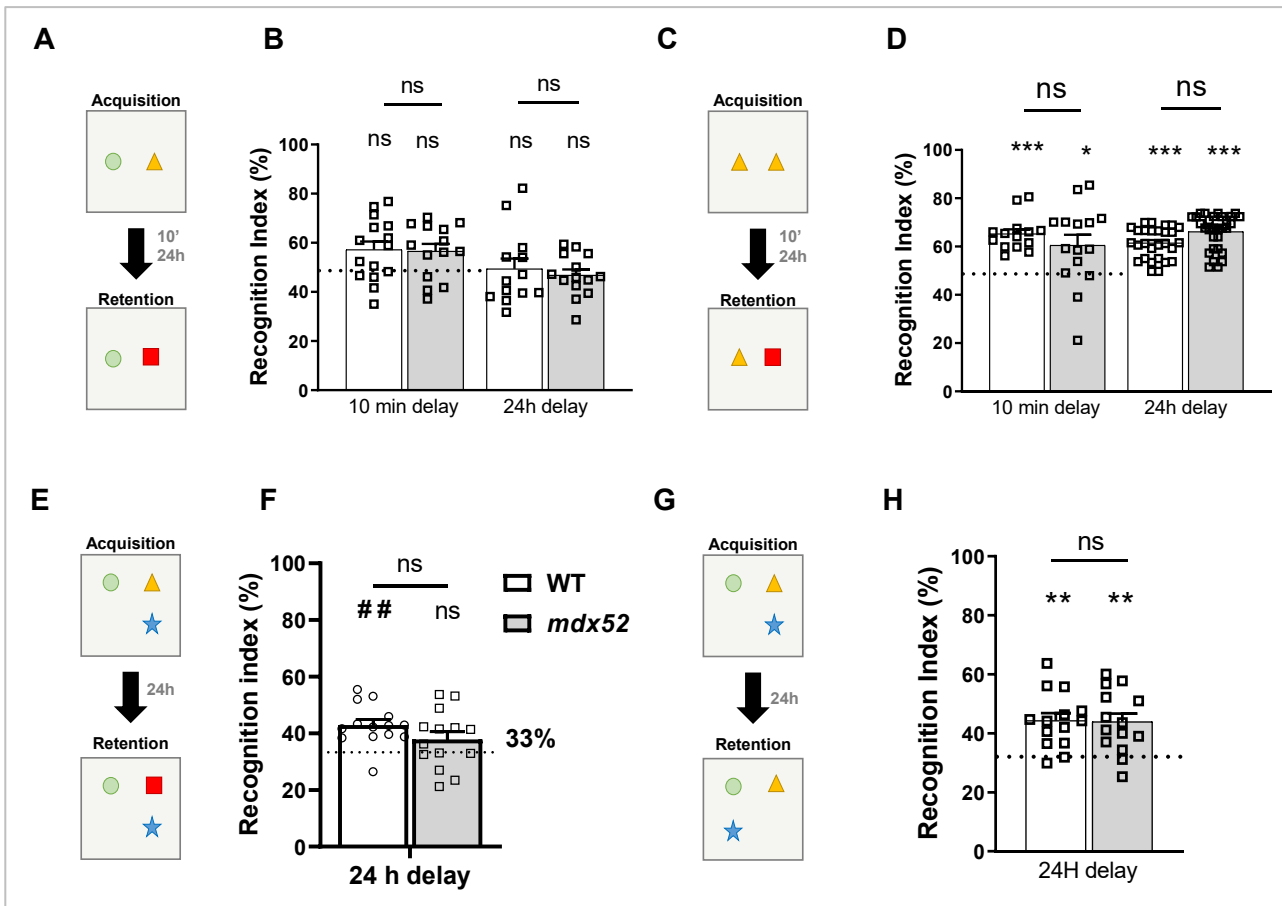


Figure 26. Spatial and non-spatial recognition memory in *mdx52* mice. (A) Schematic representation of the assay protocol for novel object recognition with a 2-different objects set at acquisition. (B) Recognition index at 10min and 24h delays. (C) Schematic representation of the assay protocol for novel object recognition with a 2-identical objects set at acquisition. (D) Recognition index at 10min and 24h delays. (E) Schematic representation of the assay protocol for novel object recognition with a 3-different objects set at acquisition. (F) Recognition index at 24h delay. (G) Schematic representation of the assay protocol for spatial object recognition with a 3-different objects set at acquisition. (H) Recognition index at 24h delay. Data are presented as mean + SEM. The percentage recognition index is calculated as the percentage of novel object exploration time over the total object exploration time measured during the 5 min retention trial. # $p < 0.05$, ## $p < 0.01$, ### $p < 0.001$ vs chance level (50% in two objects or 33.33% in three objects). Ns: non-significant difference.

This comparative study first confirm the genotype-phenotype relationship for emotional alteration deficits. The unique loss of *Dp427* leads to a less severe phenotype regardless of the genetic background, as compared to *mdx52* mice. Moreover, these results evidence the genetic background may have a substantial contribution in the expression of certain behavioral performance, such as in recognition memory tasks. This conclusion will be further developed in the general discussion of this thesis manuscript.

- II -

**Optimization of ASO-based therapeutic exon
skipping in the CNS**

ASOs-based exon skipping approaches are, so far, among the most promising therapies for DMD. In fact, it enables the restoration of the *DMD* gene reading frame and 80% of DMD patients are eligible for this strategy (Lu et al., 2000). The use of ASOs for central alterations treatment in DMD is not yet widely established. Indeed, ASO-based therapeutics injected systemically (intravenously) cannot readily cross the blood brain barrier (BBB) to target the central nervous system (CNS). Therefore, investigation of their effects in the central nervous system (CNS) requires local delivery to the CNS. Different chemistries of ASO have been developed for exon skipping strategies aiming at restoring dystrophin expression for DMD. The tcDNA-ASO, an alternative chemistry of ASOs, was the first to show ability to cross the BBB following a systemic treatment in *mdx* mouse. This treatment induced 2-4% of exon 23 skipping levels, in various brain structures including hippocampus, cortex and cerebellum. A recent study showed the feasibility and the efficacy of a local intracerebroventricular (ICV) injection of tcDNA targeting the exon 23 in *mdx* mice (Zarrouki et al., 2022). Another ASO developed for DMD was shown to induce efficient exon skipping in the brain of *mdx* mice following local ICV delivery: the PMO chemistry (Sekiguchi et al., 2009), which received the FDA approval in 2016 for the systemic treatment of DMD patients (Syed, 2016).

Material and methods: The direct delivery to the CNS of tcDNA and PMO ASO both targeting the exon 51 was compared using different injections techniques. First, we used the intracerebroventricular (ICV) delivery. The distribution was assessed by comparing unilateral and bilateral ICV. Different rates of injections were tested: a bolus rate previously reported to be efficient and a slower rate, closer to the physiological flow of the cerebrospinal fluid (CSF). The maximal reachable ASOs efficacy was analysed following repeated bolus ICV injections *via* cannula or very slow ICV *via* osmotic pumps. We then investigated a less studied method of intrathecal delivery, the intra- *cisterna magna* (ICM) delivery. ICM delivery is a less invasive procedure than the ICV and constitutes an alternative route for local delivery at a more posterior level of the brain, adjacent to the cerebellum, hindbrain, and cervical spine. A minimally invasive method for ICM delivery through the skin was defined and compared to the single and triple ICV injections. Aiming to reach the maximal efficacy, we combined ICM and ICV deliveries. The efficacy of both ASO molecules was measured by RT-qPCR to assess the level of exon 51 skipping in various CNS structures (cerebellum, hippocampus, cortex, and cervical spine) that physiologically express Dp427 and are involved in functions found to be impaired in DMD.

Results: TcDNA single ICV injection led to 20-35% of exon skipping and PMO single ICV to only 10%. Repeated delivery of tcDNA into the ventricles did not improve the efficacy and rather

demonstrated high variability. For PMO, multiple ICV induced slightly higher efficacy than single PMO ICV.

While single ICM led to 5% of skipping for both molecules, triple ICM deliveries were significantly more efficient reaching 20-35% for tcDNA and 20% for PMO.

Following combined ICM and ICV delivery, ASOs appeared distributed homogeneously across the studied structures and exon skipping efficacy reached ~35% for tcDNA and 15-20% for the PMO.

Conclusion: Despite multiple injections via various delivery routes, the efficacy of PMO-induced exon skipping did not reach that of tcDNA. The injection of maximal feasible dose in adult mice led to a maximum of 35% of exon 51 skipping across the various brain regions in the *mdx52* mice. Our results provide useful insights into the local delivery and associated efficacy of ASOs in the CNS of DMD mouse models. These findings also highlight the importance and the specificity of the delivery route, the dose and treatment conditions for each ASO-based treatments targeting the CNS.



Article

Investigating the Impact of Delivery Routes for Exon Skipping Therapies in the CNS of DMD Mouse Models

Amel Saoudi ^{1,2}, Claire Fergus ³, Talia Gileadi ⁴, Federica Montanaro ⁴, Jennifer E. Morgan ⁴, Vincent P. Kelly ³, Thomas Tensorer ⁵, Luis Garcia ¹, Cyrille Vaillend ², Francesco Muntoni ^{4,*} and Aurélie Goyenvalle ^{1,*}

- ¹ Université Paris-Saclay, UVSQ, Inserm, END-ICAP, 78000 Versailles, France
² Université Paris-Saclay, CNRS, Institut des Neurosciences Paris-Saclay, 91400 Saclay, France
³ School of BiocChemistry& Immunology, Trinity Biomedical Sciences Institute, Trinity College Dublin, Dublin D02 R590, Ireland
⁴ Dubowitz Neuromuscular Centre, UCL Great Ormond Street Institute of Child Health, 30 Guildford Street, London WC1N 1EH, UK
⁵ SQY Therapeutics-Synthena, UVSQ, 78180 Montigny le Bretonneux, France
* Correspondence: f.muntoni@ucl.ac.uk (F.M.); aurelie.goyenvalle@uvsq.fr (A.G.)

Abstract: Nucleic acid-based therapies have demonstrated great potential for the treatment of monogenetic diseases, including neurologic disorders. To date, regulatory approval has been received for a dozen antisense oligonucleotides (ASOs); however, these chemistries cannot readily cross the blood–brain barrier when administered systemically. Therefore, an investigation of their potential effects within the central nervous system (CNS) requires local delivery. Here, we studied the brain distribution and exon-skipping efficacy of two ASO chemistries, PMO and tCDNA, when delivered to the cerebrospinal fluid (CSF) of mice carrying a deletion in exon 52 of the dystrophin gene, a model of Duchenne muscular dystrophy (DMD). Following intracerebroventricular (ICV) delivery (unilateral, bilateral, bolus vs. slow rate, repeated via cannula or very slow via osmotic pumps), ASO levels were quantified across brain regions and exon 51 skipping was evaluated, revealing that tCDNA treatment invariably generates comparable or more skipping relative to that with PMO, even when the PMO was administered at higher doses. We also performed intra-cisterna magna (ICM) delivery as an alternative route for CSF delivery and found a biased distribution of the ASOs towards posterior brain regions, including the cerebellum, hindbrain, and the cervical part of the spinal cord. Finally, we combined both ICV and ICM injection methods to assess the potential of an additive effect of this methodology in inducing efficient exon skipping across different brain regions. Our results provide useful insights into the local delivery and associated efficacy of ASOs in the CNS in mouse models of DMD. These findings pave the way for further ASO-based therapy application to the CNS for neurological disease.

Keywords: ASO-based therapy; central nervous system; intracerebroventricular injection; intrathecal injection; antisense oligonucleotides; exon-skipping; Duchenne muscular dystrophy; CNS delivery

Citation: Saoudi, A.; Fergus, C.; Gileadi, T.; Montanaro, F.; Morgan, J.; Kelly, V.P.; Tensorer, T.; Garcia, L.; Vaillend, C.; Muntoni, F.; et al. Investigating the Impact of Delivery Routes for Exon Skipping Therapies in the CNS of DMD Mouse Models. *Cells* **2023**, *12*, 908. <https://doi.org/10.3390/cells12060908>

Academic Editor: Izuho Hatada

Received: 12 February 2023

Revised: 7 March 2023

Accepted: 13 March 2023

Published: 15 March 2023



Copyright: © 2023 by the authors. Licensee MDPI, Basel, Switzerland. This article is an open access article distributed under the terms and conditions of the Creative Commons Attribution (CC BY) license (<https://creativecommons.org/licenses/by/4.0/>).

1. Introduction

Antisense oligonucleotides (ASOs) hold tremendous therapeutic potential for many genetic diseases. ASOs are short, synthetic, single-stranded oligonucleotides that can bind to mRNA and non-coding RNAs to reduce, restore, or modify protein expression [1–3]. Several ASOs have already reached market approval, in particular for the treatment of neuromuscular disorders, such as spinal muscular atrophy (SMA) and Duchenne muscular dystrophy (DMD). DMD is a neuromuscular disease with an incidence of 1:5000 boys, who carry mutations in the *DMD* gene that disrupt the open-reading frame of the dystrophin protein (Dp) in muscle, heart, and brain [4,5]. The ASOs used in DMD aim to

restore the open reading frame to produce an internally deleted but still functional protein [6–8]. Over the past decade, a number of ASOs have been developed to target exons flanking different relatively common groups of DMD mutations, leading to four such therapies being conditionally approved by the FDA. These ASOs require regular (weekly) systemic administration via an intravenous route. However, none of these ASOs can address DMD brain comorbidities, which have a significant impact on the patients' quality of life. These include intellectual disability and neurobehavioral comorbidities, affecting between 30 and 50% of individuals with DMD [9,10]. The European *Brain Involvement in Dystrophinopathies* (BIND) consortium (<https://bindproject.eu/>, accessed on 6 February 2023) aims to investigate and characterize further the role of the various dystrophin isoforms in the CNS and evaluate the potential reversibility of the central deficits associated with the lack of dystrophin. In this context, we are using the exon 52-deleted *mdx52* mouse model of DMD [11], as this mutation is located in a “hot spot” region that is frequently mutated in DMD patients [10,12,13]. We previously showed that *mdx52* mice, lacking Dp427, Dp260, and Dp140, display enhanced anxiety and fearfulness and impaired associative fear learning as compared to the original Dp427 deficient-*mdx* mouse model [14]. The development of therapeutic approaches in this mouse model is thus of great interest, as it directly translates to patients' conditions. As part of our investigations, we first aimed to optimize the administration route to achieve high and widespread delivery of ASOs in the CNS of DMD mouse models.

Considering that the systemic delivery of ASO requires high doses and results in very low efficacy in the CNS, mostly due to the inability of oligonucleotides to efficiently cross the blood–brain barrier (BBB), we focused on local delivery to the CNS. One of the most common delivery method to the CNS is administration to the cerebrospinal fluid (CSF) [15,16]. CSF continuously flows in cerebral ventricles, the subarachnoid, cisternal spaces, and the spinal canal. Its direct contact with the CNS makes it an ideal delivery route to achieve widespread distribution to the CNS [17], although different regions are targeted with different efficiencies. CSF delivery can be achieved via injection into the cerebral ventricles, the lumbar intrathecal space, or the *cisterna magna*. The most commonly used delivery route to the CSF, in particular for rodents, is via intracerebroventricular (ICV) injection based on specific stereotaxic coordinates [18]. On the other hand, intrathecal (IT) delivery via lumbar puncture is a convenient delivery strategy not only because it does not require a stereotaxic set up but also because of ease of access and minimal invasiveness [19–21]. This method results in efficient drug distribution to the spinal cord in animal models and patients and is successfully used in the clinic for the administration of the ASO Nusinersen to SMA patients [22]. However, preclinical data in animal models also suggest that lumbar intrathecal delivery results in limited distribution to the supratentorial brain structures [23], which are the target for DMD therapies. As an alternative to lumbar delivery, administration into the *cisterna magna* has been used in animal models to achieve delivery closer to brain structures. This method has resulted in widespread distribution to the cerebellum, hindbrain, and spinal cord in mice [23].

In the present study, we aimed to optimize ASO efficacy in the CNS, to reach the highest possible exon-skipping levels in brain regions known to express dystrophin, such as the cerebellum, hippocampus, and cortex. We therefore evaluated different delivery methods, in particular ICV and ICM (intra-cisterna magna), using various injection regimens. Notably, we compared unilateral vs. bilateral ICV injections and a bolus vs. slow rate of injection, as well as the repeated administration of ASO using a cannula and continuous administration using osmotic pumps. Finally, we studied the feasibility and resulting effects of combining both ICM and ICV delivery methods.

Considering that ASO biodistribution in the CNS may be affected by various factors, such as ASO chemistry and charge, we used two different chemistries of ASO in this study: the Phosphorodiamidate Morpholino Oligomer (PMO) chemistry and the tricyclo-DNA (tcDNA) chemistry. PMOs have a neutral charge and are already approved by the FDA for the systemic treatment of DMD [8], while tcDNA is a charged, lipid-conjugated ASO

that has previously shown therapeutic potential in mouse models of DMD [24,25]. Overall, our detailed comparative study provides useful insights into the local delivery and associated efficacy of ASOs in the CNS of mouse models of DMD.

2. Materials and Methods

2.1. Animals and Antisense Oligonucleotides

Mdx52 mice (B6;129S-*Dmd*^{tm1Mok}) breeders were generously provided by Prof. Sasaoka Toshikuni and Dr. Motoya Katsuki (Department of Comparative & Experimental Medicine, Brain Research Institute, Niigata University, Japan) and kindly shipped to our laboratories by Dr. Jun Tanihata and Dr. Shin'ichi Takeda (National Center of Neurology and Psychiatry, Tokyo, Japan). *Mdx52* mice contain a neomycin cassette in place of exon 52 of the *DMD* gene on the X chromosome, thereby disrupting the *dmd* gene reading frame and eliminating the expression of Dp427, Dp260, and Dp140 dystrophin isoforms, but preserving the expression of Dp116 (in peripheral nerves) and of Dp71 (in brain and retina) [11] (for a review of DMD isoforms see [26]). Optimization experiments were performed using hDMD mice expressing the human dystrophin gene [27,28]. The mouse lines were backcrossed with the C57BL/6J strain for more than eight generations. At the animal facility Plateforme 2Care, UFR des Sciences de la santé, Université de Versailles-Saint Quentin (France), heterozygous females were crossed to C57BL/6J male mice to generate *mdx52* and littermate control (WT) males.

At Trinity Biomedical Sciences Institute (TBSI), Trinity College Dublin, heterozygous females were crossed to C57BL/6J males to generate *mdx52* and littermate control (WT) males. Genotypes were determined via PCR analysis of DNA from tail or ear biopsies. Mice were housed in individually ventilated cages (IVC, Tecniplast) in a specific pathogen-free facility on a 12 h light/dark cycle with access to food and water *ad libitum*. Animal care and all experimental procedures complied with the national and European legislation, approved by the French government (Ministère de l'Enseignement Supérieur et de la Recherche, Autorisation APAFiS #6518) and the Irish Health Products Regulatory Authority (Ref: AE19136/P131) and with the approval of the TCD Animal Research Ethics Committee.

The tcDNA-ex51 used in this study targets an exonic splicing enhancer within exon 51 of the dystrophin pre-mRNA (position +48 + 62, sequence GGAGATGGCAGTTTC) and was synthesized by SQY Therapeutics (Montigny-le-Bretonneux, France). Palmitic acid was conjugated at the 5' end of the tcDNA full phosphodiester via a C6-amino linker and a phosphorothioate bond as previously described [24]. M51D PMO used in this study targets the *Dmd* exon 51 splice donor site (position + 10 - 15, sequence TTGTTTATCCATACCTTCTGTTG) (Genetools LLC, Philomath, USA). For analysis of *in situ* biodistribution, a carboxyfluorescein-conjugated control PMO (CCTCTTACCTCAGTTACAATTTATA, Genetools LLC, Philomath, USA) was used. PMO was resuspended in sterile phosphate buffered saline and heated to 65 °C for 15 min before use to ensure solubility.

ASO administrations were performed using 6–8-week-old *mdx52* and WT mice anesthetized via intraperitoneal injection of a ketamine (95 mg/kg)/medetomidine (1 mg/kg) mixture. For intracerebroventricular injections (ICV), tcDNA-Ex51 or M51D PMO solutions were bilaterally injected into the lateral brain ventricles (−0.5 mm anterior and 1 mm lateral from bregma; −2 mm from pia). A volume of 5 µL was infused into each ventricle, i.e., a total volume of 10 µL of ASO corresponding to 400 µg of tcDNA (71 nmol) and 900 µg for PMO (107 nmol). The slow-bolus rate of 0.3 µL/min was compared to a bolus rate of 0.6 µL/s, which was the fastest rate achievable with the injection system (Legato 130 pump from KD scientific). For intra-cisterna magna injections (ICM), 10 µL of tcDNA-Ex51 (i.e., 400 µg) or M51D PMO (i.e., 900 µg) solutions were administered, using a 30-gauge stainless steel needle with a point 4 style bevel curved (45°) 2 mm from the tip, so that it was J-shaped.

Repeated ICV delivery was performed using cannula implants in the lateral ventricles (−0.5 mm from bregma; 1 mm lateral; −2 mm from pia) and an infusion rate of 0.6 $\mu\text{L}/\text{min}$ during each infusion, while the animals were under isoflurane anesthesia. Infusions were repeated between 3 and 5 times with a minimal recovery of 3 days between each infusion. For tcDNA, 3 and 5 infusions were performed corresponding to a total injected dose of 1 and 2 mg respectively (−176 and 352 nmol). For PMO, 4 infusions were performed corresponding to a total injected dose of 2.7 mg (−320 nmol).

For continuous slow delivery, osmotic pumps (Alzet, Model 1002) were implanted under the back skin and directly linked to the ventricle via a cannula. The osmotic pumps delivered a total volume of 100 μL of ASO solution (0.25 $\mu\text{L}/\text{hr}$ for 2 weeks), corresponding to up to 4 mg of tcDNA (−700 nmol) over the period of 2 weeks.

2.2. Biodistribution Analysis in Tissue Lysates

For tcDNA administrations, tissues were homogenized using the Precellys 24 (Bertin Instruments, France) in lysis buffer (100 mmol/l Tris-HCl, pH 8.5, 200 mmol/l NaCl, 5 mmol/l EDTA, 0.2% sodium dodecyl sulfate) containing 2 mg/mL of proteinase K (Invitrogen) (50 mg tissue/mL of buffer), followed by incubation overnight at 55 °C in a hybridization oven. After centrifugation at 14,000 rpm (Sorval ST 8R centrifuge, 75,005,719 rotor) for 15 min, tcDNA was quantified in the supernatant via a hybridization assay with a molecular beacon probe, as previously described [24]. Briefly, 10 μL of tissue lysates was incubated with a 5' Cy3-DNA complementary probe conjugated with HBQ quencher at 3' in a black non-binding 96-well plate (ThermoFischer Scientific, Rockford, IL USA), PBS was added to a final volume of 100 μL per well, and fluorescence was measured on a spectrophotometer (Ex 544 nm/Em 590 nm using FluoStar Omega, BMG Labtech, France). The amount of tcDNA in tissues was determined using a standard curve built on the measurement of known tcDNA quantities dissolved in the respective tissue lysates of saline-treated animals.

2.3. Biodistribution Analysis In Situ

In situ analysis of the biodistribution of tcDNA was performed using sagittal and coronal brain cryosections (30 μm) from brains that were fresh-frozen in powdered dry ice. Cryosections were post-fixed in a 5 min bath of acetone/methanol (1:1), and detection of tcDNA-ASO was achieved using a complementary probe conjugated to biotin, which was then revealed with a Streptavidin Alexa Fluor™ 555 conjugate (ThermoFisher Scientific, USA). Images were taken at equivalent locations and exposure times using a laser scanning confocal microscope (Zeiss LSM 700 \times 40 objective). Stacks of 9 to 12 images (1024 \times 1024 pixels) spaced by 1 μm were recorded at a resolution of 156 nm/pixel. Scan tiles images (1024 \times 1024 pixels) were taken using the ScanR Olympus HCS microscope, X40 objective.

For PMO biodistribution a carboxyfluorescein-conjugated PMO was administered via ICV or ICM. Forty-eight hours later, mice were transcardially perfused with PBS followed by 4% paraformaldehyde (PFA), and brains were harvested. Whole brains were post-fixed for 6 h in 4% PFA, followed by sucrose cryoprotection in increasing concentrations of sucrose in 1X PBS (15%, 30%) at 4 °C. A final incubation in 30% sucrose/30% OCT was performed before brains were embedded in OCT using methylbutane cooled with liquid nitrogen and stored at −80 °C.

Brains were cryosectioned sagittally and coronally (10 μm), stained with a nuclear stain, and mounted with Prolon Diamond antifade mountant (Invitrogen, Carlsbad, CA USA). Whole sections were imaged at equivalent locations and exposure times using a digital slide scanner (NanoZoomer S60, Hamamatsu, Shizuoka, Japan, 40 \times objective) at a resolution of 220 nm/pixel.

2.4. Exon 51 Skipping Analysis

For PMO-injected mice, brain regions were microdissected and stored in RNAlater (ThermoFisher Scientific, Carlsbad, CA USA) at 4 °C overnight to preserve the RNA, before removal of the RNAlater for storage at −80 °C. Total RNA was isolated from dissected brain structures using TRIzol reagent (ThermoFisher Scientific, Carlsbad, CA USA) or an RNeasy mini kit (Qiagen, Hilden, Germany) according to the manufacturer's instructions. For visualization of the exon-skipping efficacy on gels, aliquots of 1 µg of total RNA were used for RT-PCR analysis using the Access RT-PCR System (Promega, Madison, WI USA) in a 50 µL reaction using the external primers Ex49F (5'-AAACTGAAATAGCAGTTCAAGC-3') and Ex53R (5'-ACCTGTTGCGCTTCTTCCTT-3'). The cDNA synthesis was carried out at 55 °C for 10 min, followed by the PCR of 30 cycles of 95 °C (30 s), 58 °C (1 min), and 72 °C (1 min). PCR products were electrophoresed on 1.5% agarose gels.

Exon 51 skipping was also measured via Taqman quantitative PCR, as previously described (Aupy et al., 2020), using Taqman assays designed against the exon 50–51 junction (assay Mm.PT.58.41685801: forward: 5'-CAAAGCAGCCTGACCGT-3'; reverse: 5'-TGACAGTTTCCTTAGTAACCACAG-3'; probe: 5'-TGGACTGAGCACTACTGGAGCCT-3') and exon 50–53 junction (forward: 5'-GCACTACTGGAGCCTTTGAA-3'; reverse: 5'-CTTCCAGCCATTGTGTTGAATC-3'; probe: 5'-ACAGCTGCAGAACAGGAGACAACA-3') (Integrated DNA technology). One hundred and fifty nanograms of cDNA was used per reaction, and assays were carried out in triplicate. Assays were performed under fast cycling conditions on a Biorad CFX384 Touch Real-Time PCR Detection System, and data were analyzed using the absolute copy number method. For a given sample, the copy number of skipped products (exon 50–53 assay) and unskipped products (exon 50–51 assay) were determined using the standards Ex49-54Delta52 and Ex49-54Delta51+52, respectively (gBlocks gene fragments from Integrated DNA technology). Exon 51 skipping was then expressed as a percentage of total dystrophin (calculated by the addition of exon 50–51 and exon 50–53 copy numbers).

2.5. Statistical Analysis

Data are presented as means ± SEMs; statistics were performed using the GraphPad Prism8 software (San Diego, CA, USA). Repeated measures were analyzed using repeated-measure (RM) two-way analysis of variance (ANOVA) with treatment as the between-group factor and brain structure as the within-subjects factor. Significant levels were set at * $p < 0.05$, ** $p < 0.01$, *** $p < 0.001$, and **** $p < 0.0001$.

3. Results

3.1. Single ICV ASO Delivery Optimization

We first focused on one of the most commonly utilized delivery routes to the CNS in rodents, intracerebroventricular (ICV) administration (Figure S1), and evaluated the different parameters for ASO delivery. Considering that the injection volume to the ventricles is restricted to a maximum of 5 µL/hemisphere and that ASO chemistries display limited solubility, we first compared bilateral ICV injection with unilateral injection.

Adult hDMD mice received either a unilateral ICV injection of 200 µg of tcDNA-ex51 (previously described in [25]) or a bilateral ICV injection of 2 × 200 µg (i.e., a total amount of 400 µg of ASO). We first checked that unilateral ICV injection results of the distribution of ASO to both hemispheres of the brain (Figure 1A) (hemisphere effect $p = 0.5596$). While it could be expected that bilateral injection of 400 µg of ASO would lead to increased ASO levels in tissue relative to that with unilateral ICV injection of 200 µg, the concentrations in tissues were surprisingly much higher than the expected 2-fold difference following the bilateral delivery (~7.7-fold on average) (Figure 1A–C) ($p = 0.0031$ unilateral vs. bilateral). Likewise, exon 51-skipping efficacy was measured via quantitative RT-PCR and revealed

that bilateral ICV injection induced significantly higher levels of exon skipping (~6-fold change) compared to that with unilateral ICV injection ($p < 0.0001$ unilateral vs. bilateral) (Figure 1D). Based on these results, we selected bilateral injection as our standard ICV injection method for further experiments.

Next, as different rates of administration have been described in the literature [25,29], we chose to examine rapid-bolus delivery (0.6 $\mu\text{L/s}$) versus a slow-bolus rate (0.3 $\mu\text{L/min}$) for the administration of tcDNA-ASO in adult hDMD mice [28]. Both methods led to a homogenous distribution of tcDNA-Ex51 to the different CNS regions (rate effect $p = 0.1783$), although slightly higher levels of ASO were detected in the slow-bolus rate-injected tissues (Figure 1A). Exon 51-skipping levels were similar for both rates (rate effect $p = 0.51$) (Figure 1B). Considering that 0.3 $\mu\text{L/min}$ is closer to the cerebrospinal fluid (CSF) flow [30] we selected this slow-bolus rate to compare PMO and tcDNA delivery in *mdx52* mice. Eight-week-old *mdx52* mice received a bilateral ICV injection of a carboxyfluorescein-conjugated PMO in order to investigate its biodistribution. Forty-eight hours after the injection, PMO was mainly detected in the hippocampus, with some in the cortex and only very limited diffusion to the cerebellum and amygdala (Figures 1C and S2A). For tcDNA, we performed in situ hybridization using a complementary probe to directly detect the injected tcDNA-ex51, thus avoiding the need to inject a fluorescent ASO. While we were not able to easily detect the tcDNA 48 h after the ICV injection using this technique, we could clearly detect it 3 weeks and 7 weeks post-ICV (Supplementary Figure S2B,C). The tcDNA-ASO was found at a high concentration in the CA1 region of the hippocampus and in the cerebellum at both time points.

The efficacy of both PMO and tcDNA-ASOs targeting the *Dmd* exon 51, administered via bilateral ICV injection, were next compared in 8-week-old *mdx52* mice. The highest feasible dose was injected in both cases (400 μg for tcDNA and 900 μg for PMO, corresponding to 72 and 107 nmol, respectively). Seven weeks post-ICV, the levels of exon 51 skipping were measured via qPCR and showed that both tcDNA and PMO induced homogenous skipping across the different CNS structures (structure effect $p = 0.193$). The tcDNA, however, showed significantly higher efficacy in inducing exon 51 skipping, with a mean of 20–30%, compared to that with PMO, which induced 7–15% of exon 51 skipping (ASO chemistry effect $p = 0.0013$) (Figure 1D). The difference was particularly striking in the cerebellum. Exon 51 skipping in the different brain regions was also visualized on the gel after RT-PCR for both chemistries (Figure 1D right panel).

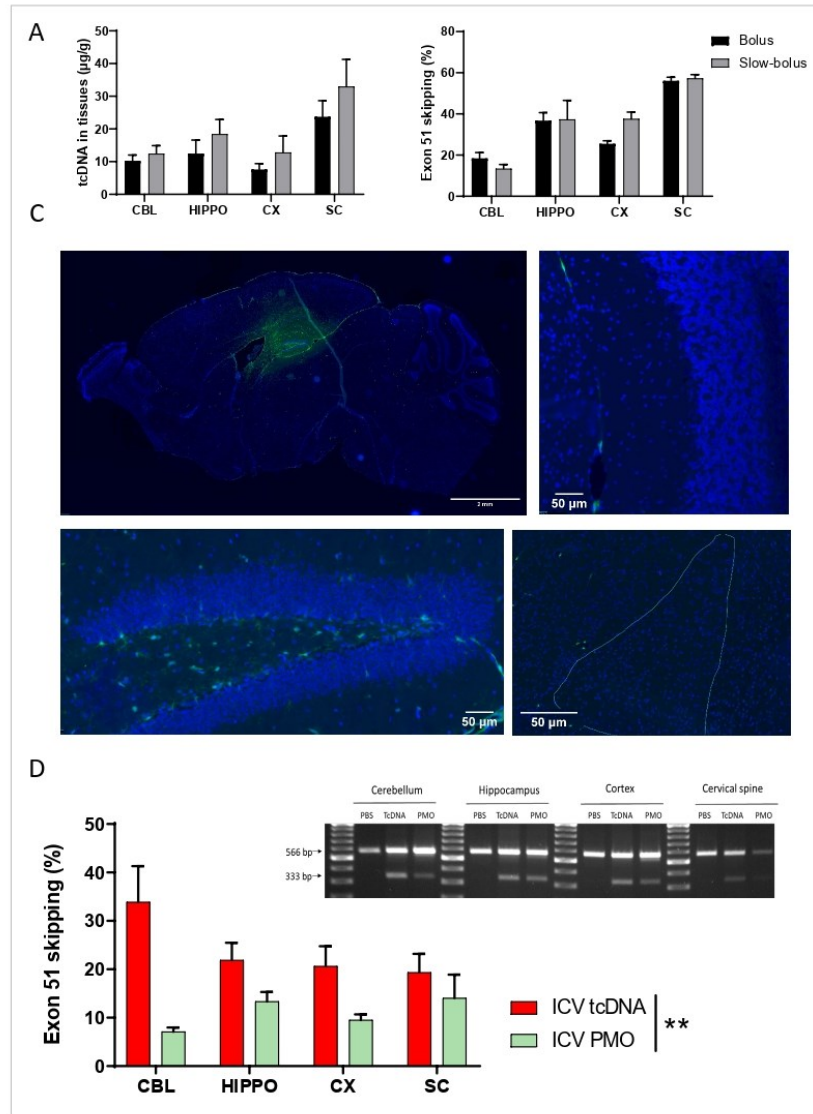


Figure 1. Quantification of tcDNA and PMO in specific brain regions and exon skipping after single ICV delivery. (A) Quantification by fluorescent hybridization assay of tcDNA-Ex51 content in various CNS tissues 4 weeks after the ICV administration using a bolus or a slow-bolus rate. Results are expressed as means \pm SEMs; $n = 4$ hDMD-tcDNA-Ex51. (B) Quantification of exon 51-skipping levels via RT-qPCR in different brain tissues 4 weeks after the ICV administration using a bolus or a slow-bolus rate. Results are expressed as means \pm SEMs; $n = 4$ hDMD-tcDNA-Ex51. (C) Carboxyfluorescein-conjugated PMO detected 48 h post-ICV slow-bolus rate delivery. Representative images show a sagittal section (scale bar 2mm), cerebellum lobules IV-V (CBL), hippocampus dentate gyrus (HIPPO), and the lateral amygdala (LA), $n = 3$, (scale bars 50 µm). (D) Left panel: quantification of exon 51-skipping levels via RT-qPCR in different brain tissues after a slow-bolus rate ICV administration. Right panel: detection of exon 51-skipped dystrophin mRNA via RT-PCR in different brain tissues 7 weeks after the ICV administration of saline (PBS), tcDNA-ex51 ($n = 5$), or PMO-ex51 ($n = 3$) in mdx52 mice. CBL: cerebellum, CX: cortex, HIPPO: hippocampus,

and SC: spinal cord (cervical region). ** $p < 0.01$ between tcDNA and PMO treatment analyzed via RM two-way ANOVA.

3.2. Repeated ICV ASO Delivery

In order to investigate whether it was possible to increase the levels of exon-skipping further, we evaluated the delivery of higher doses of ASOs. For this purpose and accounting for the maximum feasible dose for single injections, we performed repeated administrations of ASOs. Given that repeated ICV injection presents a high risk of damage to the cortex, cannula implants are commonly used for this purpose. Cannulas were implanted directly into the lateral ventricles, and delivery was repeated using anesthetized 8-week-old *mdx52* mice over a period of 2 weeks with at least 3 days between the administrations to allow for recovery. For tcDNA, two distinct treatment groups were analyzed, one receiving three injections of tcDNA (total amount, 1 mg; i.e., 176 nmol) and another group receiving five injections (total amount, 2 mg; i.e., 352 nmol). Mice treated with 2 mg of tcDNA showed tolerability issues characterized by a progressive reduction in mobility and a lack of responsiveness with weight loss. This group was thus euthanized 4 weeks after the last administration due to tolerability issues. The tcDNA quantification revealed homogeneous biodistribution through the CNS for all doses examined, although the 2 mg cannula group showed large inter-individual variability (Figure 2A) (structure effect $p = 0.8533$). Exon-skipping levels were also homogeneous in the different structures analyzed for all groups (Figure 2B). A large variability in exon-skipping levels was also observed in the 2 mg cannula group, and despite a slight tendency of this group to show higher skipping efficacy, we found no significant difference when compared to the 1 mg group or to a single ICV of 400 μg (dose effect $p = 0.5603$). These results were confirmed in the hDMD mouse model, in which we did not detect significantly higher exon skipping in the 2 mg cannula group compared to that with single ICV delivery (Figure S3A).

The repeated ICV delivery of PMO using a cannula (total amount, 2.7 mg; i.e., 320 nmol) was well tolerated and induced slightly higher exon 51-skipping levels in the various brain regions compared to that with the single bilateral ICV injection, although this was not statistically significant ($p = 0.09$ between ICV of 900 μg and repeated ICV of 2.7 mg, analyzed via RM two-way ANOVA) (Figure 2C).

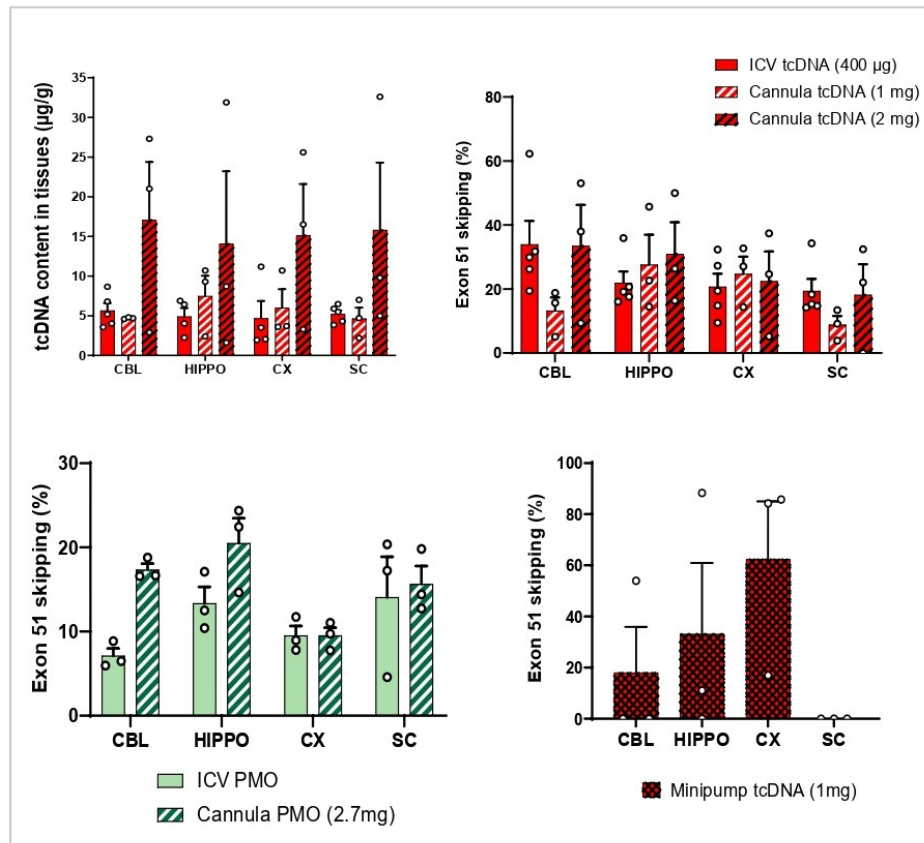


Figure 2. Repeated ICV delivery of tcDNA and PMO. (A) Quantification by fluorescent hybridization assay of tcDNA-Ex51 content in various CNS tissues after three multiple injections via a cannula implant 4 weeks after tcDNA administration. Results are expressed as means \pm SEMs; $n = 3$ *mdx52*-tcDNA-Ex51 in cannula groups. (B) Quantification of exon 51-skipping levels via RT-qPCR in different brain tissues. Results are expressed as means \pm SEMs; $n = 3$ *mdx52*-tcDNA-Ex51 in cannula groups. (C) Quantification of exon 51-skipping levels via RT-qPCR in different brain tissues 7 weeks after either single ICV slow-bolus injection or three administrations via a cannula implant of PMO. (D) Quantification of exon 51-skipping levels via RT-qPCR in different brain tissues after very slow diffusion via osmotic pumps of tcDNA. CBL: cerebellum, CX: cortex, HIPPO: hippocampus, and SC: spinal cord (cervical region). Results are expressed as means \pm SEMs; $n = 3$ *mdx52*-minipump-tcDNA-Ex51.

3.3. ICV Delivery of ASO Using Osmotic Pumps

To investigate further the possibility of achieving greater efficacy levels, we evaluated the administration of even higher doses of ASO. For that purpose, we used osmotic pumps to deliver the ASO directly to the lateral ventricles at a very slow diffusion rate. This method allows for the delivery of larger volumes (up to 100 μ L) of ASO over a sustained period of time (2 weeks), thus allowing for higher dosages of ASO reaching up to 4 mg of tcDNA-ASO (i.e., 704 nmol). Preliminary experiments were conducted in hDMD mice, which received either 2 or 4 mg of tcDNA-ex51. Mice were euthanized 4 weeks after the last administration because of tolerability issues (as reported above), and tissues were taken for analysis. Quantification of exon 51 skipping revealed lower levels in both osmotic pump groups compared to levels that were obtained after a single bilateral ICV injection of 400 μ g (analyzed at 7 weeks) (Figure S3B). For experiments in *mdx52* mice, we

lowered the dose to 1 mg to improve tolerability and this amount was indeed better tolerated. Mice were analyzed 7 weeks post-treatment, and exon-skipping levels were examined in the various brain regions (Figure 2D). This very slow diffusion method led to exon 51-skipping levels of around 18% in the cerebellum, 33% in the hippocampus, and 62% in the cortex (Figure 2D), but this was not statistically different from those with the bilateral single ICV injection of 400 µg ($p = 0.7148$ between the two treatments analyzed via two-way ANOVA), probably due to the very large variability between individuals in the osmotic pump group, making this delivery route less reliable.

3.4. Intra-Cisterna Magna Delivery of ASOs

We next investigated other CNS delivery methods that may be better tolerated and more translatable for clinical use. In particular, we delivered ASO to the CSF through intra-cisterna magna (ICM) delivery. ICM is a less invasive method than ICV, allowing for delivery directly to the spinal canal or subarachnoid space without interference with any CNS tissue, making its repeated delivery possible. The ICM route of ASO administration tends to induce higher distribution to brain regions, such as the cerebellum, hindbrain, and hippocampus, while the intrathecal route via lumbar puncture (LP) more efficiently targets the spinal cord [23]. For these reasons, we focused on ICM delivery and validated this injection technique first using a blue dye (Figure S4A). Six-week-old *mdx52* mice received an ICM delivery of blue dye, and 5 min later, the mice were euthanized and the brains were harvested. The presence of the dye was observed throughout the ventricular system indicating the correct needle placement and angle at the base of the skull. As previously performed for the ICV studies, we then determined the biodistribution of ASO 48 h following the ICM injection of a carboxyfluorescein-conjugated PMO (Figures 3A and S4). The PMO was detected brightly in the cerebellum, mostly near blood vessels, but only detected at very low levels in other brain regions. For the tcDNA, we performed fluorescent in situ hybridization 7 weeks post-ICM delivery, and high levels of ASO were also found in the cerebellum, while very little was found in the CA1 region of the hippocampus (Figure S4B).

We next assessed the molecular efficacy following single ICM injection of the maximum feasible dose of tcDNA and PMO targeting *Dmd* exon 51 (400 µg and 900 µg, respectively, as previously for the ICV injection). We examined exon-skipping levels and found a larger variability for the tcDNA as compared to that with the PMO (Figure 3B), which was further supported by an examination of the biodistribution of the tcDNA in brain structures (Figure S4C). The skipping quantification showed relatively low levels as compared to those with the ICV injection, 5 to 15% for the tcDNA depending on the structure and less than 5% in all analyzed structures for the PMO (ASO chemistry effect $p = 0.2623$) (Figure 3B).

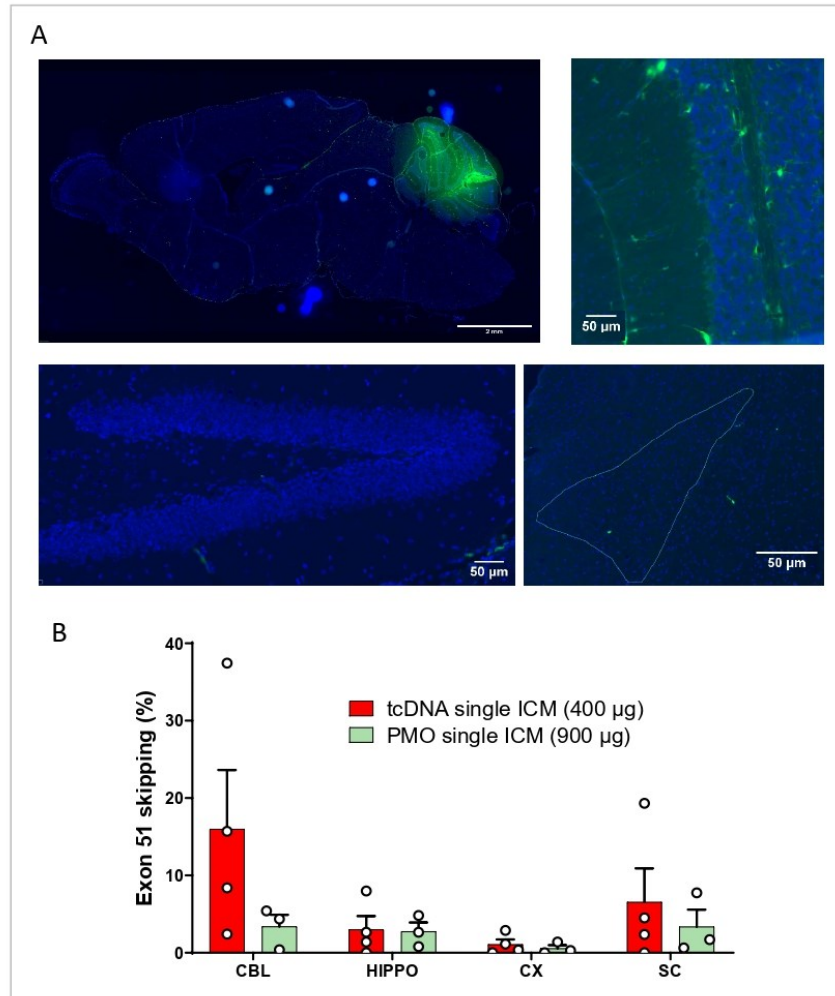


Figure 3. Single ICM delivery of tcDNA or PMO. (A) Carboxyfluorescein-conjugated PMO detected 48 h post-ICM delivery. Representative images showing a sagittal section (scale bar 2 mm), cerebellum lobules IV–V (CBL), hippocampus dentate gyrus (HIPPO), and the lateral amygdala (LA) (scale bars 50 μm); $n = 3$. (B) Quantification of exon 51-skipping levels via RT-qPCR in different brain regions (CBL: cerebellum, CX: cortex, HIPPO: hippocampus, and SC: spinal cord) after a single ICM administration of tcDNA or PMO. Results are expressed as means \pm SEMs; $n = 3$ *mdx52*-PMO and $n = 4$ *mdx52*-tcDNA. RM two-way ANOVA: structure effect $p = 0.1810$; ASO chemistry effect $p = 0.2623$.

3.5. Repeated ICM ASO Administration

As the ICM delivery allows for less invasive repeated administration, we evaluated the effect of repeated ICM injections. PMO and tcDNA were delivered three times to 8-week-old *mdx52* mice at 72 h intervals, reaching total amounts of 2.7 mg for PMO (320 nmol) and 1.2 mg for tcDNA (213 nmol). The skipping efficacy showed that overall, the triple ICM injection led to significantly higher skipping levels than single ICM injection for both tcDNA (20–40%) and PMO (10–20%) (Figures 4A and S4D,E). A comparison between tcDNA and PMO revealed higher levels of exon skipping induced by tcDNA (treatment effect $p = 0.0054$), as previously shown for ICV injections; however, high doses of PMO were better tolerated by the mice than high doses of tcDNA.

Finally, given that triple ICM injection still did not induce higher exon-skipping levels than our standard bilateral ICV injection, we tried to combine ICM and ICV delivery to increase both the efficacy and the distribution of ASO in the CNS. For PMO, *mdx52* mice received three ICM injections followed by an ICV injection as shown in Figure 4B, reaching a total amount of 3.6 mg of PMO. For tcDNA, considering that amounts totaling 1 mg or more were not well tolerated by the mice, *mdx52* mice received a single ICM injection before the ICV administration, reaching a total of 800 µg of tcDNA, which was well tolerated. Seven weeks after the ICV injection, exon-skipping levels were quantified and revealed an overall higher efficacy for the tcDNA-treated group (ASO chemistry effect $p = 0.0209$) compared to that in the PMO-treated group. However, these levels were not significantly higher than those obtained after the bilateral ICV injection of 400 µg of tcDNA ($p = 0.73$ between the two treatments analyzed via two-way ANOVA) (Figure S6A). Reassuringly however, for PMO, this combined delivery method was the most efficient one, resulting in the highest levels of exon 51 skipping obtained with this chemistry (16–22%) (Figure S6B,C).

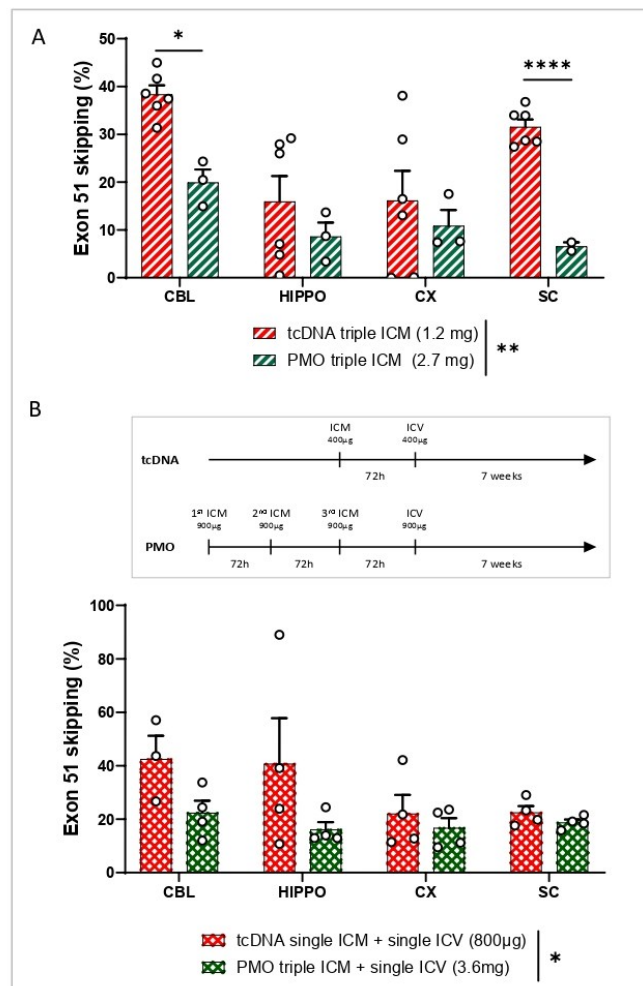


Figure 4. Repeated ICM delivery and combined ICM and ICV delivery of tcDNA or PMO in the CNS of *mdx52* mice. (A) Quantification of exon 51-skipping levels via RT-qPCR in different brain

regions (CBL: cerebellum, CX: cortex, HIPPO: hippocampus, and SC: spinal cord) after PMO or tcDNA triple ICM7 weeks after administration. Results are expressed as means \pm SEMs; $n = 6$ *mdx52*-tcDNA and $n = 3$ *mdx52*-PMO. RM two-way ANOVA: structure effect $p = 0.0182$, ASO chemistry effect ** $p = 0.0054$. (B) Quantification of exon 51-skipping levels via RT-qPCR in different brain regions (CBL: cerebellum, CX: cortex, HIPPO: hippocampus, and SC: spinal cord) after PMO triple ICM + ICV injection and tcDNA single ICM + ICV injection, analyzed 7 weeks after administration. Results are expressed as means \pm SEMs; $n = 4$ *mdx52*-tcDNA and $n = 4$ *mdx52*-PMO. RM two-way ANOVA: structure effect $p = 0.3012$, ASO chemistry effect * $p = 0.0209$. (* $p < 0.05$, **** $p < 0.0001$).

4. Discussion

In this study, we have used the delivery of ASO therapies directly to the CNS as a means to bypass the BBB, in DMD neuromuscular mouse models. We compared two different oligonucleotide chemistries: the charge-neutral PMO chemistry, which is already approved by the FDA for the treatment of DMD following intravenous delivery, and the charged, lipid-conjugated tcDNA. TcDNA is an alternative chemistry that previously showed higher efficacy in mouse models of DMD and will enter clinical evaluation in H1 2023 (clinical trial *Avance 1*, sponsored by SQY Therapeutics). We focused on delivery to the CSF as opposed to direct injections into specific structures (e.g., intra hippocampal, etc.) in order to allow a broad distribution of ASO throughout the whole CNS since dystrophin isoforms are expressed across most CNS structures [31]. We therefore gathered useful information for the potential future use of ASOs to address dystrophin deficiency in the brain.

In the first part of the study, we focused on ICV administration, which has been commonly used to deliver therapeutic agents to the CNS in rodents; however various injection rates have been described in the literature. Rigo and colleagues previously demonstrated an increased ASO potency using a rapid-bolus rate (1 $\mu\text{L}/\text{s}$) of injection compared to that with a very slow rate of 0.5 $\mu\text{L}/\text{h}$ [29]. Here, we compared a bolus rate of 0.6 $\mu\text{L}/\text{sec}$ (the maximum bolus rate achievable with our injection system) to a slow-bolus rate of 0.3 $\mu\text{L}/\text{min}$, closer to the CSF flow [30]. Our results showed no statistical difference in the resulting ASO content or exon-skipping efficacy between both rates. Considering that we successfully used the slow-bolus rate in previous studies [25] and that it is closer to CSF flow, we selected this rate for our standard ICV protocol. The bilateral ICV administration of the maximal feasible dose of tcDNA induced relatively homogenous exon-skipping efficacy across the various CNS regions, ranging from 20 to 34%. Exon-skipping levels were also homogenous within the various brain structures following PMO ICV delivery, although they were significantly lower (ranging from 7 to 14%) compared to those obtained with tcDNA.

We next used cannula implants in order to deliver higher doses of ASO delivered to the CSF. The repeated injection of PMO, reaching up to 2.7 mg, induced slightly higher exon-skipping levels than single bilateral ICV delivery. Yet the difference was not statistically significant and efficacy levels did not correlate with the higher dose administered (2.7 vs. 0.9 mg). For tcDNA, repeated delivery through a cannula induced similar levels of exon skipping compared to those with single bilateral ICV, despite the much higher doses injected. This may be explained by the type of anesthesia used during the delivery. In order to avoid repeated long anesthesia sessions, mice implanted with the cannula were subsequently anaesthetized under isoflurane when receiving the tcDNA, whereas mice from the ICV bilateral groups were anaesthetized using ketamine/medetomidine when receiving the ASO. Indeed, several studies have recently raised the impact of anesthesia on CSF flow and showed that distribution to the CSF may be different depending on the wakefulness state [32]. Moreover, Ma and colleagues demonstrated that the CSF efflux out of the brain is higher under isoflurane anesthesia compared to that under deeper chemical anesthesia using ketamine/medetomidine [33]. This suggests that ASO may be more quickly eliminated from the CSF under isoflurane anesthesia (i.e., during delivery via a cannula) than under deeper anesthesia (i.e., bilateral

ICV). This hypothesis could also explain the results obtained with the osmotic pumps, which delivered the ASO to the CSF in awake mice, since the clearance of CSF-infused tracers was shown to be increased under conscious conditions [33]. These findings are also in line with those previously reported by Rigo and colleagues that demonstrated the lower efficacy of a very slow rate of infusion (0.5 $\mu\text{L}/\text{h}$), similar to the one of the osmotic pumps that deliver the ASO continuously through a catheter implanted in the lateral ventricle, at a slow rate of 0.25 $\mu\text{L}/\text{h}$ for 2 weeks in conscious animals.

Besides the lack of improvement in exon-skipping efficacy, the administration of a high dose of tcDNA was not very well tolerated by the mice, which showed general reduced mobility and weight loss with hypoactivity and a lack of responsiveness. Such toxicities have previously been observed following the direct injection of charged ASO in the CNS of rodents [34–36] and highlight the need to perform detailed safety studies before considering the potential future application to DMD patients [37]. Furthermore, we detected particularly high variability with this procedure, thus questioning its reproducibility. PMO-treated mice did not show any tolerability issues even after receiving a very high dose up to 2.7 mg of PMO with the cannula. Yet, exon-skipping levels obtained after the repeated delivery of PMO were still lower than those obtained after a single bilateral ICV injection of tcDNA.

We next investigated ICM injection as an alternative delivery to the CSF. Because ICM injections are less invasive than ICV procedures, this route may offer an easier opportunity for repeated administration. In addition, IT delivery is well tolerated and already approved for ASO delivery in the clinic for SMA [38]. The biodistribution following ICM injection differs from that of ICV as it preferentially targets the cerebellum, hindbrain, olfactory bulb, and spinal cord in mice [23] and therefore offers an interesting alternative delivery route for ASOs. We indeed clearly detected both PMO and tcDNA in the cerebellum after a single ICM injection, while only limited signal was detected in the hippocampus and cortex. This translated into higher exon-skipping levels in the cerebellum and spinal cord of tcDNA-treated mice, which are the closest regions to the injection site. Single ICM injections induced lower efficacy than ICV for both PMO and tcDNA; however, triple ICM achieved significantly higher exon-skipping levels than single ones. Considering that the wakefulness state of the animal may have an impact on the CSF efflux and influence ASO biodistribution and efficacy as discussed above, we decided to perform the ICM administrations under ketamine/medetomidine anesthesia as opposed to isoflurane. Indeed, besides the previously mentioned studies investigating the impact of anesthesia on CSF distribution [32,33], Xavier and colleagues evaluated this parameter in the context of a cannula implant into the *cisterna magna* and recommended a mixture of ketamine/xylazine for chronic injection [39]. This may explain why repeated ICM delivery induced higher efficacy than single ICM injection, while this was not the case for repeated ICV compared to single ICV.

Finally, we investigated the combination of ICV and ICM delivery with the objective of reaching the highest achievable efficacy levels but also a wider CNS distribution of the ASO. Administration of up to 3.6 mg of PMO to the CSF was well tolerated by the mice and led to homogenous exon 51-skipping levels across the different brain structures ranging from 16% to 22%. This combined administration was the most efficient delivery method for PMO (Figures S6B and S7). In order to avoid tolerability issues observed with >1 mg of tcDNA, ICV injection of tcDNA was combined with a single ICM administration reaching 800 μg of tcDNA, which was well tolerated. This combined method also resulted in the highest efficacy levels for tcDNA ranging from 22 to 42% of exon-skipping levels, although not significantly different from those with the bilateral ICV administration of 400 μg (ranging from 19 to 34%).

5. Conclusions

Together, our study highlights the importance of the delivery route, as well as the impact of the ASO chemistry and the type of anesthesia used during injection, on ASO

distribution and molecular efficacy in the CNS. Overall, these results provide useful insights into the direct delivery of ASOs to the CNS of mice and lay the foundations for future work investigating the effects of ASO therapy in the CNS in mouse models of DMD. This work, linked to an assessment of functional rescue of the neuro-behavioral abnormalities that have been described in dystrophic mice, paves the way for the potential future clinical application of CNS-delivered ASO for individuals affected by DMD.

Supplementary Materials: The following supporting information can be downloaded at: <https://www.mdpi.com/article/10.3390/cells12060908/s1>, Figure S1: Schematic representation of the various injection methods and anatomical localization of the brain regions dissected for molecular analysis; Figure S2: Comparison of unilateral of bilateral ICV injection of tcDNA-ASO in hDMD mice; Figure S3: In situ biodistribution of PMO and tcDNA following single ICV administration; Figure S4: Comparison of single and repeated ICV delivery of tcDNA in hDMD mice; Figure S5: Biodistribution of ASO following ICM delivery; Figure S6: Comparison of various delivery routes for tcDNA and PMO; Figure S7: Summary of exon skipping efficacy following various delivery routes for tcDNA and PMO.

Author Contributions: Conceptualization and methodology, F.M. (Francesco Muntoni) and A.G.; Analysis, A.S., C.F., C.V., and T.G.; Investigation, A.G., A.S., C.F., C.V., F.M. (Francesco Muntoni), F.M. (Federica Montanaro), J.E.M., T.G., and V.P.K.; Resources, F.M. (Federica Montanaro), A.G., C.V., V.P.K., T.T.; L.G.; and F.M. (Francesco Muntoni); Writing—original draft preparation, A.S. and A.G.; Writing—review and editing, A.G., A.S., C.F., C.V., F.M. (Francesco Muntoni), J.E.M., T.G., and V.P.K.; Supervision, A.G., V.P.K., and F.M. (Francesco Muntoni); Funding acquisition, F.M. (Francesco Muntoni). All authors have read and agreed to the published version of the manuscript.

Funding: This work was supported by the European Union’s Horizon 2020 research and innovation program “Brain Involvement in Dystrophinopathies” (BIND) under grant agreement No 847826, Centre National de la Recherche Scientifique (CNRS, France), Institut National de la santé et la recherche médicale (INSERM), Université Paris-Saclay (France), and Paris Ile-de-France Region. AS received a PhD fellowship from Ministère de l’Enseignement Supérieur et de la Recherche (France). AS and CF received support from the COST Action CA17103 Delivery of Antisense RNA Therapeutics (DARTER) for a short-term scientific mission. The support of the Muscular Dystrophy UK (MDUK) for the centre funding of the Dubowitz Neuromuscular Centre is acknowledged.

Institutional Review Board Statement: The animal study protocols were approved by the Ethics Committee CNREEA47, the French government (ministère de l’enseignement supérieur et de la recherche, Autorisation APAFiS #6518), the Irish Health Products Regulatory Authority (Ref: AE19136/P131), and the TCD Animal Research Ethics Committee.

Informed Consent Statement: Not applicable.

Data Availability Statement: The primary data for this study are available from the authors upon request.

Acknowledgments: We are grateful to Toshikuni Sasaoka and Motoya Katsuki (Department of Comparative & Experimental Medicine, Brain Research Institute, Niigata University, Japan) and Jun Tanihata and Shin’ichi Takeda (National Center of Neurology and Psychiatry, Tokyo, Japan) for generating and providing the *mdx52* line used in this study. We would also like to thank Matthew Siddle for helping with some RNA extractions. We are grateful to the Zootechnic platforms of our institutes for mouse breeding, care, and genotyping.

Conflicts of Interest: TT is an employee of SQY Therapeutics, which produces tricyclo-DNA oligomers. LG is co-founder of SQY Therapeutics. The other authors declare no conflict of interest.

References

1. Gilar, M.; Belenky, A.; Smisek, D.L.; Bourque, A.; Cohen, A.S. Kinetics of Phosphorothioate Oligonucleotide Metabolism in Biological Fluids. *Nucleic Acids Res.* **1997**, *25*, 3615–3620. <https://doi.org/10.1093/nar/25.18.3615>.
2. Gripenburg, J.C.; Rapp, T.L.; Carroll, P.J.; Eberwine, J.; Dmochowski, I.J. Ruthenium-Caged Antisense Morpholinos for Regulating Gene Expression in Zebrafish Embryos. *Chem. Sci.* **2015**, *6*, 2342–2346. <https://doi.org/10.1039/C4SC03990D>.
3. Kaur, H.; Wengel, J.; Maiti, S. LNA-Modified Oligonucleotides Effectively Drive Intramolecular-Stable Hairpin to Intermolecular-Duplex State. *Biochem. Biophys. Res. Commun.* **2007**, *352*, 118–122. <https://doi.org/10.1016/j.bbrc.2006.10.155>.

4. Hoffman, E.P.; Knudson, C.M.; Campbell, K.P.; Kunkel, L.M. Subcellular Fractionation of Dystrophin to the Triads of Skeletal Muscle. *Nature* **1987**, *330*, 754–758. <https://doi.org/10.1038/330754a0>.
5. Mah, J.K.; Korngut, L.; Dykeman, J.; Day, L.; Pringsheim, T.; Jette, N. A Systematic Review and Meta-Analysis on the Epidemiology of Duchenne and Becker Muscular Dystrophy. *Neuromuscul. Disord.* **2014**, *24*, 482–491. <https://doi.org/10.1016/j.nmd.2014.03.008>.
6. Aartsma-Rus, A.; Janson, A.A.M.; Heemskerk, J.A.; De Winter, C.L.; Van Ommen, G.-J.B.; Van Deutekom, J.C.T. Therapeutic Modulation of DMD Splicing by Blocking Exonic Splicing Enhancer Sites with Antisense Oligonucleotides. *Ann. N. Y. Acad. Sci.* **2006**, *1082*, 74–76. <https://doi.org/10.1196/annals.1348.058>.
7. Dunckley, M.G.; Manoharan, M.; Villiet, P.; Eperon, I.C.; Dickson, G. Modification of Splicing in the Dystrophin Gene in Cultured Mdx Muscle Cells by Antisense Oligoribonucleotides. *Hum. Mol. Genet.* **1998**, *7*, 1083–1090. <https://doi.org/10.1093/hmg/7.7.1083>.
8. Ferlini, A.; Goyenvalle, A.; Muntoni, F. RNA-Targeted Drugs for Neuromuscular Diseases. *Science* **2021**, *371*, 29–31. <https://doi.org/10.1126/science.aba4515>.
9. Hendriksen, R.G.F.; Vles, J.S.H.; Aalbers, M.W.; Chin, R.F.M.; Hendriksen, J.G.M. Brain-Related Comorbidities in Boys and Men with Duchenne Muscular Dystrophy: A Descriptive Study. *Eur. J. Paediatr. Neurol.* **2018**, *22*, 488–497. <https://doi.org/10.1016/j.ejpn.2017.12.004>.
10. Ricotti, V.; Mandy, W.P.L.; Scoto, M.; Pane, M.; Deconinck, N.; Messina, S.; Mercuri, E.; Skuse, D.H.; Muntoni, F. Neurodevelopmental, Emotional, and Behavioural Problems in Duchenne Muscular Dystrophy in Relation to Underlying Dystrophin Gene Mutations. *Dev. Med. Child Neurol.* **2016**, *58*, 77–84. <https://doi.org/10.1111/dmcn.12922>.
11. Araki, E.; Nakamura, K.; Nakao, K.; Kameya, S.; Kobayashi, O.; Nonaka, I.; Kobayashi, T.; Katsuki, M. Targeted Disruption of Exon 52 in the Mouse Dystrophin Gene Induced Muscle Degeneration Similar to That Observed in Duchenne Muscular Dystrophy. *Biochem. Biophys. Res. Commun.* **1997**, *238*, 492–497. <https://doi.org/10.1006/bbrc.1997.7328>.
12. Colombo, P.; Nobile, M.; Tesei, A.; Civati, F.; Gandossini, S.; Mani, E.; Molteni, M.; Bresolin, N.; D'Angelo, G. Assessing Mental Health in Boys with Duchenne Muscular Dystrophy: Emotional, Behavioural and Neurodevelopmental Profile in an Italian Clinical Sample. *Eur. J. Paediatr. Neurol.* **2017**, *21*, 639–647. <https://doi.org/10.1016/j.ejpn.2017.02.007>.
13. Taylor, P.J.; Betts, G.A.; Maroulis, S.; Gilissen, C.; Pedersen, R.L.; Mowat, D.R.; Johnston, H.M.; Buckley, M.F. Dystrophin Gene Mutation Location and the Risk of Cognitive Impairment in Duchenne Muscular Dystrophy. *PLoS ONE* **2010**, *5*, e8803. <https://doi.org/10.1371/journal.pone.0008803>.
14. Saoudi, A.; Zarrouki, F.; Sebr e, C.; Izabelle, C.; Goyenvalle, A.; Vaillend, C. Emotional Behavior and Brain Anatomy of the Mdx52 Mouse Model of Duchenne Muscular Dystrophy. *Dis. Model Mech.* **2021**, *14*, dmm049028. <https://doi.org/10.1242/dmm.049028>.
15. Boursereau, R.; Donadieu, A.; Dabertrand, F.; Dubayle, D.; Morel, J.-L. Blood Brain Barrier Precludes the Cerebral Arteries to Intravenously-Injected Antisense Oligonucleotide. *Eur. J. Pharmacol.* **2015**, *747*, 141–149. <https://doi.org/10.1016/j.ejphar.2014.11.027>.
16. Crawford, L.; Rosch, J.; Putnam, D. Concepts, Technologies, and Practices for Drug Delivery Past the Blood–Brain Barrier to the Central Nervous System. *J. Control. Release* **2016**, *240*, 251–266. <https://doi.org/10.1016/j.jconrel.2015.12.041>.
17. Lehtinen, M.K.; Bjornsson, C.S.; Dymecki, S.M.; Gilbertson, R.J.; Holtzman, D.M.; Monuki, E.S. The Choroid Plexus and Cerebrospinal Fluid: Emerging Roles in Development, Disease, and Therapy. *J. Neurosci.* **2013**, *33*, 17553–17559. <https://doi.org/10.1523/JNEUROSCI.3258-13.2013>.
18. Paxinos, G.; Franklin, K. *Paxinos and Franklin's the Mouse Brain in Stereotaxic Coordinates*, 5th ed.; Elsevier: Amsterdam, The Netherlands, 2019. Available online: <https://www.elsevier.com/books/paxinos-and-franklins-the-mouse-brain-in-stereotaxic-coordinates-compact/franklin/978-0-12-816159-3> (accessed on 14 October 2022).
19. Miller, T.M.; Pestronk, A.; David, W.; Rothstein, J.; Simpson, E.; Appel, S.H.; Andres, P.L.; Mahoney, K.; Allred, P.; Alexander, K.; et al. An Antisense Oligonucleotide against SOD1 Delivered Intrathecally for Patients with SOD1 Familial Amyotrophic Lateral Sclerosis: A Phase 1, Randomised, First-in-Man Study. *Lancet Neurol.* **2013**, *12*, 435–442. [https://doi.org/10.1016/S1474-4422\(13\)70061-9](https://doi.org/10.1016/S1474-4422(13)70061-9).
20. Madan, E.; Carri e, S.; Donado, C.; Lobo, K.; Souris, M.; Laine, R.; Beers, E.; Cornelissen, L.; Darras, B.T.; Koka, A.; et al. Nusinersen for Patients with Spinal Muscular Atrophy: 1415 Doses via an Interdisciplinary Institutional Approach. *Pediatr. Neurol.* **2022**, *132*, 33–40. <https://doi.org/10.1016/j.pediatrneurol.2022.04.008>.
21. Kennedy, Z.; Gilbert, J.W.; Godinho, B.M.D.C. Intrathecal Delivery of Therapeutic Oligonucleotides for Potent Modulation of Gene Expression in the Central Nervous System. *Methods Mol. Biol.* **2022**, *2434*, 345–353. https://doi.org/10.1007/978-1-0716-2010-6_24.
22. Finkel, R.S.; Chiriboga, C.A.; Vajsar, J.; Day, J.W.; Montes, J.; De Vivo, D.C.; Yamashita, M.; Rigo, F.; Hung, G.; Schneider, E.; et al. Treatment of Infantile-Onset Spinal Muscular Atrophy with Nusinersen: A Phase 2, Open-Label, Dose-Escalation Study. *Lancet* **2016**, *388*, 3017–3026. [https://doi.org/10.1016/S0140-6736\(16\)31408-8](https://doi.org/10.1016/S0140-6736(16)31408-8).
23. Bailey, R.M.; Rozenberg, A.; Gray, S.J. Comparison of High-Dose Intracisterna Magna and Lumbar Puncture Intrathecal Delivery of AAV9 in Mice to Treat Neuropathies. *Brain Res.* **2020**, *1739*, 146832. <https://doi.org/10.1016/j.brainres.2020.146832>.
24. Relizani, K.; Echevarr a, L.; Zarrouki, F.; Gastaldi, C.; Dambrune, C.; Aupy, P.; Haeberli, A.; Komisariski, M.; Tensorer, T.; Larcher, T.; et al. Palmitic Acid Conjugation Enhances Potency of Tricyclo-DNA Splice Switching Oligonucleotides. *Nucleic Acids Res.* **2022**, *50*, 17–34. <https://doi.org/10.1093/nar/gkab1199>.

25. Zarrouki, F.; Relizani, K.; Bizot, F.; Tensorer, T.; Garcia, L.; Vaillend, C.; Goyenvalle, A. Partial Restoration of Brain Dystrophin and Behavioral Deficits by Exon Skipping in the Muscular Dystrophy X-Linked (Mdx) Mouse. *Ann. Neurol.* **2022**, *92*, 213–229. <https://doi.org/10.1002/ana.26409>.
26. Muntoni, F.; Torelli, S.; Ferlini, A. Dystrophin and Mutations: One Gene, Several Proteins, Multiple Phenotypes. *Lancet Neurol.* **2003**, *2*, 731–740. [https://doi.org/10.1016/s1474-4422\(03\)00585-4](https://doi.org/10.1016/s1474-4422(03)00585-4).
27. Bremmer-Bout, M.; Aartsma-Rus, A.; de Meijer, E.J.; Kaman, W.E.; Janson, A.A.M.; Vossen, R.H.A.M.; van Ommen, G.-J.B.; den Dunnen, J.T.; van Deutekom, J.C.T. Targeted Exon Skipping in Transgenic HDMD Mice: A Model for Direct Preclinical Screening of Human-Specific Antisense Oligonucleotides. *Mol. Ther.* **2004**, *10*, 232–240. <https://doi.org/10.1016/j.ymthe.2004.05.031>.
28. Veltrop, M.; van Vliet, L.; Hulsker, M.; Claassens, J.; Brouwers, C.; Breukel, C.; van der Kaa, J.; Linszen, M.M.; den Dunnen, J.T.; Verbeek, S.; et al. A Dystrophic Duchenne Mouse Model for Testing Human Antisense Oligonucleotides. *PLoS ONE* **2018**, *13*, e0193289. <https://doi.org/10.1371/journal.pone.0193289>.
29. Rigo, F.; Chun, S.J.; Norris, D.A.; Hung, G.; Lee, S.; Matson, J.; Fey, R.A.; Gaus, H.; Hua, Y.; Grundy, J.S.; et al. Pharmacology of a Central Nervous System Delivered 2'-O-Methoxyethyl-Modified Survival of Motor Neuron Splicing Oligonucleotide in Mice and Nonhuman Primates. *J. Pharmacol. Exp. Ther.* **2014**, *350*, 46–55. <https://doi.org/10.1124/jpet.113.212407>.
30. Simon, M.J.; Iliff, J.J. Regulation of Cerebrospinal Fluid (CSF) Flow in Neurodegenerative, Neurovascular and Neuroinflammatory Disease. *Biochim. Biophys. Acta* **2016**, *1862*, 442–451. <https://doi.org/10.1016/j.bbadis.2015.10.014>.
31. Dooreweerd, N.; Mahfouz, A.; van Putten, M.; Kaliyaperumal, R.; T' Hoen, P.A.C.; Hendriksen, J.G.M.; Aartsma-Rus, A.M.; Verschuuren, J.J.G.M.; Niks, E.H.; Reinders, M.J.T.; et al. Timing and Localization of Human Dystrophin Isoform Expression Provide Insights into the Cognitive Phenotype of Duchenne Muscular Dystrophy. *Sci. Rep.* **2017**, *7*, 12575. <https://doi.org/10.1038/s41598-017-12981-5>.
32. Xie, L.; Kang, H.; Xu, Q.; Chen, M.J.; Liao, Y.; Thiyagarajan, M.; O'Donnell, J.; Christensen, D.J.; Nicholson, C.; Iliff, J.J.; et al. Sleep Drives Metabolite Clearance from the Adult Brain. *Science* **2013**, *342*, 373–377. <https://doi.org/10.1126/science.1241224>.
33. Ma, Q.; Ries, M.; Decker, Y.; Müller, A.; Riner, C.; Bücken, A.; Fassbender, K.; Detmar, M.; Proulx, S.T. Rapid Lymphatic Efflux Limits Cerebrospinal Fluid Flow to the Brain. *Acta Neuropathol.* **2019**, *137*, 151–165. <https://doi.org/10.1007/s00401-018-1916-x>.
34. Toonen, L.J.A.; Casaca-Carreira, J.; Pellisé-Tintoré, M.; Mei, H.; Temel, Y.; Jahanshahi, A.; van Roon-Mom, W.M.C. Intracerebroventricular Administration of a 2'-O-Methyl Phosphorothioate Antisense Oligonucleotide Results in Activation of the Innate Immune System in Mouse Brain. *Nucleic Acid Ther.* **2018**, *28*, 63–73. <https://doi.org/10.1089/nat.2017.0705>.
35. Moazami, M.; Rembetsy-Brown, J.; Wang, F.; Krishnamurthy, P.M.; Brown, R.; Watts, J.K. Quantifying and Mitigating Motor Phenotypes Induced by Antisense Oligonucleotides in the Central Nervous System. *BioRxiv* **2021**. <https://doi.org/10.1101/2021.02.14.431096>.
36. Hagedorn, P.H.; Brown, J.M.; Easton, A.; Pierdomenico, M.; Jones, K.; Olson, R.E.; Mercer, S.E.; Li, D.; Loy, J.; Hog, A.M.; et al. Acute Neurotoxicity of Antisense Oligonucleotides After Intracerebroventricular Injection into Mouse Brain Can Be Predicted from Sequence Features. *Nucleic Acid Ther.* **2022**, *32*, 151–162. <https://doi.org/10.1089/nat.2021.0071>.
37. Goyenvalle, A.; Jimenez-Mallebrera, C.; van Roon, W.; Sewing, S.; Krieg, A.M.; Arechavala-Gomez, V.; Andersson, P. Considerations in the Preclinical Assessment of the Safety of Antisense Oligonucleotides. *Nucleic Acid Ther.* **2023**, *33*, 1–16. <https://doi.org/10.1089/nat.2022.0061>.
38. Finkel, R.S.; Mercuri, E.; Darras, B.T.; Connolly, A.M.; Kuntz, N.L.; Kirschner, J.; Chiriboga, C.A.; Saito, K.; Servais, L.; Tizzano, E.; et al. Nusinersen versus Sham Control in Infantile-Onset Spinal Muscular Atrophy. *N. Engl. J. Med.* **2017**, *377*, 1723–1732. <https://doi.org/10.1056/NEJMoa1702752>.
39. Xavier, A.L.R.; Hauglund, N.L.; von Holstein-Rathlou, S.; Li, Q.; Sanggaard, S.; Lou, N.; Lundgaard, I.; Nedergaard, M. Cannula Implantation into the Cisterna Magna of Rodents. *J. Vis. Exp.* **2018**, 57378. <https://doi.org/10.3791/57378>.

Disclaimer/Publisher's Note: The statements, opinions and data contained in all publications are solely those of the individual author(s) and contributor(s) and not of MDPI and/or the editor(s). MDPI and/or the editor(s) disclaim responsibility for any injury to people or property resulting from any ideas, methods, instructions or products referred to in the content.

- III -

**Therapeutic rescue of the *mdx52* behavioral
deficits**

The central deficits that we characterized in the *mdx52* mouse model in the first part of my thesis, revealed severe alterations of emotional behavioral responses and impaired fear learning and memory. These phenotypes are reminiscent of the emotional phenotype of DMD patients with similar mutation profile (Ricotti et al., 2016; Maresh et al., 2023), thus validating this model as relevant for preclinical therapeutic studies. These alterations constitute reliable behavioral outcomes to evaluate treatment efficacy.

A recent study from our group in Dp427-deficient *mdx* mice demonstrated the efficacy of ICV injection of tcDNA. The exon 23 skipping levels reached 10-30% and led to 10-30% of Dp427 re-expression in different brain structures that normally express Dp427, namely hippocampus, cortex, and cerebellum. Moreover, the treatment induced significant reduction of the abnormal unconditioned fear response and compensation of recognition memory deficits in *mdx* mice (Zarrouki et al., 2022). In the second part of my thesis project, we determined the optimal conditions for local ICV delivery route for tcDNA targeting the exon 51 to reach its maximal efficacy in the brain. Since the start codon of Dp140 lies in exon 51 (Lidov et al., 1995) its skipping exclusively rescues the Dp427 in the brain of *mdx52* mice.

Material and methods: Here, we investigated the impact of the selective rescue of brain Dp427 on the severe emotional reactivity of the *mdx52* model. *Mdx52* mice received the antisense tcDNA targeting the exon 51 by ICV injection; control groups were included: *mdx52* mice injected with the sense tcDNA sequence and WT that received saline injections. The kinetics of treatment efficacy was first assessed at the molecular level: the tcDNA biodistribution, exon 51 skipping levels and protein Dp427 re-expression at 3, 7 and 11 weeks post-ICV. The behavioral study, performed in the optimal therapeutic window within 7-9 weeks post-ICV, consisted in a test battery including paradigms to assess anxiety, in the elevated-plus maze and light/dark choice test, and to evaluate unconditioned fear responses and associative fear learning and memory.

Results: We first showed that single ICV administration of tcDNA induces restoration of 5 to 15% of Dp427 expression in hippocampus, cerebellum, and cortex. We further confirmed that dystrophin expression was stable between 7 and 11 weeks after ICV injection, which defined the optimal therapeutic window for behavioral testing. Anxiety and unconditioned fear responses were significantly improved in treated *mdx52* mice during this period. Moreover, acquisition of fear conditioning was fully rescued, while fear memory tested 24h later was only partially improved. An

additional restoration of Dp427 in skeletal and cardiac muscles by systemic treatment did not further improve the unconditioned fear response, confirming the central origin of this phenotype.

Conclusion: These findings indicate that some emotional and cognitive deficits associated with dystrophin deficiency may be reversible or at least improved by partial postnatal Dp427 rescue. This offers promising therapeutic opportunities to address the brain comorbidities associated with DMD using gene-correction strategies.

Publication 5

Published in *Molecular Therapy Nucleic Acids*, 2023

Molecular Therapy
Nucleic Acids
Original Article



Partial restoration of brain dystrophin by tricyclo-DNA antisense oligonucleotides alleviates emotional deficits in *mdx52* mice

Amel Saoudi,^{1,2} Sacha Barberat,¹ Olivier le Coz,¹ Ophélie Vacca,¹ Mathilde Doisy Caquant,¹ Thomas Tensorer,³ Eric Sliwinski,³ Luis Garcia,¹ Francesco Muntoni,⁴ Cyrille Vaillend,^{2,5} and Aurélie Goyenvalle^{1,5}

¹Université Paris-Saclay, UVSQ, Inserm, END-ICAP, 78000 Versailles, France; ²Université Paris-Saclay, CNRS, Institut des Neurosciences Paris-Saclay, 91400 Saclay, France; ³SQY Therapeutics – Synthena, UVSQ, 78180 Montigny le Bretonneux, France; ⁴The Dubowitz Neuromuscular Centre, Developmental Neurosciences Research and Teaching Department, Great Ormond Street Institute of Child Health, University College London, WC1N 1EH London, UK

The *mdx52* mouse model recapitulates a frequent mutation profile associated with brain involvement in Duchenne muscular dystrophy. Deletion of exon 52 impedes expression of two dystrophins (Dp427, Dp140) expressed in brain, and is eligible for therapeutic exon-skipping strategies. We previously showed that *mdx52* mice display enhanced anxiety and fearfulness, and impaired associative fear learning. In this study, we examined the reversibility of these phenotypes using exon 51 skipping to restore exclusively Dp427 expression in the brain of *mdx52* mice. We first show that a single intracerebroventricular administration of tricyclo-DNA antisense oligonucleotides targeting exon 51 restores 5%–15% of dystrophin protein expression in the hippocampus, cerebellum, and cortex, at stable levels between 7 and 11 week after injection. Anxiety and unconditioned fear were significantly reduced in treated *mdx52* mice and acquisition of fear conditioning appeared fully rescued, while fear memory tested 24 h later was only partially improved. Additional restoration of Dp427 in skeletal and cardiac muscles by systemic treatment did not further improve the unconditioned fear response, confirming the central origin of this phenotype. These findings indicate that some emotional and cognitive deficits associated with dystrophin deficiency may be reversible or at least improved by partial postnatal dystrophin rescue.

INTRODUCTION

Duchenne muscular dystrophy (DMD) is a neuromuscular disease that affects 1:5,000 male births and is associated with non-progressive cognitive, behavioral and neuropsychiatric comorbidities.^{1–3} DMD is caused by mutations in the dystrophin (*DMD*) gene that encodes multiple dystrophin proteins (Dp). Dystrophins are membrane-bound proteins involved in receptor and ion channel clustering in a cell- and tissue-specific manner. The dystrophins differ by their molecular weight, expression, and function. The full-length dystrophins, Dp427 M/C/P, are expressed in muscles (Dp427M) as well as in central GABAergic synapses in brain (Dp427C) and cerebellum where they contribute to the synaptic clustering of GABA_A receptors.^{4,5}

The smaller C-terminal brain dystrophins are expressed from independent internal promoters: Dp260 is selectively expressed in the retina, Dp140 shows enriched expression in the fetal human brain but its cellular localization in adult brain is still unclear,^{5,6} and Dp71 is expressed in excitatory synapses as well as in astrocyte endfeet forming the blood-brain barrier (BBB), where it plays a role in aquaporin 4 (AQP4) regulation.⁷ Mutations in the *DMD* gene lead to muscular dystrophy due to the loss of the muscle dystrophin, while the nature and severity of brain alterations in DMD patients depend on the position of the mutation and on the type and number of dystrophins affected by the mutation.³ While proximal mutations inducing the loss of the full-length Dp427 are generally associated with very modest effect on cognitive function, the more distal ones are associated with more severe deficits due to the cumulative loss of several brain dystrophins.^{8,9} Functional studies of different DMD mouse models provided an essential contribution to our understanding of the affected brain mechanisms depending on the position of the mutation and loss of different dystrophins.^{10–12} We previously demonstrated that the exon52-deleted *mdx52* mouse model,¹³ lacking Dp427, Dp260, and Dp140, shows stronger emotional alterations compared with the original Dp427-deficient-*mdx* mouse model.¹⁰ Indeed, the mutation is located in a “hot spot” region frequently found to be mutated in DMD patients (65%).^{1,3,9} The development of therapeutic approaches in this mouse model is thus of great interest, as it directly translates to patients’ condition. One of the most promising therapeutic strategies for DMD aims to restore the open reading frame to express an internally deleted but still functional protein. This so-called exon-skipping strategy is based on the use of antisense oligonucleotides (ASOs) that interfere with splicing signals or

Received 20 October 2022; accepted 16 March 2023;
<https://doi.org/10.1016/j.omtn.2023.03.009>.

⁵These authors contributed equally

Correspondence: Cyrille Vaillend, Université Paris-Saclay, CNRS, Institut des Neurosciences Paris-Saclay, 91400 Saclay, France.

E-mail: cyrille.vaillend@universite-paris-saclay.fr

Correspondence: Aurélie Goyenvalle, Université Paris-Saclay, UVSQ, Inserm, END-ICAP, 78000 Versailles, France.

E-mail: aurelie.goyenvalle@uvsq.fr



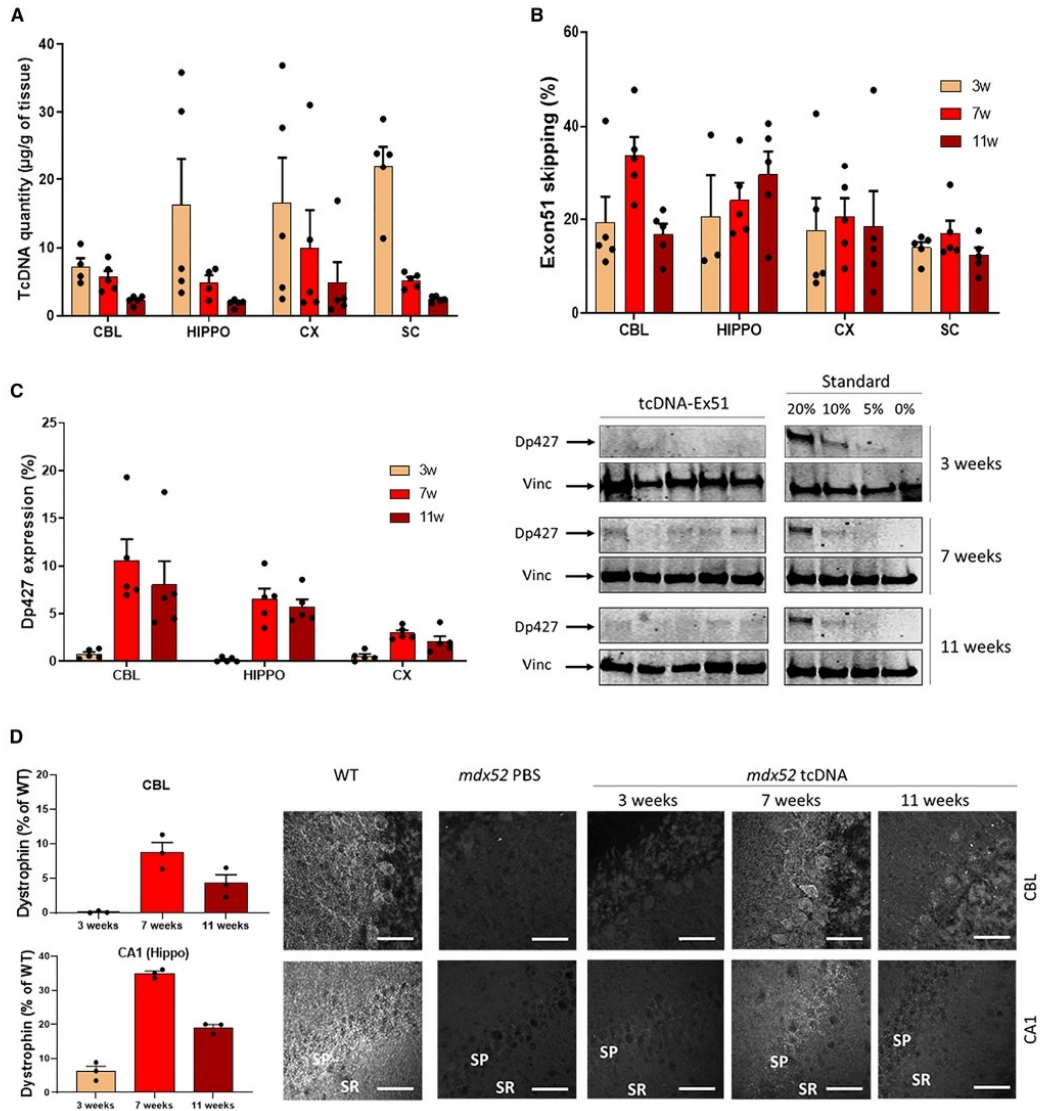


Figure 1. Optimal time frame following i.c.v. delivery of tcDNA-Ex51

(A) Quantification of fluorescent hybridization of tcDNA-Ex51 in various CNS tissues (CBL, cerebellum; HIPPO, hippocampus; CX, cortex; SC, the cervical part of the spinal cord) at 3, 7, and 11 weeks after i.c.v. administration. Results are expressed as mean \pm SEM; $n = 5$ mice per group. (B) Quantification of exon 51-skipping levels by qRT-PCR in same tissues as above at 3, 7, and 11 weeks after i.c.v. administration. (C) Dp427 protein restoration by western blot in the same brain regions as above, at 3, 7, and 11 weeks after i.c.v. administration (mean \pm SEM; $n = 5$ mice per group). Immunoblots shown in the right panel are representative examples of dystrophin restoration in the hippocampus at the different time points. A four-point standard curve made of 0%, 5%, 10%, and 20% of WT lysate (mixed with *mdx52* lysate) was loaded for

(legend continued on next page)

regulatory elements in the exon or intron, thus leading to the skipping of the targeted exon at the precursor (pre-)mRNA level.^{14–16} Previous studies in *mdx52* mice demonstrated the therapeutic potential of the exon-skipping approach to restore expression of Dp427 in muscles using naked ASO¹⁷ or vectorized sequences in AAV-U7snRNA vector.¹⁸ The feasibility of antisense-based therapies has been demonstrated in clinical trials and several ASO drugs have now been conditionally approved by the FDA.¹⁹ However, none of the currently approved ASO drugs are capable of addressing DMD brain comorbidities, mostly because of their inability to cross the BBB. Yet novel ASO chemistries or conjugates are currently being developed and may offer promising tools to treat both the dystrophic phenotype and the central deficits associated with the lack of brain dystrophin. Among these, we have previously demonstrated that tricyclo-DNA (tcDNA)-based ASOs display unprecedented uptake in many tissues including cardiac muscle and central nervous system (CNS) after intravenous administration in mouse models of DMD^{20–22} and SMA.²³ More recently, we have shown that local administration of tcDNA-based ASO in the brain of *mdx* mice lacking only Dp427 alleviates some cognitive deficits associated with DMD.²⁴

In this study, we aimed to investigate the impact of postnatal restoration of brain Dp427 in the more severe *mdx52* model, which is representative of a larger subpopulation of DMD patients. For this purpose, we used a tcDNA-ASO conjugated to palmitic acid²² and targeting dystrophin exon 51, to restore Dp427 exclusively. Given that exon 51 contains the start codon for Dp140, skipping of exon 51 indeed cannot restore Dp140 expression. We first determined the optimal therapeutic window following intracerebroventricular (i.c.v.) microinjection of tcDNA-Ex51 and then assessed its potential in rescuing behavior, using tests in which *mdx52* mice typically show deficits.¹⁰ Anxiety, unconditioned fear, and conditioned fear learning and memory were successively assessed in treated *mdx52* mice. The efficacy of the treatment was also analyzed at the molecular level, and we further evaluated the contribution of partial Dp427 restoration by systemic injection in muscles and heart to rule out the possibility of a peripheral contribution to the behavioral improvements observed.

RESULTS

Optimal time frame for Dp427 restoration following i.c.v. delivery of tcDNA-Ex51

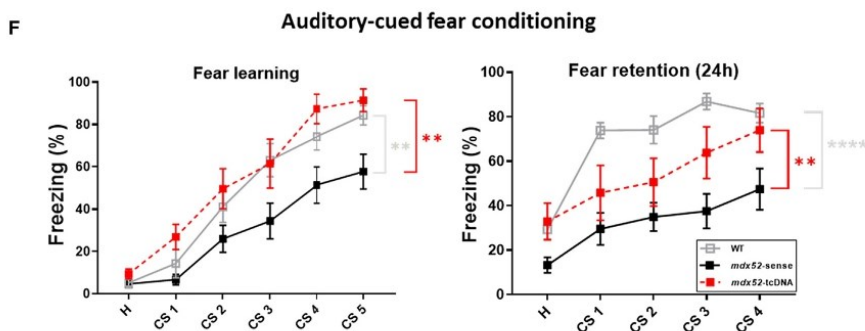
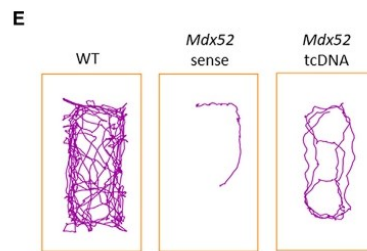
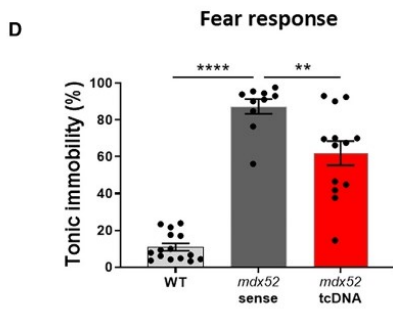
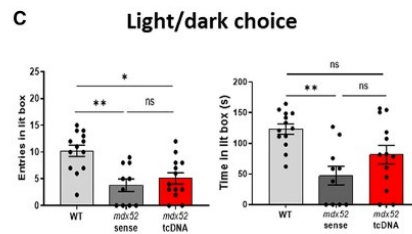
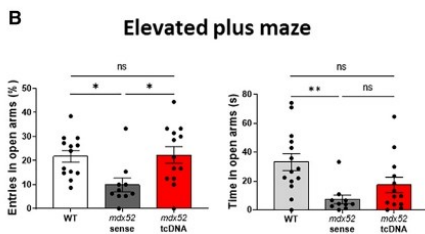
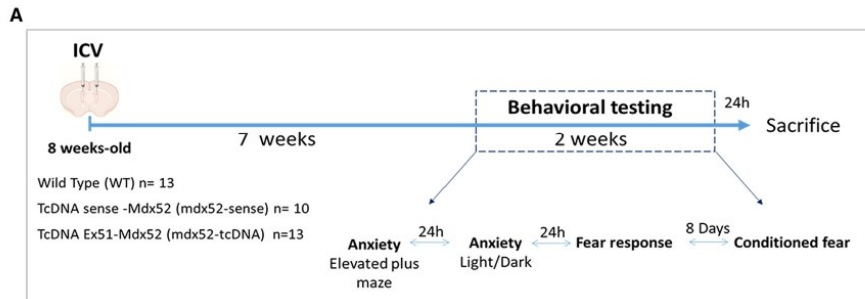
We first investigated the extent and duration of dystrophin restoration following a single injection of tcDNA-Ex51 in each lateral ventricle (bilateral i.c.v. injection) to define the optimal time frame for behavioral studies. For this experiment, 8-week-old *mdx52* mice received i.c.v. injections of a total 400 μg of tcDNA-Ex51. As described previously for tcDNA targeting exon 23,²⁴ the maximal dose was 400 μg , a limitation related to the solubility of the tcDNA-ASOs taken from a 40 mg/mL stock solution for bilateral in-

jections of a 10- μL maximal volume. Distinct groups were analyzed at three different time points: 3, 7, and 11 weeks after the i.c.v. injections. For each time point, we examined different regions of the CNS: the cerebellum, hippocampus, cortex, and the cervical part of the spinal cord. We first analyzed the biodistribution of the tcDNA by quantifying the amount of tcDNA-Ex51 in each structure using a fluorescent hybridization assay. Results presented in Figure 1A indicate that tcDNA-Ex51 was homogeneously distributed (structure effect, $p = 0.2429$) in the different regions after i.c.v. administration and that the quantity was decreasing with time as expected from previous studies (time effect, $p = 0.0036$). We then estimated the efficacy of the treatment by quantifying the levels of exon 51 skipping in the different brain regions by real time TaqMan PCR quantification (Figure 1B).

The i.c.v. injection of 400 μg of tcDNA-Ex51 induced a mean of 30% of exon 51 skipping across the various structures and levels of exon skipping appeared stable between 3 and 11 weeks after the treatment (time effect, $p = 0.3071$, structure \times time point effect ($F(6,34) = 1.195$, $p = 0.3327$). No exon 51 skipping was detected in skeletal muscles (data not shown), indicating no peripheral effect after i.c.v. delivery as shown previously.²⁴ i.c.v. injection of 400 μg of a control (sense) tcDNA induced no exon skipping in any of the analyzed regions (Figure S1). We then quantified the restoration of the dystrophin protein (Dp427) by western blot in the cerebellum, hippocampus, and cortex at the different time points (Figure 1C). Three weeks after i.c.v. administration, the levels of Dp427 were very low ($\sim 1\%$), while after 7 weeks we detected between 3% and 10% of Dp427 production in the different brain regions (structure effect, $p = 0.0042$). These levels were found to be stable between 7 and 11 weeks (time effect, $p = 0.6494$). Despite the presence of a substantial amount of skipped mRNAs, we could not detect any protein restoration in the cervical part of the spinal cord, which may be due to the very low levels of Dp427 normally expressed in this structure (Figure S2).

Dp427 re-expression was also confirmed in *in situ* sections by immunofluorescent staining. Dystrophin is normally expressed in inhibitory synapses of pyramidal neurons, showing typical punctate staining around their soma in the stratum pyramidale (SP) and in the proximal dendritic layer of the stratum radiatum (SR) within the CA1-CA3 hippocampal subfields. Accordingly, Figure 1D shows that dystrophin expression was indeed characterized by a punctate immunoreactive signal reflecting synaptic expression in wild-type (WT) mice as well as in tcDNA-Ex51-treated *mdx52* mice, while it was completely absent in PBS-treated *mdx52* mice. The level of dystrophin restoration was estimated using a semi-quantitative approach based on confocal image analysis in synapses of hippocampal neurons and in the Purkinje cell layer (PCL) and molecular cell layer (MCL) of the cerebellum.⁴ TcDNA-Ex51-treated *mdx52* mice displayed

quantification (the same standard is shown for 7 and 11 weeks since they were loaded on the same gel). Vinculin used as control for normalization. (D) Detection of the restored dystrophin protein by immunofluorescence in the cerebellar Purkinje cell layer and the molecular cell layer, as well as the stratum pyramidale (SP) and proximal stratum radiatum (SR) of the CA1 hippocampal subfield, as indicated. Groups of WT, *mdx52* mice injected with PBS (*mdx52* PBS), and tcDNA-Ex51 (*mdx52* tcDNA) were compared at 3, 7, and 11 week after i.c.v. administration (mean \pm SEM; $n = 3$ mice per group). Scale bars, 12 μm .



(legend on next page)

significant levels of dystrophin re-expression, compared with untreated *mdx52* mice, in the MCL and PCL of the cerebellum at 7- and 11-week time points, ranging from 3% to 12%, while it was barely detectable at 3 weeks. In the SP and SR layers of the CA1 region of the hippocampus, Dp427 was already detectable at low levels (~6%) at 3 weeks, reached approximately 30% at 7 weeks, and then slightly decreased to 20% at 11 weeks (Figure 1D). Dp427 expression was also detected at low levels in the basolateral nucleus of the amygdala, although quite variably between individuals which prevented accurate quantification (Figure S3). Overall, these findings indicate that the optimal therapeutic window is between 7 and 11 weeks after i.c.v. administration, when exon 51 skipping and Dp427 restoration are at their highest levels in the different brain structures.

Effect of partial Dp427 restoration on *mdx52* mice impaired behavior

To assess the functionality of the restored Dp427, groups of 8-week-old *mdx52* and WT littermates received i.c.v. injections as follows: $n = 13$ *mdx52* mice received the tcDNA-Ex51 (*mdx52*-tcDNA), $n = 10$ *mdx52* mice received the control sense sequence of tcDNA (*mdx52*-sense), and $n = 13$ WT mice received the saline solution. Within the therapeutic window determined above (between 7 and 9 weeks after the i.c.v.), the three groups of mice were submitted to behavioral testing, using a selection of tests with low motor demand that had previously highlighted robust emotional-related deficits in *mdx52* mice.¹⁰

The behavioral testing consisted of four consecutive tests separated by at least a 24-h interval (Figure 2A), starting with measures of anxiety in the elevated plus maze then in the light dark choice. In the elevated plus-maze test, anxiety results from the threat induced by the void in the elevated open arms. Global activity in the maze, reflected by the total number of arms visited, was comparable in treated and untreated *mdx52* groups (Figure S4A), while an increased number of entries into open arms was only observed in *mdx52*-tcDNA (Figure S4B). This indicates that the increased number of entries into open arms in the *mdx52*-tcDNA group could not be directly attributed to a change in global activity. As shown in Figure 2B the percent of entries in the open arms was significantly reduced in the control *mdx52*-sense group compared with WT ($p = 0.0242$), a behavioral deficit that is consistent with the deficits previously characterized in

this model. In contrast, in the tcDNA-Ex51-treated *mdx52* group the percent of entries was comparable with the WT group ($p > 0.9999$). The time spent in open arms also appeared similar between the WT and tcDNA-Ex51 groups ($p = 0.1527$) (Figure 2B), which further supports that this phenotype was rescued in this test.

The light/dark choice test that we described previously¹⁰ is based on the choice given to the mice to stay in a secure dark compartment or to explore an anxiogenic (brightly lit) compartment characterized by a gradient of illumination from the trap door (50 Lx) to the end of the compartment (600 Lx). The number of entries into the lit box was found to be comparable between the WT group and the control group *mdx52*-sense, as shown in Figure 2C. However, for the time spent in the lit compartment, which is a good marker of the anxiety level in this test, control *mdx52* mice spent significantly less time in the lit box compared with WT mice ($p = 0.0027$), thus confirming their anxiety-related phenotype. In contrast, tcDNA-Ex51-treated *mdx52* mice spent as much time as the WT mice (ns, $p = 0.1786$) (Figure 2C). The results of these two tests of anxiety suggest that tcDNA-Ex51 treatment has the potential to partly rescue the anxiety phenotype of *mdx52* mice.

The third test/manipulation evaluated the stress-induced freezing response, which is typically characterized by a complete tonic immobilization of the mouse, except for respiration, in mouse models of DMD. It is expressed as the percent time spent in tonic immobility (percent freezing) during a 5-min period following a brief (15 s) manual scruff-restraint, which is considered as a measure of unconditioned fear. Manual restraint did not induce a fear response in the WT mice (mean percent time spent immobile <20%) (Figure 2D). In contrast, in control sense-treated *mdx52* mice, the fear response was clearly expressed (>85%) during 5 min following this mild stress. The freezing behavior observed in *mdx52* mice is reminiscent of the innate antipredator behavior expressed by mice when confronted by fearful stimuli, suggesting that *mdx52* mice express a pathological increase of unconditioned fear-related behaviors. In the tcDNA-Ex51-treated *mdx52* mice, the freezing response was significantly reduced ($p = 0.0017$) compared with the control group (~60% instead of 85%). TcDNA-Ex51-treated *mdx52* mice also displayed an apparently higher mobility in the recording area (Figure 2E), yet the distance traveled was not significantly improved ($p = 0.2727$,

Figure 2. Effect of a partial restoration of Dp427 on *mdx52* mice emotional reactivity

(A) Schematic representation of the study design showing the sample sizes, the age at i.c.v. injection, the post-injection delay at which behavioral testing was initiated (7 weeks), starting with anxiety testing in the elevated plus maze and light/dark choice tests, then quantification of the unconditioned fear response (24-h intervals between tests), and finishing by auditory-cued fear conditioning 8 days later the animals were sacrificed 24 h after the last behavioral testing day and brain structures (cerebellum, hippocampus, and cortex) and spinal cord were harvested. Wild-type littermates were injected i.c.v. with saline (WT) and *mdx52* mice with 400 μ g of control tcDNA-sense (*mdx52*-sense) or tcDNA-Ex51 (*mdx52*-tcDNA). (B) Number of entries and time spent in the open arms of the elevated plus maze, expressed as percent of total arm entries. (C) Number of entries and time spent in the lit box (s) in the light/dark choice test. Results are mean \pm SEM; * $p < 0.05$, ** $p < 0.01$; Kruskal-Wallis test followed by Dunn's post-hoc tests. (D) Unconditioned fear expressed as percent time spent in tonic immobility during a 5-min period of observation following a brief scruff restraint (15 s) (mean \pm SEM; ** $p < 0.01$, *** $p < 0.005$; one-way ANOVA followed by Sidak post-hoc tests. (E) Representative tracking plots during the unconditioned fear test. (F) Auditory-cued fear conditioning. Performance during conditioning (fear learning) and memory retention sessions (fear retention at a 24-h post-conditioning delay) is expressed as the percent time spent freezing during presentation of the conditioned stimulus (tone, 30 s), which was repeated five times during conditioning (CS 1–5; each was an 80 dB tone lasting 30 s, followed by a foot shock) and repeated four times (CS 1–4) during the retention session performed 24 h later in a new context (tone delivered alone; no foot shock). Results are mean \pm SEM; * $p < 0.01$, **** $p < 0.001$ analyzed by two-way ANOVAs.

tcDNA-Ex51 vs. sense controls) (Figure S5A). These results indicate that tcDNA-Ex51 treatment and the associated partial restoration of Dp427 lower the fearfulness induced by a mild stressful event in *mdx52* mice.

Before being submitted to the fourth and last test, all mice were gently handled for a week to minimize their basal stress level. Auditory-cued fear conditioning involves learning of an aversive cue-outcome association. The conditioned fear learning and memory performances were expressed as the percent time spent freezing during presentation of the tone (conditioned stimulus, or CS) that predicts the electric shock (unconditioned stimulus, or US). This performance was analyzed during the habituation period and during the acquisition (fear learning) and retention sessions (24 h later) comparing the tcDNA-Ex51-treated *mdx52* mice with control *mdx52-sense* mice and untreated WT littermates (Figure 2F). Importantly, freezing was low in both genotypes during the initial habituation phase that preceded acquisition (Figure 2F, left panel), while strong freezing responses were conversely observed in all mice following delivery of the electrical foot shocks (Figure S6A, Kruskal-Wallis p value = 0.614). In contrast, freezing during presentation of the auditory tone (CS) progressively increases across trials, thus reflecting learning of the predictive value of CS, i.e., the CS-US association. This was typically observed in the WT mice (Figure 2F, left panel). In contrast, acquisition of fear conditioning was clearly impaired in the control *mdx52-sense* group (Figure 2F), as they exhibited a strongly reduced conditioned freezing response compared with WT ($p = 0.0090$) during presentation of the CS (group effect: $F(2,26) = 8.137$, $p = 0.0018$). In contrast, the conditioned freezing response displayed by the tcDNA-Ex51-treated *mdx52* mice was similar to the WT group ($p = 0.5464$). The deficit in learning the predictive value of the CS observed in the untreated group of *mdx52* mice was observed during the whole learning period (group \times time interaction: $F(10,130) = 1.426$, $p = 0.1756$), a result consistent with our previous study, while tcDNA-Ex51 and partial rescue of Dp427 fully restored the performance of treated *mdx52* mice to WT level.

Twenty-four hours later (retention session, Figure 2F, right panel), the control *mdx52-sense* mice showed a lower amount of freezing during the habituation phase (before CS1 delivery), which might reflect poor memory of the events experienced on the previous day. Accordingly, they also exhibited reduced quantities of freezing during the four presentations of the CS alone (not followed by electric foot shocks) (group effect: $F(2,26) = 13.47$, $p < 0.0001$), thus showing impaired fear memory. It is noteworthy that the control group (*mdx52-sense*) in this study shows a stronger memory deficit compared with our previous study.¹⁰ The major difference between the two studies is that mice of the present study have experienced intracranial surgery, which is not a trivial factor, but instead is known to potentially modify mouse behavior. To consider this parameter all groups (WT, treated and control *mdx52*) underwent the surgery in similar conditions. These results suggest that the impact of surgery was more harmful in *mdx52* mice than in WT and treated *mdx52* mice. In contrast, tcDNA-Ex51-treated *mdx52* displayed a signifi-

cantly higher performance (more freezing) compared with untreated mice ($p = 0.0415$), and this performance was similar to WT levels ($p = 0.1306$). However, performance evolution appears different (group \times time interaction: $F(8,104) = 2.668$, $p = 0.0102$), in particular in response to the first conditioning stimulus (CS1) (tone not followed by electric foot shock), since WT displayed a stronger freezing response ($p = 0.0187$).

In addition, these animals were also tested in the same apparatus for contextual fear memory and showed no impairment for this type of fear-related memory (Kruskal-Wallis, $p = 0.8474$) (Figure S6B), consistent with previous work on the *mdx* mouse model.^{11,25} This further confirms that *mdx52* mice are selectively impaired in their capacity to learn the Pavlovian CS-US association during auditory-cued fear conditioning.

Partial restoration of Dp427 associated to the behavioral rescue in tcDNA-Ex51-treated *mdx52* mice

To evaluate whether these improvements in emotional-related behaviors were in line with the molecular effects of the treatment, we analyzed the different brain regions of treated mice for tcDNA bi-distribution, exon 51 skipping levels, and Dp427 restoration at the end of the behavioral testing period. All groups of mice were therefore analyzed 9 weeks after the i.c.v. administration (24 h after the last behavioral test). Substantial amounts of the tcDNA-Ex51-ASO in the different brain regions was confirmed by fluorescent hybridization assay at this post-administration delay and revealed a homogeneous distribution of the ASO across the CNS ($p = 0.5786$) (Figure 3A). We also confirmed presence of the tcDNA-Ex51 in the hippocampus, cortex, and cerebellum by *in situ* hybridization (ISH) using a complementary probe in tissue sections. We clearly detected the tcDNA-Ex51 in the cerebellum, the CA1 hippocampus region, and the cortex (Figures 3B and S7A). However, it was not detected in the lateral nuclei of the amygdala, such as BLP, LaVm, and LaVL, nor in the striatum (CPu). Interestingly, we detected a tcDNA-Ex51 signal in surrounding regions: low levels in the medio- and centrolateral nuclei of the amygdala (BMP and CeL) and most tcDNA detected was found in the piriform cortex and the amygdalo-hippocampal area (Figure S7B).

Accordingly, qRT-PCR revealed approximately 15% of exon 51 skipping in the cerebellum, hippocampus, cortex, and the cervical part of the spinal cord (structure effect, $p = 0.1275$) (Figure 3C).

To further investigate the localization of the skipped and unskipped mRNA in the brain, we performed *in situ* hybridization using BaseScope duplex probes against exon junctions 50-51 (unskipped mRNA) and 50-53 (exon 51-skipped mRNA in *mdx52*). We successfully detected the exon 51-skipped mRNA in the brain of tcDNA-treated mice (turquoise dots in Figure 3D), while only the unskipped mRNA (red dots) was detected in sense-treated *mdx52* mice. We detected particular high expression of the *Dmd* transcript in the Purkinje cell layer of the cerebellum and in the CA1 hippocampal region, while dots in the cortex were relatively sparse. By quantifying the

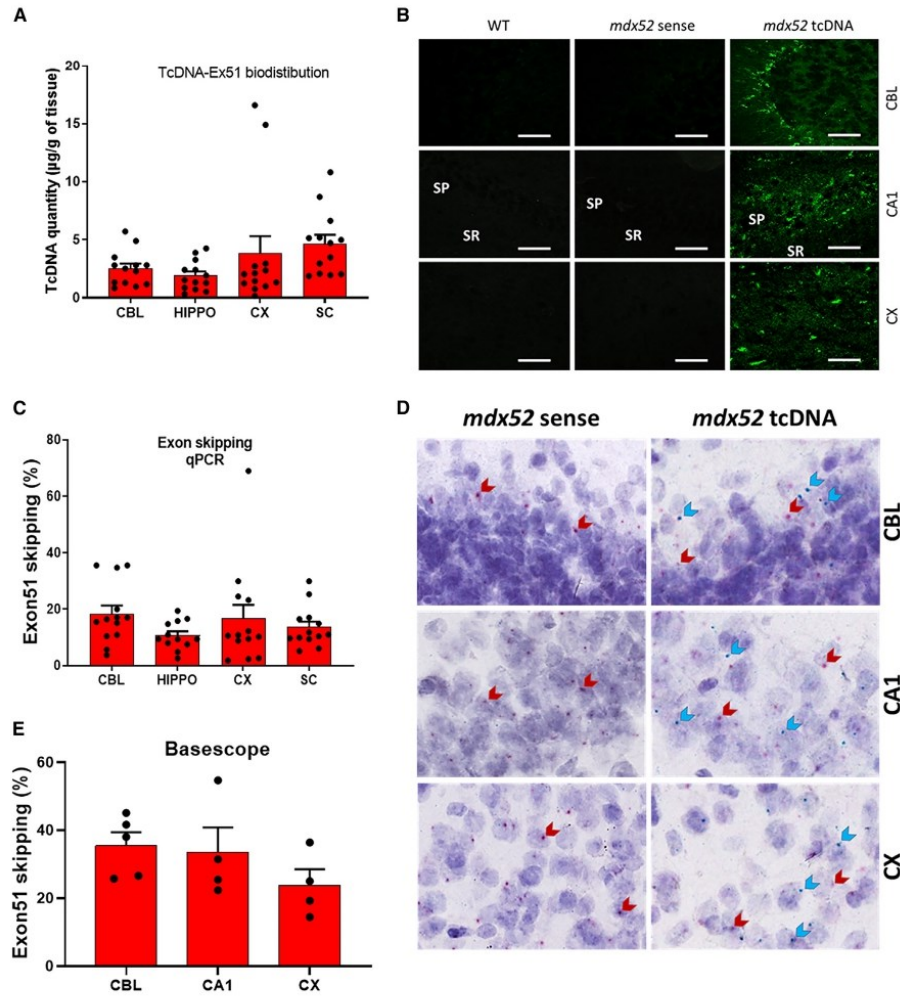


Figure 3. Detection of tcDNA-Ex51 ASO and skipped *Dmd* mRNA 9 weeks after the i.c.v. injection of tcDNA-Ex51 in *mdx52* mice

(A) Quantification by fluorescent hybridization assay of tcDNA-Ex51 content in various CNS tissues (CBL, cerebellum; HIPPO, hippocampus; CX, cortex; SC, the cervical part of the spinal cord) 9 weeks after the i.c.v. administration. Results are expressed as mean \pm SEM; $n = 13$ *mdx52*-tcDNA-Ex51. (B) Detection of tcDNA-Ex51 in different brain regions (CBL, cerebellum; CX, cortex; and CA1 of the hippocampus) by fluorescent *in situ* hybridization. (C) Quantification of exon 51-skipping levels by qRT-PCR in the same tissues as above 9 weeks after i.c.v. administration (mean \pm SEM; $n = 13$ mice per group). (D) Detection of skipped dystrophin mRNA using the BaseScope hybridization technology in the CBL, CA1 region of the hippocampus, and the CX of control-treated (*mdx52* sense) and tcDNA-Ex51-treated *mdx52* mice (*mdx52* tcDNA). BaseScope probes were directed against the exon 50-51 junction for the native (full) mRNA (red dots indicated with red arrows) and against the exon 23-skipped mRNA only detected in tcDNA-Ex51-treated *mdx52* mice (turquoise dots, indicated with blue arrows). Dark blue/purple elements are counterstained nuclei. (E) Percentage of exon 51-skipped mRNAs in the different brain regions, calculated as the total surface covered by turquoise staining (skipped mRNA) normalized to total (red + turquoise) staining (skipped and unskipped mRNA) (mean \pm SEM; $n = 4$ mice per group).

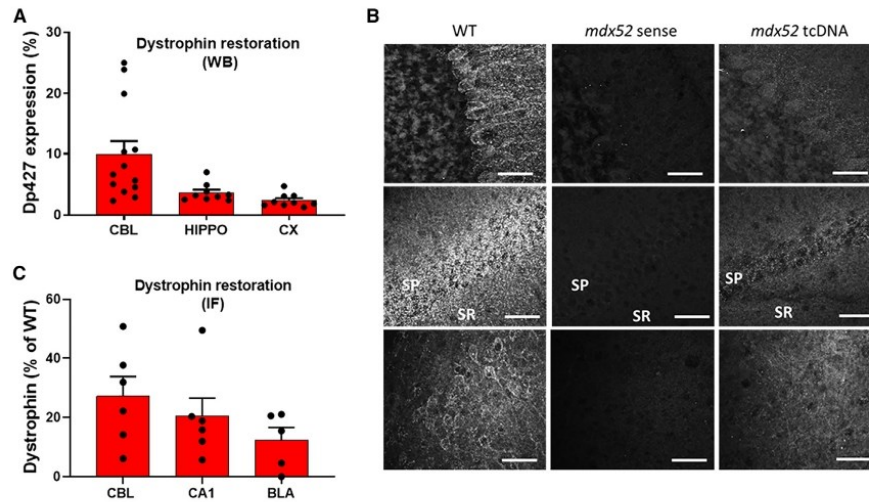


Figure 4. Partial restoration of Dp427 associated to the behavioral rescue in tcDNA-Ex51-treated *mdx52* mice

(A) Quantification of dystrophin protein restoration by western blot in different brain regions (CBL, cerebellum; HIPPO, hippocampus; CX, cortex) 9 weeks after i.c.v. administration. (B) Detection of the restored dystrophin protein by immunofluorescence in the Purkinje cell and molecular cell layers of the cerebellum, in the stratum pyramidal (SP) and proximal stratum radiatum (SR) of the CA1 region of the hippocampus, and in the basolateral nucleus of the amygdala (BLA) of WT and *mdx52* mice 9 weeks after the i.c.v. administration of tcDNA-sense sequence (*mdx52* sense) or tcDNA-Ex51 (*mdx52* tcDNA). Scale bars, 12 μ m. (C) Quantification of dystrophin restoration detected by immunofluorescence in the different structures. Results are expressed as mean \pm SEM; n = 3–6 mice per group.

relative area covered by the red and blue signals, we were able to estimate the level of exon skipping in the different brain regions. We report an average of 33.5% of exon 51 skipping in the CA1 layer of the hippocampus, 23.8% in the cortex, and 35.5% in the cerebellum (Figures S3E and S8A). Interestingly in the cerebellum, while the quantification represents the average staining across the different lobules, we were able to detect higher skipped transcripts in the lobules close to the fourth ventricle compared with more distant lobules (Figure S8B). In addition, we were also able to detect few dots corresponding to exon 51-skipped transcripts the BLA region of the amygdala (Figure S8A).

We also quantified the levels of Dp427 restoration in the various brain regions using immunoblots and found 9.9% protein levels in the cerebellum, 3.6% in the hippocampus, and 2.4% in the cortex of tcDNA-Ex51-treated *mdx52* mice (ANOVA $p = 0.0004$, CBL vs. HIP $p = 0.0019$, CBL vs. CX $p = 0.001$, HIP vs. CX $p = 0.9743$) (Figures 4A and S9). No Dp427 was detected in skeletal muscles (data not shown), indicating no peripheral effect after i.c.v. delivery. We also checked the expression of Dp140, the re-expression of which following treatment was not expected since skipping of exon 51 should remove the start codon of Dp140. Our results confirmed the absence of Dp140 in both control- and tcDNA-treated *mdx52* mice (Figure S10).

Finally, we determined the localization of the restored Dp427 using immunofluorescence techniques and the DYS-1 antibody directed

against the N terminus of the dystrophin protein (Figure 4B). This revealed approximately 25% of Dp427 restoration in the cerebellum (in both the PCL and MCL) and 20% in the CA1 region (in SP and SR layers) of the hippocampus, in line with the distribution of the tcDNA and skipped mRNA. Moreover, we found approximately 12% of Dp427 expression in the basolateral nucleus of the amygdala (Figure 4C).

Altogether, these results indicate that administration of tcDNA-Ex51 in the lateral ventricles of *mdx52* mice induces exon 51 skipping and a partial restoration of Dp427 in the cerebellum, hippocampus, and cortex of treated mice. This postnatal restoration in the range of 3%–10% of WT levels partially rescued the emotional-related deficits in this mouse model. Yet, we noticed that some parameters analyzed during the fear response (such as distance traveled shown in Figure S5A) were not rescued by the partial restoration of Dp427 in the CNS. This is intriguing given that we have previously shown that a low level of Dp427 restoration in the CNS (in the range of 2%) following systemic delivery of tcDNA-ASO could lead to the correction of the abnormal restraint-induced fear response in *mdx* mice.^{20–22} This raises questions about the involvement of the peripheral system, including skeletal and cardiac muscles, in this deficit. To further investigate this aspect and evaluate whether rescue of Dp427 in the periphery could improve the partial rescue in the restraint-induced fear response, we performed combined intravenous and central treatments.

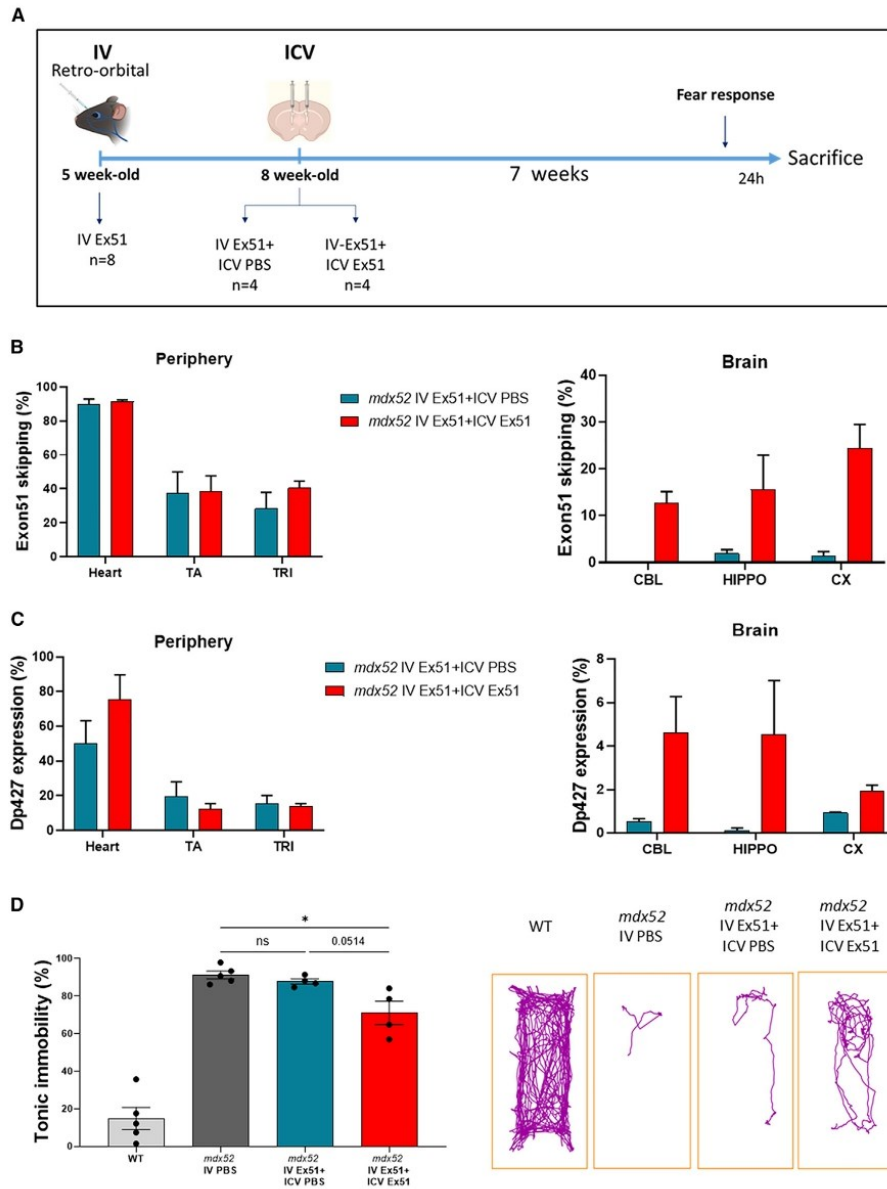


Figure 5. Combined restoration of Dp427 in muscles and brain using i.v. injection of AAV-U7-Ex51 and i.c.v. injection of tcDNA-Ex51

(A) Schematic representation of the study design showing the sample sizes, the time of i.v. and i.c.v. injections, and the post-injection delay at which fear response was assessed (7 weeks post-i.c.v.). (B) Quantification of exon 51-skipping levels by qRT-PCR in peripheral tissues (heart; TA, tibialis anterior; TRI, triceps) and brain tissues (CBL,

(legend continued on next page)

Combined restoration of Dp427 in muscles and brain

We combined a systemic treatment using the previously described AAV-U7snRNA system^{18,26} with the i.c.v. injection of tcDNA-Ex51. The experimental design is represented in Figure 5A. A group of 5-week-old *mdx52* mice was first injected intravenously with scAAV9-U7Ex51, which has been shown to rescue Dp427 expression in muscles and heart, but not in the brain.¹⁸ Half of these systemically treated *mdx52* mice also received an i.c.v. injection of tcDNA-Ex51 3 weeks later (group named i.v. Ex51 + i.c.v. Ex51, $n = 4$), while the other half received an i.c.v. injection of saline (group named i.v. Ex51 + i.c.v. PBS, $n = 4$). Groups of control *mdx52* mice ($n = 5$, only injected i.v. with PBS) and WT mice ($n = 5$) were also included in the study. Brain and muscle tissues were analyzed 7 weeks after the i.c.v. injection, which corresponds to approximately 10 weeks after the intravenous delivery of AAV, when mice were aged 15 weeks.

Exon 51 skipping levels were measured both in the CNS and in the periphery following both types of treatment (i.v. Ex51 + i.c.v. PBS or i.v. Ex51 + i.c.v. Ex51). We detected similar levels of exon 51 skipping in the periphery after both treatments, with up to 95% of exon skipping in the heart and ~40% in the tibialis anterior (TA) and triceps (TRI) (Figure 5B), confirming the peripheral effect of the AAV-U7Ex51 with no additional effect of the subsequent i.c.v. administration (treatment effect, $p = 0.5224$). In contrast, and as expected, exon 51 skipping levels in the CNS were much higher (treatment effect, $p = 0.0033$) when the initial i.v. injection of scAAV9-U7Ex51 was followed by the i.c.v. injection of tcDNA-Ex51. Exon 51 skipping was relatively homogeneous in the different regions (structure effect, $p = 0.228$) in the *mdx52* mice that received the i.c.v. injection of tcDNA-Ex51, as observed previously (Figures 1B and 3C). This was in line with the distribution of tcDNA-Ex51 in the different brain regions ($p = 0.4451$) (Figure S11). Western blot analysis also revealed comparable restoration levels of the Dp427 protein in the periphery in both treatment groups (treatment effect, $p = 0.5774$), reaching about 50% of WT levels in the heart and 15% in the TA and the TRI (Figure 5C). In the CNS, 3%–10% of Dp427 expression was detected in the different brain regions of the i.v. Ex51 + i.c.v. Ex51 group, while less than 1% was detected in the i.v. Ex51 + i.c.v. PBS group. These analyses confirmed that the i.v. Ex51 + i.c.v. PBS group displayed mostly Dp427 restoration in the periphery, while the combined i.v. Ex51 + i.c.v. Ex51 group displayed Dp427 both in the periphery and in the CNS.

The fear response was assessed in these mice and is shown in Figure 5D. A representative tracking plot for each group illustrates the mice mobility following the different treatments. The fear response of the i.v. Ex51 + i.c.v. PBS group was not different from the i.v.

PBS ($p = 0.5933$), suggesting that postnatal peripheral rescue of Dp427 had no impact on this phenotype. In contrast, the i.v. Ex51 + i.c.v. Ex51 group showed significantly lower freezing amount after acute stress induction compared with the i.v. PBS group ($p = 0.0203$) and this was also marginally significant compared with the i.v. Ex51 + i.c.v. PBS group ($p = 0.0514$) (Figure 5D). This confirms our previous results indicating that partial restoration in the CNS had a positive effect on the fear response. Importantly, however, the amount of freezing in the i.v. Ex51 + i.c.v. Ex51 group was not statistically different from *mdx52* treated with i.c.v. Ex51 only, as shown in Figure 2D (~60% of freezing) ($p = 0.3645$). Similarly, the distance traveled (Figure S4B) was not significantly improved in the i.v. Ex51 + i.c.v. Ex51 group compared with controls ($p = 0.9240$), as previously shown for i.c.v. only (Figure S5A). These results indicate no significant cumulative effect of the peripheral rescue of Dp427 over a partial central restoration on the fear response rescue in *mdx52* mice.

DISCUSSION

Cumulative loss of centrally expressed dystrophin proteins (Dp427, Dp260, Dp140, and Dp71) is associated with more severe emotional and cognitive deficits in DMD patients.^{1,9} The *mdx52* mouse model (lacking Dp427, Dp260, and Dp140) is therefore a useful model to investigate brain comorbidities in DMD and their potential reversibility. We previously confirmed that *mdx52* mice that carry a mutation profile frequently found in DMD patients display more severe phenotypes than *mdx* mice that only lack Dp427.¹⁰ In particular, *mdx52* mice display enhanced anxiety and a severe impairment in learning an amygdala-dependent Pavlovian association. In this context, we aimed to evaluate an exon-skipping approach targeting the dystrophin exon 51, which is expected to selectively restore Dp427 expression in this model. DMD patients amenable to exon 51 skipping represent the largest patient group eligible for exon skipping therapy, i.e., approximately 13% of DMD patients.²⁷ The PMO ASO eteplirsen was the first approved drug for the treatment of DMD in the US in 2016.²⁸ However, since exon 51 contains the initiation codon for Dp140, the exclusion of this exon can only rescue Dp427 (and Dp260 expressed in the retina).

In this study, we investigated the impact of Dp427 restoration on CNS alterations in the *mdx52* model. For that purpose, *mdx52* mice were treated with the maximal feasible dose (400 μ g) of tcDNA-Ex51 in the lateral brain ventricles. We first showed that tcDNA-Ex51 was homogeneously distributed in the different brain regions following i.c.v. injection, inducing approximately 20%–30% of transcripts skipped for exon 51. Interestingly, the half-life of tcDNA in brain regions was longer than what we had previously reported in skeletal muscles

cerebellum; HIPPO, hippocampus; CX, cortex) 7 weeks after the i.c.v. administration. Results are expressed as mean \pm SEM; $n = 4$ mice per group. (C) Quantification of Dp427 protein levels by western blot in peripheral tissues (heart; TA; TRI) and brain tissues (CBL; HIPPO; CX) 7 weeks after i.c.v. administration. Results are expressed as mean \pm SEM; $n = 4$ mice/group. (D) Restraint-induced unconditioned fear responses expressed as the percent time spent freezing (left panel) and representative tracking plots (right panel) for each group. *Mdx52* mice were injected i.v. when they were 5 weeks old with PBS (*mdx52* i.v. PBS) or with AAV-U7Ex51, then i.c.v. at 8 weeks old with PBS (*mdx52* i.v. Ex51 + i.c.v. PBS) or Ex51:tcDNA-Ex51 (*mdx52* i.v. Ex51 + i.c.v. Ex51) and compared with WT littermates (WT). Results are expressed as mean \pm SEM; $n = 4$ mice/group.

after systemic delivery,²² where only about 10% of ASO was found left in tissues 12 weeks after the end of the treatment. More importantly exon skipping levels were found to be very stable between 3 and 11 weeks after the injection, which is in line with previous reports indicating a particularly long lasting effect of ASO in the CNS.²⁹ Dp427 protein expression, ranging from 5% to 10% in the different brain regions appeared stable between 7 and 11 weeks after the i.c.v., which determined the optimal therapeutic window to investigate treatment effect on the behavioral phenotypes found to be impaired in this mouse model.

To evaluate the impact of Dp427 rescue on behavioral phenotypes, groups of *mdx52* mice received either a tcDNA targeting exon 51 or a control tcDNA sense sequence, and their WT littermates received saline to take the surgery bias into consideration. The animals were successively submitted to a selection of tests in which *mdx52* mice display strong deficits. Anxiety was the first central disturbance analyzed using two distinct behavioral tests. We found that treatment with tcDNA-Ex51 fully compensated the anxiety phenotype measured in the elevated plus-maze test, while emotional reactivity was only partially improved in the light/dark choice test. Interestingly, we noticed that all injected mice displayed more anxiety compared with non-injected mice in our previous study.¹⁰ The differences between WT and control *mdx52* were also lower in this study, suggesting a potential effect of the surgery, which might have partially masked or attenuated the treatment efficacy. The third test performed was the unconditioned fear response. This is one of the main behavioral outcomes in *mdx52* mice, which likely reflects a maladaptive response to mild stress and enables to measure their pathological stress reactivity. Treatment with tcDNA-Ex51 induced a significant reduction of the fear response in *mdx52* mice, despite a large variability observed between individuals. An additional parameter, the distance traveled, measured during this test, was not significantly improved, indicating a partial recovery improvement. Finally, we evaluated the effect of treatment on mouse performance in the auditory-cued fear conditioning, in which *mdx52* mice display robust impairments in acquiring and recalling fear memories. We show that treatment rescues acquisition of this Pavlovian associative learning and partially improves the recall of fear memory. This suggests that low restoration of brain Dp427 was sufficient to compensate the learning deficits but was insufficient to fully overcome the fear memory deficits during fear conditioning. These findings contrast with those reported previously in *mdx* mice with a mutation in exon 23 (hence only lacking Dp427), in which partial Dp427 restoration only slightly improved fear memory but had no effect on fear learning.²⁴ One possible explanation may be the localization of the restored Dp427, which appears higher in the cerebellum of *mdx52*-treated mice in this study than previously treated *mdx* mice, in which restoration was higher in the hippocampus.²⁴ The biodistribution of the tcDNA-Ex51 indeed appears more homogeneous across the different brain regions than in our previous study using the same dose of a tcDNA targeting the *mdx* exon 23, which may be due to sequence-specific properties of each ASO. Higher restoration of Dp427 in the cerebellum may explain this difference in fear-learning

performances; indeed, recent studies showed an involvement of the cerebellum in fear-learning tasks.³⁰ Overall, we demonstrate that the tcDNA-Ex51 central treatment improves both the emotional reactivity and emotional learning in *mdx52* mice.

While our results are particularly encouraging for the future treatments of DMD patients, they also raise many questions related to the incomplete rescue of the phenotypes. A first hypothesis to explain this partial phenotypic rescue is that the absence of Dp140 participates in the genesis of these phenotypes, but it is not restored by post-natal exon 51 skipping. This is supported by our previous observation that anxiety is more severe in *mdx52* mice compared with *mdx* mice lacking only Dp427. However, the unconditioned fear response was not completely rescued either, although previous studies reported similarly enhanced fear responses in *mdx* and *mdx52* mice,^{10,31} suggesting that this phenotype is mainly caused by the lack of Dp427. This is also supported by our previous work showing that Dp427 restoration in the brain can completely rescue the fear response in *mdx* mice.²⁴ The partial improvement in the fear response observed here in *mdx52* mice and the high inter-individual variability could alternatively be due to the low levels of Dp427 restored. Indeed, in this study, efficient exon 51 skipping (10%–30% across the different brain regions) only restored 3%–10% of Dp427 protein, while we demonstrated previously that a similar treatment with a tcDNA targeting exon 23 restored up to 25% of Dp427 in the hippocampus of *mdx* mice.²⁴ This discrepancy in dystrophin restoration between *mdx* and *mdx52* mice, which has been reported previously,¹⁸ is not due to variable skipping efficacy between exon 23 and 51, which are relatively similar (20%–30%). Instead, it was suggested that it may be due to differences in the *Dmd* mRNA levels between *mdx* and *mdx52* models, given that the *DMD* gene is subjected to transcript imbalance, limiting the amount of transcripts available in particular in the 3' region.^{32,33} However, we have also shown previously in *mdx* mice that a systemic—intravenous—treatment with tcDNA-ASO induces only very low levels of Dp427 in the brain, but normalizes the fear response.²⁰

Taking all these observations into consideration, we hypothesized that the slightly more severe muscle phenotype of *mdx52* mice compared with *mdx* mice,³⁴ also shown to be more severe on the C57Bl/6 genetic background,³⁵ could have had an impact on the fear response, which therefore could not be fully restored by intracerebral treatment only. Recent studies questioned the involvement of central and peripheral dystrophin in stressful conditions.^{36–38} Razzioli et al. indeed demonstrated that transgenic *mdx* mice expressing dystrophin or utrophin in skeletal muscles display significantly lowered fear response after a scruffing-induced stress but still not to the WT level, which does not fully account for the peripheral origin of the phenotype. Moreover, by knocking out the nSmase2/Smpd3 inflammation regulatory protein in *mdx* mice, it was found that the reduced inflammation in this model was associated with a decreased fear response.³⁷ Lindsay et al., in line with these studies showed an activation of the hypothalamic-pituitary-adrenal axis suggesting a central involvement.³⁶ In parallel, previous studies showed a fully

rescued fear response following a locally central treatment in *mdx* mice confirming a strong central origin to this phenotype.²⁴

The extent of skeletal muscle involvement in *mdx* mouse models (including the *mdx52* model) is relatively mild, in particular when the mice are young as in this study where the behavior is analyzed at age 3–4 months. For example, the mean duration of visits (total time spent in the lit compartment normalized to the number of visits) in the light/dark choice test was comparable between the *mdx52* group and their WT littermates (Figure S12), indicating no major hypoactivity in this mouse model. Yet, some specific parameters with higher muscular demand, such as the grip strength test, were previously shown to be significantly reduced in *mdx52* compared with *mdx* mice.³⁴ We therefore wondered if the absence of Dp427 in muscles and heart could contribute to the only partial rescue of the restraint-induced fear response that we observed in *mdx52* mice after treatment with tcDNA-Ex51. In the present study, we demonstrate that the peripheral restoration of Dp427 in skeletal (15% in the TA and the TRI) and cardiac (50% of WT levels) muscles using scAAV9-U7Ex51¹⁸ does not improve the fear response on its own. Moreover, a treatment combining i.v. injection of scAAV9-U7Ex51 and the i.c.v. injection of tcDNA-Ex51 does not improve further the effect on the fear response compared with i.c.v. alone of tcDNA-Ex51. These results confirm that brain Dp427 plays a major role in the genesis of the fear response phenotype.

Concluding remarks

Our results suggest that restoring Dp427 in the brain postnatally, even partially, can improve or at least alleviate some severe central comorbidities associated with DMD. More investigations are needed to explore the possibility to further improve the postnatal reversibility of these deficits. It would be interesting to investigate higher levels or structure-specific restoration of Dp427, such as in the amygdala, but also restoration at earlier time points (in neonates, for example) to see whether a more complete rescue could be achieved. Finally, considering that *mdx52* mice also lack Dp140 in the brain, it would be particularly insightful to investigate its restoration, either alone or in combination with Dp427, using exon 53 skipping. These future lines of research would help shed some light on the role of Dp140 and its involvement in the central functions. Yet, these findings are particularly encouraging at a time where new generations of ASO are being developed and may offer the exciting opportunity to treat both the dystrophic muscle phenotype and the brain comorbidities in DMD patients.

MATERIALS AND METHODS

Animals and ASOs

Exon 52-deleted X chromosome-linked muscular dystrophy mice (*mdx52* mice) were generated by the group of Dr. Katsuki Motoya.¹³ It was produced by replacement of exon 52 of the *DMD* gene by the neomycin resistance gene, thereby eliminating expression of Dp427, Dp260, and Dp140 dystrophins but preserving expression of Dp116 (in peripheral nerves) and of Dp71 (in brain and retina).¹³ The mouse line was backcrossed with the C57BL/6J strain for more

than eight generations. The mouse line has been provided by Prof. Sasaoka Toshikuni (Department of Comparative & Experimental Medicine/Brain Research Institute; Niigata University, Japan). Breeders were provided to our lab by Dr. Jun Tanihata and Dr. Shin'ichi Takeda (National Center of Neurology and Psychiatry, Tokyo, Japan). Heterozygous females were crossed with C57BL/6J males to generate *mdx52* and littermate control (WT) males in the animal facility of Neuro-PSI at Saclay (France). Genotypes were determined by PCR analysis of tail DNA. Animal care and all experimental procedures complied with the European Communities Council Directive (CEE 86/609/EEC), EU Directive 2010/63/EU, French National Committee (87/848) and Ethic Committee (Paris Center et Sud, no. 59).

The tcDNA-Ex51 used in this study targets an exonic splicing enhancer within exon 51 of the dystrophin pre-mRNA (position +48 + 62) and was synthesized by SQY Therapeutics (Montigny-le-Bretonneux, France). The control tcDNA named tcDNA-sense is the complementary sequence and was therefore not hybridizing to the target dystrophin pre-mRNA. Palmitic acid was conjugated at the 5' end of the tcDNA full phosphodiester via a C6-amino linker and a phosphorothioate bond as described previously.²²

Stereotaxic surgery and systemic injections

i.c.v. injections were performed in 6- to 8-week-old *mdx52* and WT littermate male mice deeply anesthetized by a single intraperitoneal injection of ketamine (95 mg/kg)/medetomidine (1 mg/kg). tcDNA-Ex51, tcDNA-sense, or saline solutions (phosphate-buffered saline, 0.1 mol/L) were injected bilaterally into the lateral brain ventricles (–0.5 mm from bregma; 1 mm lateral; –2 mm from dura).³⁹ A volume of 5 μ L was infused in each ventricle at a rate of 0.3 μ L/min. A total amount of 400 μ g of tcDNA-Ex51 was thus distributed bilaterally. The systemic treatment consisted in intravenous retro-orbital injections under gaseous anesthesia (2.5% isoflurane mixed with air). A group of 5-week-old male *mdx52* mice was injected with 3 E+14 vector genomes (vg) of self-complementary adeno-associated vector serotype 9 encoding the U7snRNA engineered to target dystrophin exon 51 (scAAV9-U7Ex51M), as described previously.^{18,40} Treatment of animals was pseudorandomized in each cage so that it was balanced within the litters and with comparable distribution among litters.

Experimental groups

Siblings were kept in groups (two to five per cage) under a 12-h light-dark cycle (light on: 7.00 a.m.) with food and water *ad libitum*. For the kinetics study, groups of five mice were used, and *mdx52* mice received i.c.v. injections of either tcDNA-Ex51 or saline. The animals were sacrificed at three different time points: 3, 7, and 11 weeks after i.c.v. injection (n = 5 per time point). Brains were dissected out, one hemisphere was fresh frozen in dry ice for *in situ* analysis and the other one was dissected to isolate hippocampus (HIP), cerebellum (CBL), cortex (CX), and the cervical part of the spinal cord samples that were snap-frozen in liquid nitrogen for biodistribution, qPCR, and western blot analyses.

For the behavioral study, three groups of mice were used and underwent surgery in identical conditions. Eight-week-old *mdx52* male mice were treated with the tcDNA-Ex51 (n = 13) or with the tcDNA-sense as a control (n = 10), while WT littermate males were treated with saline (n = 13). Seven weeks after i.c.v. injections, within a therapeutic window of 2 weeks, the mice were tested in a battery of behavioral tests in the following order: elevated plus maze, light/dark choice test, and restraint-induced unconditioned fear with 24 h interval. The order of the tests was specifically chosen to minimize their influence on each other. A week of gentle handling preceded the auditory-cued fear conditioning, to reduce stress before testing. Behavioral testing was performed blind to the genotype. The experimental protocol is shown in Figure 2A. For the treatment combining systemic and central injections, a separate group of *mdx52* male mice (n = 8) underwent intravenous injections of 3 E+14 vg of scAAV9-U7Ex51M. Three weeks later, half of them also received tcDNA-Ex51 by i.c.v. and the other half received saline. Seven weeks after the i.c.v. injections, these animals and their non-injected WT littermates (n = 5) were submitted to restraint-induced unconditioned fear.

Behavioral analysis

Elevated plus-maze

The maze had two facing arms enclosed with high walls (closed arms, 20 × 8 × 25 cm), two open arms without walls (20 × 8 cm), and a central area (8 × 8 cm) forming a plus sign situated above a vertical stand to elevate the maze 65 cm above the floor. Illumination was 150 lx in open and 30 lx in closed arms. Mice were individually placed at the center of the maze with the head facing a closed arm. The number of entries and time spent in open or closed arms were manually scored for 5 min.

Light-dark choice

The apparatus had 20-cm-high Plexiglas walls and consisted of a black and dark compartment (15 × 15 cm; illumination <15 lx) connected by a trap door (6 × 6 cm) to a brightly lit white compartment (40 × 15 cm). Bright illumination was provided by a light source placed at the end of the white compartment, opposite from the trap door to create an illumination gradient (50 lx close to the trap door to 600 lx close to the light), as described previously.¹⁰ Each mouse was placed in the dark compartment for 10 s, the trap door was then open, and the mouse allowed to freely explore the whole apparatus for 5 min. Step through latency, number of entries, and total time spent in the lit compartment were manually scored by the experimenter.

Restraint-induced unconditioned fear

The mouse was restrained by grasping the scruff and back skin between thumb and index fingers, while securing the tail between the third and little fingers and tilting the animal upside-down in order that the ventral part of its body faced the experimenter. After 15 s, the mouse was released to a novel cage (24 × 19 cm, with 12-cm-high walls) containing clean sawdust and then video-tracked for 5 min under dim illumination (60 lx) using the Any-maze software (Stoelting). Unconditioned fear responses induced by this short acute

stress were characterized by periods of tonic immobility (freezing) and quantified during a 5-min recording period. Complete immobilization of the mouse, except for respiration, was regarded as a freezing response.⁴¹ The percent time spent freezing was calculated for group comparisons.

Auditory-cued fear conditioning

The conditioning procedure was carried out using the StartFear system (Panlab, Barcelona) under the same conditions previously used in our studies of *mdx* and *mdx52* mice.^{10,11} The conditioning chamber (25 × 25 × 25 cm) had three black methacrylate walls, a transparent front door, a grid floor connected to a shock scrambler to deliver unconditioned stimuli (US), and a speaker mounted on the ceiling to deliver audible tones as conditioned stimuli (CS). The conditioning chamber rested on a high sensitivity weight transducer system to generate an analog signal reflecting animal's movement. The chamber was confined in a ventilated soundproof enclosure (67 × 53 × 55 cm) on an anti-vibration table with a surrounding 60-dB white noise. Interchangeable floors and walls (i.e., plain floor and white walls) were used to analyze retention of cued fear in a novel context. On the first day (acquisition), a 2-min baseline period (habituation "H") was recorded before delivery of five CS-US pairs (tone [CS], 80 dB, 10 kHz, 30 s; footshocks [US], each at 0.4 mA for 2 s) with variable and pseudo-randomly distributed intervals between pairs of stimuli (60, 120, and 180 s). On the next day (retention), the session started by placing the mouse in a different context for 2 min (H) before delivery of four CS (80 dB, 10 kHz, 30 s) separated by intervals of variable durations (60, 90, and 120 s). Animals' movements were sampled at 50 Hz for quantitative analysis (FREEZING software, Panlab). Freezing was measured during delivery of the CS (periods of 30 s) to specifically reflect associative learning performance.⁴²

tcDNA tissue quantification by fluorescent hybridization assay

Tissues were homogenized using the Precellys 24 (Bertin Instruments, France) in lysis buffer (100 mmol/L Tris-HCl [pH 8.5], 200 mmol/L NaCl, 5 mmol/L EDTA, 0.2% sodium dodecyl sulfate) containing 2 mg/mL of proteinase K (Invitrogen) (50 mg tissue/mL of buffer), followed by incubation overnight at 55°C in a hybridization oven. After centrifugation at 14,000 rpm (Sorval ST 8R centrifuge, 75005719 rotor) for 15 min, the supernatant was used in the assay. Quantification of tcDNA was performed using a hybridization assay with a molecular beacon probe as described previously.⁴³ In brief, 10 µL of tissue lysates was incubated with a 5' Cy3-DNA complementary probe conjugated with HBQ quencher at 3' in a black non-binding 96-well plates (Thermo Fischer Scientific); PBS was added to a final volume of 100 µL per well and fluorescence was measured on a spectrophotometer (Ex 544 nm/Em 590 nm using FluoStar Omega). The amount of tcDNA in tissues was determined using a standard curve build on the measurement of known tcDNA quantities dissolved in the respective tissue lysates of saline-treated animals.

RNA analyses

Total RNA was isolated from dissected brain structures using TRIzol reagent according to the manufacturer's instructions (Thermo Fisher

Scientific). For visualization of exon-skipping efficacy on gels, aliquots of 1 µg of total RNA were used for RT-PCR analysis using the Access RT-PCR System (Promega) in a 50-µL reaction using the external primers Ex49F (5'-AAACTGAAATAGCAGTTCAAGC-3') and Ex 53R-Aoki (5'-ACCTGTTCCGGCTTCTTCCTT-3'). The cDNA synthesis was carried out at 55°C for 10 min, followed by the PCR of 30 cycles of 95°C (30 s), 58°C (1 min), and 72°C (1 min). PCR products were analyzed on 1.5% agarose gels.

Exon 51 skipping was also measured by TaqMan quantitative PCR as described,¹⁸ using a TaqMan assays designed against the exon 50-51 junction (assay Mm.PT.58.41685801: forward: 5'-CAAAGCAGCCTGACCGT-3'; reverse: 5'-TGACAGTTTCTTAGTAACACAG-3'; probe: 5'-TGGACTGAGCACTACTGGAGCCT-3') and the exon 50-53 junction (forward: 5'-GCACTACTGGAGCCTTTGAA-3'; reverse: 5'-CTTCCAGCCATTGTTGAATC-3'; probe: 5'-ACAGCTGCAGAACAGGAGACAACA-3') (Integrated DNA Technology). One hundred and fifty nanograms of cDNA was used as input per reaction and all assays were carried out in triplicate. Assays were performed under fast cycling conditions on a Bio-Rad CFX384 Touch Real-Time PCR Detection System, and all data were analyzed using the absolute copy number method. For a given sample, the copy number of skipped product (exon 50-53 assay) and unskipped product (exon 50-51 assay) were determined using the standards Ex49-54Delta52 and Ex49-54Delta51 + 52, respectively (gBlocks gene fragments from Integrated DNA technology). Exon 51 skipping was then expressed as a percentage of total dystrophin transcripts (calculated by the addition of exon 50-51 and exon 50-53 copy numbers).

Western blot analyses

Protein extracts were obtained from brain structures treated with RIPA lysis and extraction buffers (Thermo Fisher Scientific) complemented with SDS powder (5% final) (Bio-Rad, France). Total protein concentration was determined with the BCA Protein Assay Kit (Thermo Fisher Scientific). Samples were denatured at 100°C for 3 min and 25 µg of protein was loaded onto NuPAGE 3%–8% Tris-acetate protein gels (Invitrogen), following the manufacturer's instructions. Dystrophin protein was detected by probing the membrane with NCL-DYS1 primary monoclonal antibody (NCL-DYS1; Novocastra, Newcastle, UK) and vinculin was detected as an internal control with the hVin-1 primary antibody (Sigma), followed by incubation with a goat anti-mouse secondary antibody (IRDye 800CW Goat anti-mouse IgG, Li-Cor, Germany). Bands were visualized using the Odyssey CLx system (Li-Cor). The quantification was done using the Empiria Studio software (Li-Cor) after normalization to internal control (vinculin) and based on a standard curve specific to each brain structure and made of a mix of WT and *mdx52* control lysates to obtain defined percentages of dystrophin (0%, 5%, 10%, and 20% of corresponding WT tissues).

In situ analysis of brain sections

Brain fresh-frozen 30-µm-thick cryosections were collected onto Superfrost+ slides and then stored at –80°C. Prior to all *in situ* ana-

lyzes, the slices were post-fixed for 5 min in a bath of acetone/methanol (1:1) at –20°C.

Biodistribution

The tcDNA distribution in the brain structures was assessed using a complementary probe conjugated to a biotin. The probe was then revealed with a streptavidin, Alexa Fluor 555 conjugate (Thermo Fisher Scientific). Images were taken at equivalent locations and exposure times using a laser scanning confocal microscope (Zeiss LSM 700, ×40 objective). Stacks of 9 to 11 images (1,024 × 1,024 pixels) spaced by 1 µm were recorded at a magnification of 156 nm/pixel. Scan tiles images (1,024 × 1,024 pixels) were taken using the ScanR Olympus HCS microscope, ×40 objective).

BaseScope analyses of *Dmd* mRNA

The BaseScope Duplex assay from Advanced Cell Diagnostics was used to detect the specific *Dmd* mRNA by ISH. Fresh frozen sections prepared as above for immunofluorescence were fixed in cold neutral buffered formalin and dehydrated in ethanol baths (50%, 70%, and 100%). The hydrogen peroxide, protease *i.v.* treatment, and RNA ISH were performed using the BaseScope Duplex reagent kit (323800, Advanced Cell Diagnostics) according to manufacturer's instructions. Specific BaseScope probes were designed against the exon 50-51 junction to detect unskipped mRNA, and against the exon 50-53 junction to specifically detect exon-51-skipped mRNA in *mdx52*. Control probes targeting peptidylprolyl isomerase B and ubiquitin C were used in parallel as positive controls, and against the bacterial dihydrodipicolinate reductase as a negative control (data not shown). At the end of the ISH, tissues were counterstained with hematoxylin Gills I (GHS132-1L, Sigma) diluted at 50% in water (30 s staining) and ammonium hydroxide 28–30 wt % (205840025, Acros Organics) diluted at 0.02% in water (30 s staining). Slides were then dried at 60°C for 45 min and mounted in Vectamount (321584, Advanced Cell Diagnostics). Images were obtained using the aperio AT2 scanner (Leica) (zoom 40×) and analyzed with ImageScope software (Leica). Signal quantification was performed in coronal sections from three mice per group at bregma –2.0 mm³⁹ from images taken along the hippocampal Ammon's horn (3,500 µm along CA1 and 1,100 µm along CA3), in the primary and secondary visual cortices above the hippocampal dentate gyrus in the same sections, as well as along the cerebellar Purkinje cell layer (4Cb, 5Cb, and 9Cb lobules) from sagittal sections (lateral 0.60 mm). Discrimination of specific signals was achieved by detection of turquoise staining (corresponding to the exon 50-51 junction) with a Hue value = 0.35 and color saturation threshold = 0.2, and red staining (corresponding to the exon 50-53 junction) with a Hue value = 0.5 and color saturation threshold = 0.14. The positive Pixel Count v.9 program of the ImageScope software was used for semiquantitative analysis of the relative area covered by each signal (rather than dot counts because of the variability in dot size).

Immunostaining

For Dp427 staining, slices were incubated first in a blocking solution for 90 min (10% normal goat serum, 0.3% Triton X-100, 1% BSA, and

10% FAB) at room temperature (RT), then overnight at 4°C with a monoclonal anti-dystrophin primary antibody (DYS1 Leica; dilution, 1/3 in 10% normal goat serum, 1% BSA), washed in PBS, and then incubated with secondary antibody Alexa 647 (1:500, 45 min, RT). Controls prepared by omitting the primary antibody showed no specific staining. Images were taken at equivalent locations and exposure times using a laser scanning confocal microscope (Zeiss LSM 700, ×40 objective). Stacks of 9 to 11 images (1,024 × 1,024 pixels) spaced by 1 μm were recorded at a magnification of 156 nm/pixel. Quantification of Dp427 re-expression in the CA1 hippocampus was performed in coronal sections (bregma –2.0 mm) and in the cerebellum on sagittal sections from three to six mice per group.

Statistical analysis

Data are presented as mean ± SEM; statistics were performed using the GraphPad Prism8 software (San Diego, CA). All data that passed the normality test (Shapiro-Wilk normality test) were analyzed using standard one-way analysis of variance (ANOVA). Kruskal-Wallis test followed by Dunn's post-hoc multiple comparison were used to analyze data that did not pass the normality test. Group comparisons were performed using two-way ANOVA with repeated measures when needed in behavioral and molecular studies, with treatment as the between-group factor and temporal or spatial variables (time in behavioral studies and different brain structure in molecular analysis) as the within factor, followed by Tukey (for one-way ANOVA) or Holm-Sidak (for two-way ANOVA) post-hoc multiple comparisons. Significance threshold was set at $p < 0.05$.

DATA AVAILABILITY

The primary data for this study are available from the authors upon request.

SUPPLEMENTAL INFORMATION

Supplemental information can be found online at <https://doi.org/10.1016/j.omtn.2023.03.009>.

ACKNOWLEDGMENTS

This work was funded by the European Union's Horizon 2020 research and innovation program "Brain Involvement in Dystrophinopathies" to F.M., C.V., and A.G., under grant agreement no. 847826. It was also supported by the Centre National de la Recherche Scientifique (CNRS, France), the Institut National de la Santé et de la Recherche Médicale (INSERM), the Université Paris-Saclay (France), Paris Ile-de-France Region, a project award from Association Monégasque contre les Myopathies (AMM, Monaco) to C.V. and a PhD fellowship from the Ministère de l'Enseignement Supérieur et de la Recherche (France) to A.S. We thank Dr. Katsuki Motoya and Prof. Sasaoka Toshiyuki (Department of Comparative & Experimental Medicine/Brain Research Institute; Niigata University, Japan), and Dr. Jun Tanihata and Dr. Shin'ichi Takeda (National Center of Neurology and Psychiatry, Tokyo, Japan) for providing the *mdx52* mouse breeders. We thank Dr. Zarrouki for his advice. We are grateful to the Zootechnic platform of our institutes for mouse breeding, care, and to the genotyping platform.

AUTHOR CONTRIBUTIONS

Conceptualization, C.V., F.M., and A.G.; methodology, A.S., C.V., and A.G.; investigation, A.S., S.B., O.I.C., O.V., M.D.C., T.T., and E.S.; writing – original draft, A.S., C.V., and A.G.; writing – review & editing, F.M., C.V., and A.G.; funding acquisition, F.M., C.V., L.G., and A.G.; supervision, C.V. and A.G.

DECLARATION OF INTERESTS

T.T. and E.S. are employees of SQY Therapeutics, which produces tri-cyclo-DNA oligomers. L.G. is a co-founder of SQY Therapeutics.

REFERENCES

- Colombo, P., Nobile, M., Tesi, A., Civati, F., Gandossini, S., Mani, E., Molteni, M., Bresolin, N., and D'Angelo, G. (2017). Assessing mental health in boys with Duchenne muscular dystrophy: emotional, behavioural and neurodevelopmental profile in an Italian clinical sample. *Eur. J. Paediatr. Neurol.* 21, 639–647. <https://doi.org/10.1016/j.ejpn.2017.02.007>.
- Hinton, V.J., Cyrulnik, S.E., Fee, R.J., Batchelder, A., Kiefel, J.M., Goldstein, E.M., Kaufmann, P., and De Vivo, D.C. (2009). Association of autistic spectrum disorders with dystrophinopathies. *Pediatr. Neurol.* 41, 339–346. <https://doi.org/10.1016/j.pediatrneurol.2009.05.011>.
- Ricotti, V., Mandy, W.P.L., Scoto, M., Pane, M., Deconinck, N., Messina, S., Mercuri, E., Skuse, D.H., and Muntoni, F. (2016). Neurodevelopmental, emotional, and behavioural problems in Duchenne muscular dystrophy in relation to underlying dystrophin gene mutations. *Dev. Med. Child Neurol.* 58, 77–84. <https://doi.org/10.1111/dmcn.12922>.
- Knaesel, I., Zuellig, R.A., Schaub, M.C., and Fritschy, J.M. (2001). Alterations in dystrophin and utrophin expression parallel the reorganization of GABAergic synapses in a mouse model of temporal lobe epilepsy. *Eur. J. Neurosci.* 13, 1113–1124. <https://doi.org/10.1046/j.0953-816x.2001.01476.x>.
- Lidov, H.G., Selig, S., and Kunkel, L.M. (1995). Dp140: a novel 140 kDa CNS transcript from the dystrophin locus. *Hum. Mol. Genet.* 4, 329–335. <https://doi.org/10.1093/hmg/4.3.329>.
- Morris, G.E., Simmons, C., and Nguyen, T.M. (1995). Apo-dystrophins (Dp140 and Dp71) and dystrophin splicing isoforms in developing brain. *Biochem. Biophys. Res. Commun.* 215, 361–367. <https://doi.org/10.1006/bbrc.1995.2474>.
- Belmaati Cherkaoui, M., Vacca, O., Izabelle, C., Boulay, A.-C., Boulogne, C., Gillet, C., Barnier, J.-V., Rendon, A., Cohen-Salmon, M., and Vaillend, C. (2021). Dp71 contribution to the molecular scaffold anchoring aquaporin-4 channels in brain macroglial cells. *Glia* 69, 954–970. <https://doi.org/10.1002/glia.23941>.
- Desguerre, I., Christov, C., Mayer, M., Zeller, R., Becane, H.-M., Bastuji-Garin, S., Leturcq, F., Chiron, C., Chelly, J., and Gherardi, R.K. (2009). Clinical heterogeneity of duchenne muscular dystrophy (DMD): definition of sub-phenotypes and predictive criteria by long-term follow-up. *PLoS One* 4, e4347. <https://doi.org/10.1371/journal.pone.0004347>.
- Taylor, P.J., Betts, G.A., Maroulis, S., Gilissen, C., Pedersen, R.L., Mowat, D.R., Johnston, H.M., and Buckley, M.F. (2010). Dystrophin gene mutation location and the risk of cognitive impairment in Duchenne muscular dystrophy. *PLoS One* 5, e8803. <https://doi.org/10.1371/journal.pone.0008803>.
- Saoudi, A., Zarrouki, F., Sebri, C., Izabelle, C., Goyenvalle, A., and Vaillend, C. (2021). Emotional behavior and brain anatomy of the *mdx52* mouse model of Duchenne muscular dystrophy. *Dis. Model. Mech.* 14, dmm049028. <https://doi.org/10.1242/dmm.049028>.
- Vaillend, C., and Chaussonot, R. (2017). Relationships linking emotional, motor, cognitive and GABAergic dysfunctions in dystrophin-deficient *mdx* mice. *Hum. Mol. Genet.* 26, 1041–1055. <https://doi.org/10.1093/hmg/ddx013>.
- Vaillend, C., Rendon, A., Misslin, R., and Ungerer, A. (1995). Influence of dystrophin-gene mutation on *mdx* mouse behavior. I. Retention deficits at long delays in spontaneous alternation and bar-pressing tasks. *Behav. Genet.* 25, 569–579. <https://doi.org/10.1007/BF02327580>.

13. Araki, E., Nakamura, K., Nakao, K., Kameya, S., Kobayashi, O., Nonaka, I., Kobayashi, T., and Katsuki, M. (1997). Targeted disruption of exon 52 in the mouse dystrophin gene induced muscle degeneration similar to that observed in Duchenne muscular dystrophy. *Biochem. Biophys. Res. Commun.* 238, 492–497. <https://doi.org/10.1006/bbrc.1997.7328>.
14. Aartsma-Rus, A., Janson, A.A.M., Heemskerk, J.A., De Winter, C.L., Van Ommen, G.-J.B., and Van Deutekom, J.C.T. (2006). Therapeutic modulation of DMD splicing by blocking exonic splicing enhancer sites with antisense oligonucleotides. *Ann. N.Y. Acad. Sci.* 1082, 74–76. <https://doi.org/10.1196/annals.1348.058>.
15. Dunckley, M.G., Manoharan, M., Villiet, P., Eperon, I.C., and Dickson, G. (1998). Modification of splicing in the dystrophin gene in cultured Mdx muscle cells by antisense oligonucleotides. *Hum. Mol. Genet.* 7, 1083–1090. <https://doi.org/10.1093/hmg/7.7.1083>.
16. Mann, C.J., Honeyman, K., Cheng, A.J., Ly, T., Lloyd, F., Fletcher, S., Morgan, J.E., Partridge, T.A., and Wilton, S.D. (2001). Antisense-induced exon skipping and synthesis of dystrophin in the mdx mouse. *Proc. Natl. Acad. Sci. USA* 98, 42–47. <https://doi.org/10.1073/pnas.98.1.42>.
17. Aoki, Y., Nakamura, A., Yokota, T., Saito, T., Okazawa, H., Nagata, T., and Takeda, S. (2010). In-frame dystrophin following exon 51-skipping improves muscle pathology and function in the exon 52-deficient mdx mouse. *Mol. Ther.* 18, 1995–2005. <https://doi.org/10.1038/mt.2010.186>.
18. Aupy, P., Zarrouki, F., Sandro, Q., Gastaldi, C., Buclez, P.-O., Mamchaoui, K., Garcia, L., Vaillend, C., and Goyenvalle, A. (2020). Long-Term efficacy of AAV9-U7snRNA-mediated exon 51 skipping in mdx52 mice. *Mol. Ther. Methods Clin. Dev.* 17, 1037–1047. <https://doi.org/10.1016/j.omtn.2020.04.025>.
19. Ferlini, A., Goyenvalle, A., and Muntoni, F. (2021). RNA-targeted drugs for neuromuscular diseases. *Science* 371, 29–31. <https://doi.org/10.1126/science.aba4515>.
20. Goyenvalle, A., Griffith, G., Babbs, A., El Andaloussi, S., Ezzat, K., Avril, A., Dugovic, B., Chaussonot, R., Ferry, A., Voit, T., et al. (2015). Functional correction in mouse models of muscular dystrophy using exon-skipping tricyclo-DNA oligomers. *Nat. Med.* 21, 270–275. <https://doi.org/10.1038/nm.3765>.
21. Relizani, K., Griffith, G., Echevarria, L., Zarrouki, F., Facchinetti, P., Vaillend, C., Leumann, C., Garcia, L., and Goyenvalle, A. (2017). Efficacy and safety profile of tricyclo-DNA antisense oligonucleotides in duchenne muscular dystrophy mouse model. *Mol. Ther. Nucleic Acids* 8, 144–157. <https://doi.org/10.1016/j.omtn.2017.06.013>.
22. Relizani, K., Echevarria, L., Zarrouki, F., Gastaldi, C., Dambrune, C., Aupy, P., Haeblerli, A., Komisariski, M., Tensorer, T., Larcher, T., et al. (2022). Palmitic acid conjugation enhances potency of tricyclo-DNA splice switching oligonucleotides. *Nucleic Acids Res.* 50, 17–34. <https://doi.org/10.1093/nar/gkab1199>.
23. Robin, V., Griffith, G., Carter, J.-P.L., Leumann, C.J., Garcia, L., and Goyenvalle, A. (2017). Efficient SMN rescue following subcutaneous tricyclo-DNA antisense oligonucleotide treatment. *Mol. Ther. Nucleic Acids* 7, 81–89. <https://doi.org/10.1016/j.omtn.2017.02.009>.
24. Zarrouki, F., Relizani, K., Bizot, F., Tensorer, T., Garcia, L., Vaillend, C., and Goyenvalle, A. (2022). Partial restoration of brain dystrophin and behavioral deficits by exon skipping in the muscular dystrophy X-linked (mdx) mouse. *Ann. Neurol.* 92, 213–229. <https://doi.org/10.1002/ana.26409>.
25. Sekiguchi, M., Zushida, K., Yoshida, M., Maekawa, M., Kamichi, S., Yoshida, M., Sahara, Y., Yuasa, S., Takeda, S., and Wada, K. (2009). A deficit of brain dystrophin impairs specific amygdala GABAergic transmission and enhances defensive behaviour in mice. *Brain* 132, 124–135. <https://doi.org/10.1093/brain/awn253>.
26. Goyenvalle, A., Vulin, A., Fougerousse, F., Leturcq, F., Kaplan, J.-C., Garcia, L., and Danos, O. (2004). Rescue of dystrophic muscle through U7 snRNA-mediated exon skipping. *Science* 306, 1796–1799. <https://doi.org/10.1126/science.1104297>.
27. Aartsma-Rus, A., Straub, V., Hemmings, R., Haas, M., Schlosser-Weber, G., Stoyanova-Beninska, V., Mercuri, E., Muntoni, F., Sepodes, B., Vroom, E., and Balabanov, P. (2017). Development of exon skipping therapies for duchenne muscular dystrophy: a critical Review and a perspective on the outstanding issues. *Nucleic Acid Therapeut.* 27, 251–259. <https://doi.org/10.1089/nat.2017.0682>.
28. Syed, Y.Y. (2016). Eteplirsen: first global approval. *Drugs* 76, 1699–1704. <https://doi.org/10.1007/s40265-016-0657-1>.
29. Rigo, F., Chun, S.J., Norris, D.A., Hung, G., Lee, S., Matson, J., Fey, R.A., Gaus, H., Hua, Y., Grundy, J.S., et al. (2014). Pharmacology of a central nervous system delivered 2'-O-Methoxyethyl-Modified survival of motor neuron splicing oligonucleotide in mice and nonhuman primates. *J. Pharmacol. Exp. Therapeut.* 350, 46–55. <https://doi.org/10.1124/jpet.113.212407>.
30. Hwang, K.-D., Kim, S.J., and Lee, Y.-S. (2022). Cerebellar circuits for classical fear conditioning. *Front. Cell. Neurosci.* 16, 836948. <https://doi.org/10.3389/fncel.2022.836948>.
31. Hashimoto, Y., Kuniishi, H., Sakai, K., Fukushima, Y., Du, X., Yamashiro, K., Hori, K., Imamura, M., Hoshino, M., Yamada, M., et al. (2022). Brain Dp140 alters glutamatergic transmission and social behaviour in the mdx52 mouse model of Duchenne muscular dystrophy. *Prog. Neurobiol.* 216, 102288. <https://doi.org/10.1016/j.pneurobio.2022.102288>.
32. Garcia-Rodriguez, R., Hiller, M., Jiménez-Gracia, L., van der Pal, Z., Balog, J., Adamczek, K., Aartsma-Rus, A., and Spitali, P. (2020). Premature termination codons in the DMD gene cause reduced local mRNA synthesis. *Proc. Natl. Acad. Sci. USA* 117, 16456–16464. <https://doi.org/10.1073/pnas.1910456117>.
33. Spitali, P., van den Bergen, J.C., Verhaart, I.E.C., Wokke, B., Janson, A.A.M., van den Eijnde, R., den Dunnen, J.T., Laros, J.F.J., Verschuren, J.J.G.M., 't Hoen, P.A.C., and Aartsma-Rus, A. (2013). DMD transcript imbalance determines dystrophin levels. *Faseb. J.* 27, 4909–4916. <https://doi.org/10.1096/fj.13-232025>.
34. Chesshyre, M., Ridout, D., Hashimoto, Y., Ookubo, Y., Torelli, S., Maresh, K., Ricotti, V., Abbott, L., Gupta, V.A., Main, M., et al. (2022). Investigating the role of dystrophin isoform deficiency in motor function in Duchenne muscular dystrophy. *J. Cachexia Sarcopenia Muscle* 13, 1360–1372. <https://doi.org/10.1002/jcsm.12914>.
35. Beastron, N., Lu, H., Macke, A., Canan, B.D., Johnson, E.K., Penton, C.M., Kaspar, B.K., Rodino-Klapac, L.R., Zhou, L., Janssen, P.M.L., and Montanaro, F. (2011). mdx^(cv) mice manifest more severe muscle dysfunction and diaphragm force deficits than do mdx Mice. *Am. J. Pathol.* 179, 2464–2474. <https://doi.org/10.1016/j.ajpath.2011.07.009>.
36. Lindsay, A., Trewin, A.J., Sadler, K.J., Laird, C., Della Gatta, P.A., and Russell, A.P. (2021). Sensitivity to behavioral stress impacts disease pathogenesis in dystrophin-deficient mice. *Faseb. J.* 35, e22034. <https://doi.org/10.1096/fj.202101163RR>.
37. Matsuzaka, Y., Tanihata, J., Ooshima, Y., Yamada, D., Sekiguchi, M., Miyatake, S., Aoki, Y., Terumitsu, M., Yashiro, R., Komaki, H., et al. (2020). The nSMase2/Smpd3 gene modulates the severity of muscular dystrophy and the emotional stress response in mdx mice. *BMC Med.* 18, 343. <https://doi.org/10.1186/s12916-020-01805-5>.
38. Razzoli, M., Lindsay, A., Law, M.L., Chamberlain, C.M., Southern, W.M., Berg, M., Osborn, J., Engeland, W.C., Metzger, J.M., Ervasti, J.M., and Bartolomucci, A. (2020). Social stress is lethal in the mdx model of Duchenne muscular dystrophy. *EBioMedicine* 55, 102700. <https://doi.org/10.1016/j.ebiom.2020.102700>.
39. Paxinos, G., and Franklin, K.B.J. (2001). *The Mouse Brain in Stereotaxic Coordinates, Second Edition 2nd edition* (Academic Press).
40. Goyenvalle, A., Babbs, A., Wright, J., Wilkins, V., Powell, D., Garcia, L., and Davies, K.E. (2012). Rescue of severely affected dystrophin/utrophin-deficient mice through scAAV-U7snRNA-mediated exon skipping. *Hum. Mol. Genet.* 21, 2559–2571. <https://doi.org/10.1093/hmg/dds082>.
41. Paylor, R., Zhao, Y., Libbey, M., Westphal, H., and Crawley, J.N. (2001). Learning impairments and motor dysfunctions in adult *lhx5*-deficient mice displaying hippocampal disorganization. *Physiol. Behav.* 73, 781–792. [https://doi.org/10.1016/s0031-9384\(01\)00515-7](https://doi.org/10.1016/s0031-9384(01)00515-7).
42. Chaussonot, R., Edeline, J.-M., Le Bec, B., El Massoufi, N., Laroche, S., and Vaillend, C. (2015). Cognitive dysfunction in the dystrophin-deficient mouse model of Duchenne muscular dystrophy: a reappraisal from sensory to executive processes. *Neurobiol. Learn. Mem.* 124, 111–122. <https://doi.org/10.1016/j.nlm.2015.07.006>.
43. Echevarria, L., Aupy, P., Relizani, K., Bestetti, T., Griffith, G., Blandel, F., Komisariski, M., Haeblerli, A., Svinartchouk, F., Garcia, L., and Goyenvalle, A. (2019). Evaluating the impact of variable phosphorothioate content in tricyclo-DNA antisense oligonucleotides in a duchenne muscular dystrophy mouse model. *Nucleic Acid Therapeut.* 29, 148–160. <https://doi.org/10.1089/nat.2018.0773>.

DISCUSSION

Duchenne muscular dystrophy is a neuromuscular disease. However, the neurological aspect of the pathology is so far not fully elucidated. Unlike the muscular dystrophy, the severity of the central deficits appear dependent on the genotype. Indeed, the position of mutations may affect the expression of one or multiple brain dystrophins and the cumulative loss of brain dystrophins is associated with more severe central deficits. Thus, due to multiple brain dystrophins and the established correlation between the genotype and the phenotype, the neurological aspect still needs to be understood. Consequently, the treatment of the central deficits is not yet established. Also, the focus was so far to treat the muscular dystrophy, which is the cause of premature death in DMD. This has led to great progress in terms of therapeutic approaches in the last decades. Currently one of the most promising strategies that may also apply to brain dystrophins, is the restoration of the reading frame by exon skipping. This innovative approach was based on the hypothesis that the reading frame maintenance is underlying the difference between BMD and DMD. Therapeutic exon skipping relies on the use of ASOs specific of certain exons making it a personalized medicine approach. The delivery of ASOs is currently the main challenge of this approach particularly to the CNS. Indeed, the CNS is naturally hermetically separated from the rest of the body by the blood brain barrier (BBB). Among ASOs used for DMD, the tc-DNA is an alternative chemistry that display increased stability and which stands out for its ability to cross the BBB after a systemic treatment. This provides a great advance to the field as it makes it possible to imagine a treatment that targets both muscular and central deficits in DMD.

Throughout this thesis work, we first characterized the *mdx52* DMD mouse model that carries a mutation profile frequently found in DMD patients and which leads to the loss of multiple brain dystrophins. The first aim was to characterize this mouse model to further investigate the central deficits and the genotype-phenotype relationship. Moreover, this could provide a reliable model with strong behavioral outcomes adequate for therapeutic preclinical studies targeting the CNS. We then investigated the therapeutic potential of ASOs specific of exon 51, as the *mdx52* model carries a deletion of exon 52 that disrupts the reading frame and skipping of exon 51 allows to restore it. We assessed the optimal treatment conditions to reach the highest levels of exon 51 skipping. Finally, we characterized the therapeutic efficacy of tcDNA-mediated exon 51 skipping to restore brain dystrophin and to alleviate certain severe behavioral deficits of the *mdx52* mouse model. Different aspects of this thesis work are discussed below in light of the obtained results.

I. Behavioral phenotyping

I.1. Genotype-phenotype relationships in DMD

In the last decades, with the extension of DMD patients lifespan, the neurological aspect of the disease appeared to be a hinder to a proper quality of life. In parallel, the increased acquaintance on the *DMD* gene and its multiple products of which numerous are expressed in the CNS shed light on the complexity of this side of the pathology. Through correlative studies of DMD patients emerged the evidence of a relationship between the mutation profiles and the severity of central deficits. The differences in mutation profiles impact the number and type of brain dystrophins expression as the more dystrophins are lost the more severe the deficits are (Desguerre et al., 2009; Taylor et al., 2010; Ricotti et al., 2016b; Colombo et al., 2017).

In order to identify the specific role and thus the involvement of each dystrophin in brain as well as the mechanisms underlying the genotype-phenotype correlation, DMD mouse models have been used. So far, the original *mdx* mouse model, lacking the full-length dystrophin (Dp427), has been largely characterized and described by our group (Vaillend et al., 1995, 1998; Chaussonot et al., 2015; Vaillend and Chaussonot, 2017).

In the present work, we investigated another mouse model, the *mdx52* mouse that lacks Dp427 (in both muscle and brain), but also Dp260 in the retina and Dp140 in the brain.

In the first part of the study, our group identified visual processing alteration in *mdx52* mice.

Dp260 is only detected in the retina where it is abundantly expressed in photoreceptors in the outer plexiform layer of the retina (OPL) (D'Souza et al., 1995; Wersinger et al., 2011). Dp427 is also found in the OPL of the mouse retina in a greater amount in cone terminals compared to rod terminals (Wersinger et al., 2011).

A previous histological examination of the *mdx52* mouse retina revealed normally organized retinal cells, similar to *mdx* mice lacking only Dp427. However, staining for β -dystroglycan was detected in the OPL of *mdx* mice, but not in *mdx52* (Kameya et al., 1997). This suggested that Dp260 and/or Dp140 are necessary for dystroglycan localization in the OPL and proper retinal functioning. It was then hypothesized that the loss of these dystrophins in *mdx52* mice could alter synaptic function between photoreceptors, bipolar and/or horizontal cells. This concur with the altered visual processing that we report here to be more severe in *mdx52* as compared to *mdx* mice (Bucher et al., 2019). Indeed, *mdx52* mice in our study exhibited affected ERG responses similarly to patients

lacking several dystrophins due to mutations in the central and distal parts of the *DMD* gene (Ricotti et al., 2016a). These findings further implement knowledge on the genotype-phenotype relationships in DMD.

Moreover, the reduced contrast sensitivity observed in *mdx52* mice in our OMR study may be compared with the reduced contrast sensitivity measured psychophysically in DMD patients (Barboni et al., 2013; Costa et al., 2011). The visual phenotype of *mdx52* mice includes key features observed in DMD patients, which may represent relevant outcome measures for further preclinical studies.

In the next parts of the thesis, we aimed to deeper characterize the emotion-related behaviors and emotional cognition of the *mdx52* mouse. We used behavioral tests that evaluate anxiety, unconditioned fear response and conditioned fear learning and memory. Emotional behavioral problems have been recognized in DMD patients (Hendriksen and Vles, 2008; Fee and Hinton, 2011) as significant changes that impact daily functioning. This includes parent-reported concerns such as behavioral outbursts, aggressiveness, anger problems, mood variations (Darke et al., 2006). Ricotti and colleagues further described that parents also report internalizing (anxious, depressive, and over-controlled) and externalizing (aggressive, hyperactive, non-compliant, and under-controlled) problems. These findings reflect the high level of anxiety and mood disorders, alone or in combination, observed in clinical practice (Ricotti et al., 2016b). Because these behaviors do not cluster with specific mutation profiles, they may likely result from the common loss of brain Dp427 in all DMD patients, perhaps due to the impact of Dp427 loss on central inhibition. Recently, Maresh et al., investigated a novel psychophysiological fear-conditioning task for the assessment of the unconditioned startle response in DMD patients. The authors provide the first evidence that boys with DMD show increased unconditioned startle response to threat, similarly to the *mdx* mouse (Maresh et al., 2023). In the mouse, this phenotype is rescued by postnatal restoration of brain Dp427 (Goyenvalle et al., 2015; Zarrouki et al., 2022b). The clinical study also confirmed that DMD participants exhibited increased anxiety symptoms. Furthermore, the DMD subgroup lacking the Dp140 had higher anxiety scores than the subgroup retaining Dp140. However, the unconditioned fear response was found to be similar for both subgroups and therefore can be attributed to deficiency of the Dp427. These findings provide insights on the severity of certain emotional phenotypes related to the loss of Dp140. In addition, the study defines an objective measure of this CNS phenotype, which will be valuable for future CNS-targeted dystrophin-restoration studies.

In our study, we compared the *mdx52* to the original Dp427-deficient *mdx* model using behavioral conditions in which visual alterations of *mdx52* do not disturb the execution or the interpretation of

the tests. A stronger emotional reactivity was characterized in *mdx52*. Thus, the cumulative loss of two main brain dystrophins results in a more severe phenotype, further supporting the genotype-phenotype correlation. These findings indicate that the *mdx52* model well mimics phenotypes of patients carrying similar genotypes, confirming its reliability for further preclinical studies.

I.2. Genetic background of DMD mouse models

It has previously been shown that the muscular dystrophy might be more severe depending on the genetic background (Beastrom et al., 2011a). In our first work we compared the *mdx* and *mdx52* mouse models which were both generated on a different genetic background: C57BL/10 and C57BL/6 respectively. In the literature, differences between these two genetic backgrounds have been reported (McLin and Steward, 2006; Deacon et al., 2007; Mortazavi et al., 2021; Flynn et al., 2021). McLin and Steward investigated the impact of the genetic background in the establishment of Kainic acid-induced seizure model. The authors reported variable profiles: while the C57BL/6 strain appeared highly resistant to the seizure, C57BL/10 was found to be highly sensitive (McLin and Steward, 2006). Kainic acid being an analogue of glutamate, the variable sensitivity of C57BL/6 and C57BL/10 mice suggest difference in the brain glutamatergic system. Mortazavi et al., through a comparative transcriptomic study, demonstrated that several genes are differentially expressed between C57BL/6 and C57BL/10 strains. Further studies reported differential genome-wide copy number variations (CNVs) between C57BL/6 and C57BL/10 strains (Flynn et al., 2021), which may influence phenotype expressions (McCarroll and Altshuler, 2007). Recently, a study reported that CNVs in *RCL1* gene, encoding an RNA 3'-terminal phosphate cyclase-like protein, are associated with a range of neuropsychiatric phenotypes (Brownstein et al., 2021). Finally, behavioral differences between the two genetic backgrounds have been reported in several studies. For example, Deacon and collaborators investigated numerous behaviors comparing C57BL/6 and C57BL/10 strains. Both strains behaved similarly in several tests, yet, C57BL/10 mice were impaired on a number of measures compared to C57BL/6, notably a marked deficit was seen in B10 mice in a spontaneous alternation task, suggesting reduced spatial working memory (Deacon et al., 2007).

To take into account the potential differences in the genetic background in our assessment of central deficits in DMD, we included a wild-type control group for each strain (littermates). We noticed

some variations between these control groups suggesting the influence of the genetic background on the behavior. We thus decided to further investigate and characterize the behavior of another DMD model, *mdx5^{cv}* which carries a proximal mutation in exon 10 that also impedes the expression of Dp427, but in a C57BL/6 background. We compared its behavior with that of *mdx52* mice in the study to assess the severity dependent on the mutation profile in models with same genetic background.

As *mdx* and *mdx5^{cv}* both lack the same dystrophin, the behavioral phenotype was expected to be similar. However, in certain tests *mdx5^{cv}* did not replicate the phenotypes of the original *mdx* mouse, indicating the impact of the background. This may also explain why some phenotypes were not replicated in the *mdx52*.

In our study, the *mdx5^{cv}* mice showed a trend for impaired recognition memory, which resembles the deficit displayed by the original *mdx* mouse, but the inter-individual variability in *mdx5^{cv}* and WT littermates does not allow to easily reach significance in this test. Recognition memory performance in *mdx52* mice was slightly impaired, but also associated with high inter-individual variability and requirement of larger samples of animals. We had to adapt the protocol to the C57BL/6 background, notably by shortening the habituation phase, in order to achieve reliable testing. Following protocol modifications, we evidenced long-term recognition memory deficits in both models without main difference in severity between them. In addition, difficulties for phenotype replication among partners' laboratories were encountered. Recognition memory performance was therefore not considered as a reliable marker for preclinical studies.

In conclusion, the deficits of *mdx* mice were not easily replicated, thus pointing to the impact of the genetic background. This collaborative work between two laboratories provided key insights on the limits of the reproducibility of behavioral studies in DMD mouse models.

Overall, despite differences dependent on the genetic background, the emotional phenotype was still more severe in *mdx52* compared to both *mdx* and *mdx5^{cv}*. These findings validate the severity of this phenotype as associated with the mutation profile, and further support reliability of emotional outcomes for preclinical studies.

II. Therapeutic exon 51 skipping optimization

II.1. ASO-based therapeutic exon skipping

The severity of the dystrophic phenotype, DMD or the milder BMD form, depends on the mutations. Indeed, deletions and duplications mutations that lead to DMD severe phenotype, disrupt the reading frame (frameshift) and prevent the protein expression. The preservation of the reading frame (in-frame) generally results in truncated but partly functional dystrophin and is associated with a BMD phenotype. This phenomenon inspired exon skipping therapeutic approaches based on splicing modulation mechanisms ([Annex I.2 for review](#)). In parallel, in revertant fibers found in DMD patients, it was shown that the splicing mechanism can lead to spontaneous skipping of one or multiple exons, thus reframing out of frame mutations. This phenomenon gives rise to a partially truncated but functional dystrophin (Burrow et al., 1991). Together, these observations led to the development of exon skipping therapy using antisense oligonucleotides (ASOs). ASOs specifically target the mutation site and induce the exclusion of one or numerous exons in order to restore the reading frame. Notably, skipping the same exon can rescue different mutations profiles; for example, the deletion of exons 47–50, 48–50, 49–50 and 52 can be restored by exon 51 skipping. In fact, exon 51 skipping represents the major applicability per mutation namely, 19.1% of the deletions in DMD (Aartsma-Rus and Ommen, 2009). Among ASOs for DMD treatment, only one type of chemistry is so far approved by the FDA for the treatment of DMD: the neutrally charged PMO. Alternative chemistries are being developed to improve the efficacy of exon skipping therapies, amongst which the charged tcDNA, which has recently been conjugated to a palmitic acid to increase further its therapeutic index. Both have previously showed skipping efficacy in the CNS of *mdx* mouse and capability to rescue to a certain extent the expression of Dp427 in different brain regions (Sekiguchi et al., 2009; Zarrouki et al., 2022b).

In the second part of this thesis work we investigated the therapeutic potential of both PMO and tcDNA targeting the exon 51 to efficiently induce exon skipping in the CNS.

II.2. ASOs therapeutics delivery to the CNS

In order to determine the therapeutic potential, we decided to locally deliver the ASOs to the cerebrospinal fluid (CSF). Indeed, the Dp427 is expressed in different CNS regions including the cortex, the hippocampus, the amygdala, the cerebellum and at very low levels in the spinal cord. Notably, shorter brain dystrophins are also widely expressed in different brain regions, further supporting this delivery method. The most commonly used delivery route is the intracerebroventricular (ICV) injection, in the CSF through the lateral ventricles. Our results demonstrated the efficacy of tcDNA to induce significant levels of exon 51 skipping (20-40%) in the different brain regions after a single dose. However, repeated injections through a cannula implant or an osmotic pumps led to toxicity at high doses. Indeed, at doses over 1 mg animals tended to be hypoactive, less reactive and lose weight. Toxicity of ASOs can be caused by type I hypersensitivity after ASO injection, however, the tolerability issues we observed emerged weeks following the ICV. Another cause may be the binding of the tcDNA to off-target mRNAs, which may impair their function. Alternatively, ASO-mediated toxicity can be caused by the chemical modifications which lead to ASO-protein interactions with subsequent immune reaction resulting in non-specific adverse events (Alhamadani et al., 2022). These hypotheses would require further investigations to determine the mechanism underlying the toxic effects of tcDNA at high doses in the CNS. For PMO which are known to be particularly safe, in particular due to their neutral charge, no tolerability issue emerged even at very high doses (up to 3.6 mg injected). Yet, even with higher doses the treatment efficacy of both ASOs did not overcome the efficacy of their respective single dose ICV delivery. One explanation can be the type of anaesthesia used during the delivery. Indeed, to avoid repeated long anaesthesia sessions, mice implanted with the cannula were subsequently anaesthetized under isoflurane when receiving the ASO, whereas mice from the ICV bilateral groups were deeper anaesthetized using ketamine/ medetomidine when receiving the ASO. Interestingly, several studies have raised the influence of anaesthesia on the CSF flow and showed that distribution to the CSF may be different depending on the wakefulness state (Xie et al., 2013). Moreover, Ma and colleagues demonstrated that the CSF efflux out of the brain is higher under isoflurane anaesthesia compared to ketamine/ medetomidine anaesthesia (Ma et al., 2019). These findings suggest a higher clearance of ASO from the CNS under isoflurane anaesthesia than deeper anaesthesia. This hypothesis is further supported by the results obtained with the osmotic pumps. The osmotic pumps delivered the ASO to the CSF of non-anesthetized mice. Notably, the clearance of CSF-infused tracers was shown to be

significantly increased in awake conditions (Ma et al., 2019). Furthermore, the study of Rigo and colleagues previously demonstrated that a very slow rate of infusion (0.5 μ l/h) led to lower efficacy (Rigo et al., 2014). In our study, the osmotic pumps were only tested for tcDNA. It was delivered continuously through a catheter implanted in the lateral ventricle, at a very slow rate of 0.25 μ l/h for 2 weeks to non-anesthetized animals. Overall, these may explain the low skipping efficacy following repeated/higher doses of ASO treatment. Interestingly, in their study Sekiguchi and colleagues injected PMO targeting the exon 23 *via* osmotic minipumps (0.5 μ l/h) (Sekiguchi et al., 2009) and reported an efficacy of 25% of skipping. A recent study of our group showed similar efficacy following a single ICV of tcDNA targeting exon 23. These additional findings suggest that the appropriate rate and anaesthesia state conditions might vary depending on the ASO.

The ICV delivery requests skull drilling and cortex crossing to reach the ventricles, making it a highly invasive procedure. In the scope of the study, we investigated an alternative delivery route to the CSF: in the intra *cisterna magna* (ICM), before the first vertebra right under the cerebellum. This procedure is less invasive as the injections are made through the skin and thus can be repeated with less burden to the mice. In addition, the intra-thecal injection holds a translational potential as it is already used in patients for the treatment of other neuromuscular disease such as SMA (Finkel et al., 2016). In light of previous differences associated with anesthesia, single ICM injections were performed under ketamine/ medetomidine anaesthesia. For both ASOs the single ICM led to lower exon skipping levels compared to the corresponding dose administered in single ICV. Still, the repeated ICM injections showed clearly higher levels than repeated ICV delivery.

Finally, we investigated the combination of ICV and ICM delivery in order to reach the highest achievable efficacy levels with a wider CNS distribution of the ASOs. Administration of up to 3.6 mg of PMO to the CSF was well tolerated by the mice. The treatment led to homogenous exon 51 skipping levels across the different brain structures ranging from 16% to 22%. This combined administration was the most efficient delivery method for PMO. Considering the tolerability issues observed with over than 1 mg of tcDNA, ICV injection of tcDNA was combined with a single ICM administration, leading to a total of 800 μ g of tcDNA administered. This combined method also resulted in the highest efficacy levels for tcDNA ranging from 22 to 42% of exon skipping levels, although not significantly different from bilateral ICV administration of 400 μ g (ranging from 19 to 34%). Overall, these findings evidenced the importance of the delivery route but also of the anesthesia on treatment efficacy. Precisely, each ASO needs to be fully tested to determine the optimal dose and route of administration but also other treatment conditions. Those may vary among ASOs and impact their efficacy.

III. Therapeutic rescue of the behavioral deficits

III.1. Behavioral rescue

Even though exon 51 skipping represents the highest applicability per mutation in DMD patients (Aartsma-Rus and Ommen, 2009), it is important to highlight that skipping this exon in the brain will not rescue the expression of Dp140 (because the initiation codon of Dp140 is located within exon 51). It is thus essential to assess the potential of Dp427 alone to restore or at least alleviate central alterations. Moreover, this may provide insights on the need of Dp140 for certain central functions. Thus, the therapeutic evaluation of exon 51 skipping is necessary to determine its relevance for DMD patients treatment targeting the CNS. The last objective of this thesis work was to assess the reversibility of emotional reactivity identified in the first part following post-natal restoration of dystrophin. Based on our optimization study, we selected a single ICV delivery of tcDNA targeting the exon 51 (tcDNA-ex51) as optimal tool.

The ICV delivery being an invasive procedure that may affect the behavioral readouts, we submitted all testing groups to the procedure in similar conditions. Control *mdx52* mice were injected with a control tcDNA sense sequence, WT were injected with saline and treated *mdx52* with the tcDNA-ex51. In certain parameters of behavioral tests the control groups *mdx52* (sense) and WT (PBS) exhibited behavioral differences compared to non-injected *mdx52* and WT from the first study. In the anxiety tests, the PBS injected WT showed slightly increased anxious phenotype. Also, sense-injected *mdx52* had more impaired fear conditioning learning. This emphasizes the possible impact of the surgery on certain phenotypes reproducibility.

Following the tcDNA-ex51 treatment, *mdx52* mice exhibited partially rescued anxiety phenotype on two dedicated tests. Moreover, during cued fear learning, *mdx52* mice behaved similarly to the WT group. Regarding the unconditioned fear, the freezing response was significantly reduced, but not back to WT level. Overall, this partial rescue demonstrates the possibility to alleviate some of the central deficits in DMD. However, these data raise many questions related to the incomplete rescue of the phenotypes. Different hypothesis will be discussed in the following parts:

- A. Impact of the muscular dystrophy
- B. Low levels of Dp427 protein rescued
- C. Dp427 only may not rescue all the phenotypes
- D. Late post-natal treatment

A. Impact of the muscular dystrophy

This hypothesis is based on the observation that *mdx52* mice present a slightly more severe muscle phenotype than *mdx* mice (Chesshyre et al., 2022). This could be attributed to the genetic background as it has been shown to be more severe on the C57Bl/6 genetic background (Beastrom et al., 2011b). The muscular dystrophy could have an impact on the fear response, which therefore may not be fully restored by central treatment only. Recently, studies questioned the involvement of central and peripheral components in *mdx* stress reactivity (Lindsay et al., 2021; Razzoli et al., 2020). Razzioli and colleagues demonstrated that transgenic *mdx* mice expressing dystrophin or utrophin in skeletal muscles display significantly lowered unconditioned fear response. Still, the WT level was not reached which already suggests that the origin of the phenotype is not strictly peripheral. Lindsay and colleagues reported an activation of the hypothalamic-pituitary-adrenal axis introducing a central involvement (Lindsay et al., 2021). In parallel, two studies showed a fully rescued unconditioned fear response in *mdx* mice following a locally central treatment confirming a strong central origin for this phenotype (Sekiguchi et al., 2009; Zarrouki et al., 2022b).

The extent of skeletal muscle involvement in *mdx* mouse models (including the *mdx52* model) is relatively mild, in particular before the age of 15 months (Pastoret and Seville, 1995). In our study, the behavioral phenotype is assessed in 3-4 months old mice, when the phenotype is still mild. Yet, some specific parameters with higher muscular demand, such as the grip strength test, was previously shown to be significantly reduced in *mdx52* compared with *mdx* mice (Chesshyre et al., 2022).

We therefore assessed whether the absence of mDp427 contributes to the only partial behavioral rescue observed in ICV treated *mdx52*. We demonstrated that the restoration of mDp427 exclusively in the periphery using scAAV9-U7Ex51 (Aupy et al., 2020) does not result in rescued unconditioned fear response. Moreover, the combined peripheral and central treatment did not further improve the fear response rescue compared to the ICV only treatment. These results confirm that brain Dp427 plays a major role in the genesis of the fear response phenotype.

B. Structure-specific Dp427 rescue

The low Dp427 levels restored by the ICV treatment might not be enough for the total rescue of behavioral phenotype. Indeed, the discrepancy phenomenon requires even higher skipping levels to reach more than 10% of Dp427 restoration. We already assessed various ways to increase the exon skipping efficacy in the optimization study. Yet, neither repeated ICV delivery nor repeated ICM injections led to increased skipping levels. Even the treatment based on combined ICV and repeated ICM showed equivalent levels compared to the single ICV. As the levels obtained by ICV appeared insufficient, a more direct local injection of ASO in specific brain structures might provide an alternative to address the behavioral rescue dependent of higher Dp427 restoration. In addition, this local delivery would allow to specifically target structures involved in these behaviors and at higher levels than those obtained by CSF circulation.

Previous studies from our group demonstrated the efficacy of intrahippocampal injections of antisense sequences targeting the exon 23 in *mdx* mice (Vaillend et al., 2010; Dallérac et al., 2011). In that study, the antisense sequence was carried by the AAV-U7 vector and the Dp427 restoration reached up to 25% in the hippocampus. One of the main disadvantage of the AAV seemed to be its limited diffusion since efficient transduction only occurred near the injection site. This particular property could be used to limit the rescue to the specific structures targeted.

Further investigations using local delivery of AAV-U7 targeting exon 51 would be interesting as they may provide higher Dp427 rescue per structure. This would allow the determination of the minimal quantity of Dp427 required in these structures to rescue the phenotype. Moreover, this might help to identify structures that require higher levels of dystrophin to properly achieve their function and thus result in a rescued phenotype. For example, we could investigate specific intra-amygdala injections, a structure that holds a great interest as it is centrally involved in emotional behaviors.

Identifying these parameters are of great interest for further systemic therapeutic approaches that aim to reach the CNS. Indeed, if the minimum amount of dystrophin rescue is not reached in specific structures (to be determined), then no phenotype rescue could be obtained.

C. Rescue of other central dystrophins

Skipping the exon 51 allows the rescue of Dp427 in the brain but also the rescue of Dp260 in the retina. In fact, we assessed the possibility of retinal rescue following an ICV delivery, but we did not manage to detect any skipping in the retina even at high doses. Previous studies demonstrated the feasibility and efficacy of intravitreal treatments to rescue Dp71 (Vacca et al., 2016; Barboni et al., 2020). This approach might be investigated for the rescue of Dp427 and Dp260 in the retina and assess its ability to alleviate visual alterations resulting from Dp260 loss. Indeed, DMD typically affects ERGs (Fitzgerald et al., 1994; Pillers et al., 1993) and visual perception is also disturbed in DMD patients (Costa et al., 2007, 2011; Barboni et al., 2021). In addition, more severe cases of retinal alterations, such as proliferative retinopathy, have been reported in DMD patients (Fagan et al., 2012; Hahn et al., 2013; Park et al., 2019; Kecik et al., 2021). Moreover, mutations affecting Dp427 may induce disturbed retinal homeostasis with increasing age and therefore be prone to develop excessive retinal neovascular changes in response to hypoxic stress (Bucher et al., 2019). Thus, retinopathies are likely to become more frequent as life expectancy increases in this population.

Nevertheless, as mentioned previously, since the first methionine initiation codon of Dp140 is located in exon 51 (Lidov et al., 1995), the skipping of exon 51 cannot lead to Dp140 rescue. This may explain why the phenotype is not fully rescued but just milder following partial Dp427 rescue in *mdx52* mice. Indeed, the loss of multiple dystrophins is shown to be associated with a more severe emotional phenotype (Maresh et al., 2023). This strongly suggests a role of Dp140 in these deficits. Further investigations are required to determine whether the additional restoration of Dp140 would lead to a more complete behavioral rescue. Skipping the exon 53 also allows to reframe the DMD transcript in *mdx52* mice, while keeping exon 51. Thus, exon 53 skipping approach could in theory restore both Dp427 and Dp140. Preliminary studies are conducted by our group in order to achieve exon 53 skipping using tcDNA-ASOs. Multiple ASOs targeting different sequences in the exon 53 were tested *in vitro* in *mdx52* myoblasts and the results revealed unexpected challenges. Indeed, in contrast with human exon 53, efficient skipping of mouse exon 53 required a combination of ASOs targeting different sequences within the exon 53. Based on these results, preliminary ICV injections of a combination of 3 tcDNA-ASO targeting exon 53 were conducted in small groups of *mdx52* mice. RT-PCR results revealed exon 53 levels ranging from 10 to 20% which are already slightly lower than those reached by tcDNA-ex51 (20-40%). Difficulties to skip the mouse exon 53 were also

reported in the literature. Hashimoto and colleagues recently reported PMO-mediated exon 53 skipping treatment *via* ICV delivery in *mdx52* mice. However, their therapeutic approach only aimed to partially skip the exon 53. Moreover, despite a particularly high dose of PMO injected (8 repeated doses of 900µg), the amount of Dp140 rescued ranged between 8 and 10% depending on the brain structure. To further assess the efficacy of Dp140 rescue, the authors actually had to inject the Dp140 mRNA in the basolateral amygdala to ensure higher levels of Dp140 (Hashimoto et al., 2022). In our group, ICV injections of the optimal combination of tcDNA ASOs are currently ongoing in large groups of animals to further assess the impact of Dp427 and Dp140 rescue on the emotional phenotype.

D. Postnatal treatment of genetic neurodevelopmental disease

Duchenne muscular dystrophy is a neurodevelopmental disease (NDD); indeed, dystrophin protein is normally expressed in the brain during the development. It is therefore possible to hypothesize that its absence during this period might not be fully reversible and thus postnatal restoration (i.e. after the developmental stages) may be too late to achieve a full restoration of central deficits. Several studies though, reported that treating the disrupted molecular and cellular mechanisms specifically in adults can compensate for or even correct specific developmental pathologies and result in real improvements in cognitive function (Ehninger et al., 2008).

In our study, animals were treated at 6-8 weeks old, which is equivalent to young human adults (adolescents), in which the brain development is almost achieved. Thus, earlier treatment (P1-2), during postnatal brain development, should be tested to assess the reversibility of the phenotype while managed earlier. Indeed, important regions of the brain including hippocampus, amygdala, nucleus accumbens, prefrontal, frontal, orbital cortex are restructured during adolescence (Giedd et al., 1996; Sowell et al., 1999; Stiles and Jernigan, 2010). Structures such as the amygdala, the hippocampus and the prefrontal cortex are known to be involved in emotional behaviors expression and control. The early rescue of dystrophin in these structures may lessen the severity of the phenotype and allow a higher rescue.

Moreover, such findings could pave the way to possible early post-natal or pre-natal treatment, as it may even prevent the emergence of some deficits. In fact, this hold a great translational potential as DMD might be detected via prenatal diagnosis and genotyping, hence providing the mutations profile.

III.2. Exon 51 skipping and Dp427 restoration discrepancy

We reported efficient exon 51 skipping up to 10-30% across the different brain regions namely, cortex, hippocampus, amygdala and cerebellum. This led to Dp427 protein levels of only 3% to 10%, while our team previously demonstrated that a similar treatment with a tcDNA targeting exon 23 restored up to 25% of Dp427 in the hippocampus of *mdx* mice (Zarrouki et al., 2022b). This discrepancy in dystrophin restoration between *mdx* and *mdx52* mice has previously been reported in brain and skeletal muscles (Aupy et al., 2020). This phenomenon does not appear to be due to variable skipping efficacy between exon 23 and 51 which are relatively similar (20-30%). Instead, it was suggested that it may be due to differences in the *Dmd* mRNA levels between *mdx* and *mdx52* models, given that the *DMD* gene is subjected to transcript imbalance limiting the amount of transcripts available in particular in the 3' region (Spitali et al., 2013; García-Rodríguez et al., 2020). This represents a main challenge to achieve efficient dystrophin rescue by exon skipping approaches because *Dmd* transcripts levels available for correction are lower than in the WT. A recent study conducted by our group reported that increasing histone acetylation using histone deacetylase inhibitors (HDACi) could help to correct the transcript imbalance. Indeed, the study showed in *mdx* mice that ASO treatment induced significantly higher Dp427 rescue while combined with HDACi compared to ASO alone (Bizot et al., 2022). These findings further support the imbalance hypothesis and provide insights on therapeutic strategies to overcome this limitation. The potential of this approach to increase the protein rescue could be interesting to assess in *mdx52* mice.

In the scope of increasing dystrophin restoration and thus possibly higher behavioral rescue, we tested an alternative tool, the AAV-U7 targeting the exon 51 (Annex II). *Mdx52* mice were injected intracerebroventricularly with 2^{E+12} vg of scAAV9-U7ex51 and then underwent the same battery of behavioral tests (anxiety, unconditioned fear and associative fear learning and memory). In contrast with tcDNA ICV treatment, the AAV-treated mice showed no improvement in all the behavioral outcomes. Consistently with previous studies, the distribution was found to be very limited as compared to ASOs injected *via* ICV delivery and higher intra-group variability was observed in the AAV-treated animals. Also, the dystrophin protein rescue was overall lower and in particular in the cerebellum. These data suggest that a minimal percent of Dp427 rescue in the cerebellum may be necessary to achieve some behavioral improvement. Studies have shown the cerebellum to be connected with fear and anxiety-related areas, such as the amygdala (Farley et al., 2016). Neuroimaging study of anxious patients revealed differential activation of the cerebellum is frequently found in many studies (Etkin et al., 2009; Talati et al., 2015). Also, fMRI in humans have

showed cerebellar involvement in the processing of various aversive stimuli and associated learning, including fear conditioning (Ernst et al., 2019; Faul et al., 2020). In rodents, studies revealed that functional integrity of cerebellar lobules was necessary for consolidating fear memories in a fear conditioning task (Sacchetti et al., 2002, 2007). Also Otsuka et al., reported that mice with altered parallel fiber (PF)-Purkinje cell (PC) synapses in the cerebellum displayed an impaired acquisition of fear memory (Otsuka et al., 2016). Overall, our results further suggest the potential importance of the cerebellum in fear related behaviors in DMD.

Another finding to be discussed is the absence of protein re-expression in the spinal cord despite detection of exon 51 skipping. This may be explained by the very low expression of Dp427 in the WT spinal cord (De Stefano et al., 1997; Masaki et al., 2001). A recent study from our group reported a physiological expression 3–4 times lower in the spinal cord compared to the cortex. The role of Dp427 in the spinal cord is still unclear. In this particular study, specific investigations on the GABA_AR and their subunits composition showed abnormal expression in *mdx* mice. An increased expression of $\alpha 3$ and $\alpha 6$ subunits as well as decreased $\alpha 4$ subunit were reported (Zarrouki et al., 2022a). These findings step further the role of Dp427 in GABAergic system in the spinal cord.

III.3. Dystrophin associated protein complexes and GABAergic system

Another point is the GABA_AR restoration and thus the GABAergic functioning dependent on synaptic Dp427. Complementary investigations are necessary to determine the impact of Dp427 rescue on its associated proteins and mechanisms. Indeed, dystrophins interact with numerous partners forming the dystrophin associated protein complexes (DGC). DGC seem to play a role on GABA_A receptors clustering regulation and the molecular composition in the synaptic and extra synaptic domains (Fritschy et al., 2003; Zarrouki et al., 2022a). In fact, a determinant contribution for receptor localization is assigned to the postsynaptic dystroglycan (DG). The lack of DG is associated with reduction of GABA_AR and other postsynaptic proteins in cerebellar Purkinje cells, with consequent severe GABAergic denervation and motor learning disability (Briatore et al., 2020). A central role of DG and α -DG glycosylation in regulating GABAergic synaptic plasticity homeostasis has also been reported in hippocampal neurons (Pribiag et al., 2014; Früh et al., 2016). In addition, the glycosylated α -DG have been reported to play a role in the regulation of GABA_ARs expression and GABAergic neurotransmission in the ventral hippocampus. Moreover, this was shown to be involved in the pathophysiological process of depressive-like behaviors induced by chronic social defeat stress

(Xie et al., 2022). Other DGC proteins such as the dystrobrevins are also involved in the clustering of GABA_ARs in cerebellar Purkinje cells. Similarly to dystrophin, loss of both β - and α -dystrobrevin disrupt GABA_AR clustering in Purkinje cells (Blake et al., 1999; Grady et al., 2006). Investigations are required on DGCs composition at the synaptic level and its proper function on GABA-R subunits composition, clustering and synaptic localization following dystrophin rescue. This could further clarify the impact of Dp427 rescue at the molecular level and determine whether the partial rescue is due to partial GABAergic system restoration.

Beyond GABAergic function, loss of Dp427 has also been associated with alterations in cholinergic nicotinic transmission in the hippocampus (Ghedini et al., 2012; Parames et al., 2014; Cohen et al., 2015). This may reflect an adaptation of the hippocampal circuit to GABAergic alterations, these circuits being strongly interacting (Albuquerque et al., 2009). The impact of Dp427 rescue on this circuit also needs to be evaluated.

Conclusion and wide perspectives

While great progress have been made regarding the muscular phenotype of DMD over the past few decades, the understanding of the neurological aspect has, however, been less extended and thus its care is still delayed. Notably, the complexity of the central facet of the pathology is a hinder and still needs to be clarified.

In DMD, both central and peripheral alterations are due to mutations in the DMD gene. This suggests that therapeutic approaches targeting the origin of the pathology might be applicable for both aspects. Yet, the central expression of the *DMD* gene is more complex due to multiple gene products in the CNS. Also, the accessibility of CNS is more difficult because of the BBB. Thus, peripheral treatment approaches require adaptation to be used for central deficits.

Overall, this thesis work stepped further the understanding of the neurological aspect of DMD. We validated the *mdx52* as a good mouse model with reliable outcomes including more severe deficits which suggest the involvement of shorter brain dystrophin (Dp140). Future studies using this model could find out more about this Dp140 function. Indeed, new deficits (Dp140-dependent) not found in mice lacking only Dp427 might be evidenced. Moreover, this mouse model appears adequate to determine the ideal therapeutic conditions and to assess the treatment of neurological alterations. Thus, the observation of only partial effects of therapies on certain outcomes suggests that sole Dp427 rescue is insufficient to compensate the deficits supporting the role of Dp140. In addition, this work provided insights on the possible postnatal reversibility of neurodevelopmental alterations in DMD.

The local central treatment is a first step to further establish a combined treatment for central and peripheral aspects of the pathology. This would be a life changing progress in DMD management.

Another progress would be the possibility to fully rescue the central alterations or prevent their appearance. The earlier the therapeutic intervention is, the higher the chances to properly manage the disease is. Early post-natal treatment or even pre-natal treatment represent promising perspectives.

Alternative therapeutic approaches could also be evaluated. Indeed, the loss of brain Dp427 leads to altered GABAergic transmission and pharmacological agents could compensate it. In addition, elucidating the molecular and cellular modifications in DMD might provide novel pharmacological targets to investigate.

More is still to be elucidated in DMD neurological aspects and underlying mechanisms to possibly expand therapeutic management of the disease to the central alterations. Further studies could help the understanding of other central deficits that appears to be worsen by Dp140 loss. Detailed complementary studies could thus investigate the working memory processes and the social alterations. Additional studies are also to be conducted to better understand and maybe manage the associated disorders found in DMD such as autistic spectrum disorders or ADHD. This might also provide insights for these pathologies and their treatment even when not associated with DMD.

In parallel with molecular and pharmacological therapies it is important to consider a non-pharmacological management for the central deficits in DMD. Hinton and Fee demonstrated the importance of resilience in DMD, through the familial and environmental support to improve patients quality of life (Fee and Hinton, 2011). An appropriate support of patients including everyday mental assistance can have a great potential and might emphasize the pharmacological treatment.

REFERENCES

- Aartsma-Rus, A., Fokkema, I., Verschuuren, J., Ginjaar, I., van Deutekom, J., van Ommen, G.-J., den Dunnen, J.T., 2009. Theoretic applicability of antisense-mediated exon skipping for Duchenne muscular dystrophy mutations. *Hum Mutat* 30, 293–299. <https://doi.org/10.1002/humu.20918>
- Aartsma-Rus, A., Goemans, N., 2019. A Sequel to the Eteplirsen Saga: Eteplirsen Is Approved in the United States but Was Not Approved in Europe. *Nucleic Acid Ther* 29, 13–15. <https://doi.org/10.1089/nat.2018.0756>
- Aartsma-Rus, A., Ommen, G.-J.B. van, 2009. Less is more: therapeutic exon skipping for Duchenne muscular dystrophy. *The Lancet Neurology* 8, 873–875. [https://doi.org/10.1016/S1474-4422\(09\)70229-7](https://doi.org/10.1016/S1474-4422(09)70229-7)
- Aartsma-Rus, A., Van Deutekom, J.C.T., Fokkema, I.F., Van Ommen, G.-J.B., Den Dunnen, J.T., 2006. Entries in the Leiden Duchenne muscular dystrophy mutation database: an overview of mutation types and paradoxical cases that confirm the reading-frame rule. *Muscle Nerve* 34, 135–144. <https://doi.org/10.1002/mus.20586>
- Abbs, S., Bobrow, M., 1992. Analysis of quantitative PCR for the diagnosis of deletion and duplication carriers in the DMD gene. *J Med Genet* 29, 191–196. <https://doi.org/10.1136/jmg.29.3.191>
- Achenbach, T.M., 1991. Manual for Child Behavior Checklist 4-18, 1991 Profile. Univ Vermont/Dept Psychiatry, Burlington, VT.
- Acland, G.M., Aguirre, G.D., Bennett, J., Aleman, T.S., Cideciyan, A.V., Bennicelli, J., Dejneka, N.S., Pearce-Kelling, S.E., Maguire, A.M., Palczewski, K., Hauswirth, W.W., Jacobson, S.G., 2005. Long-term restoration of rod and cone vision by single dose rAAV-mediated gene transfer to the retina in a canine model of childhood blindness. *Mol Ther* 12, 1072–1082. <https://doi.org/10.1016/j.ymthe.2005.08.008>
- Acosta, R., Montañez, C., Fuentes-Mera, L., Gonzalez, E., Gómez, P., Quintero-Mora, L., Mornet, D., Alvarez-Salas, L.M., Cisneros, B., 2004. Dystrophin Dp71 is required for neurite outgrowth in PC12 cells. *Exp Cell Res* 296, 265–275. <https://doi.org/10.1016/j.yexcr.2004.01.015>
- Adams, M.E., Mueller, H.A., Froehner, S.C., 2001. In vivo requirement of the alpha-syntrophin PDZ domain for the sarcolemmal localization of nNOS and aquaporin-4. *J Cell Biol* 155, 113–122. <https://doi.org/10.1083/jcb.200106158>
- Aigner, B., Rathkolb, B., Klawns, M., Sedlmeier, R., Klempt, M., Wagner, S., Michel, D., Mayer, U., Klopstock, T., de Angelis, M.H., Wolf, E., 2009. Generation of N-ethyl-N-nitrosourea-induced mouse mutants with deviations in plasma enzyme activities as novel organ-specific disease models. *Exp Physiol* 94, 412–421. <https://doi.org/10.1113/expphysiol.2008.045864>
- Albuquerque, E.X., Pereira, E.F.R., Alkondon, M., Rogers, S.W., 2009. Mammalian nicotinic acetylcholine receptors: from structure to function. *Physiol Rev* 89, 73–120. <https://doi.org/10.1152/physrev.00015.2008>
- Alessi, A., Bragg, A.D., Percival, J.M., Yoo, J., Albrecht, D.E., Froehner, S.C., Adams, M.E., 2006. gamma-Syntrophin scaffolding is spatially and functionally distinct from that of the alpha/beta syntrophins. *Exp Cell Res* 312, 3084–3095. <https://doi.org/10.1016/j.yexcr.2006.06.019>
- Alhamadani, F., Zhang, K., Parikh, R., Wu, H., Rasmussen, T.P., Bahal, R., Zhong, X.-B., Manautou, J.E., 2022. Adverse Drug Reactions and Toxicity of the Food and Drug Administration-Approved Antisense Oligonucleotide Drugs. *Drug Metab Dispos* 50, 879–887. <https://doi.org/10.1124/dmd.121.000418>
- Anna, A., Monika, G., 2018. Splicing mutations in human genetic disorders: examples, detection, and confirmation. *J Appl Genet* 59, 253–268. <https://doi.org/10.1007/s13353-018-0444-7>
- Aoki, Y., Nakamura, A., Yokota, T., Saito, T., Okazawa, H., Nagata, T., Takeda, S., 2010. In-frame dystrophin following exon 51-skipping improves muscle pathology and function in the exon 52-deficient mdx mouse. *Mol Ther* 18, 1995–2005. <https://doi.org/10.1038/mt.2010.186>

- Arahata, K., Ishiura, S., Ishiguro, T., Tsukahara, T., Sahara, Y., Eguchi, C., Ishihara, T., Nonaka, I., Ozawa, E., Sugita, H., 1988. Immunostaining of skeletal and cardiac muscle surface membrane with antibody against Duchenne muscular dystrophy peptide. *Nature* 333, 861–863. <https://doi.org/10.1038/333861a0>
- Araki, E., Nakamura, K., Nakao, K., Kameya, S., Kobayashi, O., Nonaka, I., Kobayashi, T., Katsuki, M., 1997. Targeted disruption of exon 52 in the mouse DMD gene induced muscle degeneration similar to that observed in Duchenne muscular dystrophy. *Biochem Biophys Res Commun* 238, 492–497. <https://doi.org/10.1006/bbrc.1997.7328>
- Aranmolate, A., Tse, N., Colognato, H., 2017. Myelination is delayed during postnatal brain development in the mdx mouse model of Duchenne muscular dystrophy. *BMC Neurosci* 18, 63. <https://doi.org/10.1186/s12868-017-0381-0>
- Arpan, I., Willcocks, R.J., Forbes, S.C., Finkel, R.S., Lott, D.J., Rooney, W.D., Triplett, W.T., Senesac, C.R., Daniels, M.J., Byrne, B.J., Finanger, E.L., Russman, B.S., Wang, D.-J., Tennekoon, G.I., Walter, G.A., Sweeney, H.L., Vandeborne, K., 2014. Examination of effects of corticosteroids on skeletal muscles of boys with DMD using MRI and MRS. *Neurology* 83, 974–980. <https://doi.org/10.1212/WNL.0000000000000775>
- Asadi, S., Kia, V.V., Bagheri, R., Jamali, M., Dell, S.S., 2017. Assessment of Genetic Mutations DMD, DYSF, EMD, LMNA, DUX4, DMPK, ZNF9, PABPN1 Genes Induction Duchenne Muscular Dystrophy. *SOJ Immunology* 5.
- Aupy, P., Zarrouki, F., Sandro, Q., Gastaldi, C., Buclez, P.-O., Mamchaoui, K., Garcia, L., Vaillend, C., Goyenvalle, A., 2020. Long-Term Efficacy of AAV9-U7snRNA-Mediated Exon 51 Skipping in mdx52 Mice. *Mol Ther Methods Clin Dev* 17, 1037–1047. <https://doi.org/10.1016/j.omtm.2020.04.025>
- Bagdatlioglu, E., Porcari, P., Grealley, E., Blamire, A.M., Straub, V.W., 2020. Cognitive impairment appears progressive in the mdx mouse. *Neuromuscul Disord* 30, 368–388. <https://doi.org/10.1016/j.nmd.2020.02.018>
- Banerjee, A., Rikhye, R.V., Breton-Provencher, V., Tang, X., Li, C., Li, K., Runyan, C.A., Fu, Z., Jaenisch, R., Sur, M., 2016. Jointly reduced inhibition and excitation underlies circuit-wide changes in cortical processing in Rett syndrome. *Proc Natl Acad Sci U S A* 113, E7287–E7296. <https://doi.org/10.1073/pnas.1615330113>
- Bar, S., Barnea, E., Levy, Z., Neuman, S., Yaffe, D., Nudel, U., 1990. A novel product of the Duchenne muscular dystrophy gene which greatly differs from the known isoforms in its structure and tissue distribution. *Biochem J* 272, 557–560. <https://doi.org/10.1042/bj2720557>
- Barboni, M.T.S., Dias, S.L., Silva, L.A., Damico, F.M., Vidal, K.S., Costa, M.F., Nagy, B.V., Kremers, J., Ventura, D.F., 2021. Correlations Between Dark-Adapted Rod Threshold Elevations and ERG Response Deficits in Duchenne Muscular Dystrophy. *Invest Ophthalmol Vis Sci* 62, 29. <https://doi.org/10.1167/iovs.62.4.29>
- Barboni, M.T.S., Joachimsthaler, A., Roux, M.J., Nagy, Z.Z., Ventura, D.F., Rendon, A., Kremers, J., Vaillend, C., 2022. Retinal dystrophins and the retinopathy of Duchenne muscular dystrophy. *Prog Retin Eye Res* 101137. <https://doi.org/10.1016/j.preteyeres.2022.101137>
- Barboni, M.T.S., Martins, C.M.G., Nagy, B.V., Tsai, T., Damico, F.M., da Costa, M.F., de Cassia, R., Pavanello, M., Lourenço, N.C.V., de Cerqueira, A.M.P., Zatz, M., Kremers, J., Ventura, D.F., 2016. Dystrophin Is Required for Proper Functioning of Luminance and Red-Green Cone Opponent Mechanisms in the Human Retina. *Invest Ophthalmol Vis Sci* 57, 3581–3587. <https://doi.org/10.1167/iovs.16-19287>
- Barboni, M.T.S., Nagy, B.V., de Araújo Moura, A.L., Damico, F.M., da Costa, M.F., Kremers, J., Ventura, D.F., 2013. ON and OFF Electoretinography and Contrast Sensitivity in Duchenne Muscular

- Dystrophy. *Investigative Ophthalmology & Visual Science* 54, 3195–3204. <https://doi.org/10.1167/iovs.13-11700>
- Barboni, M.T.S., Vaillend, C., Joachimsthaler, A., Liber, A.M.P., Khabou, H., Roux, M.J., Vacca, O., Vignaud, L., Dalkara, D., Guillonneau, X., Ventura, D.F., Rendon, A., Kremers, J., 2020. Rescue of Defective Electroretinographic Responses in Dp71-Null Mice With AAV-Mediated Reexpression of Dp71. *Invest Ophthalmol Vis Sci* 61, 11. <https://doi.org/10.1167/iovs.61.2.11>
- Bardoni, A., Felisari, G., Sironi, M., Comi, G., Lai, M., Robotti, M., Bresolin, N., 2000. Loss of Dp140 regulatory sequences is associated with cognitive impairment in dystrophinopathies. *Neuromuscul Disord* 10, 194–199. [https://doi.org/10.1016/s0960-8966\(99\)00108-x](https://doi.org/10.1016/s0960-8966(99)00108-x)
- Beastrom, N., Lu, H., Macke, A., Canan, B.D., Johnson, E.K., Penton, C.M., Kaspar, B.K., Rodino-Klapac, L.R., Zhou, L., Janssen, P.M.L., Montanaro, F., 2011a. mdx^(5cv) mice manifest more severe muscle dysfunction and diaphragm force deficits than do mdx Mice. *Am J Pathol* 179, 2464–2474. <https://doi.org/10.1016/j.ajpath.2011.07.009>
- Beastrom, N., Lu, H., Macke, A., Canan, B.D., Johnson, E.K., Penton, C.M., Kaspar, B.K., Rodino-Klapac, L.R., Zhou, L., Janssen, P.M.L., Montanaro, F., 2011b. mdx^(5cv) mice manifest more severe muscle dysfunction and diaphragm force deficits than do mdx Mice. *Am J Pathol* 179, 2464–2474. <https://doi.org/10.1016/j.ajpath.2011.07.009>
- Beato, M., Herrlich, P., Schütz, G., 1995. Steroid hormone receptors: many actors in search of a plot. *Cell* 83, 851–857. [https://doi.org/10.1016/0092-8674\(95\)90201-5](https://doi.org/10.1016/0092-8674(95)90201-5)
- Beggs, A.H., Koenig, M., Boyce, F.M., Kunkel, L.M., 1990. Detection of 98% of DMD/BMD gene deletions by polymerase chain reaction. *Hum Genet* 86, 45–48. <https://doi.org/10.1007/BF00205170>
- Bello, L., Campadello, P., Barp, A., Fanin, M., Semplicini, C., Sorarù, G., Caumo, L., Calore, C., Angelini, C., Pegoraro, E., 2016. Functional changes in Becker muscular dystrophy: implications for clinical trials in dystrophinopathies. *Sci Rep* 6, 32439. <https://doi.org/10.1038/srep32439>
- Belmaati Cherkaoui, M., Vacca, O., Isabelle, C., Boulay, A.-C., Boulogne, C., Gillet, C., Barnier, J.-V., Rendon, A., Cohen-Salmon, M., Vaillend, C., 2021. Dp71 contribution to the molecular scaffold anchoring aquaporine-4 channels in brain macroglial cells. *Glia* 69, 954–970. <https://doi.org/10.1002/glia.23941>
- Bérout, C., Tuffery-Giraud, S., Matsuo, M., Hamroun, D., Humbertclaude, V., Monnier, N., Moizard, M.-P., Voelckel, M.-A., Calemard, L.M., Boisseau, P., Blayau, M., Philippe, C., Cossée, M., Pagès, M., Rivier, F., Danos, O., Garcia, L., Claustres, M., 2007. Multiexon skipping leading to an artificial DMD protein lacking amino acids from exons 45 through 55 could rescue up to 63% of patients with Duchenne muscular dystrophy. *Hum Mutat* 28, 196–202. <https://doi.org/10.1002/humu.20428>
- Billard, C., Gillet, P., Signoret, J.L., Uicaut, E., Bertrand, P., Fardeau, M., Barthez-Carpentier, M.A., Santini, J.J., 1992. Cognitive functions in Duchenne muscular dystrophy: a reappraisal and comparison with spinal muscular atrophy. *Neuromuscul Disord* 2, 371–378. [https://doi.org/10.1016/s0960-8966\(06\)80008-8](https://doi.org/10.1016/s0960-8966(06)80008-8)
- Birnkrant, D.J., Bushby, K., Bann, C.M., Alman, B.A., Apkon, S.D., Blackwell, A., Case, L.E., Cripe, L., Hadjiyannakis, S., Olson, A.K., Sheehan, D.W., Bolen, J., Weber, D.R., Ward, L.M., 2018. Diagnosis and management of Duchenne muscular dystrophy, part 2: respiratory, cardiac, bone health, and orthopaedic management. *Lancet Neurol* 17, 347–361. [https://doi.org/10.1016/S1474-4422\(18\)30025-5](https://doi.org/10.1016/S1474-4422(18)30025-5)
- Bizot, F., Goossens, R., Tensorer, T., Dmitriev, S., Garcia, L., Aartsma-Rus, A., Spitali, P., Goyenvalle, A., 2022. Histone deacetylase inhibitors improve antisense-mediated exon-skipping efficacy in mdx mice. *Mol Ther Nucleic Acids* 30, 606–620. <https://doi.org/10.1016/j.omtn.2022.11.017>
- Bizot, F., Vulin, A., Goyenvalle, A., 2020. Correction to: Current Status of Antisense Oligonucleotide-Based Therapy in Neuromuscular Disorders. *Drugs* 80, 1417. <https://doi.org/10.1007/s40265-020-01375-z>

- Blake, D.J., Hawkes, R., Benson, M.A., Beesley, P.W., 1999. Different dystrophin-like complexes are expressed in neurons and glia. *J Cell Biol* 147, 645–658. <https://doi.org/10.1083/jcb.147.3.645>
- Blake, D.J., Schofield, J.N., Zuellig, R.A., Górecki, D.C., Phelps, S.R., Barnard, E.A., Edwards, Y.H., Davies, K.E., 1995. G-utrophin, the autosomal homologue of dystrophin Dp116, is expressed in sensory ganglia and brain. *Proc Natl Acad Sci U S A* 92, 3697–3701. <https://doi.org/10.1073/pnas.92.9.3697>
- Blake, D.J., Weir, A., Newey, S.E., Davies, K.E., 2002. Function and genetics of dystrophin and dystrophin-related proteins in muscle. *Physiol Rev* 82, 291–329. <https://doi.org/10.1152/physrev.00028.2001>
- Bostick, B., Yue, Y., Long, C., Duan, D., 2008. Prevention of dystrophin-deficient cardiomyopathy in twenty-one-month-old carrier mice by mosaic dystrophin expression or complementary dystrophin/utrophin expression. *Circ Res* 102, 121–130. <https://doi.org/10.1161/CIRCRESAHA.107.162982>
- Bostick, B., Yue, Y., Long, C., Marschalk, N., Fine, D.M., Chen, J., Duan, D., 2009. Cardiac expression of a mini-dystrophin that normalizes skeletal muscle force only partially restores heart function in aged Mdx mice. *Mol Ther* 17, 253–261. <https://doi.org/10.1038/mt.2008.264>
- Boulay, A.-C., Saubaméa, B., Cisternino, S., Mignon, V., Mazeraud, A., Jourden, L., Blugeon, C., Cohen-Salmon, M., 2015. The Sarcoglycan complex is expressed in the cerebrovascular system and is specifically regulated by astroglial Cx30 channels. *Front Cell Neurosci* 9, 9. <https://doi.org/10.3389/fncel.2015.00009>
- Brenman, J.E., Chao, D.S., Gee, S.H., McGee, A.W., Craven, S.E., Santillano, D.R., Wu, Z., Huang, F., Xia, H., Peters, M.F., Froehner, S.C., Bredt, D.S., 1996. Interaction of nitric oxide synthase with the postsynaptic density protein PSD-95 and alpha1-syntrophin mediated by PDZ domains. *Cell* 84, 757–767. [https://doi.org/10.1016/s0092-8674\(00\)81053-3](https://doi.org/10.1016/s0092-8674(00)81053-3)
- Bresolin, N., Castelli, E., Comi, G.P., Felisari, G., Bardoni, A., Perani, D., Grassi, F., Turconi, A., Mazzucchelli, F., Gallotti, D., 1994. Cognitive impairment in Duchenne muscular dystrophy. *Neuromuscul Disord* 4, 359–369. [https://doi.org/10.1016/0960-8966\(94\)90072-8](https://doi.org/10.1016/0960-8966(94)90072-8)
- Briatore, F., Pregno, G., Di Angelantonio, S., Frola, E., De Stefano, M.E., Vaillend, C., Sassoè-Pognetto, M., Patrizi, A., 2020. Dystroglycan Mediates Clustering of Essential GABAergic Components in Cerebellar Purkinje Cells. *Front Mol Neurosci* 13, 164. <https://doi.org/10.3389/fnmol.2020.00164>
- Brown, S., Sharpey-Schafer, E.A., 1888. XI. An investigation into the functions of the occipital and temporal lobes of the monkey's brain. *Philosophical Transactions of the Royal Society of London. (B.)* 179, 303–327. <https://doi.org/10.1098/rstb.1888.0011>
- Brownstein, C.A., Smith, R.S., Rodan, L.H., Gorman, M.P., Hojlo, M.A., Garvey, E.A., Li, J., Cabral, K., Bowen, J.J., Rao, A.S., Genetti, C.A., Carroll, D., Deaso, E.A., Agrawal, P.B., Rosenfeld, J.A., Bi, W., Howe, J., Stavropoulos, D.J., Hansen, A.W., Hamoda, H.M., Pinard, F., Caracansi, A., Walsh, C.A., D'Angelo, E.J., Beggs, A.H., Zarrei, M., Gibbs, R.A., Scherer, S.W., Glahn, D.C., Gonzalez-Heydrich, J., 2021. RCL1 copy number variants are associated with a range of neuropsychiatric phenotypes. *Mol Psychiatry* 26, 1706–1718. <https://doi.org/10.1038/s41380-021-01035-y>
- Brüinig, I., Suter, A., Knuesel, I., Lüscher, B., Fritschy, J.-M., 2002. GABAergic terminals are required for postsynaptic clustering of dystrophin but not of GABA(A) receptors and gephyrin. *J Neurosci* 22, 4805–4813. <https://doi.org/10.1523/JNEUROSCI.22-12-04805.2002>
- Bucher, F., Friedlander, M.S.H., Aguilar, E., Kurihara, T., Krohne, T.U., Usui, Y., Friedlander, M., 2019. The long DMD gene product Dp427 modulates retinal function and vascular morphology in response to age and retinal ischemia. *Neurochemistry International* 129, 104489. <https://doi.org/10.1016/j.neuint.2019.104489>
- Bulfield, G., Siller, W.G., Wight, P.A., Moore, K.J., 1984. X chromosome-linked muscular dystrophy (mdx) in the mouse. *Proc Natl Acad Sci U S A* 81, 1189–1192. <https://doi.org/10.1073/pnas.81.4.1189>
- Burger, C., Gorbatyuk, O.S., Velardo, M.J., Peden, C.S., Williams, P., Zolotukhin, S., Reier, P.J., Mandel, R.J., Muzyczka, N., 2004. Recombinant AAV viral vectors pseudotyped with viral capsids from

- serotypes 1, 2, and 5 display differential efficiency and cell tropism after delivery to different regions of the central nervous system. *Mol Ther* 10, 302–317. <https://doi.org/10.1016/j.ymthe.2004.05.024>
- Burrow, K.L., Coovert, D.D., Klein, C.J., Bulman, D.E., Kissel, J.T., Rammohan, K.W., Burghes, A.H., Mendell, J.R., 1991. Dystrophin expression and somatic reversion in prednisone-treated and untreated Duchenne dystrophy. CIDD Study Group. *Neurology* 41, 661–666. <https://doi.org/10.1212/wnl.41.5.661>
- Bushby, K., Finkel, R., Birnkrant, D.J., Case, L.E., Clemens, P.R., Cripe, L., Kaul, A., Kinnett, K., McDonald, C., Pandya, S., Poysky, J., Shapiro, F., Tomezsko, J., Constantin, C., DMD Care Considerations Working Group, 2010a. Diagnosis and management of Duchenne muscular dystrophy, part 1: diagnosis, and pharmacological and psychosocial management. *Lancet Neurol* 9, 77–93. [https://doi.org/10.1016/S1474-4422\(09\)70271-6](https://doi.org/10.1016/S1474-4422(09)70271-6)
- Bushby, K., Finkel, R., Birnkrant, D.J., Case, L.E., Clemens, P.R., Cripe, L., Kaul, A., Kinnett, K., McDonald, C., Pandya, S., Poysky, J., Shapiro, F., Tomezsko, J., Constantin, C., DMD Care Considerations Working Group, 2010b. Diagnosis and management of Duchenne muscular dystrophy, part 2: implementation of multidisciplinary care. *Lancet Neurol* 9, 177–189. [https://doi.org/10.1016/S1474-4422\(09\)70272-8](https://doi.org/10.1016/S1474-4422(09)70272-8)
- Bushby, K., Finkel, R., Wong, B., Barohn, R., Campbell, C., Comi, G.P., Connolly, A.M., Day, J.W., Flanigan, K.M., Goemans, N., Jones, K.J., Mercuri, E., Quinlivan, R., Renfroe, J.B., Russman, B., Ryan, M.M., Tulinius, M., Voit, T., Moore, S.A., Lee Sweeney, H., Abresch, R.T., Coleman, K.L., Eagle, M., Florence, J., Gappmaier, E., Glanzman, A.M., Henricson, E., Barth, J., Elfring, G.L., Reha, A., Spiegel, R.J., O'donnell, M.W., Peltz, S.W., McDonald, C.M., PTC124-GD-007-DMD STUDY GROUP, 2014. Ataluren treatment of patients with nonsense mutation dystrophinopathy. *Muscle Nerve* 50, 477–487. <https://doi.org/10.1002/mus.24332>
- Byers, T.J., Kunkel, L.M., Watkins, S.C., 1991. The subcellular distribution of dystrophin in mouse skeletal, cardiac, and smooth muscle. *J Cell Biol* 115, 411–421. <https://doi.org/10.1083/jcb.115.2.411>
- Byers, T.J., Lidov, H.G., Kunkel, L.M., 1993. An alternative dystrophin transcript specific to peripheral nerve. *Nat. Genet.* 4, 77–81. <https://doi.org/10.1038/ng0593-77>
- Calhoun, G.G., Tye, K.M., 2015. Resolving the neural circuits of anxiety. *Nat Neurosci* 18, 1394–1404. <https://doi.org/10.1038/nn.4101>
- Cannon, W.B., 1915. Bodily changes in pain, hunger, fear, and rage: an account of recent researches into the function of emotional excitement. D. Appleton and Company, New York, London.
- Caudal, D., François, V., Lafoux, A., Ledevin, M., Anegon, I., Le Guiner, C., Larcher, T., Huchet, C., 2020. Characterization of brain dystrophins absence and impact in dystrophin-deficient Dmdmdx rat model. *PLoS One* 15, e0230083. <https://doi.org/10.1371/journal.pone.0230083>
- Cearley, C.N., Wolfe, J.H., 2006. Transduction characteristics of adeno-associated virus vectors expressing cap serotypes 7, 8, 9, and Rh10 in the mouse brain. *Mol Ther* 13, 528–537. <https://doi.org/10.1016/j.ymthe.2005.11.015>
- Centonze, D., Rossi, S., Mercaldo, V., Napoli, I., Ciotti, M.T., De Chiara, V., Musella, A., Prosperetti, C., Calabresi, P., Bernardi, G., Bagni, C., 2008. Abnormal striatal GABA transmission in the mouse model for the fragile X syndrome. *Biol Psychiatry* 63, 963–973. <https://doi.org/10.1016/j.biopsych.2007.09.008>
- Chamberlain, J.S., Metzger, J., Reyes, M., Townsend, D., Faulkner, J.A., 2007. Dystrophin-deficient mdx mice display a reduced life span and are susceptible to spontaneous rhabdomyosarcoma. *FASEB J* 21, 2195–2204. <https://doi.org/10.1096/fj.06-7353com>
- Chapman, V.M., Miller, D.R., Armstrong, D., Caskey, C.T., 1989. Recovery of induced mutations for X chromosome-linked muscular dystrophy in mice. *Proc Natl Acad Sci U S A* 86, 1292–1296. <https://doi.org/10.1073/pnas.86.4.1292>

- Chappell, A.E., Gaus, H.J., Berdeja, A., Gupta, R., Jo, M., Prakash, T.P., Oestergaard, M., Swayze, E.E., Seth, P.P., 2020. Mechanisms of palmitic acid-conjugated antisense oligonucleotide distribution in mice. *Nucleic Acids Res* 48, 4382–4395. <https://doi.org/10.1093/nar/gkaa164>
- Chausseot, R., Amar, M., Fossier, P., Vaillend, C., 2019. Dp71-Dystrophin Deficiency Alters Prefrontal Cortex Excitation-Inhibition Balance and Executive Functions. *Mol Neurobiol* 56, 2670–2684. <https://doi.org/10.1007/s12035-018-1259-6>
- Chausseot, R., Edeline, J.-M., Le Bec, B., El Massioui, N., Laroche, S., Vaillend, C., 2015. Cognitive dysfunction in the dystrophin-deficient mouse model of Duchenne muscular dystrophy: A reappraisal from sensory to executive processes. *Neurobiol Learn Mem* 124, 111–122. <https://doi.org/10.1016/j.nlm.2015.07.006>
- Chelly, J., Hamard, G., Koulakoff, A., Kaplan, J.C., Kahn, A., Berwald-Netter, Y., 1990. DMD gene transcribed from different promoters in neuronal and glial cells. *Nature* 344, 64–65. <https://doi.org/10.1038/344064a0>
- Chemello, F., Bassel-Duby, R., Olson, E.N., 2020. Correction of muscular dystrophies by CRISPR gene editing. *J Clin Invest* 130, 2766–2776. <https://doi.org/10.1172/JCI136873>
- Chesshyre, M., Ridout, D., Hashimoto, Y., Ookubo, Y., Torelli, S., Maresh, K., Ricotti, V., Abbott, L., Gupta, V.A., Main, M., Ferrari, G., Kowala, A., Lin, Y.-Y., Tedesco, F.S., Scoto, M., Baranello, G., Manzur, A., Aoki, Y., Muntoni, F., 2022. Investigating the role of dystrophin isoform deficiency in motor function in Duchenne muscular dystrophy. *J Cachexia Sarcopenia Muscle* 13, 1360–1372. <https://doi.org/10.1002/jcsm.12914>
- Cibis, G.W., Fitzgerald, K.M., 2001. The negative ERG is not synonymous with nightblindness. *Trans Am Ophthalmol Soc* 99, 171–175; discussion 175-176.
- Cirak, S., Arechavala-Gomez, V., Guglieri, M., Feng, L., Torelli, S., Anthony, K., Abbs, S., Garralda, M.E., Bourke, J., Wells, D.J., Dickson, G., Wood, M.J.A., Wilton, S.D., Straub, V., Kole, R., Shrewsbury, S.B., Sewry, C., Morgan, J.E., Bushby, K., Muntoni, F., 2011. Exon skipping and dystrophin restoration in patients with Duchenne muscular dystrophy after systemic phosphorodiamidate morpholino oligomer treatment: an open-label, phase 2, dose-escalation study. *Lancet* 378, 595–605. [https://doi.org/10.1016/S0140-6736\(11\)60756-3](https://doi.org/10.1016/S0140-6736(11)60756-3)
- Clemens, P.R., Rao, V.K., Connolly, A.M., Harper, A.D., Mah, J.K., McDonald, C.M., Smith, E.C., Zaidman, C.M., Nakagawa, T., CINRG DNHS Investigators, Hoffman, E.P., 2022. Long-Term Functional Efficacy and Safety of Viltolarsen in Patients with Duchenne Muscular Dystrophy. *J Neuromuscul Dis* 9, 493–501. <https://doi.org/10.3233/JND-220811>
- Cohen, E.J., Quarta, E., Fulgenzi, G., Minciocchi, D., 2015. Acetylcholine, GABA and neuronal networks: a working hypothesis for compensations in the dystrophic brain. *Brain Res Bull* 110, 1–13. <https://doi.org/10.1016/j.brainresbull.2014.10.004>
- Colombo, P., Nobile, M., Tesei, A., Civati, F., Gandossini, S., Mani, E., Molteni, M., Bresolin, N., D'Angelo, G., 2017. Assessing mental health in boys with Duchenne muscular dystrophy: Emotional, behavioural and neurodevelopmental profile in an Italian clinical sample. *Eur J Paediatr Neurol* 21, 639–647. <https://doi.org/10.1016/j.ejpn.2017.02.007>
- Connors, N.C., Adams, M.E., Froehner, S.C., Kofuji, P., 2004. The potassium channel Kir4.1 associates with the dystrophin-glycoprotein complex via alpha-syntrophin in glia. *J Biol Chem* 279, 28387–28392. <https://doi.org/10.1074/jbc.M402604200>
- Cooper, B.J., Winand, N.J., Stedman, H., Valentine, B.A., Hoffman, E.P., Kunkel, L.M., Scott, M.O., Fischbeck, K.H., Kornegay, J.N., Avery, R.J., 1988. The homologue of the Duchenne locus is defective in X-linked muscular dystrophy of dogs. *Nature* 334, 154–156. <https://doi.org/10.1038/334154a0>

- Costa, M., Barboni, M., Ventura, D., 2011. Psychophysical measurements of luminance and chromatic spatial and temporal contrast sensitivity in Duchenne muscular dystrophy. *Psychology & Neuroscience* 4, 67–74. <https://doi.org/10.3922/j.psns.2011.1.008>
- Costa, M.F., Oliveira, A.G.F., Feitosa-Santana, C., Zatz, M., Ventura, D.F., 2007. Red-green color vision impairment in Duchenne muscular dystrophy. *Am J Hum Genet* 80, 1064–1075. <https://doi.org/10.1086/518127>
- Cotton, S., Voudouris, N.J., Greenwood, K.M., 2001. Intelligence and Duchenne muscular dystrophy: full-scale, verbal, and performance intelligence quotients. *Dev Med Child Neurol* 43, 497–501. <https://doi.org/10.1017/s0012162201000913>
- Cowen, L., Mancini, M., Martin, A., Lucas, A., Donovan, J.M., 2019. Variability and trends in corticosteroid use by male United States participants with Duchenne muscular dystrophy in the Duchenne Registry. *BMC Neurol* 19, 84. <https://doi.org/10.1186/s12883-019-1304-8>
- Cox, D.B.T., Platt, R.J., Zhang, F., 2015. Therapeutic genome editing: prospects and challenges. *Nat Med* 21, 121–131. <https://doi.org/10.1038/nm.3793>
- Cox, G.A., Phelps, S.F., Chapman, V.M., Chamberlain, J.S., 1993. New mdx mutation disrupts expression of muscle and nonmuscle isoforms of dystrophin. *Nat Genet* 4, 87–93. <https://doi.org/10.1038/ng0593-87>
- Cozzi, F., Cerletti, M., Luvoni, G.C., Lombardo, R., Brambilla, P.G., Faverzani, S., Blasevich, F., Cornelio, F., Pozza, O., Mora, M., 2001. Development of muscle pathology in canine X-linked muscular dystrophy. II. Quantitative characterization of histopathological progression during postnatal skeletal muscle development. *Acta Neuropathol* 101, 469–478. <https://doi.org/10.1007/s004010000308>
- Crawford, A.H., Hildyard, J.C.W., Rushing, S.A.M., Wells, D.J., Diez-Leon, M., Piercy, R.J., 2022. Validation of DE50-MD dogs as a model for the brain phenotype of Duchenne muscular dystrophy. *Dis Model Mech* 15, dmm049291. <https://doi.org/10.1242/dmm.049291>
- Crooke, S.T., Wang, S., Vickers, T.A., Shen, W., Liang, X.-H., 2017. Cellular uptake and trafficking of antisense oligonucleotides. *Nat. Biotechnol.* 35, 230–237. <https://doi.org/10.1038/nbt.3779>
- Crosbie, R.H., Lebakken, C.S., Holt, K.H., Venzke, D.P., Straub, V., Lee, J.C., Grady, R.M., Chamberlain, J.S., Sanes, J.R., Campbell, K.P., 1999. Membrane targeting and stabilization of sarcospan is mediated by the sarcoglycan subcomplex. *J Cell Biol* 145, 153–165. <https://doi.org/10.1083/jcb.145.1.153>
- Cyrlunik, S.E., Fee, R.J., Batchelder, A., Kiefel, J., Goldstein, E., Hinton, V.J., 2008. Cognitive and adaptive deficits in young children with Duchenne muscular dystrophy (DMD). *J Int Neuropsychol Soc* 14, 853–861. <https://doi.org/10.1017/S135561770808106X>
- Cyrlunik, S.E., Fee, R.J., De Vivo, D.C., Goldstein, E., Hinton, V.J., 2007. Delayed developmental language milestones in children with Duchenne’s muscular dystrophy. *J Pediatr* 150, 474–478. <https://doi.org/10.1016/j.jpeds.2006.12.045>
- Dallérac, G., Perronnet, C., Chagneau, C., Leblanc-Veyrac, P., Samson-Desvignes, N., Peltekian, E., Danos, O., Garcia, L., Laroche, S., Billard, J.-M., Vaillend, C., 2011. Rescue of a dystrophin-like protein by exon skipping normalizes synaptic plasticity in the hippocampus of the mdx mouse. *Neurobiol Dis* 43, 635–641. <https://doi.org/10.1016/j.nbd.2011.05.012>
- D’Angelo, M.G., Lorusso, M.L., Civati, F., Comi, G.P., Magri, F., Del Bo, R., Guglieri, M., Molteni, M., Turconi, A.C., Bresolin, N., 2011. Neurocognitive profiles in Duchenne muscular dystrophy and gene mutation site. *Pediatr Neurol* 45, 292–299. <https://doi.org/10.1016/j.pediatrneurol.2011.08.003>
- Daoud, F., Angeard, N., Demerre, B., Martie, I., Benyaou, R., Leturcq, F., Cossée, M., Deburgrave, N., Saillour, Y., Tuffery, S., Urtizbera, A., Toutain, A., Echenne, B., Frischman, M., Mayer, M., Desguerre, I., Estournet, B., Réveillère, C., Penisson-Besnier, null, Cuisset, J.M., Kaplan, J.C., Héron, D., Rivier, F., Chelly, J., 2009a. Analysis of Dp71 contribution in the severity of mental retardation

- through comparison of Duchenne and Becker patients differing by mutation consequences on Dp71 expression. *Hum Mol Genet* 18, 3779–3794. <https://doi.org/10.1093/hmg/ddp320>
- Daoud, F., Candelario-Martínez, A., Billard, J.-M., Avital, A., Khelifaoui, M., Rozenvald, Y., Guegan, M., Mornet, D., Jaillard, D., Nudel, U., Chelly, J., Martínez-Rojas, D., Laroche, S., Yaffe, D., Vaillend, C., 2009b. Role of Mental Retardation-Associated Dystrophin-Gene Product Dp71 in Excitatory Synapse Organization, Synaptic Plasticity and Behavioral Functions. *PLoS One* 4. <https://doi.org/10.1371/journal.pone.0006574>
- Darabi, R., Pan, W., Bosnakovski, D., Baik, J., Kyba, M., Perlingeiro, R.C.R., 2011. Functional myogenic engraftment from mouse iPS cells. *Stem Cell Rev Rep* 7, 948–957. <https://doi.org/10.1007/s12015-011-9258-2>
- Darke, J., Bushby, K., Le Couteur, A., McConachie, H., 2006. Survey of behaviour problems in children with neuromuscular diseases. *Eur J Paediatr Neurol* 10, 129–134. <https://doi.org/10.1016/j.ejpn.2006.04.004>
- Darmahkasih, A.J., Rybalsky, I., Tian, C., Shellenbarger, K.C., Horn, P.S., Lambert, J.T., Wong, B.L., 2020. Neurodevelopmental, behavioral, and emotional symptoms common in Duchenne muscular dystrophy. *Muscle & Nerve* 61, 466–474. <https://doi.org/10.1002/mus.26803>
- Davies, K.E., Pearson, P.L., Harper, P.S., Murray, J.M., O'Brien, T., Sarfarazi, M., Williamson, R., 1983. Linkage analysis of two cloned DNA sequences flanking the Duchenne muscular dystrophy locus on the short arm of the human X chromosome. *Nucleic Acids Res* 11, 2303–2312. <https://doi.org/10.1093/nar/11.8.2303>
- De Stefano, M.E., Zaccaria, M.L., Cavaldesi, M., Petrucci, T.C., Medori, R., Paggi, P., 1997. Dystrophin and its isoforms in a sympathetic ganglion of normal and dystrophic mdx mice: immunolocalization by electron microscopy and biochemical characterization. *Neuroscience* 80, 613–624. [https://doi.org/10.1016/s0306-4522\(97\)00003-1](https://doi.org/10.1016/s0306-4522(97)00003-1)
- Deacon, R.M.J., Thomas, C.L., Rawlins, J.N.P., Morley, B.J., 2007. A comparison of the behavior of C57BL/6 and C57BL/10 mice. *Behav Brain Res* 179, 239–247. <https://doi.org/10.1016/j.bbr.2007.02.009>
- Del Tongo, C., Carretta, D., Fulgenzi, G., Catini, C., Minciacchi, D., 2009. Parvalbumin-positive GABAergic interneurons are increased in the dorsal hippocampus of the dystrophic mdx mouse. *Acta Neuropathol* 118, 803–812. <https://doi.org/10.1007/s00401-009-0567-3>
- den Dunnen, J.T., Bakker, E., Breteler, E.G., Pearson, P.L., van Ommen, G.J., 1987. Direct detection of more than 50% of the Duchenne muscular dystrophy mutations by field inversion gels. *Nature* 329, 640–642. <https://doi.org/10.1038/329640a0>
- den Dunnen, J.T., Casula, L., Makover, A., Bakker, B., Yaffe, D., Nudel, U., van Ommen, G.J., 1991. Mapping of dystrophin brain promoter: a deletion of this region is compatible with normal intellect. *Neuromuscul Disord* 1, 327–331. [https://doi.org/10.1016/0960-8966\(91\)90118-c](https://doi.org/10.1016/0960-8966(91)90118-c)
- Den Dunnen, J.T., Grootsholten, P.M., Bakker, E., Blondin, L.A., Ginjaar, H.B., Wapenaar, M.C., van Paassen, H.M., van Broeckhoven, C., Pearson, P.L., van Ommen, G.J., 1989. Topography of the Duchenne muscular dystrophy (DMD) gene: FIGE and cDNA analysis of 194 cases reveals 115 deletions and 13 duplications. *Am J Hum Genet* 45, 835–847.
- Desguerre, I., Christov, C., Mayer, M., Zeller, R., Becane, H.-M., Bastuji-Garin, S., Leturcq, F., Chiron, C., Chelly, J., Gherardi, R.K., 2009. Clinical heterogeneity of duchenne muscular dystrophy (DMD): definition of sub-phenotypes and predictive criteria by long-term follow-up. *PLoS One* 4, e4347. <https://doi.org/10.1371/journal.pone.0004347>
- Deutsch, M., Long, M., 1999. Intron-exon structures of eukaryotic model organisms. *Nucleic Acids Res* 27, 3219–3228. <https://doi.org/10.1093/nar/27.15.3219>
- Donders, J., Taneja, C., 2009. Neurobehavioral characteristics of children with Duchenne muscular dystrophy. *Child Neuropsychol* 15, 295–304. <https://doi.org/10.1080/09297040802665777>

- Doorenweerd, N., Dumas, E.M., Ghariq, E., Schmid, S., Straathof, C.S.M., Roest, A.A.W., Wokke, B.H., Zwet, E.W. van, Webb, A.G., Hendriksen, J.G.M., Buchem, M.A. van, Verschuuren, J.J.G.M., Asllani, I., Niks, E.H., Osch, M.J.P. van, Kan, H.E., 2017. Decreased cerebral perfusion in Duchenne muscular dystrophy patients. *Neuromuscular Disorders* 27, 29–37. <https://doi.org/10.1016/j.nmd.2016.10.005>
- Dowling, P., Culligan, K., Ohlendieck, K., 2002. Distal mdx muscle groups exhibiting up-regulation of utrophin and rescue of dystrophin-associated glycoproteins exemplify a protected phenotype in muscular dystrophy. *Naturwissenschaften* 89, 75–78. <https://doi.org/10.1007/s00114-001-0289-4>
- Drachman, D.B., Toyka, K.V., Myer, E., 1974. Prednisone in Duchenne muscular dystrophy. *Lancet* 2, 1409–1412. [https://doi.org/10.1016/s0140-6736\(74\)90071-3](https://doi.org/10.1016/s0140-6736(74)90071-3)
- D’Souza, V.N., Nguyen, T.M., Morris, G.E., Karges, W., Pillers, D.A., Ray, P.N., 1995. A novel dystrophin isoform is required for normal retinal electrophysiology. *Hum. Mol. Genet.* 4, 837–842. <https://doi.org/10.1093/hmg/4.5.837>
- Duan, D., 2018a. Systemic AAV Micro-DMD gene Therapy for Duchenne Muscular Dystrophy. *Mol. Ther.* 26, 2337–2356. <https://doi.org/10.1016/j.ymthe.2018.07.011>
- Duan, D., 2018b. Micro-DMD gene Therapy Goes Systemic in Duchenne Muscular Dystrophy Patients. *Hum Gene Ther* 29, 733–736. <https://doi.org/10.1089/hum.2018.012>
- Duan, D., Goemans, N., Takeda, S., Mercuri, E., Aartsma-Rus, A., 2021. Duchenne muscular dystrophy. *Nat Rev Dis Primers* 7, 1–19. <https://doi.org/10.1038/s41572-021-00248-3>
- Dubowitz, V., 1979. Involvement of the nervous system in muscular dystrophies in man. *Ann N Y Acad Sci* 317, 431–439. <https://doi.org/10.1111/j.1749-6632.1979.tb56558.x>
- Duchenne, 1868. De la paralysie musculaire pseudo-hypertrophique, ou paralysie myo-sclérotique.
- Duchenne, G.-B. (1806-1875) A. du texte, 1861. De l’électrisation localisée et de son application à la physiologie, à la pathologie et à la thérapeutique (2e édition) / par le Dr Duchenne, de Boulogne.
- Durbeej, M., Campbell, K.P., 2002. Muscular dystrophies involving the dystrophin-glycoprotein complex: an overview of current mouse models. *Curr Opin Genet Dev* 12, 349–361. [https://doi.org/10.1016/s0959-437x\(02\)00309-x](https://doi.org/10.1016/s0959-437x(02)00309-x)
- Echigoya, Y., Lee, J., Rodrigues, M., Nagata, T., Tanihata, J., Nozohourmehrabad, A., Panesar, D., Miskew, B., Aoki, Y., Yokota, T., 2013. Mutation Types and Aging Differently Affect Revertant Fiber Expansion in Dystrophic Mdx and Mdx52 Mice. *PLOS ONE* 8, e69194. <https://doi.org/10.1371/journal.pone.0069194>
- Ehninger, D., Li, W., Fox, K., Stryker, M.P., Silva, A.J., 2008. Reversing Neurodevelopmental Disorders in Adults. *Neuron* 60, 950–960. <https://doi.org/10.1016/j.neuron.2008.12.007>
- Engelbeen, S., Aartsma-Rus, A., Koopmans, B., Loos, M., van Putten, M., 2021. Assessment of Behavioral Characteristics With Procedures of Minimal Human Interference in the mdx Mouse Model for Duchenne Muscular Dystrophy. *Front Behav Neurosci* 14, 629043. <https://doi.org/10.3389/fnbeh.2020.629043>
- Ernst, T.M., Brol, A.E., Gratz, M., Ritter, C., Bingel, U., Schlamann, M., Maderwald, S., Quick, H.H., Merz, C.J., Timmann, D., 2019. The cerebellum is involved in processing of predictions and prediction errors in a fear conditioning paradigm. *Elife* 8, e46831. <https://doi.org/10.7554/eLife.46831>
- Ervasti, J.M., Ohlendieck, K., Kahl, S.D., Gaver, M.G., Campbell, K.P., 1990. Deficiency of a glycoprotein component of the dystrophin complex in dystrophic muscle. *Nature* 345, 315–319. <https://doi.org/10.1038/345315a0>
- Ezzat, K., Aoki, Y., Koo, T., McClorey, G., Benner, L., Coenen-Stass, A., O’Donovan, L., Lehto, T., Garcia-Guerra, A., Nordin, J., Saleh, A.F., Behlke, M., Morris, J., Goyenvalle, A., Dugovic, B., Leumann, C., Gordon, S., Gait, M.J., El-Andaloussi, S., Wood, M.J.A., 2015. Self-Assembly into Nanoparticles Is Essential for Receptor Mediated Uptake of Therapeutic Antisense Oligonucleotides. *Nano Lett* 15, 4364–4373. <https://doi.org/10.1021/acs.nanolett.5b00490>

- Fagan, X.J., Levy, J., Al-Qureshi, S., Harper, C.A., 2012. Proliferative retinopathy in Duchenne muscular dystrophy and its response to bevacizumab. *Clinical & Experimental Ophthalmology* 40, 906–907. <https://doi.org/10.1111/j.1442-9071.2012.02822.x>
- Fan, Y., Maley, M., Beilharz, M., Grounds, M., 1996. Rapid death of injected myoblasts in myoblast transfer therapy. *Muscle Nerve* 19, 853–860. [https://doi.org/10.1002/\(SICI\)1097-4598\(199607\)19:7<853::AID-MUS7>3.0.CO;2-8](https://doi.org/10.1002/(SICI)1097-4598(199607)19:7<853::AID-MUS7>3.0.CO;2-8)
- Farini, A., Razini, P., Erratico, S., Torrente, Y., Meregalli, M., 2009. Cell based therapy for Duchenne muscular dystrophy. *J Cell Physiol* 221, 526–534. <https://doi.org/10.1002/jcp.21895>
- Farley, S.J., Radley, J.J., Freeman, J.H., 2016. Amygdala Modulation of Cerebellar Learning. *J Neurosci* 36, 2190–2201. <https://doi.org/10.1523/JNEUROSCI.3361-15.2016>
- Faul, L., Stjepanović, D., Stivers, J.M., Stewart, G.W., Graner, J.L., Morey, R.A., LaBar, K.S., 2020. Proximal threats promote enhanced acquisition and persistence of reactive fear-learning circuits. *Proc Natl Acad Sci U S A* 117, 16678–16689. <https://doi.org/10.1073/pnas.2004258117>
- Fee, R.J., Hinton, V.J., 2011. Resilience in Children Diagnosed with a Chronic Neuromuscular Disorder. *J Dev Behav Pediatr* 32, 644–650. <https://doi.org/10.1097/DBP.0b013e318235d614>
- Ferlini, A., Galié, N., Merlini, L., Sewry, C., Branzi, A., Muntoni, F., 1998. A novel Alu-like element rearranged in the DMD gene causes a splicing mutation in a family with X-linked dilated cardiomyopathy. *Am J Hum Genet* 63, 436–446. <https://doi.org/10.1086/301952>
- Ferlini, A., Goyenvalle, A., Muntoni, F., 2021. RNA-targeted drugs for neuromuscular diseases. *Science* 371, 29–31. <https://doi.org/10.1126/science.aba4515>
- Finkel, R.S., Chiriboga, C.A., Vajsar, J., Day, J.W., Montes, J., De Vivo, D.C., Yamashita, M., Rigo, F., Hung, G., Schneider, E., Norris, D.A., Xia, S., Bennett, C.F., Bishop, K.M., 2016. Treatment of infantile-onset spinal muscular atrophy with nusinersen: a phase 2, open-label, dose-escalation study. *Lancet* 388, 3017–3026. [https://doi.org/10.1016/S0140-6736\(16\)31408-8](https://doi.org/10.1016/S0140-6736(16)31408-8)
- Finkel, R.S., Flanigan, K.M., Wong, B., Bönnemann, C., Sampson, J., Sweeney, H.L., Reha, A., Northcutt, V.J., Elfring, G., Barth, J., Peltz, S.W., 2013. Phase 2a study of ataluren-mediated dystrophin production in patients with nonsense mutation Duchenne muscular dystrophy. *PLoS One* 8, e81302. <https://doi.org/10.1371/journal.pone.0081302>
- Fitzgerald, K.M., Cibis, G.W., Giambrone, S.A., Harris, D.J., 1994. Retinal signal transmission in Duchenne muscular dystrophy: evidence for dysfunction in the photoreceptor/depolarizing bipolar cell pathway. *J Clin Invest* 93, 2425–2430. <https://doi.org/10.1172/JCI117250>
- Flynn, J.M., Brown, E.J., Clark, A.G., 2021. Copy number evolution in simple and complex tandem repeats across the C57BL/6 and C57BL/10 inbred mouse lines. *G3 (Bethesda)* 11, jkab184. <https://doi.org/10.1093/g3journal/jkab184>
- Foust, K.D., Nurre, E., Montgomery, C.L., Hernandez, A., Chan, C.M., Kaspar, B.K., 2009. Intravascular AAV9 preferentially targets neonatal neurons and adult astrocytes. *Nat Biotechnol* 27, 59–65. <https://doi.org/10.1038/nbt.1515>
- Frank, D.E., Schnell, F.J., Akana, C., El-Husayni, S.H., Desjardins, C.A., Morgan, J., Charleston, J.S., Sardone, V., Domingos, J., Dickson, G., Straub, V., Guglieri, M., Mercuri, E., Servais, L., Muntoni, F., SKIP-NMD Study Group, 2020. Increased dystrophin production with golodirsen in patients with Duchenne muscular dystrophy. *Neurology* 94, e2270–e2282. <https://doi.org/10.1212/WNL.0000000000009233>
- Fritschy, J.-M., Panzanelli, P., Tyagarajan, S.K., 2012. Molecular and functional heterogeneity of GABAergic synapses. *Cell Mol Life Sci* 69, 2485–2499. <https://doi.org/10.1007/s00018-012-0926-4>
- Fritschy, J.-M., Schweizer, C., Brünic, I., Lüscher, B., 2003. Pre- and post-synaptic mechanisms regulating the clustering of type A gamma-aminobutyric acid receptors (GABAA receptors). *Biochem Soc Trans* 31, 889–892. <https://doi.org/10.1042/bst0310889>

- Früh, S., Romanos, J., Panzanelli, P., Bürgisser, D., Tyagarajan, S.K., Campbell, K.P., Santello, M., Fritschy, J.-M., 2016. Neuronal Dystroglycan Is Necessary for Formation and Maintenance of Functional CCK-Positive Basket Cell Terminals on Pyramidal Cells. *J Neurosci* 36, 10296–10313. <https://doi.org/10.1523/JNEUROSCI.1823-16.2016>
- Fuenzalida, M., Espinoza, C., Pérez, M.Á., Tapia-Rojas, C., Cuitino, L., Brandan, E., Inestrosa, N.C., 2016. Wnt signaling pathway improves central inhibitory synaptic transmission in a mouse model of Duchenne muscular dystrophy. *Neurobiol Dis* 86, 109–120. <https://doi.org/10.1016/j.nbd.2015.11.018>
- Fujimoto, T., Itoh, K., Yaoi, T., Fushiki, S., 2014. Somatodendritic and excitatory postsynaptic distribution of neuron-type dystrophin isoform, Dp40, in hippocampal neurons. *Biochem Biophys Res Commun* 452, 79–84. <https://doi.org/10.1016/j.bbrc.2014.08.064>
- García-Cruz, C., Aragón, J., Lourdel, S., Annan, A., Roger, J.E., Montanez, C., Vaillend, C., 2022. Tissue- and cell-specific whole-transcriptome meta-analysis from brain and retina reveals differential expression of dystrophin complexes and new dystrophin spliced isoforms. *Human Molecular Genetics* ddac236. <https://doi.org/10.1093/hmg/ddac236>
- García-Rodríguez, R., Hiller, M., Jiménez-Gracia, L., van der Pal, Z., Balog, J., Adamzek, K., Aartsma-Rus, A., Spitali, P., 2020. Premature termination codons in the DMD gene cause reduced local mRNA synthesis. *Proc Natl Acad Sci U S A* 117, 16456–16464. <https://doi.org/10.1073/pnas.1910456117>
- Gaus, H.J., Gupta, R., Chappell, A.E., Østergaard, M.E., Swayze, E.E., Seth, P.P., 2019. Characterization of the interactions of chemically-modified therapeutic nucleic acids with plasma proteins using a fluorescence polarization assay. *Nucleic Acids Res* 47, 1110–1122. <https://doi.org/10.1093/nar/gky1260>
- Gehring, N.H., Roignant, J.-Y., 2021. Anything but Ordinary – Emerging Splicing Mechanisms in Eukaryotic Gene Regulation. *Trends in Genetics* 37, 355–372. <https://doi.org/10.1016/j.tig.2020.10.008>
- Ghedini, P.C., Avellar, M.C.W., De Lima, T.C.M., Lima-Landman, M.T.R., Lapa, A.J., Souccar, C., 2012. Quantitative changes of nicotinic receptors in the hippocampus of dystrophin-deficient mice. *Brain Res* 1483, 96–104. <https://doi.org/10.1016/j.brainres.2012.09.021>
- Giedd, J.N., Vaituzis, A.C., Hamburger, S.D., Lange, N., Rajapakse, J.C., Kaysen, D., Vauss, Y.C., Rapoport, J.L., 1996. Quantitative MRI of the temporal lobe, amygdala, and hippocampus in normal human development: ages 4-18 years. *J Comp Neurol* 366, 223–230. [https://doi.org/10.1002/\(SICI\)1096-9861\(19960304\)366:2<223::AID-CNE3>3.0.CO;2-7](https://doi.org/10.1002/(SICI)1096-9861(19960304)366:2<223::AID-CNE3>3.0.CO;2-7)
- Girlanda, P., Quartarone, A., Buceti, R., Sinicropi, S., Macaione, V., Saad, F.A., Messina, L., Danieli, G.A., Ferreri, G., Vita, G., 1997. Extra-muscle involvement in dystrophinopathies: an electroretinography and evoked potential study. *J Neurol Sci* 146, 127–132. [https://doi.org/10.1016/s0022-510x\(96\)00292-4](https://doi.org/10.1016/s0022-510x(96)00292-4)
- Goemans, N., Mercuri, E., Belousova, E., Komaki, H., Dubrovsky, A., McDonald, C.M., Kraus, J.E., Loubakos, A., Lin, Z., Champion, G., Wang, S.X., Campbell, C., DEMAND III study group, 2018. A randomized placebo-controlled phase 3 trial of an antisense oligonucleotide, drisapersen, in Duchenne muscular dystrophy. *Neuromuscul. Disord.* 28, 4–15. <https://doi.org/10.1016/j.nmd.2017.10.004>
- Goemans, N.M., Tulinius, M., van den Akker, J.T., Burm, B.E., Ekhart, P.F., Heuvelmans, N., Holling, T., Janson, A.A., Platenburg, G.J., Sipkens, J.A., Sitsen, J.M.A., Aartsma-Rus, A., van Ommen, G.-J.B., Buyse, G., Darin, N., Verschuuren, J.J., Champion, G.V., de Kimpe, S.J., van Deutekom, J.C., 2011. Systemic administration of PRO051 in Duchenne’s muscular dystrophy. *N Engl J Med* 364, 1513–1522. <https://doi.org/10.1056/NEJMoa1011367>
- Goemans, N.M., Tulinius, M., van den Hauwe, M., Kroksmark, A.-K., Buyse, G., Wilson, R.J., van Deutekom, J.C., de Kimpe, S.J., Loubakos, A., Champion, G., 2016. Long-Term Efficacy, Safety, and Pharmacokinetics of Drisapersen in Duchenne Muscular Dystrophy: Results from an Open-Label Extension Study. *PLoS ONE* 11, e0161955. <https://doi.org/10.1371/journal.pone.0161955>

- Górecki, D.C., Barnard, E.A., 1995. Specific expression of G-dystrophin (Dp71) in the brain. *Neuroreport* 6, 893–896. <https://doi.org/10.1097/00001756-199504190-00017>
- Górecki, D.C., Monaco, A.P., Derry, J.M., Walker, A.P., Barnard, E.A., Barnard, P.J., 1992. Expression of four alternative dystrophin transcripts in brain regions regulated by different promoters. *Hum. Mol. Genet.* 1, 505–510. <https://doi.org/10.1093/hmg/1.7.505>
- Gowers, W., 1879. Pseudo-hypertrophic muscular paralysis: a clinical lecture. *Lancet*.
- Goyenvalle, A., Babbs, A., Wright, J., Wilkins, V., Powell, D., Garcia, L., Davies, K.E., 2012. Rescue of severely affected dystrophin/utrophin-deficient mice through scAAV-U7snRNA-mediated exon skipping. *Hum Mol Genet* 21, 2559–2571. <https://doi.org/10.1093/hmg/dds082>
- Goyenvalle, A., Griffith, G., Babbs, A., El Andaloussi, S., Ezzat, K., Avril, A., Dugovic, B., Chaussonot, R., Ferry, A., Voit, T., Amthor, H., Bühr, C., Schürch, S., Wood, M.J.A., Davies, K.E., Vaillend, C., Leumann, C., Garcia, L., 2015. Functional correction in mouse models of muscular dystrophy using exon-skipping tricyclo-DNA oligomers. *Nat Med* 21, 270–275. <https://doi.org/10.1038/nm.3765>
- Goyenvalle, A., Leumann, C., Garcia, L., 2016. Therapeutic Potential of Tricyclo-DNA antisense oligonucleotides. *J Neuromuscul Dis* 3, 157–167. <https://doi.org/10.3233/JND-160146>
- Goyenvalle, A., Vulin, A., Fougousse, F., Leturcq, F., Kaplan, J.-C., Garcia, L., Danos, O., 2004. Rescue of dystrophic muscle through U7 snRNA-mediated exon skipping. *Science* 306, 1796–1799. <https://doi.org/10.1126/science.1104297>
- Grady, R.M., Wozniak, D.F., Ohlemiller, K.K., Sanes, J.R., 2006. Cerebellar synaptic defects and abnormal motor behavior in mice lacking alpha- and beta-dystrobrevin. *J Neurosci* 26, 2841–2851. <https://doi.org/10.1523/JNEUROSCI.4823-05.2006>
- Gripenburg, J.C., Rapp, T.L., Carroll, P.J., Eberwine, J., Dmochowski, I.J., 2015. Ruthenium-Caged Antisense Morpholinos for Regulating Gene Expression in Zebrafish Embryos. *Chem Sci* 6, 2342–2346. <https://doi.org/10.1039/C4SC03990D>
- Hagedorn, P.H., Persson, R., Funder, E.D., Albæk, N., Diemer, S.L., Hansen, D.J., Møller, M.R., Papargyri, N., Christiansen, H., Hansen, B.R., Hansen, H.F., Jensen, M.A., Koch, T., 2018. Locked nucleic acid: modality, diversity, and drug discovery. *Drug Discov. Today* 23, 101–114. <https://doi.org/10.1016/j.drudis.2017.09.018>
- Hahn, P., Lin, P., Fekrat, S., 2013. Ultra-widefield Imaging of Duchenne Muscular Dystrophy-associated Proliferative Retinal Vasculopathy Improved With Panretinal Laser Photocoagulation Alone. *Ophthalmic Surgery, Lasers and Imaging Retina* 44, 293–295. <https://doi.org/10.3928/23258160-20130503-17>
- Hakim, C.H., Grange, R.W., Duan, D., 2011. The passive mechanical properties of the extensor digitorum longus muscle are compromised in 2- to 20-mo-old mdx mice. *J Appl Physiol* (1985) 110, 1656–1663. <https://doi.org/10.1152/japplphysiol.01425.2010>
- Hashimoto, Y., Kuniishi, H., Sakai, K., Fukushima, Y., Du, X., Yamashiro, K., Hori, K., Imamura, M., Hoshino, M., Yamada, M., Araki, T., Sakagami, H., Takeda, S., Itaka, K., Ichinohe, N., Muntoni, F., Sekiguchi, M., Aoki, Y., 2022. Brain Dp140 alters glutamatergic transmission and social behaviour in the mdx52 mouse model of Duchenne muscular dystrophy. *Prog Neurobiol* 216, 102288. <https://doi.org/10.1016/j.pneurobio.2022.102288>
- Heier, C.R., Yu, Q., Fiorillo, A.A., Tully, C.B., Tucker, A., Mazala, D.A., Uaesoontrachoon, K., Srinivassane, S., Damsker, J.M., Hoffman, E.P., Nagaraju, K., Spurney, C.F., 2019. Vamorolone targets dual nuclear receptors to treat inflammation and dystrophic cardiomyopathy. *Life Sci Alliance* 2, e201800186. <https://doi.org/10.26508/lsa.201800186>
- Helleringer, R., Verger, D.L., Li, X., Isabelle, C., Chaussonot, R., Belmaati-Cherkaoui, M., Dammak, R., Decottignies, P., Daniel, H., Galante, M., Vaillend, C., 2018. Cerebellar synapse properties and

- cerebellum-dependent motor and non-motor performance in Dp71-null mice. *Disease Models & Mechanisms* 11. <https://doi.org/10.1242/dmm.033258>
- Hendriksen, J.G.M., Vles, J.S.H., 2008. Neuropsychiatric disorders in males with duchenne muscular dystrophy: frequency rate of attention-deficit hyperactivity disorder (ADHD), autism spectrum disorder, and obsessive-compulsive disorder. *J Child Neurol* 23, 477–481. <https://doi.org/10.1177/0883073807309775>
- Hildyard, J.C.W., Crawford, A.H., Rawson, F., Riddell, D.O., Harron, R.C.M., Piercy, R.J., 2020. Single-transcript multiplex in situ hybridisation reveals unique patterns of dystrophin isoform expression in the developing mammalian embryo. *Wellcome Open Res* 5. <https://doi.org/10.12688/wellcomeopenres.15762.2>
- Hinton, V.J., Cyrulnik, S.E., Fee, R.J., Batchelder, A., Kiefel, J.M., Goldstein, E.M., Kaufmann, P., De Vivo, D.C., 2009. Association of autistic spectrum disorders with dystrophinopathies. *Pediatr Neurol* 41, 339–346. <https://doi.org/10.1016/j.pediatrneurol.2009.05.011>
- Hinton, V.J., De Vivo, D.C., Fee, R., Goldstein, E., Stern, Y., 2004. Investigation of Poor Academic Achievement in Children with Duchenne Muscular Dystrophy. *Learn Disabil Res Pract* 19, 146–154. <https://doi.org/10.1111/j.1540-5826.2004.00098.x>
- Hinton, V.J., DE VIVO, D.C., NEREO, N.E., GOLDSTEIN, E., STERN, Y., 2001. Selective deficits in verbal working memory associated with a known genetic etiology: The neuropsychological profile of Duchenne muscular dystrophy. *J Int Neuropsychol Soc* 7, 45–54.
- Hinton, V.J., De Vivo, D.C., Nereo, N.E., Goldstein, E., Stern, Y., 2000. Poor verbal working memory across intellectual level in boys with Duchenne dystrophy. *Neurology* 54, 2127–2132. <https://doi.org/10.1212/wnl.54.11.2127>
- Hinton, V.J., Fee, R.J., De Vivo, D.C., Goldstein, E., 2007. Poor Facial Affect Recognition Among Boys with Duchenne Muscular Dystrophy. *J Autism Dev Disord* 37, 1925–1933. <https://doi.org/10.1007/s10803-006-0325-5>
- Hinton, V.J., Nereo, N.E., Fee, R.J., Cyrulnik, S.E., 2006. Social behavior problems in boys with Duchenne muscular dystrophy. *J Dev Behav Pediatr* 27, 470–476. <https://doi.org/10.1097/00004703-200612000-00003>
- Hirawat, S., Welch, E.M., Elfring, G.L., Northcutt, V.J., Paushkin, S., Hwang, S., Leonard, E.M., Almstead, N.G., Ju, W., Peltz, S.W., Miller, L.L., 2007. Safety, tolerability, and pharmacokinetics of PTC124, a nonaminoglycoside nonsense mutation suppressor, following single- and multiple-dose administration to healthy male and female adult volunteers. *J Clin Pharmacol* 47, 430–444. <https://doi.org/10.1177/0091270006297140>
- Hoffman, E.P., Brown, R.H., Kunkel, L.M., 1987. Dystrophin: the protein product of the Duchenne muscular dystrophy locus. *Cell* 51, 919–928. [https://doi.org/10.1016/0092-8674\(87\)90579-4](https://doi.org/10.1016/0092-8674(87)90579-4)
- Hoffman, E.P., Gorospe, J.R.M., 1991. Chapter 8 The Animal Models of Duchenne Muscular Dystrophy: Windows on the Pathophysiological Consequences of Dystrophin Deficiency, in: Mooseker, M.S., Morrow, J.S. (Eds.), *Current Topics in Membranes, Ordering the Membrane-Cytoskeleton Trilayer*. Academic Press, pp. 113–154. [https://doi.org/10.1016/S0070-2161\(08\)60785-6](https://doi.org/10.1016/S0070-2161(08)60785-6)
- Hoffman, E.P., Morgan, J.E., Watkins, S.C., Partridge, T.A., 1990. Somatic reversion/suppression of the mouse mdx phenotype in vivo. *J Neurol Sci* 99, 9–25. [https://doi.org/10.1016/0022-510x\(90\)90195-s](https://doi.org/10.1016/0022-510x(90)90195-s)
- Hogan, A., Shepherd, L., Chabot, J., Quenneville, S., Prescott, S.M., Topham, M.K., Gee, S.H., 2001. Interaction of gamma 1-syntrophin with diacylglycerol kinase-zeta. Regulation of nuclear localization by PDZ interactions. *J Biol Chem* 276, 26526–26533. <https://doi.org/10.1074/jbc.M104156200>
- Holder, E., Maeda, M., Bies, R.D., 1996. Expression and regulation of the dystrophin Purkinje promoter in human skeletal muscle, heart, and brain. *Hum. Genet.* 97, 232–239. <https://doi.org/10.1007/bf02265272>

- Hugnot, J.P., Gilgenkrantz, H., Vincent, N., Chafey, P., Morris, G.E., Monaco, A.P., Berwald-Netter, Y., Koulakoff, A., Kaplan, J.C., Kahn, A., 1992. Distal transcript of the DMD gene initiated from an alternative first exon and encoding a 75-kDa protein widely distributed in nonmuscle tissues. *Proc Natl Acad Sci U S A* 89, 7506–7510. <https://doi.org/10.1073/pnas.89.16.7506>
- Iannitti, T., Morales-Medina, J.C., Palmieri, B., 2014. Phosphorothioate oligonucleotides: effectiveness and toxicity. *Curr Drug Targets* 15, 663–673.
- Im, W.B., Phelps, S.F., Copen, E.H., Adams, E.G., Slightom, J.L., Chamberlain, J.S., 1996. Differential expression of dystrophin isoforms in strains of mdx mice with different mutations. *Hum Mol Genet* 5, 1149–1153. <https://doi.org/10.1093/hmg/5.8.1149>
- Imbert, M., Dias-Florencio, G., Goyenvalle, A., 2017. Viral Vector-Mediated Antisense Therapy for Genetic Diseases. *Genes (Basel)* 8. <https://doi.org/10.3390/genes8020051>
- Jacobs, P.A., Hunt, P.A., Mayer, M., Bart, R.D., 1981. Duchenne muscular dystrophy (DMD) in a female with an X/autosome translocation: further evidence that the DMD locus is at Xp21. *Am J Hum Genet* 33, 513–518.
- Järver, P., O'Donovan, L., Gait, M.J., 2014. A chemical view of oligonucleotides for exon skipping and related drug applications. *Nucleic Acid Ther* 24, 37–47. <https://doi.org/10.1089/nat.2013.0454>
- Jeronimo, G., Nozoe, K.T., Polesel, D.N., Moreira, G.A., Tufik, S., Andersen, M.L., 2016. Impact of corticotherapy, nutrition, and sleep disorder on quality of life of patients with Duchenne muscular dystrophy. *Nutrition* 32, 391–393. <https://doi.org/10.1016/j.nut.2015.09.004>
- Jung, D., Filliol, D., Metz-Boutigue, M.H., Rendon, A., 1993. Characterization and subcellular localization of the dystrophin-protein 71 (Dp71) from brain. *Neuromuscul Disord* 3, 515–518. [https://doi.org/10.1016/0960-8966\(93\)90107-u](https://doi.org/10.1016/0960-8966(93)90107-u)
- Kameya, S., Araki, E., Katsuki, M., Mizota, A., Adachi, E., Nakahara, K., Nonaka, I., Sakuragi, S., Takeda, S., Nabeshima, Y., 1997. Dp260 disrupted mice revealed prolonged implicit time of the b-wave in ERG and loss of accumulation of beta-dystroglycan in the outer plexiform layer of the retina. *Hum Mol Genet* 6, 2195–2203. <https://doi.org/10.1093/hmg/6.13.2195>
- Kecik, M., Stangos, A., Malclès, A., 2021. Bilateral Visual Acuity Loss in a 28-Year-Old Man With Duchenne Muscular Dystrophy. *JAMA Ophthalmology* 139, 1035–1036. <https://doi.org/10.1001/jamaophthalmol.2020.6852>
- Kelly, R.M., Strick, P.L., 2003. Cerebellar loops with motor cortex and prefrontal cortex of a nonhuman primate. *J Neurosci* 23, 8432–8444. <https://doi.org/10.1523/JNEUROSCI.23-23-08432.2003>
- Kinali, M., Arechavala-Gomez, V., Feng, L., Cirak, S., Hunt, D., Adkin, C., Guglieri, M., Ashton, E., Abbs, S., Nihoyannopoulos, P., Garralda, M.E., Rutherford, M., McCulley, C., Popplewell, L., Graham, I.R., Dickson, G., Wood, M.J.A., Wells, D.J., Wilton, S.D., Kole, R., Straub, V., Bushby, K., Sewry, C., Morgan, J.E., Muntoni, F., 2009. Local restoration of dystrophin expression with the morpholino oligomer AVI-4658 in Duchenne muscular dystrophy: a single-blind, placebo-controlled, dose-escalation, proof-of-concept study. *Lancet Neurol* 8, 918–928. [https://doi.org/10.1016/S1474-4422\(09\)70211-X](https://doi.org/10.1016/S1474-4422(09)70211-X)
- Kingston, H.M., Sarfarazi, M., Thomas, N.S., Harper, P.S., 1984. Localisation of the Becker muscular dystrophy gene on the short arm of the X chromosome by linkage to cloned DNA sequences. *Hum Genet* 67, 6–17. <https://doi.org/10.1007/BF00270551>
- Klein, R.L., Dayton, R.D., Tatom, J.B., Henderson, K.M., Henning, P.P., 2008. AAV8, 9, Rh10, Rh43 vector gene transfer in the rat brain: effects of serotype, promoter and purification method. *Mol Ther* 16, 89–96. <https://doi.org/10.1038/sj.mt.6300331>
- Kleschevnikov, A.M., Belichenko, P.V., Faizi, M., Jacobs, L.F., Htun, K., Shamloo, M., Mobley, W.C., 2012. Deficits in cognition and synaptic plasticity in a mouse model of Down syndrome ameliorated by

- GABAB receptor antagonists. *J Neurosci* 32, 9217–9227. <https://doi.org/10.1523/JNEUROSCI.1673-12.2012>
- Klimczak, R.R., Koerber, J.T., Dalkara, D., Flannery, J.G., Schaffer, D.V., 2009. A novel adeno-associated viral variant for efficient and selective intravitreal transduction of rat Müller cells. *PLoS One* 4, e7467. <https://doi.org/10.1371/journal.pone.0007467>
- Knuesel, I., Mastrocola, M., Zuellig, R.A., Bornhauser, B., Schaub, M.C., Fritschy, J.M., 1999. Short communication: altered synaptic clustering of GABAA receptors in mice lacking dystrophin (mdx mice). *Eur J Neurosci* 11, 4457–4462. <https://doi.org/10.1046/j.1460-9568.1999.00887.x>
- Koenig, M., Beggs, A.H., Moyer, M., Scherpf, S., Heindrich, K., Bettecken, T., Meng, G., Müller, C.R., Lindlöf, M., Kaariainen, H., de la Chapelle, A., Kiuru, A., Savontaus, M.L., Gilgenkrantz, H., Récan, D., Chelly, J., Kaplan, J.C., Covone, A.E., Archidiacono, N., Romeo, G., Liechti-Gailati, S., Schneider, V., Braga, S., Moser, H., Darras, B.T., Murphy, P., Francke, U., Chen, J.D., Morgan, G., Denton, M., Greenberg, C.R., Wrogemann, K., Blonden, L.A., van Paassen, M.B., van Ommen, G.J., Kunkel, L.M., 1989. The molecular basis for Duchenne versus Becker muscular dystrophy: correlation of severity with type of deletion. *Am J Hum Genet* 45, 498–506.
- Koenig, M., Hoffman, E.P., Bertelson, C.J., Monaco, A.P., Feener, C., Kunkel, L.M., 1987. Complete cloning of the Duchenne muscular dystrophy (DMD) cDNA and preliminary genomic organization of the DMD gene in normal and affected individuals. *Cell* 50, 509–517. [https://doi.org/10.1016/0092-8674\(87\)90504-6](https://doi.org/10.1016/0092-8674(87)90504-6)
- Koenig, M., Kunkel, L.M., 1990. Detailed analysis of the repeat domain of dystrophin reveals four potential hinge segments that may confer flexibility. *J Biol Chem* 265, 4560–4566.
- Koenig, M., Monaco, A.P., Kunkel, L.M., 1988. The complete sequence of dystrophin predicts a rod-shaped cytoskeletal protein. *Cell* 53, 219–228. [https://doi.org/10.1016/0092-8674\(88\)90383-2](https://doi.org/10.1016/0092-8674(88)90383-2)
- Konieczny, P., Swiderski, K., Chamberlain, J.S., 2013. Gene and cell-mediated therapies for muscular dystrophy. *Muscle Nerve* 47, 649–663. <https://doi.org/10.1002/mus.23738>
- Kornegay, J.N., Tuler, S.M., Miller, D.M., Levesque, D.C., 1988. Muscular dystrophy in a litter of golden retriever dogs. *Muscle Nerve* 11, 1056–1064. <https://doi.org/10.1002/mus.880111008>
- Krasowska, E., Zabłocki, K., Górecki, D.C., Swinny, J.D., 2014. Aberrant location of inhibitory synaptic marker proteins in the hippocampus of dystrophin-deficient mice: implications for cognitive impairment in duchenne muscular dystrophy. *PLoS One* 9, e108364. <https://doi.org/10.1371/journal.pone.0108364>
- Kretschmer, F., Kretschmer, V., Kunze, V.P., Kretzberg, J., 2013. OMR-arena: automated measurement and stimulation system to determine mouse visual thresholds based on optomotor responses. *PLoS One* 8, e78058. <https://doi.org/10.1371/journal.pone.0078058>
- Kretschmer, F., Sajgo, S., Kretschmer, V., Badea, T.C., 2015. A system to measure the Optokinetic and Optomotor response in mice. *J Neurosci Methods* 256, 91–105. <https://doi.org/10.1016/j.jneumeth.2015.08.007>
- Kudoh, H., Ikeda, H., Kakitani, M., Ueda, A., Hayasaka, M., Tomizuka, K., Hanaoka, K., 2005. A new model mouse for Duchenne muscular dystrophy produced by 2.4 Mb deletion of DMD gene using Cre-loxP recombination system. *Biochem Biophys Res Commun* 328, 507–516. <https://doi.org/10.1016/j.bbrc.2004.12.191>
- Kueh, S.L.L., Dempster, J., Head, S.I., Morley, J.W., 2011. Reduced postsynaptic GABAA receptor number and enhanced gaboxadol induced change in holding currents in Purkinje cells of the dystrophin-deficient mdx mouse. *Neurobiol Dis* 43, 558–564. <https://doi.org/10.1016/j.nbd.2011.05.002>
- Kueh, S.L.L., Head, S.I., Morley, J.W., 2008. GABA(A) receptor expression and inhibitory post-synaptic currents in cerebellar Purkinje cells in dystrophin-deficient mdx mice. *Clin Exp Pharmacol Physiol* 35, 207–210. <https://doi.org/10.1111/j.1440-1681.2007.04816.x>

- Kurreck, J., 2003. Antisense technologies. Improvement through novel chemical modifications. *Eur J Biochem* 270, 1628–1644. <https://doi.org/10.1046/j.1432-1033.2003.03555.x>
- Kwon, J.B., ETTYREDDY, A.R., VANKARA, A., BOHNING, J.D., DEVLIN, G., HAUSCHKA, S.D., ASOKAN, A., GERSBACH, C.A., 2020. In Vivo Gene Editing of Muscle Stem Cells with Adeno-Associated Viral Vectors in a Mouse Model of Duchenne Muscular Dystrophy. *Mol Ther Methods Clin Dev* 19, 320–329. <https://doi.org/10.1016/j.omtm.2020.09.016>
- Lander, E.S., Linton, L.M., Birren, B., Nusbaum, C., Zody, M.C., Baldwin, J., Devon, K., Dewar, K., Doyle, M., FitzHugh, W., Funke, R., Gage, D., Harris, K., Heaford, A., Howland, J., Kann, L., Lehoczy, J., LeVine, R., McEwan, P., McKernan, K., Meldrim, J., Mesirov, J.P., Miranda, C., Morris, W., Naylor, J., Raymond, C., Rosetti, M., Santos, R., Sheridan, A., Sougnez, C., Stange-Thomann, Y., Stojanovic, N., Subramanian, A., Wyman, D., Rogers, J., Sulston, J., Ainscough, R., Beck, S., Bentley, D., Burton, J., Clee, C., Carter, N., Coulson, A., Deadman, R., Deloukas, P., Dunham, A., Dunham, I., Durbin, R., French, L., Grafham, D., Gregory, S., Hubbard, T., Humphray, S., Hunt, A., Jones, M., Lloyd, C., McMurray, A., Matthews, L., Mercer, S., Milne, S., Mullikin, J.C., Mungall, A., Plumb, R., Ross, M., Shownkeen, R., Sims, S., Waterston, R.H., Wilson, R.K., Hillier, L.W., McPherson, J.D., Marra, M.A., Mardis, E.R., Fulton, L.A., Chinwalla, A.T., Pepin, K.H., Gish, W.R., Chissoe, S.L., Wendl, M.C., Delehaanty, K.D., Miner, T.L., Delehaanty, A., Kramer, J.B., Cook, L.L., Fulton, R.S., Johnson, D.L., Minx, P.J., Clifton, S.W., Hawkins, T., Branscomb, E., Predki, P., Richardson, P., Wenning, S., Slezak, T., Doggett, N., Cheng, J.F., Olsen, A., Lucas, S., Elkin, C., Uberbacher, E., Frazier, M., Gibbs, R.A., Muzny, D.M., Scherer, S.E., Bouck, J.B., Sodergren, E.J., Worley, K.C., Rives, C.M., Gorrell, J.H., Metzker, M.L., Naylor, S.L., Kucherlapati, R.S., Nelson, D.L., Weinstock, G.M., Sakaki, Y., Fujiyama, A., Hattori, M., Yada, T., Toyoda, A., Itoh, T., Kawagoe, C., Watanabe, H., Totoki, Y., Taylor, T., Weissenbach, J., Heilig, R., Saurin, W., Artiguenave, F., Brottier, P., Bruls, T., Pelletier, E., Robert, C., Wincker, P., Smith, D.R., Doucette-Stamm, L., Rubenfield, M., Weinstock, K., Lee, H.M., Dubois, J., Rosenthal, A., Platzer, M., Nyakatura, G., Taudien, S., Rump, A., Yang, H., Yu, J., Wang, J., Huang, G., Gu, J., Hood, L., Rowen, L., Madan, A., Qin, S., Davis, R.W., Federspiel, N.A., Abola, A.P., Proctor, M.J., Myers, R.M., Schmutz, J., Dickson, M., Grimwood, J., Cox, D.R., Olson, M.V., Kaul, R., Raymond, C., Shimizu, N., Kawasaki, K., Minoshima, S., Evans, G.A., Athanasiou, M., Schultz, R., Roe, B.A., Chen, F., Pan, H., Ramsier, J., Lehrach, H., Reinhardt, R., McCombie, W.R., de la Bastide, M., Dedhia, N., Blöcker, H., Hornischer, K., Nordsiek, G., Agarwala, R., Aravind, L., Bailey, J.A., Bateman, A., Batzoglou, S., Birney, E., Bork, P., Brown, D.G., Burge, C.B., Cerutti, L., Chen, H.C., Church, D., Clamp, M., Copley, R.R., Doerks, T., Eddy, S.R., Eichler, E.E., Furey, T.S., Galagan, J., Gilbert, J.G., Harmon, C., Hayashizaki, Y., Haussler, D., Hermjakob, H., Hokamp, K., Jang, W., Johnson, L.S., Jones, T.A., Kasif, S., Kasprzyk, A., Kennedy, S., Kent, W.J., Kitts, P., Koonin, E.V., Korf, I., Kulp, D., Lancet, D., Lowe, T.M., McLysaght, A., Mikkelsen, T., Moran, J.V., Mulder, N., Pollara, V.J., Ponting, C.P., Schuler, G., Schultz, J., Slater, G., Smit, A.F., Stupka, E., Szustakowki, J., Thierry-Mieg, D., Thierry-Mieg, J., Wagner, L., Wallis, J., Wheeler, R., Williams, A., Wolf, Y.I., Wolfe, K.H., Yang, S.P., Yeh, R.F., Collins, F., Guyer, M.S., Peterson, J., Felsenfeld, A., Wetterstrand, K.A., Patrinos, A., Morgan, M.J., de Jong, P., Catanese, J.J., Osoegawa, K., Shizuya, H., Choi, S., Chen, Y.J., Szustakowki, J., International Human Genome Sequencing Consortium, 2001. Initial sequencing and analysis of the human genome. *Nature* 409, 860–921. <https://doi.org/10.1038/35057062>
- Lanfossi, M., Cozzi, F., Bugini, D., Colombo, S., Scarpa, P., Morandi, L., Galbiati, S., Cornelio, F., Pozza, O., Mora, M., 1999. Development of muscle pathology in canine X-linked muscular dystrophy. I. Delayed postnatal maturation of affected and normal muscle as revealed by myosin isoform analysis and utrophin expression. *Acta Neuropathol* 97, 127–138. <https://doi.org/10.1007/s004010050965>

- Le Guiner, C., Montus, M., Servais, L., Cherel, Y., Francois, V., Thibaud, J.-L., Wary, C., Matot, B., Larcher, T., Guigand, L., Dutilleul, M., Domenger, C., Allais, M., Beuvin, M., Moraux, A., Le Duff, J., Devaux, M., Jaulin, N., Guilbaud, M., Latournerie, V., Veron, P., Boutin, S., Leborgne, C., Desgue, D., Deschamps, J.-Y., Moullec, S., Fromes, Y., Vulin, A., Smith, R.H., Laroudie, N., Barnay-Toutain, F., Rivière, C., Bucher, S., Le, T.-H., Delaunay, N., Gasmi, M., Kotin, R.M., Bonne, G., Adjali, O., Masurier, C., Hogrel, J.-Y., Carlier, P., Moullier, P., Voit, T., 2014. Forelimb treatment in a large cohort of dystrophic dogs supports delivery of a recombinant AAV for exon skipping in Duchenne patients. *Mol. Ther.* 22, 1923–1935. <https://doi.org/10.1038/mt.2014.151>
- Le Hir, M., Goyenvalle, A., Peccate, C., Précigout, G., Davies, K.E., Voit, T., Garcia, L., Lorain, S., 2013. AAV genome loss from dystrophic mouse muscles during AAV-U7 snRNA-mediated exon-skipping therapy. *Mol Ther* 21, 1551–1558. <https://doi.org/10.1038/mt.2013.121>
- Lederfein, D., Levy, Z., Augier, N., Mornet, D., Morris, G., Fuchs, O., Yaffe, D., Nudel, U., 1992. A 71-kilodalton protein is a major product of the Duchenne muscular dystrophy gene in brain and other nonmuscle tissues. *Proc. Natl. Acad. Sci. U.S.A.* 89, 5346–5350. <https://doi.org/10.1073/pnas.89.12.5346>
- Lee, M., Kim, H., 2019. Therapeutic application of the CRISPR system: current issues and new prospects. *Hum Genet* 138, 563–590. <https://doi.org/10.1007/s00439-019-02028-2>
- Lee, Y., Rio, D.C., 2015. Mechanisms and Regulation of Alternative Pre-mRNA Splicing. *Annu Rev Biochem* 84, 291–323. <https://doi.org/10.1146/annurev-biochem-060614-034316>
- Lei, B., Zhang, K., Yue, Y., Ghosh, A., Duan, D., 2009. Adeno-associated virus serotype-9 efficiently transduces the retinal outer plexiform layer. *Mol Vis* 15, 1374–1382.
- Lenk, U., Hanke, R., Thiele, H., Speer, A., 1993. Point mutations at the carboxy terminus of the human DMD gene: implications for an association with mental retardation in DMD patients. *Hum Mol Genet* 2, 1877–1881. <https://doi.org/10.1093/hmg/2.11.1877>
- Li, D., Long, C., Yue, Y., Duan, D., 2009. Sub-physiological sarcoglycan expression contributes to compensatory muscle protection in mdx mice. *Hum Mol Genet* 18, 1209–1220. <https://doi.org/10.1093/hmg/ddp015>
- Li, D., Yue, Y., Duan, D., 2008. Preservation of muscle force in Mdx3cv mice correlates with low-level expression of a near full-length dystrophin protein. *Am J Pathol* 172, 1332–1341. <https://doi.org/10.2353/ajpath.2008.071042>
- Lidov, H.G., Byers, T.J., Kunkel, L.M., 1993. The distribution of dystrophin in the murine central nervous system: an immunocytochemical study. *Neuroscience* 54, 167–187. [https://doi.org/10.1016/0306-4522\(93\)90392-s](https://doi.org/10.1016/0306-4522(93)90392-s)
- Lidov, H.G., Byers, T.J., Watkins, S.C., Kunkel, L.M., 1990. Localization of dystrophin to postsynaptic regions of central nervous system cortical neurons. *Nature* 348, 725–728. <https://doi.org/10.1038/348725a0>
- Lidov, H.G., Kunkel, L.M., 1997. Dp140: alternatively spliced isoforms in brain and kidney. *Genomics* 45, 132–139. <https://doi.org/10.1006/geno.1997.4905>
- Lidov, H.G., Selig, S., Kunkel, L.M., 1995a. Dp140: a novel 140 kDa CNS transcript from the dystrophin locus. *Hum Mol Genet* 4, 329–335. <https://doi.org/10.1093/hmg/4.3.329>
- Lidov, H.G., Selig, S., Kunkel, L.M., 1995b. Dp140: a novel 140 kDa CNS transcript from the dystrophin locus. *Hum. Mol. Genet.* 4, 329–335. <https://doi.org/10.1093/hmg/4.3.329>
- Lindsay, A., Trewin, A.J., Sadler, K.J., Laird, C., Della Gatta, P.A., Russell, A.P., 2021. Sensitivity to behavioral stress impacts disease pathogenesis in dystrophin-deficient mice. *FASEB J* 35, e22034. <https://doi.org/10.1096/fj.202101163RR>
- Liu, X.S., Wu, H., Krzisch, M., Wu, X., Graef, J., Muffat, J., Hnisz, D., Li, C.H., Yuan, B., Xu, C., Li, Y., Vershkov, D., Cacace, A., Young, R.A., Jaenisch, R., 2018. Rescue of Fragile X Syndrome Neurons

- by DNA Methylation Editing of the FMR1 Gene. *Cell* 172, 979–992.e6. <https://doi.org/10.1016/j.cell.2018.01.012>
- Lorain, S., Gross, D.-A., Goyenvallé, A., Danos, O., Davoust, J., Garcia, L., 2008. Transient immunomodulation allows repeated injections of AAV1 and correction of muscular dystrophy in multiple muscles. *Mol Ther* 16, 541–547. <https://doi.org/10.1038/sj.mt.6300377>
- Lu, Q.L., 2021. Revertant Phenomenon in DMD and LGMD2I and Its Therapeutic Implications: A Review of Study Under Mentorship of Terrence Partridge. *J Neuromuscul Dis* 8, S359–S367. <https://doi.org/10.3233/JND-210692>
- Lu, Q.L., Mann, C.J., Lou, F., Bou-Gharios, G., Morris, G.E., Xue, S., Fletcher, S., Partridge, T.A., Wilton, S.D., 2003. Functional amounts of dystrophin produced by skipping the mutated exon in the mdx dystrophic mouse. *Nat Med* 9, 1009–1014. <https://doi.org/10.1038/nm897>
- Lu, Q.L., Morris, G.E., Wilton, S.D., Ly, T., Artem'yeva, O.V., Strong, P., Partridge, T.A., 2000. Massive idiosyncratic exon skipping corrects the nonsense mutation in dystrophic mouse muscle and produces functional revertant fibers by clonal expansion. *J Cell Biol* 148, 985–996. <https://doi.org/10.1083/jcb.148.5.985>
- Lu, Q.L., Rabinowitz, A., Chen, Y.C., Yokota, T., Yin, H., Alter, J., Jadoon, A., Bou-Gharios, G., Partridge, T., 2005. Systemic delivery of antisense oligoribonucleotide restores dystrophin expression in body-wide skeletal muscles. *Proc Natl Acad Sci U S A* 102, 198–203. <https://doi.org/10.1073/pnas.0406700102>
- Lue, Y.-J., Chen, S.-S., Lu, Y.-M., 2017. Quality of life of patients with Duchenne muscular dystrophy: from adolescence to young men. *Disabil Rehabil* 39, 1408–1413. <https://doi.org/10.1080/09638288.2016.1196398>
- Lynch, G.S., Hinkle, R.T., Chamberlain, J.S., Brooks, S.V., Faulkner, J.A., 2001. Force and power output of fast and slow skeletal muscles from mdx mice 6–28 months old. *J Physiol* 535, 591–600. <https://doi.org/10.1111/j.1469-7793.2001.00591.x>
- Ma, Q., Ries, M., Decker, Y., Müller, A., Riner, C., Bückner, A., Fassbender, K., Detmar, M., Proulx, S.T., 2019. Rapid lymphatic efflux limits cerebrospinal fluid flow to the brain. *Acta Neuropathol* 137, 151–165. <https://doi.org/10.1007/s00401-018-1916-x>
- Mah, J.K., Korngut, L., Dykeman, J., Day, L., Pringsheim, T., Jette, N., 2014. A systematic review and meta-analysis on the epidemiology of Duchenne and Becker muscular dystrophy. *Neuromuscul Disord* 24, 482–491. <https://doi.org/10.1016/j.nmd.2014.03.008>
- Manning, J., Kulbida, R., Rai, P., Jensen, L., Bouma, J., Singh, S.P., O'Malley, D., Yilmazer-Hanke, D., 2014. Amitriptyline is efficacious in ameliorating muscle inflammation and depressive symptoms in the mdx mouse model of Duchenne muscular dystrophy. *Exp Physiol* 99, 1370–1386. <https://doi.org/10.1113/expphysiol.2014.079475>
- Maresh, K., Papageorgiou, A., Ridout, D., Harrison, N.A., Mandy, W., Skuse, D., Muntoni, F., 2023. Startle responses in Duchenne muscular dystrophy: a novel biomarker of brain dystrophin deficiency. *Brain* 146, 252–265. <https://doi.org/10.1093/brain/awac048>
- Masaki, T., Matsumura, K., Hirata, A., Yamada, H., Hase, A., Shimizu, T., Yorifuji, H., Motoyoshi, K., Kamakura, K., 2001. Expression of dystroglycan complex in satellite cells of dorsal root ganglia. *Acta Neuropathol* 101, 174–178. <https://doi.org/10.1007/s004010000276>
- Matsumura, K., Campbell, K.P., 1994. Dystrophin-glycoprotein complex: its role in the molecular pathogenesis of muscular dystrophies. *Muscle Nerve* 17, 2–15. <https://doi.org/10.1002/mus.880170103>
- Matsumura, K., Nonaka, I., Tomé, F.M., Arahata, K., Collin, H., Leturcq, F., Récan, D., Kaplan, J.C., Fardeau, M., Campbell, K.P., 1993. Mild deficiency of dystrophin-associated proteins in Becker muscular

- dystrophy patients having in-frame deletions in the rod domain of dystrophin. *Am J Hum Genet* 53, 409–416.
- McCarroll, S.A., Altshuler, D.M., 2007. Copy-number variation and association studies of human disease. *Nat Genet* 39, S37–S42. <https://doi.org/10.1038/ng2080>
- McGreevy, J.W., Hakim, C.H., McIntosh, M.A., Duan, D., 2015. Animal models of Duchenne muscular dystrophy: from basic mechanisms to gene therapy. *Dis Model Mech* 8, 195–213. <https://doi.org/10.1242/dmm.018424>
- McLin, J.P., Steward, O., 2006. Comparison of seizure phenotype and neurodegeneration induced by systemic kainic acid in inbred, outbred, and hybrid mouse strains. *Eur J Neurosci* 24, 2191–2202. <https://doi.org/10.1111/j.1460-9568.2006.05111.x>
- Mendell, J.R., Goemans, N., Lowes, L.P., Alfano, L.N., Berry, K., Shao, J., Kaye, E.M., Mercuri, E., Eteplirsen Study Group and Telethon Foundation DMD Italian Network, 2016. Longitudinal effect of eteplirsen versus historical control on ambulation in Duchenne muscular dystrophy. *Ann. Neurol.* 79, 257–271. <https://doi.org/10.1002/ana.24555>
- Mendell, J.R., Kissel, J.T., Amato, A.A., King, W., Signore, L., Prior, T.W., Sahenk, Z., Benson, S., McAndrew, P.E., Rice, R., 1995. Myoblast transfer in the treatment of Duchenne’s muscular dystrophy. *N Engl J Med* 333, 832–838. <https://doi.org/10.1056/NEJM199509283331303>
- Mendell, J.R., Rodino-Klapac, L.R., Sahenk, Z., Roush, K., Bird, L., Lowes, L.P., Alfano, L., Gomez, A.M., Lewis, S., Kota, J., Malik, V., Shontz, K., Walker, C.M., Flanigan, K.M., Corridore, M., Kean, J.R., Allen, H.D., Shilling, C., Melia, K.R., Sazani, P., Saoud, J.B., Kaye, E.M., Eteplirsen Study Group, 2013. Eteplirsen for the treatment of Duchenne muscular dystrophy. *Ann Neurol* 74, 637–647. <https://doi.org/10.1002/ana.23982>
- Mendell, J.R., Sahenk, Z., Lehman, K., Nease, C., Lowes, L.P., Miller, N.F., Iammarino, M.A., Alfano, L.N., Nicholl, A., Al-Zaidy, S., Lewis, S., Church, K., Shell, R., Cripe, L.H., Potter, R.A., Griffin, D.A., Pozsgai, E., Dugar, A., Hogan, M., Rodino-Klapac, L.R., 2020. Assessment of Systemic Delivery of rAAVrh74.MHCK7.micro-dystrophin in Children With Duchenne Muscular Dystrophy: A Nonrandomized Controlled Trial. *JAMA Neurol* 77, 1122–1131. <https://doi.org/10.1001/jamaneurol.2020.1484>
- Mento, G., Tarantino, V., Bisiacchi, P.S., 2011. The neuropsychological profile of infantile Duchenne muscular dystrophy. *Clin Neuropsychol* 25, 1359–1377. <https://doi.org/10.1080/13854046.2011.617782>
- Mercuri, E., Bönnemann, C.G., Muntoni, F., 2019. Muscular dystrophies. *Lancet* 394, 2025–2038. [https://doi.org/10.1016/S0140-6736\(19\)32910-1](https://doi.org/10.1016/S0140-6736(19)32910-1)
- Millay, D.P., Sargent, M.A., Osinska, H., Baines, C.P., Barton, E.R., Vuagniaux, G., Sweeney, H.L., Robbins, J., Molckentin, J.D., 2008. Genetic and pharmacologic inhibition of mitochondrial-dependent necrosis attenuates muscular dystrophy. *Nat Med* 14, 442–447. <https://doi.org/10.1038/nm1736>
- Miller, G., Tunnecliffe, M., Douglas, P.S., 1985. IQ, prognosis and Duchenne muscular dystrophy. *Brain Dev* 7, 7–9. [https://doi.org/10.1016/s0387-7604\(85\)80053-x](https://doi.org/10.1016/s0387-7604(85)80053-x)
- Miranda, R., Laroche, S., Vaillend, C., 2016. Reduced neuronal density in the CA1 anterodorsal hippocampus of the mdx mouse. *Neuromuscul Disord* 26, 775–781. <https://doi.org/10.1016/j.nmd.2016.08.006>
- Miranda, R., Nagapin, F., Bozon, B., Laroche, S., Aubin, T., Vaillend, C., 2015. Altered social behavior and ultrasonic communication in the dystrophin-deficient mdx mouse model of Duchenne muscular dystrophy. *Mol Autism* 6, 60. <https://doi.org/10.1186/s13229-015-0053-9>
- Miranda, R., Nudel, U., Laroche, S., Vaillend, C., 2011. Altered presynaptic ultrastructure in excitatory hippocampal synapses of mice lacking dystrophins Dp427 or Dp71. *Neurobiol Dis* 43, 134–141. <https://doi.org/10.1016/j.nbd.2011.02.017>

- Miranda, R., Sébrié, C., Degrouard, J., Gillet, B., Jaillard, D., Laroche, S., Vaillend, C., 2009. Reorganization of inhibitory synapses and increased PSD length of perforated excitatory synapses in hippocampal area CA1 of dystrophin-deficient mdx mice. *Cereb Cortex* 19, 876–888. <https://doi.org/10.1093/cercor/bhn135>
- Miyatake, S., Mizobe, Y., Takizawa, H., Hara, Y., Yokota, T., Takeda, S., Aoki, Y., 2018. Exon Skipping Therapy Using Phosphorodiamidate Morpholino Oligomers in the mdx52 Mouse Model of Duchenne Muscular Dystrophy. *Methods Mol Biol* 1687, 123–141. https://doi.org/10.1007/978-1-4939-7374-3_9
- Moizard, M.P., Toutain, A., Fournier, D., Berret, F., Raynaud, M., Billard, C., Andres, C., Moraine, C., 2000. Severe cognitive impairment in DMD: obvious clinical indication for Dp71 isoform point mutation screening. *Eur J Hum Genet* 8, 552–556. <https://doi.org/10.1038/sj.ejhg.5200488>
- Molecule of the month. Ataluren, 2010. *Drug News Perspect* 23, 135.
- Monaco, A.P., Bertelson, C.J., Liechti-Gallati, S., Moser, H., Kunkel, L.M., 1988. An explanation for the phenotypic differences between patients bearing partial deletions of the DMD locus. *Genomics* 2, 90–95. [https://doi.org/10.1016/0888-7543\(88\)90113-9](https://doi.org/10.1016/0888-7543(88)90113-9)
- Monaco, A.P., Bertelson, C.J., Middlesworth, W., Colletti, C.A., Aldridge, J., Fischbeck, K.H., Bartlett, R., Pericak-Vance, M.A., Roses, A.D., Kunkel, L.M., 1985. Detection of deletions spanning the Duchenne muscular dystrophy locus using a tightly linked DNA segment. *Nature* 316, 842–845. <https://doi.org/10.1038/316842a0>
- Montarras, D., Morgan, J., Collins, C., Relaix, F., Zaffran, S., Cumano, A., Partridge, T., Buckingham, M., 2005. Direct isolation of satellite cells for skeletal muscle regeneration. *Science* 309, 2064–2067. <https://doi.org/10.1126/science.1114758>
- Morris, G.E., Simmons, C., Nguyen, T.M., 1995. Apo-dystrophins (Dp140 and Dp71) and dystrophin splicing isoforms in developing brain. *Biochem Biophys Res Commun* 215, 361–367. <https://doi.org/10.1006/bbrc.1995.2474>
- Morrison-Nozik, A., Anand, P., Zhu, H., Duan, Q., Sabeh, M., Prosdocimo, D.A., Lemieux, M.E., Nordsborg, N., Russell, A.P., MacRae, C.A., Gerber, A.N., Jain, M.K., Haldar, S.M., 2015. Glucocorticoids enhance muscle endurance and ameliorate Duchenne muscular dystrophy through a defined metabolic program. *Proc Natl Acad Sci U S A* 112, E6780-6789. <https://doi.org/10.1073/pnas.1512968112>
- Mortazavi, M., Ren, Y., Saini, S., Antaki, D., Pierre, C.St., Williams, A., Sohni, A., Wilkinson, M., Gymrek, M., Sebat, J., Palmer, A.A., 2021. Polymorphic SNPs, short tandem repeats and structural variants are responsible for differential gene expression across C57BL/6 and C57BL/10 substrains. *bioRxiv* 2020.03.16.993683. <https://doi.org/10.1101/2020.03.16.993683>
- Moulton, H.M., Moulton, J.D., 2010. Morpholinos and their peptide conjugates: therapeutic promise and challenge for Duchenne muscular dystrophy. *Biochim Biophys Acta* 1798, 2296–2303. <https://doi.org/10.1016/j.bbame.2010.02.012>
- Muntoni, F., Fisher, I., Morgan, J.E., Abraham, D., 2002. Steroids in Duchenne muscular dystrophy: from clinical trials to genomic research. *Neuromuscul Disord* 12 Suppl 1, S162-165. [https://doi.org/10.1016/s0960-8966\(02\)00101-3](https://doi.org/10.1016/s0960-8966(02)00101-3)
- Muntoni, F., Mateddu, A., Serra, G., 1991. Passive avoidance behaviour deficit in the mdx mouse. *Neuromuscul Disord* 1, 121–123. [https://doi.org/10.1016/0960-8966\(91\)90059-2](https://doi.org/10.1016/0960-8966(91)90059-2)
- Muntoni, F., Torelli, S., Ferlini, A., 2003. Dystrophin and mutations: one gene, several proteins, multiple phenotypes. *The Lancet Neurology* 2, 731–740. [https://doi.org/10.1016/S1474-4422\(03\)00585-4](https://doi.org/10.1016/S1474-4422(03)00585-4)
- Naidoo, M., Anthony, K., 2020. Dystrophin Dp71 and the Neuropathophysiology of Duchenne Muscular Dystrophy. *Mol Neurobiol* 57, 1748–1767. <https://doi.org/10.1007/s12035-019-01845-w>
- Nance, M.E., Shi, R., Hakim, C.H., Wasala, N.B., Yue, Y., Pan, X., Zhang, T., Robinson, C.A., Duan, S.X., Yao, G., Yang, N.N., Chen, S.-J., Wagner, K.R., Gersbach, C.A., Duan, D., 2019. AAV9 Edits Muscle

- Stem Cells in Normal and Dystrophic Adult Mice. *Mol Ther* 27, 1568–1585. <https://doi.org/10.1016/j.ymthe.2019.06.012>
- Neely, J.D., Amiry-Moghaddam, M., Ottersen, O.P., Froehner, S.C., Agre, P., Adams, M.E., 2001. Syntrophin-dependent expression and localization of Aquaporin-4 water channel protein. *Proc Natl Acad Sci U S A* 98, 14108–14113. <https://doi.org/10.1073/pnas.241508198>
- Nelson, C.E., Robinson-Hamm, J.N., Gersbach, C.A., 2017. Genome engineering: a new approach to gene therapy for neuromuscular disorders. *Nat Rev Neurol* 13, 647–661. <https://doi.org/10.1038/nrneurol.2017.126>
- Nguyen, F., Cherel, Y., Guigand, L., Goubault-Leroux, I., Wyers, M., 2002. Muscle lesions associated with dystrophin deficiency in neonatal golden retriever puppies. *J Comp Pathol* 126, 100–108. <https://doi.org/10.1053/jcpa.2001.0526>
- Nicholson, L.V., Johnson, M.A., Bushby, K.M., Gardner-Medwin, D., 1993. Functional significance of dystrophin positive fibres in Duchenne muscular dystrophy. *Arch Dis Child* 68, 632–636. <https://doi.org/10.1136/adc.68.5.632>
- Nico, B., Frigeri, A., Nicchia, G.P., Corsi, P., Ribatti, D., Quondamatteo, F., Herken, R., Girolamo, F., Marzullo, A., Svelto, M., Roncali, L., 2003. Severe alterations of endothelial and glial cells in the blood-brain barrier of dystrophic mdx mice. *Glia* 42, 235–251. <https://doi.org/10.1002/glia.10216>
- Nico, B., Paola Nicchia, G., Frigeri, A., Corsi, P., Mangieri, D., Ribatti, D., Svelto, M., Roncali, L., 2004. Altered blood-brain barrier development in dystrophic MDX mice. *Neuroscience* 125, 921–935. <https://doi.org/10.1016/j.neuroscience.2004.02.008>
- Nobile, C., Galvagni, F., Marchi, J., Roberts, R., Vitiello, L., 1995. Genomic organization of the human DMD gene across the major deletion hot spot and the 3' region. *Genomics* 28, 97–100. <https://doi.org/10.1006/geno.1995.1111>
- Nudel, U., Zuk, D., Einat, P., Zeelon, E., Levy, Z., Neuman, S., Yaffe, D., 1989. Duchenne muscular dystrophy gene product is not identical in muscle and brain. *Nature* 337, 76–78. <https://doi.org/10.1038/337076a0>
- Omori, Y., Araki, F., Chaya, T., Kajimura, N., Irie, S., Terada, K., Muranishi, Y., Tsujii, T., Ueno, S., Koyasu, T., Tamaki, Y., Kondo, M., Amano, S., Furukawa, T., 2012. Presynaptic Dystroglycan–Pikachurin Complex Regulates the Proper Synaptic Connection between Retinal Photoreceptor and Bipolar Cells. *J. Neurosci.* 32, 6126–6137. <https://doi.org/10.1523/JNEUROSCI.0322-12.2012>
- Orlandi, C., Omori, Y., Wang, Y., Cao, Y., Ueno, A., Roux, M.J., Condomitti, G., Wit, J. de, Kanagawa, M., Furukawa, T., Martemyanov, K.A., 2018. Transsynaptic Binding of Orphan Receptor GPR179 to Dystroglycan-Pikachurin Complex Is Essential for the Synaptic Organization of Photoreceptors. *Cell Reports* 25, 130-145.e5. <https://doi.org/10.1016/j.celrep.2018.08.068>
- Otsuka, S., Konno, K., Abe, M., Motohashi, J., Kohda, K., Sakimura, K., Watanabe, M., Yuzaki, M., 2016. Roles of Cbln1 in Non-Motor Functions of Mice. *J Neurosci* 36, 11801–11816. <https://doi.org/10.1523/JNEUROSCI.0322-16.2016>
- Oudet, C., Hanauer, A., Clemens, P., Caskey, T., Mandel, J.L., 1992. Two hot spots of recombination in the DMD gene correlate with the deletion prone regions. *Hum Mol Genet* 1, 599–603. <https://doi.org/10.1093/hmg/1.8.599>
- Pane, M., Scalise, R., Berardinelli, A., D'Angelo, G., Ricotti, V., Alfieri, P., Moroni, I., Hartley, L., Pera, M.C., Baranello, G., Catteruccia, M., Casalino, T., Romeo, D.M., Graziano, A., Gandioli, C., Bianco, F., Mazzone, E.S., Lombardo, M.E., Scoto, M., Sivo, S., Palermo, C., Gualandi, F., Sormani, M.P., Ferlini, A., Bertini, E., Muntoni, F., Mercuri, E., 2013. Early neurodevelopmental assessment in Duchenne muscular dystrophy. *Neuromuscul Disord* 23, 451–455. <https://doi.org/10.1016/j.nmd.2013.02.012>

- Parames, S.F., Coletta-Yudice, E.D., Nogueira, F.M., Nering de Sousa, M.B., Hayashi, M.A., Lima-Landman, M.T.R., Lapa, A.J., Souccar, C., 2014. Altered acetylcholine release in the hippocampus of dystrophin-deficient mice. *Neuroscience* 269, 173–183. <https://doi.org/10.1016/j.neuroscience.2014.03.050>
- Park, S.H., Jo, Y.J., Lee, J.J., Park, S.W., Lee, J.E., 2019. Proliferative Retinopathy Developed in a Duchenne Muscular Dystrophy Patient with Normal Cardiac Function. *J Retin* 4, 36–39. <https://doi.org/10.21561/jor.2019.4.1.36>
- Partridge, T.A., Morgan, J.E., Coulton, G.R., Hoffman, E.P., Kunkel, L.M., 1989. Conversion of mdx myofibres from dystrophin-negative to -positive by injection of normal myoblasts. *Nature* 337, 176–179. <https://doi.org/10.1038/337176a0>
- Pascual Pascual, S.I., Molano, J., Pascual-Castroviejo, I., 1998. Electroretinogram in Duchenne/Becker muscular dystrophy. *Pediatr Neurol* 18, 315–320. [https://doi.org/10.1016/s0887-8994\(97\)00208-7](https://doi.org/10.1016/s0887-8994(97)00208-7)
- Pastoret, C., Seville, A., 1995. mdx mice show progressive weakness and muscle deterioration with age. *J Neurol Sci* 129, 97–105. [https://doi.org/10.1016/0022-510x\(94\)00276-t](https://doi.org/10.1016/0022-510x(94)00276-t)
- Péault, B., Rudnicki, M., Torrente, Y., Cossu, G., Tremblay, J.P., Partridge, T., Gussoni, E., Kunkel, L.M., Huard, J., 2007. Stem and progenitor cells in skeletal muscle development, maintenance, and therapy. *Mol Ther* 15, 867–877. <https://doi.org/10.1038/mt.sj.6300145>
- Pereira da Silva, J.D., Campos, D.V., Nogueira-Bechara, F.M., Stilhano, R.S., Han, S.W., Sinigaglia-Coimbra, R., Lima-Landman, M.T.R., Lapa, A.J., Souccar, C., 2018. Altered release and uptake of gamma-aminobutyric acid in the cerebellum of dystrophin-deficient mice. *Neurochem Int* 118, 105–114. <https://doi.org/10.1016/j.neuint.2018.06.001>
- Perronnet, C., Chagneau, C., Le Blanc, P., Samson-Desvignes, N., Mornet, D., Laroche, S., De La Porte, S., Vaillend, C., 2012. Upregulation of brain utrophin does not rescue behavioral alterations in dystrophin-deficient mice. *Hum Mol Genet* 21, 2263–2276. <https://doi.org/10.1093/hmg/dds047>
- Petrof, B.J., 2002. Molecular pathophysiology of myofiber injury in deficiencies of the dystrophin-glycoprotein complex. *Am J Phys Med Rehabil* 81, S162-174. <https://doi.org/10.1097/01.PHM.0000029775.54830.80>
- Pillers, D.A., Bulman, D.E., Weleber, R.G., Sigesmund, D.A., Musarella, M.A., Powell, B.R., Murphey, W.H., Westall, C., Panton, C., Becker, L.E., 1993. Dystrophin expression in the human retina is required for normal function as defined by electroretinography. *Nat Genet* 4, 82–86. <https://doi.org/10.1038/ng0593-82>
- Politano, L., 2021. Read-through approach for stop mutations in Duchenne muscular dystrophy. An update. *Acta Myol* 40, 43–50. <https://doi.org/10.36185/2532-1900-041>
- Poysky, J., 2007. Behavior patterns in Duchenne muscular dystrophy: Report on the Parent Project Muscular Dystrophy behavior workshop 8–9 of December 2006, Philadelphia, USA. *Neuromuscular Disorders* 17, 986–994. <https://doi.org/10.1016/j.nmd.2007.06.465>
- Preethish-Kumar, V., Shah, A., Polavarapu, K., Kumar, M., Safai, A., Vengalil, S., Nashi, S., Deepha, S., Govindaraj, P., Afsar, M., Rajeswaran, J., Nalini, A., Saini, J., Ingalhalikar, M., 2022. Disrupted structural connectome and neurocognitive functions in Duchenne muscular dystrophy: classifying and subtyping based on Dp140 dystrophin isoform. *J Neurol* 269, 2113–2125. <https://doi.org/10.1007/s00415-021-10789-y>
- Pribrag, H., Peng, H., Shah, W.A., Stellwagen, D., Carbonetto, S., 2014. Dystroglycan mediates homeostatic synaptic plasticity at GABAergic synapses. *Proc Natl Acad Sci U S A* 111, 6810–6815. <https://doi.org/10.1073/pnas.1321774111>
- Prosser, E.J., Murphy, E.G., Thompson, M.W., 1969. Intelligence and the gene for Duchenne muscular dystrophy. *Arch Dis Child* 44, 221–230.

- Rafael, J.A., Nitta, Y., Peters, J., Davies, K.E., 2000. Testing of SHIRPA, a mouse phenotypic assessment protocol, on Dmd(mdx) and Dmd(mdx3cv) dystrophin-deficient mice. *Mamm Genome* 11, 725–728. <https://doi.org/10.1007/s003350010149>
- Ramos, J., Chamberlain, J.S., 2015. Gene Therapy for Duchenne muscular dystrophy. *Expert Opin Orphan Drugs* 3, 1255–1266. <https://doi.org/10.1517/21678707.2015.1088780>
- Rando, T.A., 2001. The dystrophin-glycoprotein complex, cellular signaling, and the regulation of cell survival in the muscular dystrophies. *Muscle Nerve* 24, 1575–1594.
- Rapaport, D., Passos-Bueno, M.R., Brandão, L., Love, D., Vainzof, M., Zatz, M., 1991. Apparent association of mental retardation and specific patterns of deletions screened with probes cf56a and cf23a in Duchenne muscular dystrophy. *American Journal of Medical Genetics* 39, 437–441. <https://doi.org/10.1002/ajmg.1320390414>
- Rasic, M.V., Vojinovic, D., Pesovic, J., Mijalkovic, G., Lukic, V., Mladenovic, J., Kosac, A., Novakovic, I., Maksimovic, N., Romac, S., Todorovic, S., Pavicevic, S.D., 2014. Intellectual Ability in the Duchenne Muscular Dystrophy and DMD gene Mutation Location. *Balkan Journal of Medical Genetics* 17, 25–35. <https://doi.org/10.2478/bjmg-2014-0071>
- Razzoli, M., Lindsay, A., Law, M.L., Chamberlain, C.M., Southern, W.M., Berg, M., Osborn, J., Engeland, W.C., Metzger, J.M., Ervasti, J.M., Bartolomucci, A., 2020. Social stress is lethal in the mdx model of Duchenne muscular dystrophy. *EBioMedicine* 55, 102700. <https://doi.org/10.1016/j.ebiom.2020.102700>
- Relizani, K., Echevarría, L., Zarrouki, F., Gastaldi, C., Dambrune, C., Aupy, P., Haerberli, A., Komisariski, M., Tensorer, T., Larcher, T., Svinartchouk, F., Vaillend, C., Garcia, L., Goyenville, A., 2022. Palmitic acid conjugation enhances potency of tricyclo-DNA splice switching oligonucleotides. *Nucleic Acids Res* 50, 17–34. <https://doi.org/10.1093/nar/gkab1199>
- Relizani, K., Griffith, G., Echevarría, L., Zarrouki, F., Facchinetti, P., Vaillend, C., Leumann, C., Garcia, L., Goyenville, A., 2017. Efficacy and Safety Profile of Tricyclo-DNA Antisense Oligonucleotides in Duchenne Muscular Dystrophy Mouse Model. *Mol Ther Nucleic Acids* 8, 144–157. <https://doi.org/10.1016/j.omtn.2017.06.013>
- Renneberg, D., Leumann, C.J., 2002. Watson-Crick base-pairing properties of tricyclo-DNA. *J Am Chem Soc* 124, 5993–6002. <https://doi.org/10.1021/ja025569+>
- Rice, M.L., Wong, B., Horn, P.S., Yang, M.B., 2018. Cataract development associated with long-term glucocorticoid therapy in Duchenne muscular dystrophy patients. *Journal of American Association for Pediatric Ophthalmology and Strabismus* 22, 192–196. <https://doi.org/10.1016/j.jaapos.2018.01.017>
- Ricotti, V., Jäggle, H., Theodorou, M., Moore, A.T., Muntoni, F., Thompson, D.A., 2016a. Ocular and neurodevelopmental features of Duchenne muscular dystrophy: a signature of dystrophin function in the central nervous system. *Eur J Hum Genet* 24, 562–568. <https://doi.org/10.1038/ejhg.2015.135>
- Ricotti, V., Mandy, W.P.L., Scoto, M., Pane, M., Deconinck, N., Messina, S., Mercuri, E., Skuse, D.H., Muntoni, F., 2016b. Neurodevelopmental, emotional, and behavioural problems in Duchenne muscular dystrophy in relation to underlying DMD gene mutations. *Dev Med Child Neurol* 58, 77–84. <https://doi.org/10.1111/dmcn.12922>
- Ricotti, V., Spinty, S., Roper, H., Hughes, I., Tejura, B., Robinson, N., Layton, G., Davies, K., Muntoni, F., Tinsley, J., 2016c. Safety, Tolerability, and Pharmacokinetics of SMT C1100, a 2-Arylbenzoxazole Utrrophin Modulator, following Single- and Multiple-Dose Administration to Pediatric Patients with Duchenne Muscular Dystrophy. *PLoS One* 11, e0152840. <https://doi.org/10.1371/journal.pone.0152840>
- Rigo, F., Chun, S.J., Norris, D.A., Hung, G., Lee, S., Matson, J., Fey, R.A., Gaus, H., Hua, Y., Grundy, J.S., Krainer, A.R., Henry, S.P., Bennett, C.F., 2014. Pharmacology of a Central Nervous System Delivered

- 2'-O-Methoxyethyl-Modified Survival of Motor Neuron Splicing Oligonucleotide in Mice and Nonhuman Primates. *J Pharmacol Exp Ther* 350, 46–55. <https://doi.org/10.1124/jpet.113.212407>
- Roberts, R.G., Bobrow, M., Bentley, D.R., 1992. Point mutations in the DMD gene. *Proc Natl Acad Sci U S A* 89, 2331–2335. <https://doi.org/10.1073/pnas.89.6.2331>
- Roberts, R.G., Gardner, R.J., Bobrow, M., 1994. Searching for the 1 in 2,400,000: a review of DMD gene point mutations. *Hum Mutat* 4, 1–11. <https://doi.org/10.1002/humu.1380040102>
- Romo-Yáñez, J., Rodríguez-Martínez, G., Aragón, J., Siqueiros-Márquez, L., Herrera-Salazar, A., Velasco, I., Montanez, C., 2020. Characterization of the expression of dystrophins and dystrophin-associated proteins during embryonic neural stem/progenitor cell differentiation. *Neurosci Lett* 736, 135247. <https://doi.org/10.1016/j.neulet.2020.135247>
- Rubenstein, J.L.R., Merzenich, M.M., 2003. Model of autism: increased ratio of excitation/inhibition in key neural systems. *Genes Brain Behav* 2, 255–267. <https://doi.org/10.1034/j.1601-183x.2003.00037.x>
- Sacchetti, B., Baldi, E., Lorenzini, C.A., Bucherelli, C., 2002. Cerebellar role in fear-conditioning consolidation. *Proc Natl Acad Sci U S A* 99, 8406–8411. <https://doi.org/10.1073/pnas.112660399>
- Sacchetti, B., Sacco, T., Strata, P., 2007. Reversible inactivation of amygdala and cerebellum but not perirhinal cortex impairs reactivated fear memories. *Eur J Neurosci* 25, 2875–2884. <https://doi.org/10.1111/j.1460-9568.2007.05508.x>
- Saito, T., Kawai, M., Kimura, E., Ogata, K., Takahashi, T., Kobayashi, M., Takada, H., Kuru, S., Mikata, T., Matsumura, T., Yonemoto, N., Fujimura, H., Sakoda, S., 2017. Study of Duchenne muscular dystrophy long-term survivors aged 40 years and older living in specialized institutions in Japan. *Neuromuscul Disord* 27, 107–114. <https://doi.org/10.1016/j.nmd.2016.11.012>
- Saoudi, A., Zarrouki, F., Sebrié, C., Isabelle, C., Goyenvalle, A., Vaillend, C., 2021. Emotional behavior and brain anatomy of the mdx52 mouse model of Duchenne muscular dystrophy. *Dis Model Mech* 14, dmm049028. <https://doi.org/10.1242/dmm.049028>
- Sarig, R., Mezger-Lallemand, V., Gitelman, I., Davis, C., Fuchs, O., Yaffe, D., Nudel, U., 1999. Targeted inactivation of Dp71, the major non-muscle product of the DMD gene: differential activity of the Dp71 promoter during development. *Hum Mol Genet* 8, 1–10. <https://doi.org/10.1093/hmg/8.1.1>
- Schmidt, W.M., Uddin, M.H., Dysek, S., Moser-Thier, K., Pirker, C., Höger, H., Ambros, I.M., Ambros, P.F., Berger, W., Bittner, R.E., 2011. DNA damage, somatic aneuploidy, and malignant sarcoma susceptibility in muscular dystrophies. *PLoS Genet* 7, e1002042. <https://doi.org/10.1371/journal.pgen.1002042>
- Schultz, B.R., Chamberlain, J.S., 2008. Recombinant adeno-associated virus transduction and integration. *Mol Ther* 16, 1189–1199. <https://doi.org/10.1038/mt.2008.103>
- Sekiguchi, M., Zushida, K., Yoshida, M., Mikiharu, Maekawa, M., Kamichi, S., Yoshida, Mizuko, Sahara, Y., Yuasa, S., Takeda, S., Wada, K., 2009. A deficit of brain dystrophin impairs specific amygdala GABAergic transmission and enhances defensive behaviour in mice. *Brain* 132, 124–135. <https://doi.org/10.1093/brain/awn253>
- Sesay, A.K., Errington, M.L., Levita, L., Bliss, T.V., 1996. Spatial learning and hippocampal long-term potentiation are not impaired in mdx mice. *Neurosci Lett* 211, 207–210. [https://doi.org/10.1016/0304-3940\(96\)12747-6](https://doi.org/10.1016/0304-3940(96)12747-6)
- Seth, P.P., Siwkowski, A., Allerson, C.R., Vasquez, G., Lee, S., Prakash, T.P., Kinberger, G., Migawa, M.T., Gaus, H., Bhat, B., Swayze, E.E., 2008. Design, synthesis and evaluation of constrained methoxyethyl (cMOE) and constrained ethyl (cEt) nucleoside analogs. *Nucleic Acids Symp Ser (Oxf)* 553–554. <https://doi.org/10.1093/nass/nrn280>
- Seto, J.T., Ramos, J.N., Muir, L., Chamberlain, J.S., Odom, G.L., 2012. Gene replacement therapies for duchenne muscular dystrophy using adeno-associated viral vectors. *Curr Gene Ther* 12, 139–151. <https://doi.org/10.2174/156652312800840603>

- Sharp, N.J.H., Kornegay, J.N., Van Camp, S.D., Herbstreith, M.H., Secore, S.L., Kettle, S., Hung, W.-Y., Constantinou, C.D., Dykstra, M.J., Roses, A.D., Bartlett, R.J., 1992. An error in dystrophin mRNA processing in golden retriever muscular dystrophy, an animal homologue of Duchenne muscular dystrophy. *Genomics* 13, 115–121. [https://doi.org/10.1016/0888-7543\(92\)90210-J](https://doi.org/10.1016/0888-7543(92)90210-J)
- Shi, Y., 2017. Mechanistic insights into precursor messenger RNA splicing by the spliceosome. *Nat Rev Mol Cell Biol* 18, 655–670. <https://doi.org/10.1038/nrm.2017.86>
- Sicinski, P., Geng, Y., Ryder-Cook, A.S., Barnard, E.A., Darlison, M.G., Barnard, P.J., 1989. The molecular basis of muscular dystrophy in the mdx mouse: a point mutation. *Science* 244, 1578–1580. <https://doi.org/10.1126/science.2662404>
- Singewald, N., Schmuckermair, C., Whittle, N., Holmes, A., Ressler, K.J., 2015. Pharmacology of cognitive enhancers for exposure-based therapy of fear, anxiety and trauma-related disorders. *Pharmacol Ther* 149, 150–190. <https://doi.org/10.1016/j.pharmthera.2014.12.004>
- Skuk, D., Goulet, M., Roy, B., Chapdelaine, P., Bouchard, J.-P., Roy, R., Dugré, F.J., Sylvain, M., Lachance, J.-G., Deschênes, L., Senay, H., Tremblay, J.P., 2006. Dystrophin expression in muscles of duchenne muscular dystrophy patients after high-density injections of normal myogenic cells. *J Neuropathol Exp Neurol* 65, 371–386. <https://doi.org/10.1097/01.jnen.0000218443.45782.81>
- Skuk, D., Goulet, M., Tremblay, J.P., 2011. Transplanted myoblasts can migrate several millimeters to fuse with damaged myofibers in nonhuman primate skeletal muscle. *J Neuropathol Exp Neurol* 70, 770–778. <https://doi.org/10.1097/NEN.0b013e31822a6baa>
- Smith, R.A., Newcombe, R.G., Sibert, J.R., Harper, P.S., 1991. Assessment of locomotor function in young boys with Duchenne muscular dystrophy. *Muscle Nerve* 14, 462–469. <https://doi.org/10.1002/mus.880140513>
- Smith, R.A., Sibert, J.R., Harper, P.S., 1990. Early development of boys with Duchenne muscular dystrophy. *Dev Med Child Neurol* 32, 519–527. <https://doi.org/10.1111/j.1469-8749.1990.tb16978.x>
- Snow, W.M., Anderson, J.E., Jakobson, L.S., 2013. Neuropsychological and neurobehavioral functioning in Duchenne muscular dystrophy: a review. *Neurosci Biobehav Rev* 37, 743–752. <https://doi.org/10.1016/j.neubiorev.2013.03.016>
- Sowell, E.R., Thompson, P.M., Holmes, C.J., Batth, R., Jernigan, T.L., Toga, A.W., 1999. Localizing Age-Related Changes in Brain Structure between Childhood and Adolescence Using Statistical Parametric Mapping. *NeuroImage* 9, 587–597. <https://doi.org/10.1006/nimg.1999.0436>
- Spencer-Smith, M., Anderson, V., 2009. Healthy and abnormal development of the prefrontal cortex. *Dev Neurorehabil* 12, 279–297. <https://doi.org/10.3109/17518420903090701>
- Spitali, P., van den Bergen, J.C., Verhaart, I.E.C., Wokke, B., Janson, A.A.M., van den Eijnde, R., den Dunnen, J.T., Laros, J.F.J., Verschuuren, J.J.G.M., 't Hoen, P.A.C., Aartsma-Rus, A., 2013. DMD transcript imbalance determines dystrophin levels. *FASEB J* 27, 4909–4916. <https://doi.org/10.1096/fj.13-232025>
- Stedman, H.H., Sweeney, H.L., Shrager, J.B., Maguire, H.C., Panettieri, R.A., Petrof, B., Narusawa, M., Leferovich, J.M., Sladky, J.T., Kelly, A.M., 1991. The mdx mouse diaphragm reproduces the degenerative changes of Duchenne muscular dystrophy. *Nature* 352, 536–539. <https://doi.org/10.1038/352536a0>
- Steffens, R., Leumann, C.J., 1999. Synthesis and Thermodynamic and Biophysical Properties of Tricyclo-DNA. *J. Am. Chem. Soc.* 121, 3249–3255. <https://doi.org/10.1021/ja983570w>
- Steffens, R., Leumann, C.J., 1997. Tricyclo-DNA: A Phosphodiester-Backbone Based DNA Analog Exhibiting Strong Complementary Base-Pairing Properties. *J. Am. Chem. Soc.* 119, 11548–11549. <https://doi.org/10.1021/ja972597x>
- Stiles, J., Jernigan, T.L., 2010. The Basics of Brain Development. *Neuropsychol Rev* 20, 327–348. <https://doi.org/10.1007/s11065-010-9148-4>

- Summerton, J., Weller, D., 1997. Morpholino antisense oligomers: design, preparation, and properties. *Antisense Nucleic Acid Drug Dev* 7, 187–195. <https://doi.org/10.1089/oli.1.1997.7.187>
- Syed, Y.Y., 2016. Eteplirsen: First Global Approval. *Drugs* 76, 1699–1704. <https://doi.org/10.1007/s40265-016-0657-1>
- Tadayoni, R., Rendon, A., Soria-Jasso, L.E., Cisneros, B., 2012. Dystrophin Dp71: the smallest but multifunctional product of the Duchenne muscular dystrophy gene. *Mol Neurobiol* 45, 43–60. <https://doi.org/10.1007/s12035-011-8218-9>
- Tanaka, A., Woltjen, K., Miyake, K., Hotta, A., Ikeya, M., Yamamoto, T., Nishino, T., Shoji, E., Sehara-Fujisawa, A., Manabe, Y., Fujii, N., Hanaoka, K., Era, T., Yamashita, S., Isobe, K.-I., Kimura, E., Sakurai, H., 2013. Efficient and reproducible myogenic differentiation from human iPS cells: prospects for modeling Miyoshi Myopathy in vitro. *PLoS One* 8, e61540. <https://doi.org/10.1371/journal.pone.0061540>
- Tang, X., Jaenisch, R., Sur, M., 2021. The role of GABAergic signalling in neurodevelopmental disorders. *Nat Rev Neurosci* 22, 290–307. <https://doi.org/10.1038/s41583-021-00443-x>
- Tarköy, M., Leumann, C., 1993. Synthesis and Pairing Properties of Decanucleotides from (3'S,5'R)-2'-Deoxy-3', 5'-ethanoβ-D-ribofuranosyladenine and -thymine. *Angewandte Chemie International Edition in English* 32, 1432–1434. <https://doi.org/10.1002/anie.199314321>
- Taylor, P.J., Betts, G.A., Maroulis, S., Gilissen, C., Pedersen, R.L., Mowat, D.R., Johnston, H.M., Buckley, M.F., 2010. DMD gene mutation location and the risk of cognitive impairment in Duchenne muscular dystrophy. *PLoS One* 5, e8803. <https://doi.org/10.1371/journal.pone.0008803>
- Tedesco, F.S., Gerli, M.F.M., Perani, L., Benedetti, S., Ungaro, F., Cassano, M., Antonini, S., Tagliafico, E., Artusi, V., Longa, E., Tonlorenzi, R., Ragazzi, M., Calderazzi, G., Hoshiya, H., Cappellari, O., Mora, M., Schoser, B., Schneiderat, P., Oshimura, M., Bottinelli, R., Sampaolesi, M., Torrente, Y., Broccoli, V., Cossu, G., 2012. Transplantation of genetically corrected human iPSC-derived progenitors in mice with limb-girdle muscular dystrophy. *Sci Transl Med* 4, 140ra89. <https://doi.org/10.1126/scitranslmed.3003541>
- Tinsley, J., Robinson, N., Davies, K.E., 2015. Safety, tolerability, and pharmacokinetics of SMT C1100, a 2-arylbenzoxazole utrophin modulator, following single- and multiple-dose administration to healthy male adult volunteers. *J Clin Pharmacol* 55, 698–707. <https://doi.org/10.1002/jcph.468>
- Tinsley, J.M., Blake, D.J., Davies, K.E., 1993. Apo-dystrophin-3: a 2.2kb transcript from the DMD locus encoding the dystrophin glycoprotein binding site. *Hum Mol Genet* 2, 521–524. <https://doi.org/10.1093/hmg/2.5.521>
- Tinsley, J.M., Fairclough, R.J., Storer, R., Wilkes, F.J., Potter, A.C., Squire, S.E., Powell, D.S., Cozzoli, A., Capogrosso, R.F., Lambert, A., Wilson, F.X., Wren, S.P., De Luca, A., Davies, K.E., 2011. Daily treatment with SMT C1100, a novel small molecule utrophin upregulator, dramatically reduces the dystrophic symptoms in the mdx mouse. *PLoS One* 6, e19189. <https://doi.org/10.1371/journal.pone.0019189>
- Tokarz, S.A., Duncan, N.M., Rash, S.M., Sadeghi, A., Dewan, A.K., Pillers, D.A., 1998. Redefinition of dystrophin isoform distribution in mouse tissue by RT-PCR implies role in nonmuscle manifestations of duchenne muscular dystrophy. *Mol Genet Metab* 65, 272–281. <https://doi.org/10.1006/mgme.1998.2763>
- Tozawa, T., Itoh, K., Yaoi, T., Tando, S., Umekage, M., Dai, H., Hosoi, H., Fushiki, S., 2012. The shortest isoform of dystrophin (Dp40) interacts with a group of presynaptic proteins to form a presumptive novel complex in the mouse brain. *Mol Neurobiol* 45, 287–297. <https://doi.org/10.1007/s12035-012-8233-5>

- Tsai, H.-H., Niu, J., Munji, R., Davalos, D., Chang, J., Zhang, H., Tien, A.-C., Kuo, C.J., Chan, J.R., Daneman, R., Fancy, S.P.J., 2016. Oligodendrocyte precursors migrate along vasculature in the developing nervous system. *Science* 351, 379–384. <https://doi.org/10.1126/science.aad3839>
- Tuffery, S., Lenk, U., Roberts, R.G., Coubes, C., Demaille, J., Claustres, M., 1995. Protein truncation test: analysis of two novel point mutations at the carboxy-terminus of the human DMD gene associated with mental retardation. *Hum Mutat* 6, 126–135. <https://doi.org/10.1002/humu.1380060205>
- Turner, P.R., Westwood, T., Regen, C.M., Steinhardt, R.A., 1988. Increased protein degradation results from elevated free calcium levels found in muscle from mdx mice. *Nature* 335, 735–738. <https://doi.org/10.1038/335735a0>
- Uttley, L., Carlton, J., Woods, H.B., Brazier, J., 2018. A review of quality of life themes in Duchenne muscular dystrophy for patients and carers. *Health Qual Life Outcomes* 16, 237. <https://doi.org/10.1186/s12955-018-1062-0>
- Vacca, O., Charles-Messance, H., El Mathari, B., Sene, A., Barbe, P., Fouquet, S., Aragón, J., Darche, M., Giocanti-Aurégan, A., Paques, M., Sahel, J.-A., Tadayoni, R., Montañez, C., Dalkara, D., Rendon, A., 2016. AAV-mediated gene therapy in Dystrophin-Dp71 deficient mouse leads to blood-retinal barrier restoration and oedema reabsorption. *Hum Mol Genet* 25, 3070–3079. <https://doi.org/10.1093/hmg/ddw159>
- Vaillend, C., Billard, J.-M., 2002. Facilitated CA1 hippocampal synaptic plasticity in dystrophin-deficient mice: role for GABAA receptors? *Hippocampus* 12, 713–717. <https://doi.org/10.1002/hipo.10068>
- Vaillend, C., Billard, J.M., Claudepierre, T., Rendon, A., Dutar, P., Ungerer, A., 1998. Spatial discrimination learning and CA1 hippocampal synaptic plasticity in mdx and mdx3cv mice lacking DMD gene products. *Neuroscience* 86, 53–66. [https://doi.org/10.1016/s0306-4522\(98\)00023-2](https://doi.org/10.1016/s0306-4522(98)00023-2)
- Vaillend, C., Billard, J.-M., Laroche, S., 2004. Impaired long-term spatial and recognition memory and enhanced CA1 hippocampal LTP in the dystrophin-deficient Dmd(mdx) mouse. *Neurobiol Dis* 17, 10–20. <https://doi.org/10.1016/j.nbd.2004.05.004>
- Vaillend, C., Chaussonot, R., 2017a. Relationships linking emotional, motor, cognitive and GABAergic dysfunctions in dystrophin-deficient mdx mice. *Human Molecular Genetics* 26, 1041–1055. <https://doi.org/10.1093/hmg/ddx013>
- Vaillend, C., Chaussonot, R., 2017b. Relationships linking emotional, motor, cognitive and GABAergic dysfunctions in dystrophin-deficient mdx mice. *Hum Mol Genet* 26, 1041–1055. <https://doi.org/10.1093/hmg/ddx013>
- Vaillend, C., Perronnet, C., Ros, C., Gruszczynski, C., Goyenvallé, A., Laroche, S., Danos, O., Garcia, L., Peltekian, E., 2010. Rescue of a dystrophin-like protein by exon skipping in vivo restores GABAA-receptor clustering in the hippocampus of the mdx mouse. *Mol Ther* 18, 1683–1688. <https://doi.org/10.1038/mt.2010.134>
- Vaillend, C., Rendon, A., Misslin, R., Ungerer, A., 1995a. Influence of dystrophin-gene mutation on mdx mouse behavior. I. Retention deficits at long delays in spontaneous alternation and bar-pressing tasks. *Behav Genet* 25, 569–579. <https://doi.org/10.1007/BF02327580>
- Vaillend, C., Rendon, A., Misslin, R., Ungerer, A., 1995b. Influence of dystrophin-gene mutation on mdx mouse behavior. I. Retention deficits at long delays in spontaneous alternation and bar-pressing tasks. *Behav Genet* 25, 569–579. <https://doi.org/10.1007/BF02327580>
- Vaillend, C., Zarrouki, F., Vacca, O., 2019. Gene Therapy for Central Nervous System in Duchenne Muscular Dystrophy, in: *Muscle Gene Therapy*. Springer International Publishing, pp. 417–438. https://doi.org/10.1007/978-3-030-03095-7_24
- Vajda, Z., Pedersen, M., Füchtbauer, E.-M., Wertz, K., Stødkilde-Jørgensen, H., Sulyok, E., Dóczi, T., Neely, J.D., Agre, P., Frøkiaer, J., Nielsen, S., 2002. Delayed onset of brain edema and mislocalization of

- aquaporin-4 in dystrophin-null transgenic mice. *Proc Natl Acad Sci U S A* 99, 13131–13136. <https://doi.org/10.1073/pnas.192457099>
- Valentine, B.A., Cooper, B.J., Cummings, J.F., de Lahunta, A., 1990. Canine X-linked muscular dystrophy: morphologic lesions. *J Neurol Sci* 97, 1–23. [https://doi.org/10.1016/0022-510x\(90\)90095-5](https://doi.org/10.1016/0022-510x(90)90095-5)
- Valentine, B.A., Cooper, B.J., Cummings, J.F., deLahunta, A., 1986. Progressive muscular dystrophy in a golden retriever dog: light microscope and ultrastructural features at 4 and 8 months. *Acta Neuropathol* 71, 301–310. <https://doi.org/10.1007/BF00688053>
- Valentine, B.A., Winand, N.J., Pradhan, D., Moise, N.S., de Lahunta, A., Kornegay, J.N., Cooper, B.J., 1992. Canine X-linked muscular dystrophy as an animal model of Duchenne muscular dystrophy: a review. *Am J Med Genet* 42, 352–356. <https://doi.org/10.1002/ajmg.1320420320>
- van Deutekom, J.C., Janson, A.A., Ginjaar, I.B., Frankhuizen, W.S., Aartsma-Rus, A., Bremmer-Bout, M., den Dunnen, J.T., Koop, K., van der Kooi, A.J., Goemans, N.M., de Kimpe, S.J., Ekhart, P.F., Venneker, E.H., Platenburg, G.J., Verschuuren, J.J., van Ommen, G.-J.B., 2007. Local dystrophin restoration with antisense oligonucleotide PRO051. *N Engl J Med* 357, 2677–2686. <https://doi.org/10.1056/NEJMoa073108>
- van Dommelen, P., van Dijk, O., de Wilde, J.A., Verkerk, P.H., 2020. Early developmental milestones in Duchenne muscular dystrophy. *Dev Med Child Neurol* 62, 1198–1204. <https://doi.org/10.1111/dmcn.14623>
- van Putten, M., Lloyd, E.M., de Greef, J.C., Raz, V., Willmann, R., Grounds, M.D., 2020. Mouse models for muscular dystrophies: an overview. *Dis Model Mech* 13, dmm043562. <https://doi.org/10.1242/dmm.043562>
- Vandenbergh, L.H., Bell, P., Maguire, A.M., Xiao, R., Hopkins, T.B., Grant, R., Bennett, J., Wilson, J.M., 2013. AAV9 targets cone photoreceptors in the nonhuman primate retina. *PLoS One* 8, e53463. <https://doi.org/10.1371/journal.pone.0053463>
- Verhaart, I.E.C., Aartsma-Rus, A., 2019. Therapeutic developments for Duchenne muscular dystrophy. *Nat Rev Neurol* 15, 373–386. <https://doi.org/10.1038/s41582-019-0203-3>
- Vulin, A., Barthélémy, I., Goyenvall, A., Thibaud, J.-L., Beley, C., Griffith, G., Benchaouir, R., le Hir, M., Unterfinger, Y., Lorain, S., Dreyfus, P., Voit, T., Carlier, P., Blot, S., Garcia, L., 2012. Muscle function recovery in golden retriever muscular dystrophy after AAV1-U7 exon skipping. *Mol Ther* 20, 2120–2133. <https://doi.org/10.1038/mt.2012.181>
- Wagner, K.R., Kuntz, N.L., Koenig, E., East, L., Upadhyay, S., Han, B., Shieh, P.B., 2021. Safety, tolerability, and pharmacokinetics of casimersen in patients with Duchenne muscular dystrophy amenable to exon 45 skipping: A randomized, double-blind, placebo-controlled, dose-titration trial. *Muscle Nerve* 64, 285–292. <https://doi.org/10.1002/mus.27347>
- Wahl, M.C., Will, C.L., Lührmann, R., 2009. The spliceosome: design principles of a dynamic RNP machine. *Cell* 136, 701–718. <https://doi.org/10.1016/j.cell.2009.02.009>
- Waite, A., Tinsley, C.L., Locke, M., Blake, D.J., 2009. The neurobiology of the dystrophin-associated glycoprotein complex. *Ann Med* 41, 344–359. <https://doi.org/10.1080/07853890802668522>
- Waldrop, D.M., Lawlor, D.M., Vetter, T.M., Frair, E., Beatka, M., Meng, D.H., Iammarino, M., Powers, B., Harris, J., Kaler, M., Simmons, D.T., Wein, D.N., Flanigan, D.K., 2020. LATE BREAKING NEWS ORAL PRESENTATION: LBO 3 Expression of apparent full-length dystrophin in skeletal muscle in a first-in-human gene therapy trial using the scAAV9.U7-ACCA vector. *Neuromuscular Disorders* 30, S166–S167. <https://doi.org/10.1016/j.nmd.2020.09.008>
- Walmsley, G.L., Arechavala-Gomez, V., Fernandez-Fuente, M., Burke, M.M., Nagel, N., Holder, A., Stanley, R., Chandler, K., Marks, S.L., Muntoni, F., Shelton, G.D., Piercy, R.J., 2010. A duchenne muscular dystrophy gene hot spot mutation in dystrophin-deficient cavalier king charles spaniels is amenable to exon 51 skipping. *PLoS ONE* 5, e8647. <https://doi.org/10.1371/journal.pone.0008647>

- Wang, D., Zhang, F., Gao, G., 2020. CRISPR-Based Therapeutic Genome Editing: Strategies and In Vivo Delivery by AAV Vectors. *Cell* 181, 136–150. <https://doi.org/10.1016/j.cell.2020.03.023>
- Wang, G.-S., Cooper, T.A., 2007. Splicing in disease: disruption of the splicing code and the decoding machinery. *Nat Rev Genet* 8, 749–761. <https://doi.org/10.1038/nrg2164>
- Wang, Y., Marino-Enriquez, A., Bennett, R.R., Zhu, M., Shen, Y., Eilers, G., Lee, J.-C., Henze, J., Fletcher, B.S., Gu, Z., Fox, E.A., Antonescu, C.R., Fletcher, C.D.M., Guo, X., Raut, C.P., Demetri, G.D., van de Rijn, M., Ordog, T., Kunkel, L.M., Fletcher, J.A., 2014. Dystrophin is a tumor suppressor in human cancers with myogenic programs. *Nat Genet* 46, 601–606. <https://doi.org/10.1038/ng.2974>
- Wasala, N.B., Shin, J.-H., Lai, Y., Yue, Y., Montanaro, F., Duan, D., 2018. Cardiac-Specific Expression of Δ H2-R15 Mini-Dystrophin Normalized All Electrocardiogram Abnormalities and the End-Diastolic Volume in a 23-Month-Old Mouse Model of Duchenne Dilated Cardiomyopathy. *Hum Gene Ther* 29, 737–748. <https://doi.org/10.1089/hum.2017.144>
- Wein, N., Vulin, A., Falzarano, M.S., Szgyarto, C.A.-K., Maiti, B., Findlay, A., Heller, K.N., Uhlén, M., Bakthavachalu, B., Messina, S., Vita, G., Passarelli, C., Brioschi, S., Bovolenta, M., Neri, M., Gualandi, F., Wilton, S.D., Rodino-Klapac, L.R., Yang, L., Dunn, D.M., Schoenberg, D.R., Weiss, R.B., Howard, M.T., Ferlini, A., Flanigan, K.M., 2014. Translation from a DMD exon 5 IRES results in a functional dystrophin isoform that attenuates dystrophinopathy in humans and mice. *Nat Med* 20, 992–1000. <https://doi.org/10.1038/nm.3628>
- Wells, D.J., 2018. Tracking progress: an update on animal models for Duchenne muscular dystrophy. *Dis Model Mech* 11. <https://doi.org/10.1242/dmm.035774>
- Wersinger, E., Bordais, A., Schwab, Y., Sene, A., Bénard, R., Alunni, V., Sahel, J.-A., Rendon, A., Roux, M.J., 2011. Reevaluation of dystrophin localization in the mouse retina. *Invest Ophthalmol Vis Sci* 52, 7901–7908. <https://doi.org/10.1167/iovs.11-7519>
- Wheeler, M.T., Zarnegar, S., McNally, E.M., 2002. Zeta-sarcoglycan, a novel component of the sarcoglycan complex, is reduced in muscular dystrophy. *Hum Mol Genet* 11, 2147–2154. <https://doi.org/10.1093/hmg/11.18.2147>
- Wicksell, R.K., Kihlgren, M., Melin, L., Eeg-Olofsson, O., 2004. Specific cognitive deficits are common in children with Duchenne muscular dystrophy. *Dev Med Child Neurol* 46, 154–159. <https://doi.org/10.1017/s0012162204000283>
- Wickstrom, E., 1986. Oligodeoxynucleotide stability in subcellular extracts and culture media. *J. Biochem. Biophys. Methods* 13, 97–102.
- Wilkinson, M.E., Charenton, C., Nagai, K., 2020. RNA Splicing by the Spliceosome. *Annu Rev Biochem* 89, 359–388. <https://doi.org/10.1146/annurev-biochem-091719-064225>
- Williamson, R.A., Henry, M.D., Daniels, K.J., Hrstka, R.F., Lee, J.C., Sunada, Y., Ibraghimov-Beskrovnaya, O., Campbell, K.P., 1997. Dystroglycan is essential for early embryonic development: disruption of Reichert's membrane in *Dag1*-null mice. *Hum Mol Genet* 6, 831–841. <https://doi.org/10.1093/hmg/6.6.831>
- Wilton, S.D., Dye, D.E., Blechynden, L.M., Laing, N.G., 1997. Revertant fibres: a possible genetic therapy for Duchenne muscular dystrophy? *Neuromuscul Disord* 7, 329–335. [https://doi.org/10.1016/s0960-8966\(97\)00058-8](https://doi.org/10.1016/s0960-8966(97)00058-8)
- Wright, J.F., 2008. Manufacturing and characterizing AAV-based vectors for use in clinical studies. *Gene Ther* 15, 840–848. <https://doi.org/10.1038/gt.2008.65>
- Wu, W.-C., Bradley, S.P., Christie, J.M., Pugh, J.R., 2022. Mechanisms and Consequences of Cerebellar Purkinje Cell Disinhibition in a Mouse Model of Duchenne Muscular Dystrophy. *J Neurosci* 42, 2103–2115. <https://doi.org/10.1523/JNEUROSCI.1256-21.2022>

- Xie, L., Kang, H., Xu, Q., Chen, M.J., Liao, Y., Thiyagarajan, M., O'Donnell, J., Christensen, D.J., Nicholson, C., Iliff, J.J., Takano, T., Deane, R., Nedergaard, M., 2013. Sleep Drives Metabolite Clearance from the Adult Brain. *Science* 342, 10.1126/science.1241224. <https://doi.org/10.1126/science.1241224>
- Xie, W.-L., Zheng, H.-L., Li, H.-H., Lu, J.-J., Xue, S.-G., Luo, Y., Ma, C., Liu, J.-F., Hu, Z.-L., Ni, L., Jin, Y., Wang, F., Chen, J.-G., 2022. Deficiency of Glycosylated α -Dystroglycan in Ventral Hippocampus Bridges the Destabilization of Gamma-Aminobutyric Acid Type A Receptors With the Depressive-like Behaviors of Male Mice. *Biol Psychiatry* 91, 593–603. <https://doi.org/10.1016/j.biopsych.2021.10.022>
- Yilmaz, O., Karaduman, A., Topaloğlu, H., 2004. Prednisolone therapy in Duchenne muscular dystrophy prolongs ambulation and prevents scoliosis. *Eur J Neurol* 11, 541–544. <https://doi.org/10.1111/j.1468-1331.2004.00866.x>
- Young, H.K., Barton, B.A., Waisbren, S., Portales Dale, L., Ryan, M.M., Webster, R.I., North, K.N., 2008. Cognitive and psychological profile of males with Becker muscular dystrophy. *J Child Neurol* 23, 155–162. <https://doi.org/10.1177/0883073807307975>
- Yude, C., Goodman, R., McConachie, H., 1998. Peer problems of children with hemiplegia in mainstream primary schools. *J Child Psychol Psychiatry* 39, 533–541.
- Zamecnik, P.C., Stephenson, M.L., 1978. Inhibition of Rous sarcoma virus replication and cell transformation by a specific oligodeoxynucleotide. *Proc Natl Acad Sci U S A* 75, 280–284. <https://doi.org/10.1073/pnas.75.1.280>
- Zarrouki, F., Goutal, S., Vacca, O., Garcia, L., Tournier, N., Goyenvalle, A., Vaillend, C., 2022a. Abnormal Expression of Synaptic and Extrasynaptic GABAA Receptor Subunits in the Dystrophin-Deficient mdx Mouse. *Int J Mol Sci* 23, 12617. <https://doi.org/10.3390/ijms232012617>
- Zarrouki, F., Relizani, K., Bizot, F., Tensorer, T., Garcia, L., Vaillend, C., Goyenvalle, A., 2022b. Partial restoration of brain dystrophin and behavioral deficits by exon skipping in the muscular dystrophy X-linked (mdx) mouse. *Ann Neurol*. <https://doi.org/10.1002/ana.26409>
- Zhang, H., Yang, B., Mu, X., Ahmed, S.S., Su, Q., He, R., Wang, H., Mueller, C., Sena-Estevés, M., Brown, R., Xu, Z., Gao, G., 2011. Several rAAV vectors efficiently cross the blood-brain barrier and transduce neurons and astrocytes in the neonatal mouse central nervous system. *Mol Ther* 19, 1440–1448. <https://doi.org/10.1038/mt.2011.98>
- Zhang, W., Peterson, M., Beyer, B., Frankel, W.N., Zhang, Z., 2014. Loss of MeCP2 from forebrain excitatory neurons leads to cortical hyperexcitation and seizures. *J Neurosci* 34, 2754–2763. <https://doi.org/10.1523/JNEUROSCI.4900-12.2014>
- Zincarelli, C., Soltys, S., Rengo, G., Rabinowitz, J.E., 2008. Analysis of AAV serotypes 1-9 mediated gene expression and tropism in mice after systemic injection. *Mol Ther* 16, 1073–1080. <https://doi.org/10.1038/mt.2008.76>

ANNEXES

I. Scientific publications

1. Altered visual processing in the *mdx52* mouse model of Duchenne muscular dystrophy

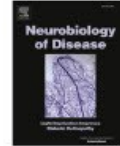
Neurobiology of Disease 152 (2021) 105288



Contents lists available at ScienceDirect

Neurobiology of Disease

journal homepage: www.elsevier.com/locate/ynbdi



Altered visual processing in the *mdx52* mouse model of Duchenne muscular dystrophy

Mirella Telles Salgueiro Barboni^{a,b,1}, André Maurício Passos Liber^{b,1},
Anneka Joachimsthaler^{c,d,1}, Amel Saoudi^{e,f}, Aurélie Goyenvalle^f, Alvaro Rendon^g, Jérôme
E. Roger^h, Dora Fix Ventura^b, Jan Kremers^{c,d,*,2}, Cyrille Vaillend^{e,*,2}

^a Department of Ophthalmology, Semmelweis University, Budapest, Hungary

^b Department of Experimental Psychology, University of Sao Paulo, Sao Paulo, Brazil

^c Section for Retinal Physiology, University Hospital Erlangen, Erlangen, Germany

^d Animal Physiology, Department of Biology, FAU Erlangen-Nürnberg, Erlangen, Germany

^e Université Paris-Saclay, CNRS, Institut des Neurosciences Paris Saclay, 91190 Gif-sur-Yvette, France

^f Université de Versailles, St-Quentin, INSERM U1179, IIA BAHN CSM, Montigny-Le Bretonneux, France

^g Department of Therapeutics, Sorbonne University, Institut de la Vision, Paris, France

^h Paris-Saclay Institute of Neuroscience, CERTE-Retina France, CNRS, Université Paris-Saclay, Orsay 91405, France

ARTICLE INFO

Keywords:

Retina
Dystrophin
Electroretinogram
Photoreceptors
B-wave
Duchenne muscular dystrophy
Mouse model
Dp427
Dp260
Dp140

ABSTRACT

The *mdx52* mouse model of Duchenne muscular dystrophy (DMD) is lacking exon 52 of the *DMD* gene that is located in a hotspot mutation region causing cognitive deficits and retinal anomalies in DMD patients. This deletion leads to the loss of the dystrophin proteins, Dp427, Dp260 and Dp140, while Dp71 is preserved. The flash electroretinogram (ERG) in *mdx52* mice was previously characterized by delayed dark-adapted b-waves. A detailed description of functional ERG changes and visual performances in *mdx52* mice is, however, lacking. Here an extensive full-field ERG repertoire was applied in *mdx52* mice and WT littermates to analyze retinal physiology in scotopic, mesopic and photopic conditions in response to flash, sawtooth and/or sinusoidal stimuli. Behavioral contrast sensitivity was assessed using quantitative optomotor response (OMR) to sinusoidally modulated luminance gratings at 100% or 50% contrast. The *mdx52* mice exhibited reduced amplitudes and delayed implicit times in dark-adapted ERG flash responses, particularly in their b-wave and oscillatory potentials, and diminished amplitudes of light-adapted flash ERGs. ERG responses to sawtooth stimuli were also diminished and delayed for both mesopic and photopic conditions in *mdx52* mice and the first harmonic amplitudes to photopic sine-wave stimuli were smaller at all temporal frequencies. OMR indices were comparable between genotypes at 100% contrast but significantly reduced in *mdx52* mice at 50% contrast. The complex ERG alterations and disturbed contrast vision in *mdx52* mice include features observed in DMD patients and suggest altered photoreceptor-to-bipolar cell transmission possibly affecting contrast sensitivity. The *mdx52* mouse is a relevant model to appraise the roles of retinal dystrophins and for preclinical studies related to DMD.

1. Introduction

Duchenne muscular dystrophy (DMD) is an X-linked neuromuscular disease affecting muscle tissues and the nervous system. It is due to a variety of genetic mutations (Koenig et al., 1987) that impede expression of several dystrophin-gene products (*DMD* gene, MIM: 300377)

expressed from independent internal promoters in a tissue and cell-specific manner (Fig. 1 A). Dystrophins are membrane-bound cytoskeletal proteins known to play a central role in a scaffold of glycoproteins, the dystrophin-associated glycoprotein complex (DAGC). The DAGC includes the transmembrane dystroglycan complex, a receptor for extracellular-matrix proteins involved in the clustering of various

* Corresponding author at: Neuroscience Paris-Saclay Institute, Université Paris Saclay, CNRS UMR9197, Bât. 446, rue Claude Bernard, 91405 Orsay cedex, France.

** Corresponding author at: Section for Retinal Physiology, University of Erlangen-Nuremberg, Germany.

E-mail addresses: jan.kremers@uk-erlangen.de (J. Kremers), cyrille.vaillend@universite-paris-saclay.fr (C. Vaillend).

¹ M.T.S.B., A.M.P.L., and A.J. contributed equally to the paper.

² J.K. and C.V. are equally responsible for the research work.

<https://doi.org/10.1016/j.nbd.2021.105288>

Received 22 September 2020; Received in revised form 26 January 2021; Accepted 3 February 2021

Available online 5 February 2021

0969-9961/© 2021 The Authors. Published by Elsevier Inc. This is an open access article under the CC BY-NC-ND license

<http://www.elsevier.com/locate/ynbdi>

membrane receptors and ion channels, and key intracellular signaling proteins such as syntrophins (Pilgram et al., 2010; Waite et al., 2009).

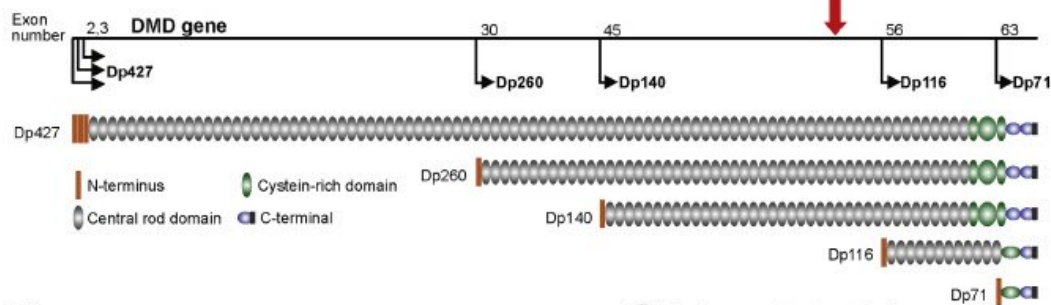
The main clinical characteristic of DMD is a progressive muscular degeneration leading to premature death due to the loss of the full-length dystrophin protein (Dp427) (Hauser and Chamberlain, 1996; Hoffman et al., 1987). In addition, through non-invasive electroretinography (ERG) and behavioral measurements, it has been established that impaired cognitive performance, neurodevelopmental problems, altered retinal physiology, and altered contrast and color discrimination are characteristic of DMD (Ricotti et al., 2016b; Ricotti et al., 2016a; Snow et al., 2013). The severity of these non-muscle phenotypes increases as larger numbers of dystrophins (Dp427, Dp260, Dp140, and Dp71) expressed in the central nervous system (CNS) are affected by distal mutations (Daoud et al., 2008; Desguerre et al., 2009; Pillers et al., 1999a; Ricotti et al., 2016b; Taylor et al., 2010). DMD is therefore associated with heterogeneous and complex genotype-phenotype relationships depending on the mutation position, since distinct dystrophins interact with different molecular partners in specific cell types throughout the CNS (Perronnet and Vaillend, 2010).

All known dystrophin proteins – except Dp116 – have been detected in various cell types and subcellular domains in the mouse retina (Fig. 1 B). The roles of dystrophins in retinal physiology however remain unclear. The mRNAs coding for Dp427, Dp260, and Dp140 have all been detected in the outer nuclear and plexiform layers (ONL/OPL) and the Dp427 mRNA has been specifically detected in bipolar and amacrine

cells in the inner nuclear layer (INL) of the mouse retina (Wersinger et al., 2011). Both Dp427 and Dp260 proteins have been detected in photoreceptor terminals (Fig. 1 C). Dp260, a retina-specific dystrophin, is likely to contribute to signal transmission at the synapse between rod photoreceptors and depolarizing (On-) bipolar cells, whereas Dp427 is more strongly expressed in cone-associated synapses (Wersinger et al., 2011). The shortest dystrophin protein, Dp71, is involved in the clustering of the potassium Kir4.1 and aquaporin AQP4 channels in Müller glial-cell endfeet (Tadayoni et al., 2012). Interestingly, the severity of the ERG alterations, particularly leading to electronegative scotopic ERGs, varies depending on the mutation or deletion position in DMD patients (Pillers et al., 1999a; Ricotti et al., 2016a) and DMD mouse models (Bucher et al., 2019; Pillers et al., 1999b). In addition, alterations of the ERG correlate with the neurodevelopmental outcome (Ricotti et al., 2016a). Thus, the ERG may be regarded as a potential biomarker for assessing the severity of the neurological defects and their responsiveness to genetic therapies targeting the CNS.

The ERG is a well-recognized non-invasive tool used for clinical detection of retinopathies and experimental investigation of physiological processing in the retina, as well as of the effects of therapeutic interventions in animal models of human retinal disorders (Cuenca et al., 2014; Pardue and Peachey, 2014). ERG recordings in mice (Kremers and Tanimoto, 2018) allow a functional dissection of distinct retinal mechanisms such as the On- and Off-pathways in vivo (Barboni et al., 2020; Barboni et al., 2013; Tsai et al., 2016) and have been

A DMD Gene and Gene Products



B Expression of Dystrophins in the Retina

	Dp427	Dp260	Dp140	Dp116	Dp71
Photoreceptor layer	-	-	-	-	-
ONL/OPL/INL*	+	+	+	-	-
OPL: Rod/cone terminals#	+	+	-	-	-
OPL: Horizontal cells	-	-	-	-	-
INL: Bipolar cells*	+	-	-	-	-
INL: Amacrine cells*	+	-	-	-	-
GCL: Ganglion cells	-	-	-	-	-
ILM: Müller-cell endfeet	-	-	-	-	+

C Photoreceptor terminal

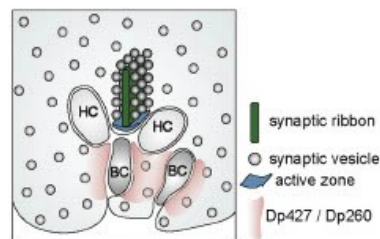


Fig. 1. Schematic overview of DMD-gene products and their expression in the retina. (A) Genetic organisation of the DMD-gene. The DMD gene (depicted by the black line) contains 79 exons. The exon numbers above the gene indicate the first exons transcribed from alternative internal promoters and the thin black arrows show the transcription start sites and the resultant dystrophin proteins for each start site. The dystrophin proteins contain four subdivisions: An N-terminus, a spectrin-like central rod domain of variable size, a cysteine-rich domain and a C-terminus. The red arrow represents the position of exon-52 that is deleted in *mdx52* mice. (B) A table summarizing the known sites of expression of dystrophins in the various retinal layers, cell-types, and/or subcellular domains. *: Detection of corresponding mRNA only. Dp427 was found proportionally more strongly expressed in cone- than in rod-associated synapses when compared with Dp260 (Wersinger et al., 2011). ONL: outer nuclear layer; OPL: outer plexiform layer; INL: inner nuclear layer; GCL: ganglion cell layer; ILM: inner limiting membrane. (C) Schematic representing the localization of Dp427 and/or Dp260 (pink) in photoreceptor terminals as suggested by others (adapted from Wersinger et al., 2011). HC: Horizontal-cell dendrites; BC: Bipolar-cell dendrites.

successfully applied to a variety of mouse models of retinal disorders (Collin et al., 2020).

In DMD mouse models, studies of electrophysiological dysfunction of the retina are still scarce and/or lack fine-level analyses of the involved cellular mechanisms. Our recent studies in *mdx*^{3Cv} mice lacking all dystrophins (Tsai et al., 2016) and in Dp71-null mice lacking only Dp71 (Barboni et al., 2020) suggest that the profile of ERG alterations is more complex than the originally described changes in b:a-wave ratios. In both patients and mice, ERGs may also display hallmarks of specific defective cellular pathways, as also suggested by some of our studies with DMD patients (Barboni et al., 2016; Barboni et al., 2013).

A detailed study of the ERG defects caused by genetic alteration in a distal hotspot area between introns 43 and 55 is still missing, although they represent a large part (approximately 70% of exonic deletions) of the alterations occurring in the human DMD gene (Bladen et al., 2015; Juan-Mateu et al., 2015). These deletions are associated with a loss of several dystrophins (Dp427, Dp260 and Dp140). The same dystrophins are also missing in the exon 52-deficient *mdx* mouse model (*mdx52*) (Araki et al., 1997). A pioneering study of ERGs in *mdx52* mice (Kameya et al., 1997) revealed the presence of delayed scotopic b-waves with normal amplitudes. This is at variance with the ERG deficits of patients bearing similar mutations, displaying not only delayed but also reduced b-wave amplitudes (De Becker et al., 1994; Girlanda et al., 1997; Ino-ue et al., 1997; Pascual Pascual et al., 1998; Pillers et al., 1999a; Ricotti et al., 2016a; Sigesmund et al., 1994).

In the present study, our main objectives were (1) to determine whether the study of retinal functions in *mdx52* mice could support the current hypothesis that distal mutations affecting several dystrophins lead to a more severe deficit than proximal mutations and (2) to identify specific outcome measures that could be relevant for future preclinical studies. We aimed to obtain a full characterization of the ERG deficits in *mdx52* mice by recording an extensive ERG repertoire using a variety of visual stimuli in scotopic, mesopic and photopic conditions, in order to probe the activity of different retinal cell populations and pathways. Moreover, optomotor response (OMR) measurements to sinusoidally modulated luminance gratings at 100% and 50% (Michelson) contrasts complemented the characterization of the visual phenotype in *mdx52* mice.

We demonstrate that flash ERGs have reduced amplitudes and longer implicit times, but also more complex alterations of the a-waves, oscillatory potentials, On- and Off-responses and responses to sinusoidal luminance modulation. Altered behavioral contrast sensitivity was also observed. We conclude that the *mdx52* mouse displays some key visual features reported in DMD patients and may therefore represent an interesting model to investigate the pathophysiological mechanisms affected by the loss of CNS dystrophins and their response to gene therapies. Comparison of the ERG data with those obtained in other mouse models for DMD gives insight of the roles of the different dystrophins in the physiology of the retina.

2. Material and methods

2.1. Animals

Exon 52-deleted X chromosome-linked muscular dystrophy mice (*mdx52* mice) were produced by replacement of exon 52 of the DMD gene by the neomycin resistance gene, thereby eliminating expression of Dp427, Dp260 and Dp140 dystrophins but preserving expression of Dp116 (in peripheral nerves) and of Dp71 (in brain and retina) (Araki et al., 1997) (see Fig. 1 A). The mouse line was backcrossed with the C57BL/6 J strain for more than eight generations. Breeders were generously provided by Dr. Jun Tanihata and Dr. Shin'ichi Takeda (National Center of Neurology and Psychiatry, Tokyo, Japan). Heterozygous females were crossed with C57BL/6Jrj male mice to generate *mdx52* and littermate control (WT) males in the animal facility of NeuroPSI at Université Paris-Saclay in Orsay (France). The genotype was

determined by PCR analysis of tail DNA. The mice were kept under a standard 12-h light-dark cycle (light on 7.00 a.m.) with food and water ad libitum. ERG recordings were performed in young-adult mice at age 3–4 months (*mdx52*: 104.2 ± 22.8 days; WT littermates: 98.7 ± 19.3 days). All experiments adhered to the ARVO Statement for the Use of Animals in Ophthalmic and Vision Research and were conducted following the guidelines of the local mouse facility (agreement D91–471-104) in compliance with European Directive 2010/63/EU and French National Committee (87/848). The protocols were approved by the French Ethics Committee (Paris Centre et Sud, #59).

2.2. ERG recordings

2.2.1. Animal preparation

ERGs were recorded from 20 eyes of 10 *mdx52* male mice and 12 eyes of six WT male littermates. Protocols and procedures have been described in detail elsewhere (Barboni et al., 2020; Tsai et al., 2016). Briefly, prior to testing, mice were dark-adapted for at least 12 h. Animal handling, preparation and electrode placement were performed under deep red illumination to keep the retina dark-adapted. Mice were anesthetized by an intramuscular injection of 25:5 mg/kg of 10% ketamine (ketamine 1000; Virbac, France), 2% xylazine (Rompun; Bayer Healthcare, Puteaux, France) in saline. During ERG recordings, the mice were positioned on a water-heated platform (38 °C) to maintain body temperature during anesthesia. Subcutaneous injections of 0.9% saline (300 µl before recordings, 100 µl after recordings) were given to prevent dehydration. Pupils were fully dilated using eye drops of 0.5% Tropicamide (Mydriaticum; Thea, France) and 5% phenylephrine (Neosynephrine FAURE; Europhtha, Monaco) (1 drop each). To prevent corneal ulcerations and/or eye infection a drop of Tevemixine and N.A.C (TVM lab, France) was applied after ERG recordings. Contact lens electrodes (Ø 3.2 mm; Mayo Corporation, Inazawa, Japan) filled with Corneregel® (Dr. Mann Pharma, Berlin, Germany) were positioned on the corneas of the two eyes. They served as active electrodes. Two reference needle electrodes were placed subcutaneously medial to the two ears. A ground needle electrode was positioned subcutaneously at the base of the tail.

2.2.2. Apparatus and general conditions

Binocular recordings of full-field ERGs and stimulus presentations were controlled by a RetiPort system (Roland Consult, Brandenburg, Germany) using a Ganzfeld bowl (Q450SC, Roland Consult). All signals were amplified 100,000 times, band-pass filtered between 1 and 300 Hz, and digitized at a rate of 512 (flashes) or 2048 Hz (flicker). ERGs were measured in the order of increasing mean luminance to minimize the dark adaptation time interval to the following stimulus condition.

2.2.3. Scotopic flashes

Dark-adapted rod and mixed rod-cone mediated ERG responses were recorded to flashes of -3.7 , -2.7 , -1.7 , -0.7 , and $0.3 \log \text{ cd.s/m}^2$ (white light) strengths on a dark background. The number of repeats (sweeps) decreased with increasing flash strength (12, 10, 8, 8, and 4, respectively). The inter-stimulus interval was progressively increased with increasing flash strength (1, 2, 5, 10 and 20 s, respectively), thereby maintaining a dark-adapted state. Similarly, the interval between each condition increased from 10 to 120 s as the flash strength increased.

2.2.4. Mesopic responses to rapid-On and rapid-Off sawtooth stimuli

Rapid-On and -Off sawtooth stimuli, eliciting On- (to instantaneous luminance increments) and Off-responses (to instantaneous luminance decrements) respectively, were delivered at a mean luminance of 1 cd/m^2 (white light). The sawtooth was presented at 4 Hz (i.e. with a period of 250 ms) and 100% luminance (Michelson) contrast. Before recording the On- and then the Off-responses, the mouse was adapted to the 1 cd/m^2 mean luminance for 2 min. Signals from the first two seconds after stimulus onset, were discarded to avoid onset artefacts. Averages of 20

sweeps of 1 s each were obtained.

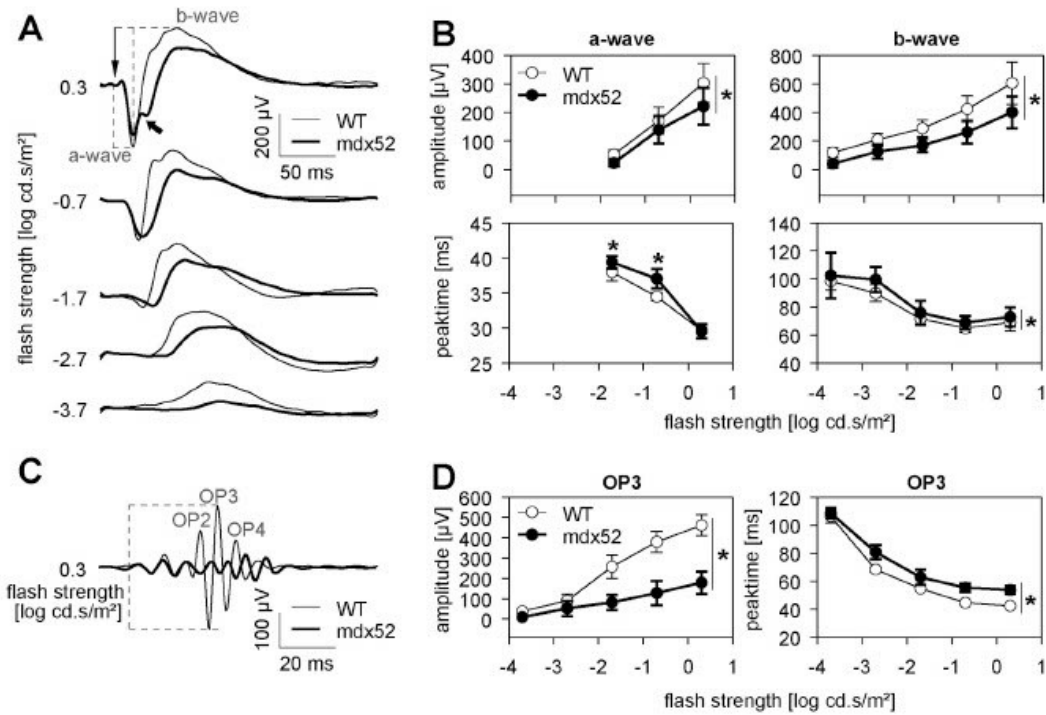
2.2.5. Photopic flashes

0.3 log cd.s/m² white flashes on a 25 cd/m² white background were delivered after a preadaptation period of 2 min. Twenty flashes with an inter-stimulus interval of 1 s were averaged.

2.2.6. Photopic sine-wave

After a preadaptation period of 2 min to 60 cd/m² background, sinusoidal luminance modulation (100% Michelson contrast; 60 cd/m² mean luminance, white light) at 10 temporal frequencies between 3 and 30 Hz were measured randomly. Averages of 20 sweeps, each lasting 1 s, were obtained. The first two seconds of recording were discarded to avoid onset artefacts.

Dark-adapted (scotopic) flash response



Light-adapted (photopic) flash response

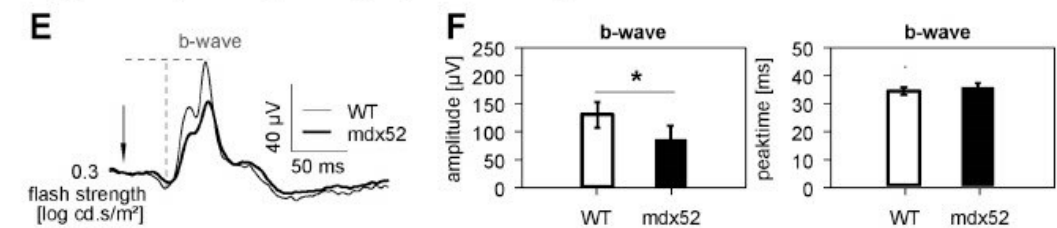


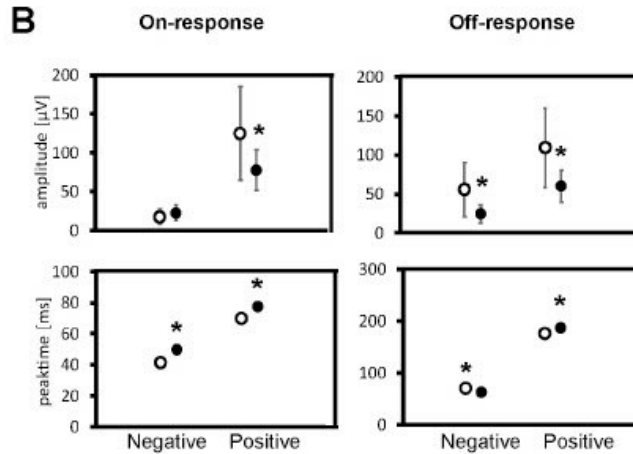
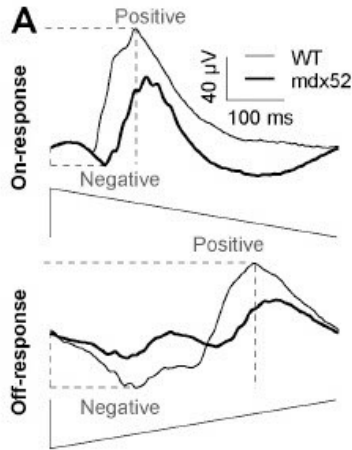
Fig. 2. Dark- and light-adapted flash responses. (A) Average dark-adapted (scotopic) flash ERGs in WT (thin traces) and *mdx52* mice (bold traces). (B) Mean (\pm one standard deviation) amplitudes (μ V; upper plots) and implicit times (ms; lower plots) of scotopic a- and b-waves, as indicated, in WT (open symbols) and *mdx52* mice (filled symbols). (C) Average OP traces isolated from the strongest scotopic flash (0.3 log cd.s/m²). (D) Mean (\pm one standard deviation) amplitude and implicit time of OP3 as a function of flash intensity in WT (open symbols) and *mdx52* (filled symbols) mice. (E) Averaged light-adapted (photopic) flash ERGs in WT (thin traces) and *mdx52* mice (bold traces). (F) Histograms showing the mean (\pm one standard deviation) amplitude and implicit time of the photopic b-wave. Significant effects are marked with an asterisk ($p < 0.05$). Dotted lines in A, C and E show the physiological hallmarks used for measurement of response implicit times and/or amplitudes (see the Methods section for details). Recordings made in 20 eyes of 10 *mdx52* mice and 12 eyes of 6 WT littermates.

2.2.7. Photopic On- and Off-sawtooth responses

Rapid-On and -Off sawtooth stimuli (white light) for incremental (On-) and decremental (Off-) responses were delivered with a mean luminance of 60 cd/m². As in the mesopic condition, the temporal profile was a 250 ms period (i.e. delivered at 4 Hz) with 100%

luminance contrast. Signals from the first two stimulus cycles were discarded to avoid onset artefacts. Averages of 40 episodes of 1 s each were obtained.

Mesopic sawtooth



Photopic sawtooth

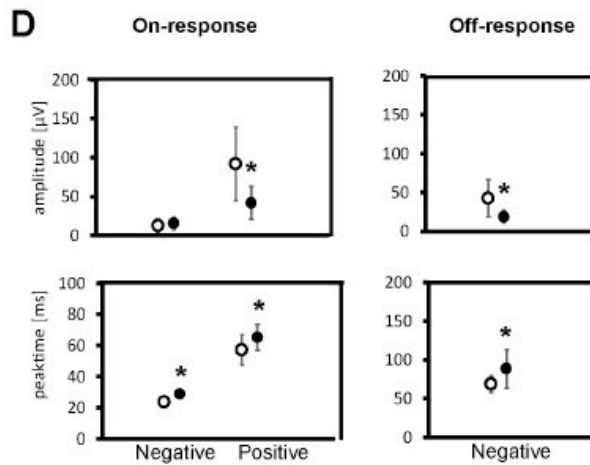
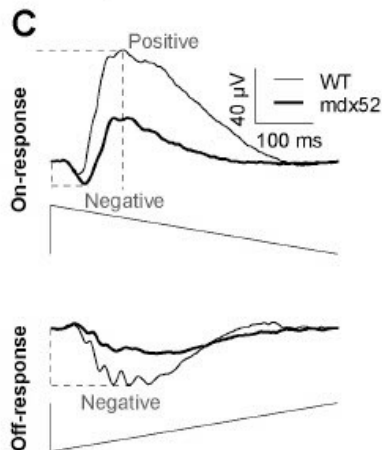


Fig. 3. Sawtooth On- and Off-responses. (A) Averaged responses of On- and Off-mediated mesopic ERG responses of *mdx52* (bold traces) and WT (thin traces) mice. Below the traces, representations of the luminance modulation for the rapid-On and the rapid-Off protocols are shown. (B) Mean (\pm one standard deviation) amplitudes (μ V; upper plots) and peak times (ms; lower plots) for the negative and positive components obtained with mesopic stimulation in WT (open symbols) and *mdx52* mice (filled symbols). (C) Averaged responses of On- and Off-mediated photopic ERG responses of *mdx52* (bold traces) and WT (thin traces) mice. Below the traces, representations of the average modulation for the rapid-On and the rapid-Off protocols are shown. (D) Mean (\pm one standard deviation) amplitudes (μ V; upper plots) and peak times (ms; lower plots) for the negative and positive components obtained with photopic stimulation in WT (open symbols) and *mdx52* mice (filled symbols). All parameters, except the negative amplitude of the On-mediated response and the negative peak time of the Off-mediate response are significantly different between the groups (marked with an asterisk; $p < 0.05$). Dotted lines in A, C and E show the physiological hallmarks used for measurement of response implicit times and/or amplitudes (see the Methods section for details). Recordings made in 20 eyes of 10 *mdx52* mice and 12 eyes of 6 WT littermates.

2.3. ERG signal processing

ERG components were analyzed offline by peak/trough detection, baseline measurements and Fourier analysis using self-written Matlab® routines (The Mathworks Inc., Natick, Massachusetts, United States) and Excel spreadsheets (Microsoft Office 2010, ©Microsoft Corporation, Redmond, WA, USA). The oscillatory potentials (OPs) were isolated and removed from the ERGs by a variable filter method (Harazny et al., 2009). ERGs without OPs were used to measure a- and b-wave parameters. Isolated OPs were also obtained through the variable filter method and analyzed.

As shown in Fig. 2 A, the amplitude of the scotopic a-wave was defined as the difference in μV between the baseline (average of recordings 17 ms before the occurrence of the flash) and the minimum within 50 ms after stimulus onset. The amplitude of the scotopic b-wave was the difference in μV between a-wave trough and the peak of the b-wave. The implicit times corresponded to the intervals between the stimulus onset and the peaks of the a-wave and of the b-wave (shown as dotted lines in Fig. 2 A). We also analyzed the amplitudes and implicit times of OP2, OP3, and OP4, but quantitative data are only shown for the highest (OP3) in Fig. 2 D.

The b-waves of the light-adapted flash ERG were measured as above. In agreement with previous data (Barboni et al., 2020; Tsai et al., 2016) both the photopic a-waves and the photopic negative responses were found to be very small and, thus, were not included in the quantitative analyses.

For the On- and Off-ERGs (Fig. 3 A, C), the baseline was defined as the average of the first 5 ms of each response after the rapid luminance change. The first troughs were taken from baseline, with subsequent component amplitudes measured from the preceding peak or trough. Steady-state ERGs in response to sine-wave modulation were Fourier analyzed to obtain the amplitudes and phases of the first harmonic (fundamental) components. Noise was defined as the mean of the amplitudes at the stimulus frequencies ± 1 Hz. The first harmonic phase values were included in subsequent analyses only if the signal-to-noise ratio for the responses were equal to or larger than 2. The relationship between phases and temporal frequencies between 3 and 30 Hz were evaluated by calculating the slope of the corresponding linear regressions.

2.4. Optomotor response (OMR)

Real time video tracking and automated measurements of compensatory head movements in freely moving mice were performed using an OMR recording setup (Phenoxys, Berlin, Germany). Each mouse was freely moving and placed on a platform (5 cm in diameter) in the center of four computer controlled LCD monitors (for details see Kretschmer et al., 2013, 2015). Visual stimuli were sinusoidally modulated luminance gratings generated by four LCD screens (60 Hz refresh rate; OkraArena, Phenoxys GmbH, Berlin, Germany), presented with a constant rotation. Video tracking considered the animal's distance to the monitors, thereby keeping the spatial frequency of the retinal image constant and providing data for automated OMR quantifications.

OMRs were recorded using two different Michelson contrasts and different spatial frequencies (presented in random order) in two distinct cohorts of mice: 100% contrast ($n = 8$ mice per genotype) or 50% contrast ($n = 10$ *mdx52* and 8 WT littermates). Similarly, as in the ERG recordings, the mice were 3–4 months of age. All stimuli were presented for 60 s randomly in either clockwise or counterclockwise direction. The measurements were completed in three trials for each animal, which we had previously validated as an optimal number of replicates to reduce the variability of individual's scores. At 100% contrast, OMRs were recorded in response to sinusoidal gratings at 12 spatial frequencies between 0.0125 and 0.5 cycles per degree (cpd). At 50% contrast, sinusoidal gratings were presented at 10 different spatial frequencies between 0.0125 and 0.4 cpd.

The number of head movements recorded at a speed range from 2 to 14 degrees per second in the same direction as the stimulus (n_{Correct}) and in the opposite direction ($n_{\text{Incorrect}}$) were used to calculate the OMR indices ($n_{\text{Correct}} / n_{\text{Incorrect}}$) at each spatial frequency.

2.5. Statistics

All ERG and OMR data were expressed as means \pm standard deviation (for ERG) and \pm standard error (for OMR). Genotype and group differences were analyzed using one or two-way ANOVAs depending on the presence of a within-subject repeated measure (strength, frequency). Univariate *t*-test was used to compare OMRs with baseline (test value = 1). *p* values < 0.05 were considered statistically significant.

3. Results

3.1. Dark- and light-adapted flash ERGs

We first describe responses to flash stimuli in scotopic and photopic conditions to evaluate the integrity of rod, cone and bipolar cell-mediated retinal physiology in the conventional ERG, and of the retinal network that generates OPs (Frishman, 2006). Both dark-adapted (scotopic) and light-adapted (photopic) ERGs were altered in *mdx52* mice compared with WT littermates. In the two genotypes, all tested stimulus strengths elicited a positive component (b-wave) in the dark-adapted flash ERG that dominated the responses, while a negative a-wave was detectable at flash strengths above $-1.7 \log \text{cd.s/m}^2$ (Fig. 2 A). The amplitudes of the a-waves ($F(2,58) = 384.14$; $p < 0.001$) and the b-waves ($F(4,120) = 273.44$; $p < 0.001$) of the dark-adapted flash ERGs increased with increasing flash strength responses in both genotypes. As shown in Fig. 2 B, the mean amplitudes of a-waves and b-waves (upper plots) were clearly reduced in *mdx52* mice compared to WT mice (a-waves: genotype effect, $F(1,29) = 9.66$, $p = 0.004$; genotype \times intensity interaction, $F(2,58) = 5.79$; $p < 0.01$; b waves: genotype effect, $F(1,30) = 36.95$, $p < 0.001$; genotype \times intensity interaction, $F(4,120) = 7.29$, $p < 0.001$). Moreover, implicit times were significantly increased in *mdx52* mice, for both the a-wave (genotype effect: $F(1,30) = 19.71$; $p < 0.001$; genotype \times intensity interaction: $F(2,60) = 21.87$; $p < 0.001$) and the b-wave (genotype effect: $F(1,27) = 10.39$, $p < 0.01$), with no significant genotype \times intensity interaction: ($F(4,108) = 0.95$; $p > 0.4$). Additionally, the scotopic ERG in *mdx52* mice showed a shoulder on the ascending limb of the b-wave at the highest flash strength (arrow in Fig. 2 A; upper plots), which was consistently found in all *mdx52* mice but never observed in WT mice.

OPs were extracted from the response to brightest dark-adapted flash ($0.3 \log \text{cd.s/m}^2$) (Fig. 2 C–D). The amplitudes of all OPs were drastically reduced in *mdx52* mice compared with WT (Fig. 2 C). As shown in Fig. 2 D, a quantitative analysis of the largest OP (OP3) confirmed the presence of significantly reduced amplitudes (genotype effect: $F(1,30) = 206.08$; $p < 0.001$; genotype \times intensity interaction: $F(4,120) = 80.59$; $p < 0.001$) and of an implicit time elongation in *mdx52* mice (genotype effect: $F(1,30) = 111.34$; $p < 0.001$; genotype \times intensity interaction: $F(4,120) = 13.68$; $p < 0.001$).

As shown in Fig. 2 E, the photopic b-wave amplitudes were significantly decreased in *mdx52* mice ($F(1,30) = 13.55$; $p < 0.01$), while implicit times (Fig. 2 F) were comparable in the two genotypes ($F(1,30) = 3.34$; $p = 0.078$).

This first set of stimulus protocols revealed a general reduction of amplitudes and longer implicit times in all retinal responses to flashes in *mdx52* mice.

3.2. Sawtooth On and Off ERGs

To further assess the integrity of the pathways involving On- and Off-bipolar cells that underlie the responses to luminance increases and decreases, we next describe the responses to mesopic and photopic

rapid-On and rapid-Off sawtooth stimuli. Mesopic On-responses (Fig. 3 A) exhibited an initial small negative component followed by a larger positive component. Mesopic Off-responses also displayed an initial negative deflection followed by a positive component. While the absolute amplitudes of the negative component of mesopic On-responses were similar in the two genotypes ($F(1,30) = 1.86$; $p > 0.1$), the positive-component amplitudes were significantly reduced in *mdx52* compared to WT mice (Fig. 3 B, upper plots) ($F(1,30) = 9.59$; $p < 0.01$). Mesopic Off-response amplitudes were also reduced for both the negative ($F(1,30) = 13.89$; $p < 0.005$) and positive ($F(1,30) = 15.27$; $p < 0.001$) components. Implicit times of the mesopic On-responses (Fig. 3 B, lower plots) were significantly longer in *mdx52* mice compared to WT mice (negative component, $F(1,30) = 12.02$, $p < 0.005$; positive component, $F(1,30) = 7.96$, $p < 0.01$). Implicit times of mesopic Off-responses were also significantly different between genotypes. However, they were shorter in *mdx52* mice for the negative component ($F(1,30) = 7.96$, $p = 0.008$) and longer for the positive component ($F(1,30) = 12.72$, $p = 0.001$).

Photopic On- and Off-responses are shown in Fig. 3 C–D. As in the mesopic condition, the photopic On-response exhibited an initial small negative component followed by a larger positive component. However, the implicit times of the photopic components were substantially shorter than those of the mesopic responses. In contrast, the photopic Off-response only displayed a negative component. As for the mesopic responses, the amplitude of the negative component photopic On-response was similar in the two genotypes ($F(1,30) = 0.748$, $p > 0.3$), while its

positive component was significantly smaller in *mdx52* mice ($F(1,30) = 17.40$; $p < 0.001$). The amplitude of the negative wavelet of the photopic Off-response was reduced in *mdx52* mice (negative component $F(1,30) = 16.64$; $p < 0.001$). Implicit times of photopic sawtooth responses (Fig. 3 D, lower plots) were all significantly increased in *mdx52* mice (negative On-component: $F(1,30) = 42.26$, $p < 0.001$; positive On-component: $F(1,30) = 5.74$, $p < 0.05$; negative Off-component: $F(1,30) = 6.30$; $p < 0.05$).

In conclusion, sawtooth stimuli elicited responses that were largely reduced in amplitude and delayed in implicit times in *mdx52* mice.

3.3. ERGs to luminance sine-wave modulations

Sine-wave stimuli were used to test the post-receptoral cone-driven mechanisms that underlie temporal luminance processing. Responses to sine-wave modulation were used to analyze the first harmonic amplitudes and phases at 10 temporal frequencies from 3 to 30 Hz (Fig. 4 B). Mean amplitudes were reduced in *mdx52* mice compared to WT mice (genotype effect: $F(1,28) = 26.03$; $p < 0.001$; genotype x frequency interaction: $F(9,252) = 7.60$; $p < 0.001$). The relationship between phases and frequency were approximately linear, indicating that the response phases are mainly determined by a delay. The slopes of the linear regressions through the phase data are proportional to the apparent delay. The slopes of the linear regressions were 23.9 degree/Hz for *mdx52* and 24.5 degree/Hz for WT mice, corresponding to apparent delays of 66.46 ms and 68.14 ms, respectively.

Sine-wave responses

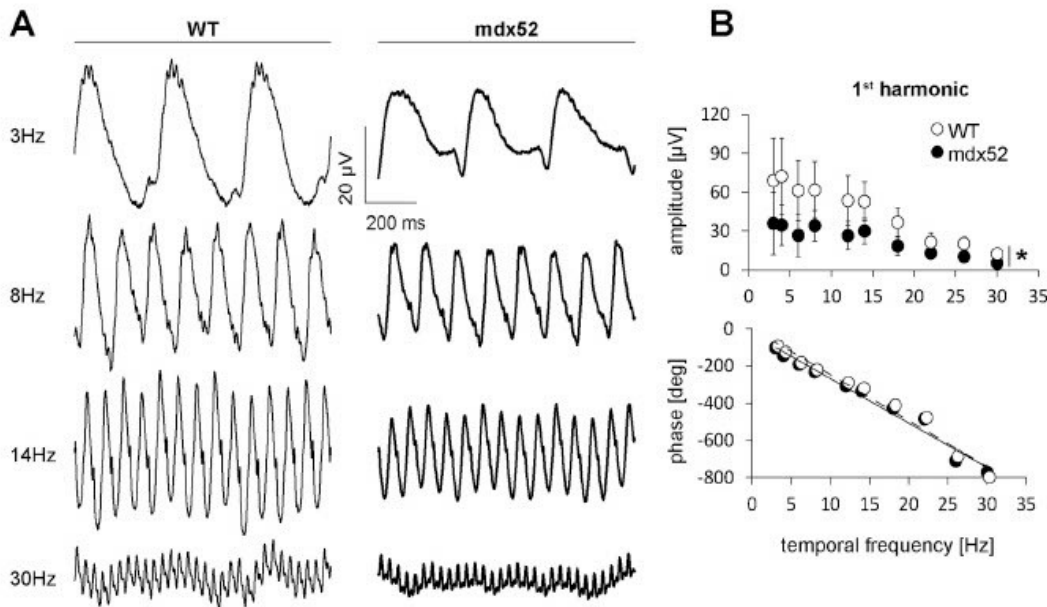


Fig. 4. Responses to sine-wave stimuli. (A) Averaged responses of WT (thin traces, left) and *mdx52* mice (bold traces, right) to sine-wave stimuli at 3, 8, 14 and 30 Hz. (B) Mean (\pm one standard deviation) first harmonic amplitudes (μ V, top) and phases (degrees, bottom) as a function of temporal frequency between 3 and 30 Hz in WT (open symbols) and *mdx52* mice (filled symbols). Response amplitudes were different between groups at all frequencies (marked with an asterisk; genotype effect: $p < 0.05$; two-group comparisons: all $p < 0.01$), phases were similar in the two groups. Linear regressions to the phase data are shown for *mdx52* (black line) and WT (dashed line) mice. Slopes of the linear regressions are 23.9 degree/Hz for *mdx52* and 24.5 degree/Hz for WT mice corresponding to apparent delays of 66.46 ms and 68.14 ms, respectively. Recordings made in 20 eyes of 10 *mdx52* mice and 12 eyes of 6 WT littermates.

Thus, *mdx52* mice displayed major alterations in the ERG amplitudes in response to sine-wave stimuli without a change in the delays.

3.4. Optomotor response (OMR)

The optomotor response (OMR) to achromatic sinusoidal gratings was measured. OMR indices were obtained from three trials, averaged for each mouse and group means \pm SEM were plotted as a function of spatial frequency (Fig. 5). Note that the OMR indices for both *mdx52* and WT mice were higher at 100% contrast (Fig. 5A) than at 50% contrast (Fig. 5B), indicating a stronger reflex at 100% contrast.

We then compared if the OMR values differed in the two groups. We excluded the OMR values at those spatial frequencies where they did not differ (Univariate *t*-test) from a value of one in both groups, because a value of one indicates no specific response to the stimulus. Therefore, at 100% of contrast the values at 0.012, 0.375, 0.4, 0.45, and 0.5 cpd were not included in the statistical analysis, whereas at 50% contrast those at 0.012, 0.375, and 0.4 cpd were not used.

At 100% contrast, there was no significant difference between genotypes (genotype effect: $F(1,14) = 3.291$; $p = 0.091$; genotypes \times frequencies interaction: $F(6,84) = 0.300$; $p = 0.935$), while OMR indices were significantly reduced in *mdx52* mice compared to WT at 50% contrast (genotype effect: $F(1,16) = 6.112$; $p = 0.025$; genotypes \times frequencies interaction: $F(6,96) = 1.754$; $p = 0.117$).

4. Discussion

The present report details the deficits in response to visual stimuli displayed by the *mdx52* mouse, a DMD transgenic model holding a deletion in a hotspot region of the *DMD* gene. We found that the deletion of exon 52 in this mouse is associated with: i) dark-adapted (scotopic) responses with reduced amplitude and delayed implicit times, particularly affecting the b-waves and oscillatory potentials; ii) diminished light-adapted (photopic) flash ERG responses; iii) reduced amplitudes and/or delayed implicit times of On- and Off-responses in mesopic and photopic conditions; iv) lower amplitudes of the fundamental harmonic components in ERG responses to sine-wave luminance modulation; and v) lower OMR indices with 50% contrast stimuli. We thus demonstrate that the cumulative loss of Dp427, Dp260 and Dp140 in the mouse retina leads to a complex impaired visual phenotype.

4.1. Profile of ERG alterations in *mdx52* mice

Our results indicate that both photoreceptor (the main contributor to the a-wave) and inner retina/bipolar cell (b-wave, OPs) functions are altered in scotopic conditions. Prolonged implicit times of the scotopic

b-wave were previously described in an ERG study in *mdx52* mice, but no significant amplitude reduction was reported (Kameya et al., 1997). In contrast, the results of our present study clearly demonstrate the presence of reduced a- and b-wave- as well as OP-amplitudes. The contradictory findings might be due to differences in the ERG methods, related to the use of a short dark-adaptation time (30 min) in the study of Kameya et al. (Kameya et al., 1997) compared to the longer adaptation (overnight) in the present study. In *mdx4Cv* mice, a mouse model with a mutation in exon 53 disrupting expression of the same dystrophins as in the *mdx52* mouse (Im et al., 1996), there was a trend toward a reduction in the b-wave amplitude (Pillers et al., 1999b). However, this reduction did not reach statistical significance, which might be attributable to the small number of recorded eyes (4–5 eyes). Furthermore, the authors used 5–6 months old mice and age effects on the ERGs cannot be excluded. Finally, they used congenic C57BL/6 mice as controls instead of littermates, making a comparison less straightforward.

Our data suggest that the prolonged implicit times of scotopic flash ERG responses, possibly reflecting a general delay in photoreceptor-to-bipolar cell transmission, are associated with the reduced amplitudes of the a- and b-waves and of the OPs. Reduced and delayed OPs may be a consequence of the changes in the signal transmission at the photoreceptor synapses. However, they may also reflect additional disturbances in amacrine cell feedback interactions (Wachtmeister and Dowling, 1978), because the reduction in OP amplitudes is larger than the reductions of the a- and b-waves (cf. Fig. 2B and D). This would be in line with the detection of Dp427 mRNAs in mouse amacrine cells (Wersinger et al., 2011). The reduced photopic flash ERGs indicate that cone driven responses are also affected.

In addition to flash ERGs defects, *mdx52* mice also showed diminished On- and Off-mediated sawtooth responses in both mesopic and photopic conditions, suggesting that the On- and Off-cone pathways are also defective. The reduced amplitudes of photopic sine-wave flicker responses further support that cone-driven post-receptoral systems are altered in *mdx52* mice. Furthermore, the phases in response to photopic sinusoidal stimuli were not altered indicating that, in contrast to the rod-driven pathways, cone-driven responses are not delayed. In agreement with this result, the implicit times in the photopic flashes were also not altered. The delay differences in the responses to the photopic sawtooth are relatively small and may suggest that the responses are partially still driven by rods. In conclusion, the loss of Dp427, Dp260 and Dp140 in *mdx52* mice results in a complex ERG phenotype characterized by multiple alteration of retinal physiological mechanisms which are likely to involve dysfunctions of both rod and cone photoreceptors but also of the bipolar and amacrine cells connected to them. Moreover, we cannot exclude an additional or downstream functional change of ganglion cells, due to expression of Dp427 in these cells (Bucher et al., 2019) and/

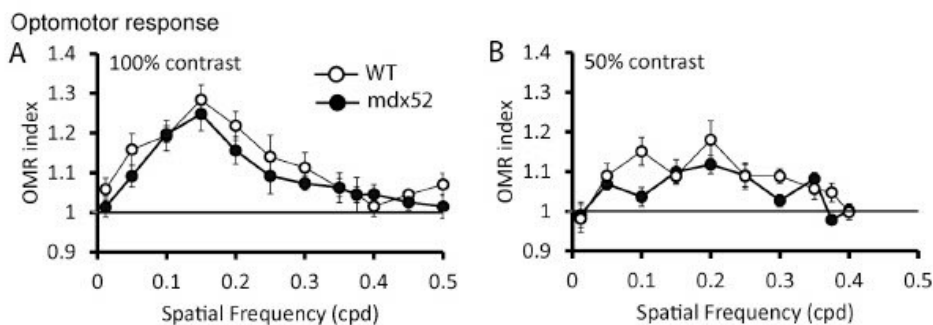


Fig. 5. Optomotor response. The mean OMR indices (\pm SEM) are plotted as a function of spatial frequency for each genotype. The baseline (1; horizontal line) represents unspecific head movements. OMR was measured in two distinct cohorts of *mdx52* (filled symbols) and WT littermate mice (open symbols) at 100% contrast (A, $n = 8$ per genotype) and 50% contrast (B, $n = 10$ *mdx52* and 8 WT littermate mice).

or due to secondary changes resulting from altered photoreceptor inputs.

4.2. Involvement of distinct retinal dystrophins in the *mdx52* phenotype

The abnormal dark- and light-adapted flash ERGs observed in *mdx52* mice indicate that part of the functional deficits may originate at the rod and cone synapses. This is in agreement with the finding that the absent dystrophins in this mouse model (Dp427, Dp260, and Dp140) are normally expressed in the outer plexiform layer (OPL) of the retina (Claudepierre et al., 1999; Rodius et al., 1997; Wersinger et al., 2011). However, the precise localization of the different dystrophins in the retina still remains to be specified, as it is currently based on the detection of their specific mRNA and immunolocalization using pan-specific antibodies that may recognize several dystrophins, due to high sequence homology among the shorter C-terminal dystrophins (Dp260, Dp140, Dp71). The current knowledge on the main expression patterns of dystrophins in retina are summarized in Fig. 1 and detailed below. It appears that some dystrophins may be expressed in several retinal layers and/or cell types, but there is also evidence in other tissues that a given cell type may express several dystrophins (e.g., (Aranmolate et al., 2017)). Single-cell transcriptomic profiling may likely help to specify the expression patterns of retinal dystrophins. However, many conventional single-cell RNA-seq technologies still suffer from inherent limitations regarding cell capture efficiency and specificity, capacity to recover complete transcriptomes and reliability to detect low-abundance transcripts. Nonetheless, the recent developments in single-cell sequencing strategies, allowing RNA 5' end or full-length coverage, will be more suitable for identification of the unique transcription start-site and precise annotation of each dystrophin promoter, as well as for effective quantification of transcript levels (Adiconis et al., 2018; Hestand et al., 2010; Liu and Trapnell, 2016). It has been suggested that the differences between the broad expression patterns revealed by in situ hybridization and the rather localized expression of dystrophins using immunohistochemistry might be due to scaffolding and microdomain concentration of dystrophin proteins (Kameya et al., 1997). In this context, transcriptomic approaches should therefore be complemented by development of specific antibodies and/or proteomic analyses (Choi et al., 2020) to better define expression levels of the distinct dystrophins and their spatial distribution in retinal layers.

Nevertheless, the main dystrophin proteins detected in retina, Dp427, Dp260, Dp140 and Dp71 clearly show preferential expression in distinct cell types and/or subcellular domains of the retina (Fig. 1 B) and are likely to play distinct roles in retinal structure and/or physiology. Hence, we propose that the ERG alterations in the *mdx52* model result from cumulative dysfunctions due to the absence of Dp427, Dp260 and Dp140. A previous histological examination of the *mdx52* mouse retina revealed normally organized retinal cells in an orderly layered anatomical arrangement, similar to WT and *mdx* mice (Kameya et al., 1997). Punctate staining of β -dystroglycan, the transmembrane component of the complex associated with dystrophins, was detected in the OPL of WT and *mdx* mice, but was absent in the *mdx52* OPL. This suggests an altered synaptic function between photoreceptors, bipolar and/or horizontal cells in *mdx52* mice, in agreement with our present ERG data. Although this suggested that Dp260 and/or Dp140 are necessary for dystroglycan localization in the OPL, mGluR6 was not affected, implying that the loss of these dystrophins may affect generation of the b-wave independently of accumulation or maintenance of mGluR6. The selective roles of the distinct dystrophins in retinal physiology still remain to be specified, yet the localization of dystrophins in several cell types and the comparison of ERG phenotypes among specific DMD mouse model enable to propose working hypotheses.

Retinal Dp427 is found in the OPL of the mouse retina in a greater amount in cone terminals compared to rod terminals (Wersinger et al., 2011). Its mRNA was also detected in the INL, suggesting expression in amacrine and bipolar cells. Accordingly, the selective loss of Dp427 in

mdx mice affects the structure of the first synapse between photoreceptor and bipolar cells, but recent studies also suggest impaired function of amacrine and ganglion cells (Catalani et al., 2020; Persiconi et al., 2020). Interestingly, *mdx* mice, at the same age as the *mdx52* mice in the present study, show minor reductions of the amplitudes of scotopic a- and b-wave and minor changes in photopic conditions and in 30 Hz flicker responses (Bucher et al., 2019). Functional studies in mice older than 6 months are scarce and their interpretation may be biased by the progression of muscular dystrophy leading to the appearance of confounding factors that may also impact the CNS (for instance inflammation, presence of higher levels of blood-circulating enzymes that may degrade cell extracellular matrix). Thus, older *mdx* mice (>15 months old) show greater reduction in flash response amplitudes attributed to additional stressors like hypoxia, perhaps related to the absence of Dp427 in vascular smooth muscles (Bucher et al., 2019). However, the amplitude changes that we report here in *mdx52* mice (between 35 and 60% for the b-wave and 20–55% for the a-wave) are much larger than in *mdx* mice (of maximally 23–26%). In conclusion, the selective absence of Dp427 in *mdx* mice during retinal development has a relatively small impact on its retinal physiology, leading to a phenotype that is substantially less severe than that found in the *mdx52* mouse. However, we cannot rule out a putative contribution of Dp427 loss to the reduced OP amplitudes, due to amacrine cell dysfunction.

Dp260 is selectively expressed in the retina (D'Souza et al., 1995) and its expression level progressively increases during the synaptic maturation phase in the developing retina (Rodius et al., 1997). Conversely, this is the only dystrophin whose expression progressively decreases concomitantly with photoreceptor degeneration in the RCS rat model (Claudepierre et al., 1999), suggesting a key role for Dp260 in synaptogenesis. Accordingly, Dp260 was detected in the mouse OPL in both rod and cone ribbon synapses around the invaginated On-bipolar cell dendritic tips (Fig. 1 C) (Blank et al., 1999; Wersinger et al., 2011). Delayed b-waves and OPs have been reported in *mdx^{2Cv}* mice lacking Dp427 and Dp260, but not in the Dp427-deficient *mdx* mouse, suggesting that increases in implicit times may be caused by Dp260 deficiency (Pillers et al., 1999a, 1999b). This may also explain the increased delays in the *mdx52* mouse.

A trend toward reduced amplitude of flash ERG responses was previously found in *mdx^{2Cv}* (lacking Dp427 and Dp260) and *mdx^{4Cv}* mice (lacking Dp427, Dp260 and Dp140). The changes in flash response amplitudes and implicit times were found to be comparable in the two mouse strains (Pillers et al., 1999b), suggesting that an additional loss of Dp140 does not aggravate the ERG alterations. In conclusion, these data support a main role for Dp260 but not for Dp140 in photoreceptor-to-bipolar cell transmission.

The role of Dp140 and its localization in the nervous system are poorly understood. Dp140 mRNA has been detected in the soma of photoreceptors, but no specific antibodies were available to determine protein expression at the cellular level. Moreover, it is possible that its expression is relatively low in adult tissue compared to other dystrophins, as it has been mostly detected in CNS during embryonic development (Morris et al., 1995). As mentioned above, the flash ERGs of *mdx^{2Cv}* and *mdx^{4Cv}* mice are comparable (Pillers et al., 1999b) suggesting a minor role of Dp140. However, in the present study we demonstrate significant changes in a-wave amplitude and implicit times that were not detected in the original study of *mdx^{4Cv}* mice but suggesting that Dp140 may aggravate the consequences of Dp427 loss. Likewise, a putative role of Dp140 in the altered sawtooth and sine-wave responses observed in *mdx52* mice cannot be ruled out. A more detailed ERG study in e.g. the *mdx^{2Cv}* mice (which do not lack Dp140) will be helpful to test this hypothesis.

Interestingly, the scotopic ERG in *mdx52* mice showed a shoulder on the ascending limb of the b-wave at the highest flash strength. This has also been reported in mouse models for congenital stationary night blindness (CSNB) with mutations in the *CACNA1F* gene in which the signal transmission in photoreceptor ribbon synapses is affected (Regus-

Leidig et al., 2014). This indicates that the physiological changes in the *mdx52* resembles those in the CNS models.

Retinal Dp71 is selectively expressed in Müller glial cells and plays an important role in retinal homeostasis due to its functional interactions with aquaporin-4 water channels and Kir4.1 potassium channels (Tadayoni et al., 2012). We recently found that a selective loss of Dp71 causes subtle amplitude reductions of the b-wave in scotopic and photopic flash ERGs and of the photopic sine-wave and On-mediated sawtooth responses, with no change in implicit times (Barboni et al., 2020). Interestingly, Dp71 is the only preserved dystrophin in the retina of *mdx52* mice. A comparison of ERG defects in *mdx52* mice and *mdx3Cv* mice lacking all dystrophins could be relevant to determine if the loss of Dp71 has a simple additive effect worsening the phenotype described here in *mdx52* mice. However, comparisons suggest more complex genotype-phenotype relationships. For example, we have shown here the presence of reduced a-wave amplitudes in *mdx52* mice, while this was not found in *mdx3Cv* mice. The light-adapted b-wave amplitudes were found to be reduced in *mdx52* mice (present study), in Dp71-null mice (Barboni et al., 2020) and in *mdx3Cv* mice. Response delays of light-adapted b-waves were only observed in *mdx3Cv* mice (Tsai et al., 2016), possibly as a result of the additional loss of Dp71 in these mice. In conclusion, there are some similarities, but also discrepancies between *mdx52*, Dp71-null and *mdx3Cv* mouse models, which do not favor the simple hypothesis that a cumulative loss of several dystrophins result in the addition of the effects induced by the loss of each dystrophin. This suggests more complex functional relationships between retinal dystrophins: The cumulative loss of several dystrophins may aggravate some phenotypes but also lead to distinct patterns of ERG alterations.

4.3. Altered vision of contrasts in *mdx52* mice

The innate optomotor response (OMR) to rotating sinusoidal luminance gratings were comparable in *mdx52* and WT mice at 100% contrast, but they were significantly reduced in *mdx52* mice at 50% contrast. Interestingly, this appears to have some translational relevance, because the visual acuity measured with standard high-contrast optotypes is preserved in DMD patients, while threshold contrasts to static gratings was increased (Costa et al., 2011). Impaired functional autophagy has been recently observed in ganglion cells from *mdx* mice (Catalani et al., 2020), indicating that the photoreceptor/bipolar cell defects due to Dp427 loss are not compensated and may affect neural pathways involved in OMR and visual sensitivity. However, it must be taken into account that distinct neural pathways lead to an OMR and to visual contrast sensitivity.

This apparent alteration of visual contrast sensitivity should be taken into consideration in future behavioral studies, since it may slightly affect performance in some tasks involving orientation and/or decision based on the processing of visual cues. OMRs have not been studied in other mouse models of DMD. The present results should therefore be considered a starting point for future work on DMD mouse models, to study the effects of dystrophin absence on retinal and central visual pathways and for comparisons with data obtained from DMD patients.

4.4. Relevance of the *mdx52* model for translational studies

Among DMD mouse models, the *mdx3Cv* mouse (Cox et al., 1993) has long been considered a standard model to study the effects of dystrophin down-regulation on retinal physiology (Pillers et al., 1995). The *mdx3Cv* mouse has a strongly reduced expression of all dystrophins due to a nonsense mutation in intron 65, and it displays a complex ERG phenotype resembling that of most DMD patients (Pillers et al., 1999b; Pillers et al., 1995; Tsai et al., 2016). However, this mouse model does not represent the most prevalent genetic condition in DMD patients, where the more frequent mutations (50% of patients) are within exons 43–55. The *mdx52* mouse, therefore, is likely a better model for DMD than the

mdx3Cv mouse. Importantly, the expression of dystrophins is not completely disrupted in *mdx3Cv* mice because they show residual dystrophin expression and reduced dysfunctions as compared to other models (Li et al., 2008; Vaillend and Ungerer, 1999). Moreover, the intronic mutation in *mdx3Cv* mice is not a target for genetic therapies based on exon-skipping strategies. On the other hand, *mdx52* mice have a deletion of exon 52 and are therefore better suited for future preclinical studies (Miyatake et al., 2018; Mizobe et al., 2018). Importantly, functional and preclinical studies in DMD mouse models currently involve early treatment administration in immature animals followed by evaluation of outcome measures after an optimal therapeutic window of several weeks or months, that is, at the same adult age at which we observed ERG defects and altered contrast vision in the present study. Our detailed characterization of the *mdx52* ERG phenotype may therefore be essential when developing tools for the genetic restoration of dystrophin proteins in the CNS.

In face of these considerations it is important to compare ERG data from patients with those of DMD mouse models. In humans, specific ERG alterations have not yet been extensively correlated with specific dystrophins expressed in the retina. Visual symptoms in DMD patients are less restrictive for daily routine than other limitations. However, increased life expectancy due to improved care and therapies of muscle dysfunction may increase the importance of concomitant treatment of retinopathies, as they may degrade progressively with age (Bucher et al., 2019).

The complex ERG phenotype of *mdx52* mice includes key features previously observed in DMD patients lacking several dystrophins due to mutations in the central and distal parts of the DMD gene, particularly with regard to the reduced amplitude of the flash ERG responses (Girlanda et al., 1997; Ino-ue et al., 1997; Jensen et al., 1995; Pascual Pascual et al., 1998; Pillers et al., 1999a; Ricotti et al., 2016a; Sigismund et al., 1994) and OP amplitudes (Tremblay et al., 1994). Similar to the findings in the *mdx52* mice, flash a-waves are less affected than b-waves in DMD patients (Ricotti et al., 2016a). In contrast, DMD patients holding mutations that alter expression of Dp427, Dp260 and Dp140 (similar as in the *mdx52* mouse), only show alterations in photopic On-responses (Barboni et al., 2013), whereas both photopic On- and Off-mediated ERG responses are affected in *mdx52* mice.

As mentioned above, the reduced contrast sensitivity for OMR triggering in *mdx52* mice may be compared with the reduced contrast sensitivity in DMD patients measured psychophysically (Barboni et al., 2013; Costa et al., 2011), even though OMRs and visual perception employ different neural pathways. To establish a better correlation between data from patients and from mouse models of DMD, it will be interesting to perform OMR measurements in DMD patients for a direct comparison.

5. Conclusion

This study highlights the need to reappraise visual dysfunction in both patients and mouse models of DMD with new methods allowing the collection of a detailed repertoire of ERG parameters and of measurements of contrast sensitivity. This is required to achieve powerful comparisons aiming at specifying the complex genotype-phenotype relationships due to the loss of distinct dystrophins. We unveiled that the *mdx52* model displays a profile of ERG alterations that cannot be inferred from previous studies in other mouse models of DMD. Our results suggest complex functional relationships among retinal dystrophins, where the cumulative loss of several dystrophins may aggravate some phenotypes but also lead to distinct patterns of ERG alterations. Importantly, the ERG profile of *mdx52* mice includes key features observed in DMD patients, which may represent relevant outcome measures and indications of CNS dysfunction for future preclinical studies.

Funding sources

This study was supported by the Centre National de la Recherche Scientifique (CNRS), the Université Paris-Sud (France), the DIM Gene Therapy Region Ile-de-France to JER, the Deutscher Akademischer Austauschdienst (DAAD #57513929) in Germany and Tempus Public Foundation in Hungary to JK and MTSB, the Sao Paulo Research Foundation (FAPESP # 2019/007771 to AMPL; 2016/04538-3 and 2014/26818-2 to DFV), the National Council for Scientific and Technological Development (CNPq grant number 404239/2016-1 to MTSB), a project award from the Association Monegasque contre les Myopathies (AMM, Monaco) to CV, a National Research, Development, and Innovation Fund of Hungary OTKA (PD134799), a fellowship from Campus France (dossier 931,824 L) and a short-term scientific mission from COST Action CA17103 to MTSB and a CNPq 1A productivity fellowship (CNPq 309,409/2015-2) to DFV.

Declaration of Competing Interest

The authors declare no competing interests.

Acknowledgements

We are grateful to Dr. Shin'ichi Takeda and Dr. Jun Tanihata (National Center of Neurology and Psychiatry, Tokyo, Japan) for kindly providing *mdx52* mouse breeders. We also thank the Zootecnic platform of the Institut des Neurosciences Paris Saclay for mouse breeding, care and genotyping.

References

- Adiconis, X., Haber, A.L., Simmons, S.K., Levy Moonshine, A., Ji, Z., Busby, M.A., Shi, X., Jacques, J., Lancaster, M.A., Pan, J.Q., Regev, A., Levin, J.Z., 2018. Comprehensive comparative analysis of 5'-end RNA-sequencing methods. *Nat. Methods* 15, 505–511. <https://doi.org/10.1038/s41592-018-0014-2>.
- Araki, E., Nakamura, K., Nakao, K., Kameya, S., Kobayashi, O., Nonaka, I., Kobayashi, T., Katuki, M., 1997. Targeted disruption of exon 52 in the mouse dystrophin gene induced muscle degeneration similar to that observed in Duchenne muscular dystrophy. *Biochem. Biophys. Res. Commun.* 238, 492–497. <https://doi.org/10.1006/bbrc.1997.7328>.
- Aranmolate, A., Tse, N., Colognato, H., 2017. Myelination is delayed during postnatal brain development in the *mdx* mouse model of Duchenne muscular dystrophy. *BMC Neurosci.* 18, 63. <https://doi.org/10.1186/s12868-017-0381-0>.
- Barboni, M.T.S., Nagy, B.V., de Araújo Moura, A.L., Damico, F.M., da Costa, M.F., Kremers, J., Ventura, D.F., 2013. ON and OFF electroretinography and contrast sensitivity in Duchenne muscular dystrophy. *Invest. Ophthalmol. Vis. Sci.* 54, 3195–3204. <https://doi.org/10.1167/iovs.13-11700>.
- Barboni, M.T.S., Martins, C.M.G., Nagy, B.V., Tsai, T., Damico, F.M., da Costa, M.F., de Cassia, R., Pavanello, M., Lourenço, N.C.V., de Cerqueira, A.M.P., Zatz, M., Kremers, J., Ventura, D.F., 2016. Dystrophin is required for proper functioning of luminance and red-green cone opponent mechanisms in the human retina. *Invest. Ophthalmol. Vis. Sci.* 57, 3581–3587. <https://doi.org/10.1167/iovs.16-19287>.
- Barboni, M.T.S., Vaillend, C., Joachimsthaler, A., Liber, A.M.P., Khabou, H., Roux, M.J., Vacca, O., Vignaud, L., Dalkara, D., Guillonnet, X., Ventura, D.F., Rendon, A., Kremers, J., 2020. Rescue of Defective Electroretinographic Responses in Dp71-null mice with AAV-mediated Reexpression of Dp71. *Invest. Ophthalmol. Vis. Sci.* 61, 11. <https://doi.org/10.1167/iovs.61.2.11>.
- Bladen, C.L., Salgado, D., Monges, S., Poncuberta, M.E., Kekou, K., Kosma, K., Dawkins, H., Lamont, L., Roy, A.J., Chamova, T., Guergueltcheva, V., Chan, S., Korogut, L., Campbell, C., Dai, Y., Wang, J., Barišić, N., Brabec, P., Lahdetie, J., Walter, M.C., Schreiber-Katz, O., Karcagi, V., Garani, M., Viswanathan, V., Bayat, F., Buccella, F., Kimura, E., Koeke, Z., van den Bergen, J.C., Rodrigues, M., Roxburgh, R., Lusakovska, A., Kostera-Pruszczyk, A., Zimowski, J., Santos, R., Neagu, E., Artemieva, S., Rasic, V.M., Vojinovic, D., Posada, M., Bloetzer, C., Jeannot, P.-Y., Joncourt, P., Díaz-Manera, J., Gallardo, E., Karaduman, A.A., Topaloglu, H., El Sherif, R., Stringer, A., Shatillo, A.V., Martin, A.S., Peay, H.L., Bellgard, M.I., Kirschner, J., Flanagan, K.M., Straub, V., Bushby, K., Verschuuren, J., Aartsma-Rus, A., Bérout, C., Lochmüller, H., 2015. The TREAT-NMD DMD global database: analysis of more than 7,000 Duchenne muscular dystrophy mutations. *Hum. Mutat.* 36, 395–402. <https://doi.org/10.1002/humu.22758>.
- Blank, M., Koulen, P., Blake, D.J., Kröger, S., 1999. Dystrophin and beta-dystroglycan in photoreceptor terminals from normal and *mdx3Cv* mouse retinae. *Eur. J. Neurosci.* 11, 2121–2133. <https://doi.org/10.1046/j.1460-9568.1999.00636.x>.
- Bucher, F., Friedlander, M.S., Aguilar, E., Kurihara, T., Krohne, T.U., Usui, Y., Friedlander, M., 2019. The long dystrophin gene product Dp427 modulates retinal function and vascular morphology in response to age and retinal ischemia. *Neurochem. Int.* 104489 <https://doi.org/10.1016/j.neuint.2019.104489>.
- Catalani, E., Bongioni, S., Taddei, A.R., Mezzetti, M., Silvestri, F., Cozzoli, M., Zecchini, S., Giovarelli, M., Perrotta, C., De Palma, C., Clementi, E., Ceci, M., Prantera, G., Cervia, D., 2020. Defects of full-length dystrophin trigger retinal neuron damage and synapse alterations by disrupting functional autophagy. *Cell. Mol. Life Sci.* <https://doi.org/10.1007/s00018-020-03598-5>.
- Choi, J.R., Yong, K.W., Choi, J.Y., Cowie, A.C., 2020. Single-cell RNA sequencing and its combination with protein and DNA analyses. *Cells* 9. <https://doi.org/10.3390/cells9051130>.
- Claudepierre, T., Rodius, F., Prasson, M., Fontaine, V., Picaud, S., Dreyfus, H., Mornet, D., Rendon, A., 1999. Differential distribution of dystrophins in rat retina. *Invest. Ophthalmol. Vis. Sci.* 40, 1520–1529.
- Collin, G.B., Gogna, N., Chang, B., Damkham, N., Pinkney, J., Hyde, L.F., Stone, L., Naggert, J.K., Nishina, P.M., Krebs, M.P., 2020. Mouse models of inherited retinal degeneration with photoreceptor cell loss. *Cells* 9. <https://doi.org/10.3390/cells9040931>.
- Costa, M.F., Barboni, M.T.S., Ventura, D.F., 2011. Psychophysical measurements of luminance and chromatic spatial and temporal contrast sensitivity in Duchenne muscular dystrophy. *Psychology & Neurosci.* 4, 67–74. <https://doi.org/10.3922/j.pnns.2011.1.008>.
- Cox, G.A., Phelps, S.F., Chapman, V.M., Chamberlain, J.S., 1993. New *mdx* mutation disrupts expression of muscle and nonmuscle isoforms of dystrophin. *Nat. Genet.* 4, 87–93. <https://doi.org/10.1038/ng0593-87>.
- Cuenca, N., Fernández-Sánchez, L., Campello, L., Manes, V., De la Villa, P., Lax, P., Pinilla, I., 2014. Cellular responses following retinal injuries and therapeutic approaches for neurodegenerative diseases. *Prog. Retin. Eye Res.* 43, 17–75. <https://doi.org/10.1016/j.preteyeres.2014.07.001>.
- Daoud, F., Candelario-Martínez, A., Billard, J.-M., Avital, A., Khelifaoui, M., Rozenvald, Y., Guegan, M., Mornet, D., Jaillard, D., Nudel, U., Chelly, J., Martínez-Rojas, D., Laroche, S., Yaffe, D., Vaillend, C., 2008. Role of mental retardation-associated dystrophin-gene product Dp71 in excitatory synapse organization, synaptic plasticity and behavioral functions. *PLoS One* 4, e6574. <https://doi.org/10.1371/journal.pone.0006574>.
- De Becker, L., Riddell, D.C., Dooley, J.M., Tremblay, F., 1994. Correlation between electroretinogram findings and molecular analysis in the Duchenne muscular dystrophy phenotype. *Br. J. Ophthalmol.* 78, 719–722. <https://doi.org/10.1136/bjo.78.9.719>.
- Desguerre, I., Christov, C., Mayer, M., Zeller, R., Becane, H.-M., Bastuji-Garin, S., Leturcq, F., Chiron, C., Chelly, J., Gherardi, R.K., 2009. Clinical heterogeneity of duchenne muscular dystrophy (DMD): definition of sub-phenotypes and predictive criteria by long-term follow-up. *PLoS One* 4, e4347. <https://doi.org/10.1371/journal.pone.0004347>.
- D'Souza, V.N., Nguyen, T.M., Morris, G.E., Karges, W., Pillers, D.A., Ray, P.N., 1995. A novel dystrophin isoform is required for normal retinal electrophysiology. *Hum. Mol. Genet.* 4, 837–842. <https://doi.org/10.1093/hmg/4.5.837>.
- Frishman, L.J., 2006. *Origins of the Electroretinogram*, in: Principles and Practice of Clinical Electrophysiology of Vision. MIT Press, Cambridge, pp. 139–183.
- Girlanda, P., Quararone, A., Buceti, R., Sinicropi, S., Macraione, V., Saad, F.A., Messina, L., Danielli, G.A., Ferreri, G., Vita, G., 1997. Extra-muscle involvement in dystrophinopathies: an electroretinography and evoked potential study. *J. Neurol.* 346, 127–132. [https://doi.org/10.1016/s0022-510x\(96\)00292-4](https://doi.org/10.1016/s0022-510x(96)00292-4).
- Harazny, J., Scholz, M., Buder, T., Lausen, B., Kremers, J., 2009. Electrophysiological deficits in the retina of the DBA/2J mouse. *Doc. Ophthalmol.* 119, 181–197. <https://doi.org/10.1007/s10633-009-9194-5>.
- Hauser, M.A., Chamberlain, J.S., 1996. Progress towards gene therapy for Duchenne muscular dystrophy. *J. Endocrinol.* 149, 373–378.
- Hestrand, M.S., Klingenhoff, A., Scherf, M., Ariyurek, Y., Ramos, Y., van Wokum, W., Suzuki, M., Werner, T., van Ommen, G.-J.B., den Dunnen, J.T., Harbers, M., 't Hoen, P.A.C., 2010. Tissue-specific transcript annotation and expression profiling with complementary next-generation sequencing technologies. *Nucleic Acids Res.* 38, e165 <https://doi.org/10.1093/nar/gkq602>.
- Hoffman, E.P., Brown, R.H., Kunkel, L.M., 1987. Dystrophin: the protein product of the Duchenne muscular dystrophy locus. *Cell* 51, 919–928.
- Im, W.B., Phelps, S.F., Copen, E.H., Adams, E.G., Slighton, J.L., Chamberlain, J.S., 1996. Differential expression of dystrophin isoforms in strains of *mdx* mice with different mutations. *Hum. Mol. Genet.* 5, 1149–1153. <https://doi.org/10.1093/hmg/5.8.1149>.
- Inoue, M., Honda, S., Nishio, H., Matsuo, M., Nakamura, H., Yamamoto, M., 1997. Genotype and electroretinal heterogeneity in Duchenne muscular dystrophy. *Exp. Eye Res.* 65, 861–864. <https://doi.org/10.1006/exer.1997.0389>.
- Jensen, H., Warburg, M., Sjög, O., Schwartz, M., 1995. Duchenne muscular dystrophy: negative electroretinograms and normal dark adaptation. Reappraisal of assignment of X linked incomplete congenital stationary night blindness. *J. Med. Genet.* 32, 348–351. <https://doi.org/10.1136/jmg.32.5.348>.
- Juan-Mateu, J., Gonzalez-Quereda, L., Rodriguez, M.J., Baena, M., Verdura, E., Nascimento, A., Ortiz, C., Baiget, M., Gallano, P., 2015. DMD mutations in 576 Dystrophinopathy families: a step forward in genotype-phenotype correlations. *PLoS One* 10, e0135189. <https://doi.org/10.1371/journal.pone.0135189>.
- Kameya, S., Araki, E., Katuki, M., Mizota, A., Adachi, E., Nakahara, K., Nonaka, I., Sakuragi, S., Takeda, S., Nabeshima, Y., 1997. Dp260 disrupted mice revealed prolonged implicit time of the b-wave in ERG and loss of accumulation of beta-dystroglycan in the outer plexiform layer of the retina. *Hum. Mol. Genet.* 6, 2195–2203.
- Koenig, M., Hoffman, E.P., Bertelson, C.J., Monaco, A.P., Feener, C., Kunkel, L.M., 1987. Complete cloning of the Duchenne muscular dystrophy (DMD) cDNA and preliminary genomic organization of the DMD gene in normal and affected individuals. *Cell* 50, 509–517.

- Kremers, J., Tanimoto, N., 2018. Measuring retinal function in the mouse. *Methods Mol. Biol.* 1753, 27–40. https://doi.org/10.1007/978-1-4939-7720-8_2.
- Kretschmer, F., Kretschmer, V., Kunze, V.P., Kretzberg, J., 2013. OMR-arena: automated measurement and stimulation system to determine mouse visual thresholds based on optomotor responses. *PLoS One* 8, e78058. <https://doi.org/10.1371/journal.pone.0078058>.
- Kretschmer, F., Sajjo, S., Kretschmer, V., Bades, T.C., 2015. A system to measure the optokinetic and Optomotor response in mice. *J. Neurosci. Methods* 256, 91–105. <https://doi.org/10.1016/j.jneumeth.2015.08.007>.
- Li, D., Yue, Y., Duan, D., 2008. Preservation of muscle force in Mdx3cv mice correlates with low-level expression of a near full-length dystrophin protein. *Am. J. Pathol.* 172, 1332–1341. <https://doi.org/10.2353/ajpath.2008.071042>.
- Liu, S., Trapnell, C., 2016. Single-cell transcriptome sequencing: recent advances and remaining challenges. *PLoS Res* 5. <https://doi.org/10.12688/pl000research.7223.1>.
- Miyatake, S., Mizobe, Y., Takizawa, H., Hara, Y., Yokota, T., Takeda, S., Aoki, Y., 2018. Exon skipping therapy using Phosphorodiamidate Morpholino oligomers in the mdx52 mouse model of Duchenne muscular dystrophy. *Methods Mol. Biol.* 1687, 123–141. https://doi.org/10.1007/978-1-4939-7374-3_9.
- Mizobe, Y., Miyatake, S., Takizawa, H., Hara, Y., Yokota, T., Nakamura, A., Takeda, S., Aoki, Y., 2018. In vivo evaluation of single-exon and multiexon skipping in mdx52 mice. *Methods Mol. Biol.* 1828, 275–292. https://doi.org/10.1007/978-1-4939-8651-4_17.
- Morris, G.E., Simmons, C., Nguyen, T.M., 1995. Apo-dystrophins (Dp140 and Dp71) and dystrophin splicing isoforms in developing brain. *Biochem. Biophys. Res. Commun.* 215, 361–367. <https://doi.org/10.1006/bbrc.1995.2474>.
- Pardue, M.T., Peachey, N.S., 2014. Mouse b-wave mutants. *Doc. Ophthalmol.* 128, 77–89. <https://doi.org/10.1007/s10633-013-9424-8>.
- Pascual Pascual, S.I., Molano, J., Pascual-Castroviejo, I., 1998. Electroretinogram in Duchenne/Becker muscular dystrophy. *Pediatr. Neurol.* 18, 315–320. [https://doi.org/10.1016/s0887-8994\(97\)00208-7](https://doi.org/10.1016/s0887-8994(97)00208-7).
- Perronet, C., Vaillend, C., 2010. Dystrophins, utrophins, and associated scaffolding complexes: role in mammalian brain and implications for therapeutic strategies. *J. Biomed. Biotechnol.* 2010, 849426. <https://doi.org/10.1155/2010/849426>.
- Persiconi, L., Cosmi, F., Guadagno, N.A., Lupo, G., De Stefano, M.E., 2020. Dystrophin Is Required for the Proper Timing in Retinal Histogenesis: A Thorough Investigation on the mdx Mouse Model of Duchenne Muscular Dystrophy. <https://doi.org/10.3389/fnins.2020.00760>.
- Pilgram, G.S.K., Potikanond, S., Baines, R.A., Pradkin, L.G., Noordermeer, J.N., 2010. The roles of the dystrophin-associated glycoprotein complex at the synapse. *Mol. Neurobiol.* 41, 1–21. <https://doi.org/10.1007/s12035-009-8089-5>.
- Pillers, D.A., Weleber, R.G., Woodward, W.R., Green, D.G., Chapman, V.M., Ray, P.N., 1995. mdxCv3 mouse is a model for electroretinography of Duchenne/Becker muscular dystrophy. *Invest. Ophthalmol. Vis. Sci.* 36, 462–466.
- Pillers, D.A., Fitzgerald, K.M., Duncan, N.M., Rash, S.M., White, R.A., Dwinell, S.J., Powell, B.R., Schnur, R.E., Ray, P.N., Gibis, G.W., Weleber, R.G., 1999a. Duchenne/Becker muscular dystrophy: correlation of phenotype by electroretinography with sites of dystrophin mutations. *Hum. Genet.* 105, 2–9.
- Pillers, D.A., Weleber, R.G., Green, D.G., Rash, S.M., Dally, G.Y., Howard, P.L., Powers, M.R., Hood, D.C., Chapman, V.M., Ray, P.N., Woodward, W.R., 1999b. Effects of dystrophin isoforms on signal transduction through neural retina: genotype-phenotype analysis of duchenne muscular dystrophy mouse mutants. *Mol. Genet. Metab.* 66, 100–110. <https://doi.org/10.1006/mgme.1998.2784>.
- Regus-Leidig, H., Atorf, J., Feigenspan, A., Kremers, J., Maw, M.A., Brandsstätter, J.H., 2014. Photoreceptor degeneration in two mouse models for congenital stationary night blindness type 2. *PLoS One* 9, e86769. <https://doi.org/10.1371/journal.pone.0086769>.
- Ricotti, V., Jigle, H., Theodorou, M., Moore, A.T., Muntoni, F., Thompson, D.A., 2016a. Ocular and neurodevelopmental features of Duchenne muscular dystrophy: a signature of dystrophin function in the central nervous system. *Eur. J. Hum. Genet.* 24, 562–568. <https://doi.org/10.1038/ejhg.2015.135>.
- Ricotti, V., Mandy, W.P.L., Scoto, M., Pane, M., Deconinck, N., Messina, S., Mercuri, E., Skuse, D.H., Muntoni, F., 2016b. Neurodevelopmental, emotional, and behavioural problems in Duchenne muscular dystrophy in relation to underlying dystrophin gene mutations. *Dev. Med. Child Neurol.* 58, 77–84. <https://doi.org/10.1111/dmcn.12922>.
- Rodius, P., Claudepierre, T., Rosat-Vargas, H., Cisneros, B., Montanez, C., Dreyfus, H., Mornet, D., Rendon, A., 1997. Dystrophins in developing retina: Dp260 expression correlates with synaptic maturation. *Neuroreport* 8, 2383–2387. <https://doi.org/10.1097/00001756-199707070-00056>.
- Sigsmund, D.A., Weleber, R.G., Pillers, D.A., Westall, C.A., Pantou, C.M., Powell, B.R., Heon, E., Murphy, W.H., Musarella, M.A., Ray, P.N., 1994. Characterization of the ocular phenotype of Duchenne and Becker muscular dystrophy. *Ophthalmology* 101, 856–865.
- Snow, W.M., Anderson, J.E., Jakobson, L.S., 2013. Neuropsychological and neurobehavioral functioning in Duchenne muscular dystrophy: a review. *Neurosci. Biobehav. Rev.* 37, 743–752. <https://doi.org/10.1016/j.neubiorev.2013.03.016>.
- Tadayoni, R., Rendon, A., Soria-Jasso, L.E., Cisneros, B., 2012. Dystrophin Dp71: the smallest but multifunctional product of the Duchenne muscular dystrophy gene. *Mol. Neurobiol.* 45, 43–60. <https://doi.org/10.1007/s12035-011-8218-9>.
- Taylor, P.J., Betts, G.A., Maroulis, S., Gillissen, C., Pedersen, R.L., Mowat, D.R., Johnston, H.M., Buckley, M.F., 2010. Dystrophin gene mutation location and the risk of cognitive impairment in Duchenne muscular dystrophy. *PLoS One* 5, e8803. <https://doi.org/10.1371/journal.pone.0008803>.
- Tremblay, F., De Becker, I., Dooley, J.M., Riddell, D.C., 1994. Duchenne muscular dystrophy: negative scotopic bright-flash electroretinogram but not congenital stationary night blindness. *Can. J. Ophthalmol.* 29, 274–279.
- Tsai, T.I., Barboni, M.T.S., Nagy, B.V., Roux, M.J., Rendon, A., Ventura, D.F., Kremers, J., 2016. Asymmetrical functional deficits of ON and OFF retinal processing in the mdx3cv mouse model of Duchenne muscular dystrophy. *Invest. Ophthalmol. Vis. Sci.* 57, 5788–5798. <https://doi.org/10.1167/iovs.16-19432>.
- Vaillend, C., Ungerer, A., 1999. Behavioral characterization of mdx3cv mice deficient in C-terminal dystrophins. *Neuromuscul. Disord.* 9, 296–304. [https://doi.org/10.1016/s0960-8966\(99\)00029-2](https://doi.org/10.1016/s0960-8966(99)00029-2).
- Wachtmeister, L., Dowling, J.E., 1978. The oscillatory potentials of the mudpuppy retina. *Invest. Ophthalmol. Vis. Sci.* 17, 1176–1188.
- Waite, A., Tinsley, C.L., Locke, M., Blake, D.J., 2009. The neurobiology of the dystrophin-associated glycoprotein complex. *Ann. Med.* 41, 344–359. <https://doi.org/10.1080/07853890802668522>.
- Werninger, E., Bordaïs, A., Schwab, Y., Sene, A., Bénard, R., Alunni, V., Sahel, J.-A., Rendon, A., Roux, M.J., 2011. Reevaluation of dystrophin localization in the mouse retina. *Invest. Ophthalmol. Vis. Sci.* 52, 7901–7908. <https://doi.org/10.1167/iovs.11-7519>.

2. RNA splicing modulation: Therapeutic progress and perspectives



médicine/sciences 2021 ; 37 : 625-31

» Les avancées en recherches génétique et génomique ne cessent d'accroître nos connaissances des maladies héréditaires. Un nombre croissant de ces maladies relève d'épissages aberrants qui représentent des cibles idéales pour les approches correctives centrées sur l'ARN. De nouvelles stratégies, en particulier médicamenteuses, visant à exclure ou à ré-inclure des exons lors du processus d'épissage, ont ainsi émergé et plusieurs molécules ont récemment obtenu des autorisations de mise sur le marché, notamment pour le traitement de la dystrophie musculaire de Duchenne et de l'amyotrophie spinale, suscitant de plus en plus d'intérêt et d'espoir. Parmi ces molécules, les oligonucléotides antisens, ou ASO, ont connu un réel essor et font l'objet de progrès constants en matière de modifications chimiques et de conception. Toutefois, leur biodistribution après administration par voie générale demeure souvent limitée, et le développement de chimies alternatives plus performantes et de nouveaux systèmes d'adressage est devenu un axe de recherche très actif. En parallèle, l'utilisation de petites molécules présentant une excellente biodistribution, ou de vecteurs viraux pour véhiculer les séquences antisens, est également explorée. Dans cette Synthèse, nous présentons les dernières avancées de ces approches de modulation d'épissage à travers deux exemples de maladies neuromusculaires. Nous discutons de leurs avantages et des principales limitations actuelles. «

Les stratégies thérapeutiques fondées sur la modulation de l'épissage de l'ARN messager (ARNm) sont actuellement en pleine expansion, notamment grâce à de récents succès dans le traitement de certaines maladies neuromusculaires. Au cours de la dernière

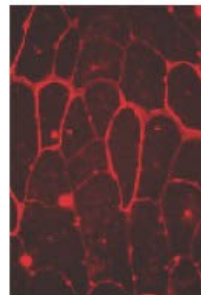
Vignette (Photo © Theresinha Evangelista).

m/s n° 6-7, vol. 37, juin-juillet 2021
<https://doi.org/10.1051/medsci/2021091>

Les approches thérapeutiques de modulation de l'épissage

Avancées et perspectives

Amel Saoudi^{1,2}, Aurélie Goyenvalle^{1,3}



¹Université Paris-Saclay, UVSQ, Inserm, END-ICAP, Handicap neuromusculaire - physiopathologie, biothérapie et pharmacologie appliquées, 78000 Versailles, France.

²Université Paris-Saclay, CNRS, Institut des neurosciences Paris Saclay, 91190 Gif-sur-Yvette, France.

³Laboratoire international associé Biothérapies appliquées aux handicaps neuromusculaires (LIA BAHN), Centre scientifique de Monaco, Monaco.
aurelie.goyenvalle@uvsq.fr

décennie, plusieurs molécules ont obtenu des autorisations de mise sur le marché (AMM) pour le traitement de la dystrophie musculaire de Duchenne (DMD) et de l'amyotrophie spinale (SMA), et de nouvelles générations de molécules sont désormais en cours de développement. La possibilité d'agir sur l'épissage des ARN pré-messagers (pré-ARNm) présente un intérêt majeur pour de nombreuses maladies génétiques causées par des mutations affectant l'épissage. La modulation de l'ARN repose sur l'utilisation de divers outils moléculaires, tels que des petites molécules actives, au premier rang desquelles les oligonucléotides antisens (ASO), qui peuvent être administrés directement ou véhiculés par des vecteurs viraux. Les ASO sont des oligonucléotides synthétiques de 12 à 30 nucléotides conçus pour se lier à un ARNm ou à un ARN non codant par appariement de bases Watson-Crick (guanine-cytosine et adénine-uracile), dans le but de moduler l'expression de ces ARN. Les ASO ont été utilisés pour la première fois en 1978 par Zamecnik et Stephenson afin d'inactiver l'expression des gènes [1], mais la technique a rapidement évolué, notamment grâce aux progrès faits en termes de modifications chimiques, ce qui a permis d'élargir considérablement les champs d'applications possibles. Alors que les premiers ASO, de type phosphodiester (PO) non modifiés, étaient rapidement dégradés dans la circulation sanguine, diverses modifications ont progressivement été introduites dans leur squelette/structure chimique afin d'augmenter leur stabilité et leur affinité pour l'ARN [2]. L'une des premières modifications a été le remplacement d'un des atomes d'oxygène du groupement phosphate PO₄ par un atome de soufre, créant ainsi des liens phosphorothioate (ou thiophosphate) (PS). Cette substitution a non seulement permis d'améliorer la résis-

REVUES



SYNTHÈSE

625

tance endogène des ASO aux nucléases, mais a aussi offert un avantage significatif en termes de pharmacocinétique. En effet, les ASO-PS (ASO de type phosphorothioate) présentent une affinité accrue pour de nombreuses protéines [3, 4], ce qui facilite leur distribution et leur absorption cellulaires par rapport à leurs homologues phosphodiester. Cependant, les modifications de type PS sont également connues pour être à l'origine d'effets indésirables dus à leur affinité pour certaines protéines plasmiques, conférant parfois aux ASO-PS un profil toxicologique indésirable [5]. Afin d'améliorer leur résistance aux nucléases et leur affinité pour les ARNm ciblés, des ASO de deuxième génération ont été alors développés, avec l'introduction de modifications chimiques en position 2' du ribose, telles que les 2'-méthyl (2'OMe) et 2'-méthoxyéthyl (2'MOE) [6], ou par des changements substantiels dans la structure du sucre, conduisant à une grande variété de molécules, comme les morpholinos (ou PMO pour *phosphoroamidate morpholino oligomer*) [7] et les oligonucléotides de type contraint (LNA pour *locked nucleic acid* [8] et cEt pour *2'-4'-constrained ethyl* [9]).

Ces avancées en matière de modifications chimiques ont incontestablement contribué au succès de certains ASO. Le domaine de la modulation d'épissage a cependant connu plusieurs tentatives infructueuses, mettant en évidence les limites des outils actuels.

Nous proposons ici de faire le point sur l'état actuel des thérapies fondées sur la modulation d'épissage et de mettre en perspectives leurs progrès récents à travers les développements précliniques et cliniques réalisés pour deux maladies : la dystrophie musculaire de Duchenne et l'amyotrophie spinale.

Le saut d'exon thérapeutique pour la dystrophie musculaire de Duchenne

La première approche de modulation de l'épissage à avoir été évaluée en clinique fut le saut d'exon thérapeutique développé pour traiter la dystrophie musculaire de Duchenne (DMD). La DMD est une maladie neuromusculaire sévère liée au chromosome X et affectant 1 naissance sur 5 000 naissances d'enfants de sexe masculin. Elle se caractérise par une faiblesse musculaire progressive et une dégénérescence des muscles, dues à des mutations dans le gène *DMD*, qui modifient le cadre de lecture et empêchent la production de la dystrophine, une protéine qui joue un rôle mécanique et signalétique entre le cytosquelette d'actine et la matrice extracellulaire. L'approche du saut d'exon thérapeutique pour la DMD vise à éliminer un exon lors de l'épissage, en utilisant des ASO masquant les sites d'épissage, afin de restaurer le cadre de lecture original, ce qui permet la production d'une dystrophine, parfois nommée quasi-dystrophine, qui, bien que légèrement tronquée, reste fonctionnelle (Figure 1). Plusieurs chimies d'ASO ont été développées pour la DMD dans le but d'augmenter la stabilité des ASO et leur affinité pour l'ARN cible. Parmi celles-là, le 2'OMe chargé (ou drisapersen) et le PMO non chargé (ou étéplirsén) ont été les premiers ASO utilisés pour cibler l'exon 51 du gène *DMD*. Malgré des résultats encourageants dans les études cliniques initiales [10], un grand essai de phase III évaluant l'administration par voie sous-cutanée du drisapersen n'a pas démontré

d'avantages cliniques significatifs ni d'augmentation évidente de la dystrophine [11]. Ces résultats décevants, ainsi que l'observation de certains effets secondaires, tels qu'une protéinurie et des réactions au niveau du site d'injection, ont conduit la *Food and Drugs Administration* (FDA) des États-Unis à rejeter le drisapersen, conduisant ainsi à l'arrêt de tous les programmes cliniques utilisant des 2'OMe pour la DMD, y compris ceux ciblant d'autres exons (les exons 45, 44 et 53).

En revanche, l'injection du PMO (étéplirsén) par voie intraveineuse a conduit à des niveaux de production faibles mais significatifs de la dystrophine, ce qui lui a permis d'obtenir en décembre 2016, non sans controverse, une autorisation de mise sur le marché de la FDA, l'étéplirsén devenant ainsi le premier ASO modulateur d'épissage à être approuvé aux États-Unis [12]. D'autres ASO de type PMO, ciblant l'exon 53 ont, par la suite, été approuvés par la FDA en décembre 2019 (golodirsén) et en août 2020 (viltolarsén) sur la base d'une faible restauration de dystrophine (en moyenne 1 % pour le golodirsén et 2,8 % pour le viltolarsén chez les patients traités par 80 mg/kg de PMO) [13, 14]. Un autre PMO ciblant l'exon 45 (le casimersén) vient également d'être approuvé par la FDA en février 2021 sur la base d'une restauration de dystrophine de 1,7 %¹ chez les patients traités par 30 mg/kg de PMO. En dépit de ces apparents succès, les niveaux de dystrophine restaurés dans les biopsies de patients traités par ces PMO restent extrêmement faibles et, en 2018, l'Agence européenne des médicaments (AEM) a émis un avis négatif concernant l'étéplirsén [12], jugeant que le rapport bénéfice-risque actuel n'était pas positif et que l'utilisation de la dystrophine comme biomarqueur était encore prématurée. Afin de fournir des preuves concluantes de l'efficacité clinique de ces molécules, de vastes études de phase III contrôlées contre placebo sont en cours avec l'étéplirsén, le golodirsén et le casimersén.

L'une des limitations principales des ASO de première génération demeure leur adressage médiocre aux tissus cibles, comme les muscles squelettiques ou le cœur. Il a notamment été montré que l'absorption musculaire des PMO dépendait de la présence de foyers inflammatoires associés aux lésions dystrophiques, ainsi que de la fusion des myoblastes et des monocytes chargés en PMO au voisinage des fibres musculaires endommagées [15]. L'amélioration de l'adressage des ASO à leurs tissus cibles représente aujourd'hui un défi majeur dans

¹ Résultats non publiés communiqués par Sarepta : <https://investorrelations.sarepta.com/news-releases/news-release-details/sarepta-therapeutics-announces-positive-expression-results>.

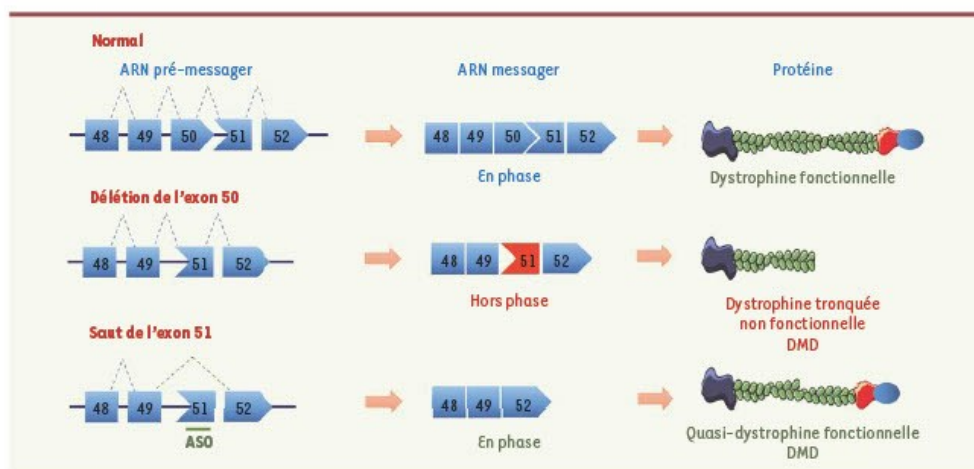


Figure 1. Principe du saut d'exon thérapeutique pour le traitement de la DMD. L'utilisation d'ASO vise à masquer les sites clés d'épissage, afin d'exclure un exon (par exemple, ici, l'exon 51) pour restaurer le cadre de lecture de l'ARNm DMD, permettant ainsi la synthèse d'une protéine quasi-dystrophine, légèrement plus courte que la dystrophine, mais tout de même fonctionnelle (similaire aux quasi-dystrophines produites par les patients atteints de myopathie de Becker).

le domaine de la modulation d'épissage thérapeutique ; de nouvelles générations de molécules antisens visant à relever ce défi sont en cours de développement [16].

Nouvelles générations d'ASO et alternatives à l'adressage

Des ASO dits « stéréopurs » ont récemment été développés dans le but d'optimiser les propriétés de biodistribution des ASO présentant des liaisons PS ainsi que leur profil toxicologique. Étant donné que le squelette phosphorothioate est chiral, un ASO-PS de 20 nucléotides est en fait un mélange de 2¹⁹ stéréoisomères différents qui ne sont pas tous aussi efficaces, ni bien tolérés. Un ASO « stéréopur » a été ainsi sélectionné en fonction de la chiralité R ou S de chaque phosphate. Un candidat « stéréopur » optimisé pour le saut de l'exon 51 (suvodirsén) a ainsi démontré une restauration de dystrophine bien supérieure (environ 52 % de restauration *versus* 1 % obtenu avec les autres types d'ASO) dans des cellules isolées de patients présentant une DMD. Cependant, son évaluation clinique en phase II/III (NCT03907072) n'a montré aucune induction de l'expression de la dystrophine après des administrations intraveineuses, et le développement clinique du suvodirsén pour la DMD a été suspendu.

La recherche de chimies alternatives d'ASO a conduit à l'identification des tricyclo-ADN (tcDNA) comme des ASO prometteurs pour les approches de modulation d'épissage thérapeutiques [17, 18]. Les tricyclo-ADN sont des analogues synthétiques de conformation contrainte, ayant notamment démontré des propriétés de biodistribution intéressantes, y compris une capacité à franchir la barrière hémato-encéphalique après une administration par voie générale [19] (→).

(→) Voir la Nouvelle de A. Ceylan et al., *m/s* n° 3, mars 2015, page 253

Cet avantage ouvre des perspectives uniques de pouvoir traiter à la fois la maladie musculaire et les comorbidités de la DMD dues à l'absence de dystrophine dans le cerveau. Un essai clinique de phase I/II est programmé en France pour fin 2021 par la société *SQY Therapeutics*.

La conjugaison des ASO à des peptides facilitant leur pénétration dans les cellules (appelés CPP pour *cell-penetrating peptide*) ou à des anticorps, tels que ceux ciblant le récepteur de la transferrine [20], est également étudiée pour améliorer une administration ciblée. Les CPP sont de courts peptides cationiques et/ou amphipathiques, qui facilitent la translocation des ASO à travers les membranes cellulaires ainsi que leur sortie des endosomes. Certains de ces ASO conjugués à de tels peptides, tels que les PPMO (*peptide-conjugated phosphoramide morpholino oligomer*) ont démontré une efficacité très supérieure à leurs homologues non conjugués, permettant notamment une restauration significative de la production de dystrophine dans le cœur de souris modèles de la maladie [21]. Une étude de phase I/II est actuellement en cours avec un PPMO ciblant l'exon 51, et *Sarepta Therapeutics* a récemment communiqué des résultats préliminaires encourageants, notamment en comparaison de patients traités par l'éteplirsén (le PMO équivalent, mais non conjugué à un peptide).

Afin de pérenniser l'effet des ASO, et ainsi d'éviter la nécessité d'une administration récurrente (potentiellement à vie), il a été proposé de vectoriser les séquences antisens dans des vecteurs recombinants dérivés des virus adéno-associés (AAV). Pour cela, les séquences antisens sont insérées dans un ARN U7snRNA (*U7 small-nuclear RNA*) optimisé. L'ARN U7snRNA est un petit ARN nucléaire non codant qui est naturellement impliqué dans la maturation des pré-ARNm des histones. Pour en faire un outil de modulation d'épissage, la séquence antisens naturelle du U7snRNA est remplacée par une séquence antisens d'intérêt (ciblant par exemple un exon du gène *DMD*). Grâce à cette inclusion dans l'ARN U7snRNA, et sa vectorisation dans un vecteur de type AAV, la séquence antisens est directement adressée et exprimée dans le noyau, de façon continue sous le contrôle du promoteur naturel de l'ARN U7snRNA. Des études précliniques, réalisées dans des modèles murins de DMD [19, 22] et chez le chien *Golden retriever muscular dystrophy* (GRMD)² [23, 24], ont montré que cette approche permet une localisation subcellulaire appropriée des séquences antisens avec les pré-ARNm, grâce à l'accumulation des particules U7snRNP dans le noyau [25], ainsi qu'une restauration de l'expression de dystrophine jusqu'à cinq ans post-injection chez le chien GRMD. À la suite de ces résultats encourageants, un essai clinique de phase I/II (NCT04240314) pour le saut de l'exon 2 a été entrepris chez des patients atteints de DMD et présentant une duplication de cet exon. Les duplications d'exon représentent en effet 11 % des mutations touchant le gène *DMD*, et la duplication de l'exon 2 est la plus commune chez les patients [26]. Le saut d'exon ciblant les duplications vise à restaurer une dystrophine complète et donc entièrement fonctionnelle, ce qui présente un avantage significatif par rapport aux quasi-dystrophines résultant de l'élimination d'exon(s) interne(s) pour corriger le cadre de lecture ou les mutations non-sens. Les résultats préliminaires de cette étude de phase I/II ont été présentés lors du 25^e congrès de la *World Muscle Society* (WMS) en octobre 2020 [27] et ont révélé, chez les 2 patients traités, une diminution de respectivement 95 % et 81 % des niveaux de créatine kinase sérique (typiquement élevés chez les patients atteints de DMD) à trois mois post-injection, et une réexpression respective de 5,8 % et 1,4 % de dystrophine, confirmant le potentiel thérapeutique de cette approche vectorisée. L'ensemble des données désormais disponibles sur les thérapies de modulation d'épissage pour la DMD suggère que l'adressage ciblé des ASO médicaments représente la limitation majeure qui entrave leur efficacité lorsqu'ils sont administrés par voie générale. En revanche, pour d'autres maladies neuromusculaires, telles que la SMA, pour laquelle les motoneurones sont les principales cellules cibles, ce problème d'adressage a pu être contourné en utilisant une voie d'administration ciblée et a ainsi conduit à des succès beaucoup plus marquants.

La modulation d'épissage pour l'amyotrophie spinale

L'amyotrophie spinale (SMA) est une maladie autosomique récessive du motoneurone avec une incidence de 1/10 000 naissances. Elle est

causée par des mutations dans le gène *SMN1* (*survival motor neuron 1*) codant la protéine SMN, impliquée dans la maturation des ARNm via l'assemblage du spliceosome. Les patients atteints de SMA sont classés en 4 groupes (type 1 à 4) selon l'âge de début de la maladie et l'importance du déficit de la force musculaire, mais la variante la plus commune est la SMA de type 1, qui représente 60 % des cas. Elle affecte les nourrissons, qui n'acquièrent jamais la capacité de s'asseoir et survivent rarement au-delà de l'âge de 2 ans. Il existe une copie centromérique du gène, appelée *SMN2*, qui ne diffère du gène *SMN1* que par quelques nucléotides, dont une substitution C->T qui entraîne un épissage alternatif de l'exon 7 et qui ne permet la production que de 10 % de protéine SMN, une production insuffisante pour contrebalancer le manque de SMN et maintenir la survie et le fonctionnement normal des motoneurones. Diverses thérapies incluant des ASO et des petites molécules ont été mises au point pour moduler l'épissage du gène *SMN2* et permettre la ré-inclusion de cet exon 7 afin de produire davantage de protéine SMN (Figure 2).

Les ASO pour l'amyotrophie spinale

Plusieurs classes d'ASO ont été développées pour interférer avec l'épissage de l'ARNm *SMN2*, parmi lesquelles un ASO de type 2^{MOE-PS} de 18 nucléotides, nommé nusinersen (commercialisé sous le nom de Spinraza®). Celui-ci a démontré des résultats particulièrement prometteurs, initialement dans les modèles murins de SMA [28-30], puis dans les études cliniques. Tout comme les autres ASO utilisés actuellement en clinique, le nusinersen ne traverse pas la barrière hématoencéphalique et nécessite des injections intrathécales directes, administrées sous la forme d'une phase de chargement (4 administrations sur une période de deux mois), suivie d'injections trimestrielles. Plusieurs essais cliniques randomisés ont été réalisés par *Ionis pharmaceuticals* et *Biogen*, et ont permis de démontrer l'efficacité du nusinersen chez plusieurs centaines de patients atteints de SMA [31] (→).

(→) Voir la Synthèse de E. Gargaun, m/s hors série n° 2, novembre 2019, page 11

Dans l'étude multicentrique ENDEAR de phase III, en double aveugle, la survie et l'acquisition de nouvelles capacités psychomotrices chez des patients SMA de type 1 ont notamment conduit à l'interruption prématurée de l'étude contrôlée contre placebo, permettant ainsi à tous les participants de recevoir le médicament. Le nusinersen a été approuvé par la FDA fin décembre 2016 et par l'AEM en juin 2017. Il représente probablement le plus grand succès de la thérapie à base d'ASO. Toutefois, plusieurs défis demeurent et, bien que le nusi-

² Ce modèle de chien atteint de myopathie de Duchenne présente spontanément une anomalie dans le gène *DMD* ; il s'agit d'une mutation entraînant la perte de l'exon 7 du gène.

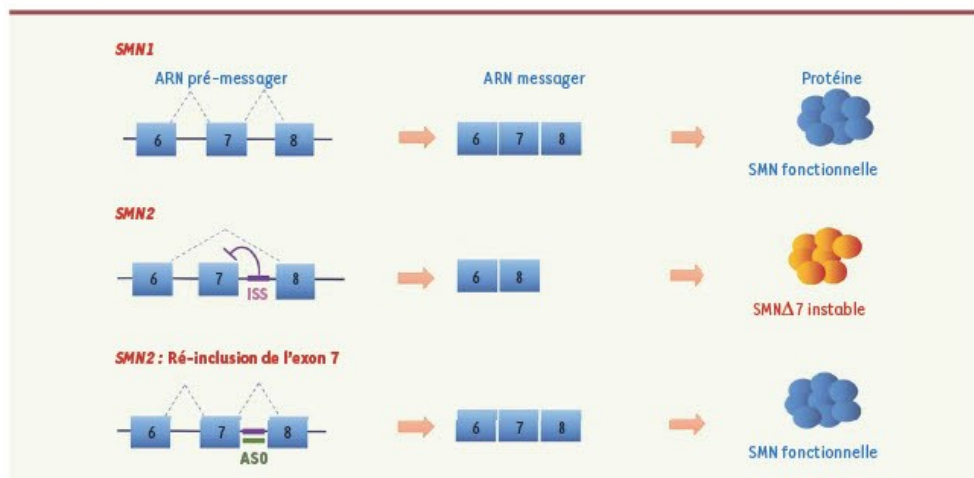


Figure 2. Modulation de l'épissage de SMN2 pour le traitement de l'amyotrophie spinale (SMA). L'utilisation d'ASO ou de petites molécules dans le contexte de la SMA vise à renforcer l'inclusion de l'exon 7 dans l'ARNm SMN2 afin de produire une protéine SMN fonctionnelle. ISS : motif intronique inhibiteur d'épissage (*Intronic splicing silencer*).

nersen induise une amélioration clinique robuste et significative chez les patients atteints de SMA de type 1 (mesurée par une réponse positive significative du test HINE [*Hammersmith Infant Neurological Examination*]), de nombreux enfants conservent un handicap résiduel significatif en raison du stade avancé de la maladie avant le début du traitement. Dans ce cadre, les résultats d'une étude de phase II en cours chez des nourrissons pré-symptomatiques susceptibles de développer une SMA de type 1 ou 2, a fourni des données extrêmement encourageantes sur l'efficacité d'un traitement pré-symptomatique, puisque 88 % des patients traités sont parvenus à marcher de manière indépendante [32]. Au vu de ces résultats exceptionnels, le dépistage néonatal de la maladie a commencé dans de nombreux pays.

Néanmoins, le mode d'administration actuel par injections intrathécales ne permet pas de traiter l'atteinte d'organes périphériques rapportée dans la SMA, telle que les dysfonctionnements cardiaques, et représente également un risque de lésions tissulaires ou d'infection après de multiples administrations. Des chimies alternatives d'ASO telles que les PPM0 [33] ou les tcDNA [18] ont démontré leur capacité à franchir la barrière hémato-encéphalique après administration par voie générale, notamment dans des modèles de souris SMA de type 3, permettant d'envisager un bénéfice thérapeutique suite à des injections intraveineuses plutôt qu'intrathécales. Au-delà de ces nouvelles générations d'ASO, de petites molécules très prometteuses ont également été développées pour moduler l'ARNm de SMN2.

Les petites molécules pour l'amyotrophie spinale

Le risdiplam est une petite molécule issue de la recherche du laboratoire *PTC Therapeutics* et développée par le laboratoire *Roche/Genentech*, permettant de moduler l'épissage de l'exon 7 du gène

SMN2 et ainsi de favoriser son inclusion dans l'ARNm de SMN2, via le renforcement de l'interaction entre le spliceosome (ou épissosome) et le site d'épissage 5' (5'SS) de l'exon 7 de SMN2 [34]. Le risdiplam permet en effet de stabiliser une adénine non hybridée au niveau de la jonction exon-intron, transformant ainsi le 5'SS « faible » de l'exon 7 en un site d'épissage nettement plus fort. Ce type de composés étant capable de traverser la barrière hémato-encéphalique avec une excellente biodistribution [35], le risdiplam peut être administré par voie orale, ce qui présente un avantage indiscutable pour les patients. Les résultats préliminaires de deux essais internationaux de phase II/III (l'essai FIREFISH dans la SMA de type 1 et l'essai SUNFISH randomisé, en double aveugle contre placebo, dans la SMA de type 2 ou 3) ont confirmé l'efficacité du risdiplam sur les fonctions motrices et respiratoires des patients. Sur la base de ces résultats, la FDA a accordé une AMM au risdiplam le 7 août 2020 pour les SMA de type 1, 2 et 3 aux États-Unis. Il est commercialisé sous le nom de *Evsrydi®*. En Europe, *Roche* a déposé une demande d'AMM en août 2020 à l'AEM qui a accepté une évaluation accélérée, ce qui signifie que le processus d'évaluation peut être ramené de 15 à 9 mois. Des essais sont actuellement toujours en cours pour évaluer ce médicament sur un grand groupe de patients atteints de SMA, représentatifs de la population concernée par cette maladie : les essais FIREFISH et SUNFISH se poursuivent ; l'essai JEWELFISH est en cours chez des

patients âgés de 6 mois à 60 ans, ayant déjà été traités par d'autres molécules, et l'essai RAINBOWFISH est en cours chez des nourrissons âgés de moins de 6 semaines et pré-symptomatiques. Une autre molécule modifiant la maturation de l'ARNm *SMN2*, le branaplam, a été identifiée par *Novartis Pharmaceuticals* lors d'un crible à haut débit. Elle permet de stabiliser l'interaction entre l'épissosome et le pré-ARNm *SMN2* [36]. En raison des résultats encourageants obtenus dans un modèle sévère de souris SMA, démontrant une augmentation significative de l'expression de la protéine SMN et de la survie des animaux, le branaplam est actuellement en cours d'évaluation clinique chez des patients SMA de type I (NCT02268552).

Conclusions et perspectives

Les thérapies par modulation d'ARN ont fait des progrès impressionnants au cours des dernières années, comme l'illustrent les récentes autorisations de mise sur le marché de plusieurs médicaments, et le nombre croissant d'essais cliniques évaluant ce type de stratégie. Ces succès récents suscitent optimisme et espoir pour le développement de futures thérapies de modulation d'épissage. Cependant, le bénéfice clinique de ces approches dépend de façon critique du tissu ciblé et de la voie d'administration, notamment dans le cas des oligonucléotides antisens (ASO). En effet, le potentiel thérapeutique des ASO administrés par voie générale est bien loin de celui obtenu avec des ASO injectés localement, comme en témoigne le succès du nusinersen, administré par voie intrathécale, comparé à l'effet beaucoup plus mitigé induit par l'éteplirsen pour la DMD, qui n'a d'ailleurs toujours pas reçu d'AMM en Europe. Cela s'explique par la biodistribution extrêmement limitée des ASO injectés par voie générale : il est estimé que seulement 1 % environ des ASO atteint le compartiment cellulaire ciblé (comme les muscles squelettiques ou cardiaque) après une administration par voies intraveineuse ou sous-cutanée [37]. L'amélioration de la distribution ciblée (en particulier au système nerveux central ou au muscle cardiaque, dans le cas des maladies neuromusculaires) représente aujourd'hui le principal défi identifié dans le domaine de la modulation d'épissage induite par les ASO. Le développement de chimies alternatives plus performantes ou de nouveaux systèmes d'administration est devenu un axe de recherche très actif ces dernières années [16]. Le développement récent et la commercialisation d'ASO incorporant des conjugués GalNAc (N-acétylgalactosamine), présentant une supériorité thérapeutique de 20 à 30 fois, ont confirmé la possibilité de créer de meilleurs ASO. Inspirée par le succès des conjugués GalNAc, la conjugaison d'ASO à divers ligands, tels que des peptides, des lipides et des anticorps, est actuellement explorée [38], et ouvre la voie vers de futures thérapies toujours plus innovantes. ♦

SUMMARY

RNA splicing modulation: Therapeutic progress and perspectives

Advances in genetic and genomic research continue to increase our knowledge of hereditary diseases, and an increasing number of them are being attributed to aberrant splicing, thus representing ideal

targets for RNA modulation therapies. New strategies to skip or re-include exons during the splicing process have emerged and are now widely evaluated in the clinic. Several drugs have recently been approved in particular for the treatment of Duchenne muscular dystrophy and spinal muscular atrophy. Among these molecules, antisense oligonucleotides, or ASOs, have gained increasing interest and have constantly been improved over the years through chemical modifications and design. However, their limited biodistribution following systemic administration still represents a major hurdle and the development of more potent alternative chemistries or new delivery systems has become a very active line of research in the past few years. In parallel, the use of small molecules with excellent biodistribution properties or of viral vectors to convey antisense sequences is also being investigated. In this review, we summarize the recent advances in splicing therapies through two examples of neuromuscular diseases and we discuss their main benefits and current limitations. ♦

LIENS D'INTÉRÊT

Les auteurs déclarent n'avoir aucun lien d'intérêt concernant les données publiées dans cet article.

RÉFÉRENCES

- Zamecnik PC, Stephenson ML. Inhibition of Rous sarcoma virus replication and cell transformation by a specific oligodeoxynucleotide. *Proc Natl Acad Sci USA* 1978 ; 75 : 280-4.
- Wickstrom E. Oligodeoxynucleotide stability in subcellular extracts and culture media. *J Biochem Biophys Methods* 1986 ; 13 : 97-102.
- Gaus HJ, Gupta R, Chappell AE, et al. Characterization of the interactions of chemically-modified therapeutic nucleic acids with plasma proteins using a fluorescence polarization assay. *Nucleic Acids Res* 2019 ; 47 : 1110-22.
- Crooke ST, Wang S, Vickers TA, et al. Cellular uptake and trafficking of antisense oligonucleotides. *Nat Biotechnol* 2017 ; 35 : 230-7.
- Crooke ST, Baker BF, Witztum JL, et al. The effects of 2'-O-methoxyethyl containing antisense oligonucleotides on platelets in human clinical trials. *Nucleic Acid Ther* 2017 ; 27 : 121-9.
- Gayenwalle A, Leumann C, Garcia L. Therapeutic Potential of Tricyclo-DNA antisense oligonucleotides. *J Neuromuscul Dis* 2016 ; 3 : 157-67.
- Summerton J, Weller D. Morpholino antisense oligomers: design, preparation, and properties. *Antisense Nucleic Acid Drug Dev* 1997 ; 7 : 187-95.
- Hagedorn PH, Persson R, Funder ED, et al. Locked nucleic acid: modality, diversity, and drug discovery. *Drug Discov Today* 2018 ; 23 : 101-14.
- Seth PP, Smlkowski A, Allerson CR, et al. Design, synthesis and evaluation of constrained methoxyethyl (cmOE) and constrained ethyl (cEt) nucleoside analogs. *Nucleic Acids Symp Ser (Oxf)* 2008 ; 553-4.
- Goemans NM, Tulinius M, Akker JT van der, et al. Systemic administration of PRO051 in Duchenne's muscular dystrophy. *N Engl J Med* 2011 ; 364 : 1513-22.
- Goemans M, Mercuri E, Belousova E, et al. A randomized placebo-controlled phase 3 trial of an antisense oligonucleotide, disaspersen, in Duchenne muscular dystrophy. *Neuromuscul Disord* 2018 ; 28 : 4-15.
- Aartsma-Rus A, Goemans N. A sequel to the Eteplirsen saga: eteplirsen is approved in the United States but was not approved in Europe. *Nucleic Acid Ther* 2019 ; 29 : 13-5.
- Heo YA. Golodisfen: first approval. *Drugs* 2020 ; 80 : 329-33.
- Komaki H, Takeshima Y, Matsumura T, et al. Viltolarsen in Japanese Duchenne muscular dystrophy patients: a phase 1/2 study. *Ann Clin Transl Neurol* 2020 ; 7 : 2393-408.

RÉFÉRENCES

15. Kovak JS, Hogarth MW, Boehler JF, et al. Myoblasts and macrophages are required for therapeutic morpholino antisense oligonucleotide delivery to dystrophic muscle. *Nat Commun* 2017 ; 8 : 941.
16. Roberts TC, Langer R, Wood MJA. Advances in oligonucleotide drug delivery. *Nat Rev Drug Discov* 2020 ; 19 : 673-94.
17. Goyenvalle A, Griffith G, Babbs A, et al. Functional correction in mouse models of muscular dystrophy using exon-skipping tricyclo-DNA oligomers. *Nat Med* 2015 ; 21 : 270-5.
18. Robin V, Griffith G, Carter J-PL, et al. Efficient SMN rescue following subcutaneous tricyclo-DNA antisense oligonucleotide treatment. *Mol Ther Nucleic Acids* 2017 ; 7 : 81-9.
19. Goyenvalle A, Griffith G, Avril A, et al. Un nouvel outil pour le traitement de la myopathie de Duchenne : les tricyclo-ADN. *Med Sci (Paris)* 2015 ; 31 : 253-6.
20. Suga T, Terada M, Oikawa T, et al. Development of antibody-siRNA conjugate targeted to cardiac and skeletal muscles. *J Control Release* 2016 ; 237 : 1-13.
21. Betts C, Saleh AF, Azumov AA, et al. Pip6-PMO, a new generation of peptide-oligonucleotide conjugates with improved cardiac exon skipping activity for DMD treatment. *Mol Ther Nucleic Acids* 2012 ; 1 : e38.
22. Goyenvalle A, Babbs A, Wright J, et al. Rescue of severely affected dystrophin/utrophin-deficient mice through scAAV-U7snRNA-mediated exon skipping. *Hum Mol Genet* 2012 ; 21 : 2559-71.
23. Vulin A, Barthélémy I, Goyenvalle A, et al. Muscle Function recovery in golden retriever muscular dystrophy after AAV1-U7 exon skipping. *Mol Ther* 2012 ; 20 : 2120-33.
24. Le Guiner C, Monbus M, Servais L, et al. Forelimb treatment in a large cohort of dystrophic dogs supports delivery of a recombinant AAV for exon skipping in Duchenne patients. *Mol Ther* 2014 ; 22 : 1923-35.
25. Grimm C, Stefanovic B, Schümperli D. The low abundance of U7 snRNA is partly determined by its Sm binding site. *EMBO J* 1993 ; 12 : 1229-38.
26. Wein M, Vulin A, Falzarano MS, et al. Translation from a DMD exon 5 IRES results in a functional dystrophin isoform that attenuates dystrophinopathy in humans and mice. *Nat Med* 2014 ; 20 : 992-1000.
27. Waldrop M. Expression of apparent full-length dystrophin in skeletal muscle in a first-in-human gene therapy trial using the scAAV9.U7-ACCA vector. *Neuromuscul Disord* 2020 ; S166-7.
28. Singh NK, Singh NN, Androphy EJ, et al. Splicing of a critical exon of human survival motor neuron is regulated by a unique silencer element located in the last intron. *Mol Cell Biol* 2006 ; 26 : 1333-46.
29. Hua Y, Sahashi K, Hung G, et al. Antisense correction of SMN2 splicing in the CNS rescues necrosis in a type III SMA mouse model. *Genes Dev* 2010 ; 24 : 1634-44.
30. Hua Y, Sahashi K, Rigo F, et al. Peripheral SMN restoration is essential for long-term rescue of a severe SMA mouse model. *Nature* 2011 ; 478 : 123-6.
31. Gargaun E. Les oligonucléotides anti-sens dans la SMA : retour d'expérience et données de la littérature. *Med Sci (Paris)* 2019 ; 35 (hors série n° 2) : 11-4.
32. De Vivo DC, Bertini E, Swoboda KJ, et al. Nusinersen initiated in infants during the presymptomatic stage of spinal muscular atrophy: Interim efficacy and safety results from the Phase 2 NURTURE study. *Neuromuscul Disord* 2019 ; 29 : 842-56.
33. Hammond SM, Hazell G, Shabarpoor F, et al. Systemic peptide-mediated oligonucleotide therapy improves long-term survival in spinal muscular atrophy. *Proc Natl Acad Sci USA* 2016 ; 113 : 10962-7.
34. Campagne S, Boigner S, Rüdisser S, et al. Structural basis of a small molecule targeting RNA for a specific splicing correction. *Nat Chem Biol* 2019 ; 15 : 1191-8.
35. Poirier A, Weetall M, Heinig K, et al. Risdipram distributes and increases SMN protein in both the central nervous system and peripheral organs. *Pharmacol Res Perspect* 2018 ; 6 : e00447.
36. Cheung AK, Hurley B, Kerrigan R, et al. Discovery of small molecule splicing modulators of survival motor neuron-2 (SMN2) for the treatment of spinal muscular atrophy (SMA). *J Med Chem* 2018 ; 61 : 11021-36.
37. Godfrey C, Desvrat LR, Smedsrød B, et al. Delivery is key: lessons learnt from developing splice-switching antisense therapies. *EMBO Mol Med* 2017 ; 9 : 545-57.
38. Bizot F, Vulin A, Goyenvalle A. Current status of antisense oligonucleotide-based therapy in neuromuscular disorders. *Drugs* 2020 ; 80 : 1397-415.

TIRÉS À PART
A. Goyenvalle

REVUES



SYNTHÈSE



Global Registry for COL6-related dystrophies

Registre global des dystrophies liées au collagène de type VI

S'inscrire sur : www.collagen6.org

Ou contactez-nous par e-mail à l'adresse : collagen6registry@ncl.ac.uk

La traduction française sera bientôt disponible sur le site web.



Muscular Dystrophy UK
fighting muscle-wasting conditions



cureCMD
a cure is among us



AFMTELETHON
INNOVER POUR GUERIR



fsrmm
fondation suisse de recherche sur les maladies musculaires

II. AAV-U7 targeting the exon 51 for behavioral rescue

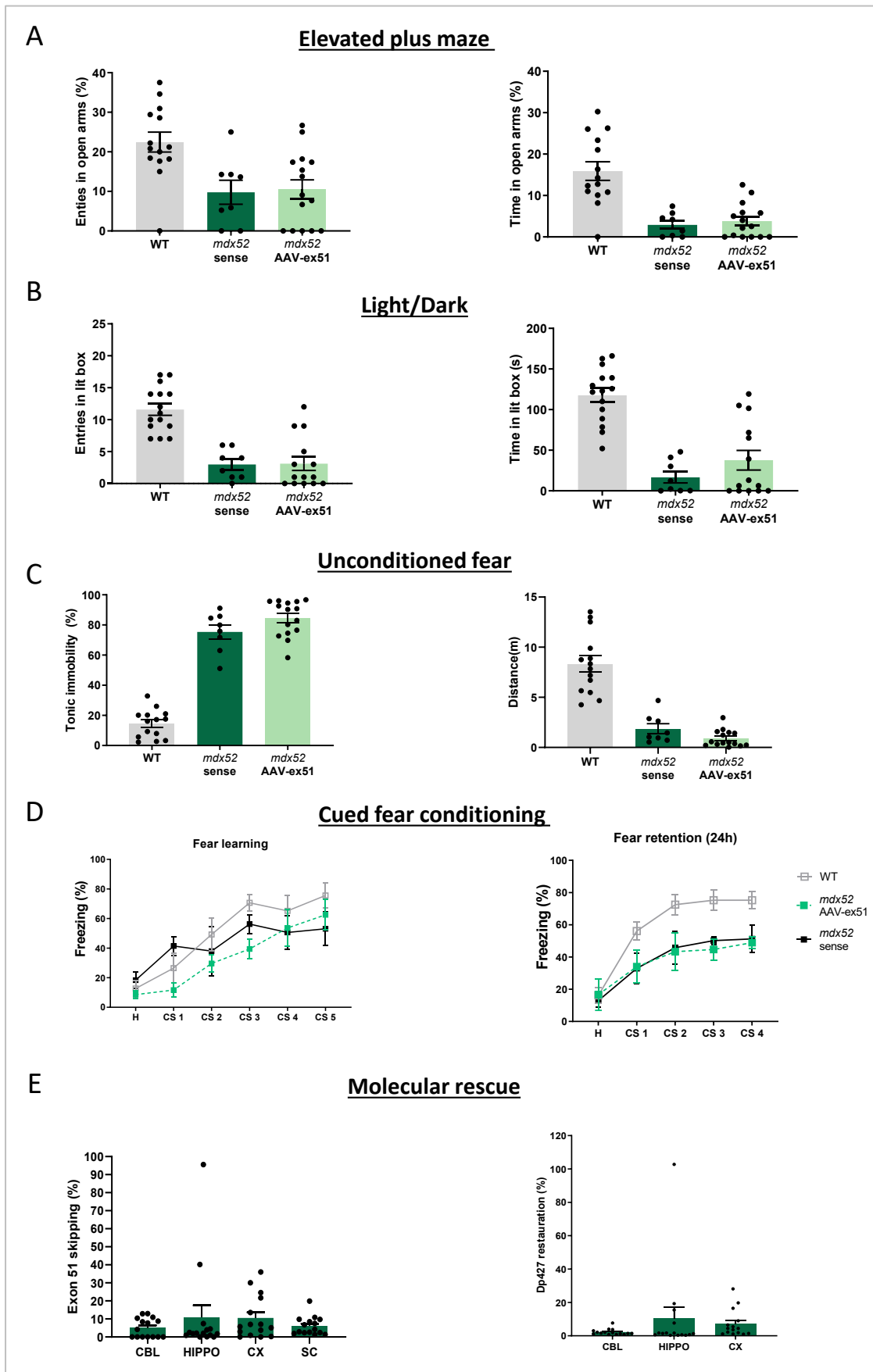


Figure 27. Effect of AAV-mediated partial restoration of Dp427 on *mdx52* mice emotional reactivity. 8 weeks-old mice underwent ICV injections: *mdx52* (n=15) received 2E+12 vg of scAAV9-U7ex51, *mdx52* control (n= 8) received scAAV9-U7scramble and the WT (n= 15) saline. (A) Number of entries and time spent in the open arms of the elevated plus maze, expressed as % of total. (B) Number of entries and time spent in the lit box (s) in the light/dark choice test. Results are means \pm SEM, * p <0.05 and ** p <0.01, Kruskal-Wallis test followed by Dunn's post-hoc tests. (C) Unconditioned fear expressed as percent time spent in tonic immobility and total distance travelled during a 5-min period of observation following a brief scruff restraint (15 s) (means \pm SEM, ** p <0.01 and *** p <0.005; one-way ANOVA followed by Sidak post-hoc tests. (D) Auditory-cued fear conditioning. Performance during conditioning (Fear learning) and memory retention sessions (Fear retention at a 24h post-conditioning delay) is expressed as the percent time spent freezing during presentation of the conditioned stimulus (tone, 30 s), which was repeated five times during conditioning (CS 1-5; each was an 80 dB tone lasting 30s, followed by a footshock) and repeated four times (CS1-4) during the retention session performed 24h later in a new context (tone delivered alone; no footshock). Results are means \pm SEM, ** p <0.01 and **** p <0.001 analyzed by Two-way ANOVAs. (E) The molecular rescue expressed by the percent of exon 51 skipping (left) and percent of Dp427 protein restoration in the cerebellum (CBL), the hippocampus (HIPPO), the cortex (CX) and the spinal cord (SC). Results are means \pm SEM.

III. Thesis summary (French)

La DMD est une maladie génétique récessive liée à l’X qui touche 1/5000 jeunes garçons. Chez les patients DMD, les différents profils de mutations conduisent à une altération progressive des muscles squelettiques, tandis que les troubles neurocognitifs, sensoriels et neuropsychiatriques, présentent une variabilité liée à la position de la mutation dans le gène *DMD*. Ces mutations empêchent l’expression des Dystrophines (Dp), protéines associées à la membrane dans différents tissus notamment le muscle squelettique et le système nerveux central (SNC). Le modèle étudié dans ce projet, la souris *mdx52*, porte une délétion de l’exon 52, un profil de mutation dans une région du gène fréquemment altérée chez les patients (63%). Cette délétion conduit à une perte d’expression de plusieurs dystrophines du SNC (Dp427, Dp260, Dp140). Ce profil de mutation est associé à des altérations centrales sévères chez les patients. De façon intéressante, ce modèle est éligible à des approches thérapeutiques par saut d’exon. Mon projet de thèse s’est organisé autour de trois axes principaux :

1. La caractérisation du phénotype comportemental de la souris *mdx52* en comparaison d’un modèle classique et connu, la souris *mdx* uniquement déficiente en Dp427.

Une étude des troubles émotionnels utilisant une batterie de tests nous a permis de mettre en évidence chez la souris *mdx52* une réactivité émotionnelle plus marquée que chez la souris *mdx*. Ceci confirme la relation entre le génotype et le phénotype observée chez les patients.

D’autre part, les altérations cognitives impliquant différents types de mémoire de reconnaissance dans le modèle *mdx52* ont également fait l’objet d’une seconde étude.

2. L’optimisation de l’approche de saut d’exon thérapeutique par administration d’oligonucléotides antisens de type tricyclo-DNA (tcDNA) pour corriger l’ARNm de la Dp427

Afin de restaurer des niveaux optimaux de Dp427 cérébrale, nous avons tout d’abord optimisé les conditions d’administration de tcDNA ciblant l’exon 51. Dans ce contexte, j’ai comparé des monoinjections intra-cérébro-ventriculaires de tcDNA à des injections répétées (*via* l’insertion d’une canule) ou à une infusion lente *via* l’implantation de mini-pompes osmotiques. La biodistribution des tcDNAs, les niveaux de saut d’exon obtenus (RT-qPCR) et les niveaux de protéine restaurée (WB, IF) dans différentes structures cérébrales ont été analysés.

D’autre part, j’ai aussi comparé l’ICV à l’injection d’une seule dose ou de trois doses répétées de tcDNA dans la *cisterna magna* (ICM). La combinaison d’une ICM et d’une ICV a également été

testée. La biodistribution et les taux de saut d'exon 51 (RT-qPCR) détectés dans les différentes structures à la suite des ICMs de TcDNA (simples, répétées ou encore combinées à l'ICV) ont été comparés à des injections similaires d'une autre chimie d'oligonucléotides antisens : les PMO, ayant reçu une autorisation de mise sur le marché pour le traitement de la DMD et actuellement utilisés par nos collaborateurs. Cette étude a permis de mettre en évidence l'ICV comme étant le mode d'injection idéal pour les tcDNA.

Nous avons validé une fenêtre d'efficacité post-ICV du traitement dans le but de réaliser les tests de comportement. Pour cela, la cinétique des niveaux de saut d'exon 51 et de restauration de Dp427 à différents délais (3, 7 et 11 semaines) post-ICV a été étudiée. L'ensemble de ces travaux suggère qu'une seule injection ICV est la procédure la mieux tolérée et la plus efficace permettant de restaurer une expression partielle de Dp427 dans plusieurs structures cérébrales, stable entre 7 et 11 semaines post-injection.

3. L'application de cette thérapie et l'analyse de son efficacité à compenser les déficits comportementaux des souris *mdx52* suite à des injections ICV

En utilisant les conditions optimales déterminées dans l'axe 2, des *mdx52* ont été traitées par ICV afin d'évaluer l'impact d'une restauration partielle de Dp427 sur la réactivité émotionnelle caractéristique de ce modèle. Les tests comportementaux utilisés sont ceux dans lesquels il a été démontré dans l'axe 1 que les souris *mdx52* présentent des déficits (tests d'anxiété: labyrinthe en croix surélevé, test de choix clair/obscur; peur conditionnée à un son ; peur inconditionnée induite par un léger stress).

Les résultats montrent un effet encourageant de la thérapie: une restauration de l'anxiété dans le labyrinthe en croix surélevé, mais aussi de l'acquisition et de la mémoire d'une peur conditionnée, ainsi qu'une amélioration significative de la réponse de peur inconditionnée. Un traitement systémique combiné au traitement local par ICV a également été étudié. Ceci a montré qu'une restauration du phénotype musculaire ne semble pas augmenter l'efficacité du traitement par ICV, ce qui confirme que ce phénotype a une origine essentiellement centrale. La biodistribution (hybridation *in situ* et lysats), les taux de saut d'exon 51 (BaseScope et qPCR) et les taux de restauration protéique (IF et WB) ont été analysés suite aux études comportementales. La restauration comportementale a été induite par une réexpression de seulement de 5-10% de Dp427 dans plusieurs structures cérébrales.

Titre : Neurobiologie des atteintes centrales et saut d'exon thérapeutique dans un modèle murin de dystrophie musculaire de Duchenne

Mots clés : DMD, Neurobiologie, Saut d'exon, Déficience intellectuelle, Trouble neurodéveloppemental

Résumé :

La dystrophie musculaire de Duchenne (DMD) est un syndrome neuromusculaire associé à des troubles comportementaux et cognitifs pouvant entraîner une déficience intellectuelle et des troubles neuropsychiatriques (TSA, TDAH, TOC). La nature et la gravité des dysfonctionnements cognitifs et des altérations centrales dépendent de la position des mutations au sein du gène DMD. En effet, cela peut affecter différemment l'expression de plusieurs dystrophines cérébrales codées à partir de promoteurs internes, qui ont des fonctions diverses dans divers types de cellules au cours du développement et dans le cerveau adulte. Ce travail de recherche multidisciplinaire et collaboratif fait partie du projet financé par l'Europe BIND (Behavioural Involvement In Dystrophinopathies). La première partie visait à clarifier les relations génotype-phénotype des anomalies centrales dans cette maladie ainsi que leurs bases moléculaires et neuroanatomiques. La deuxième partie visait à développer des approches thérapeutiques précliniques de saut d'exon pour corriger le gène dmd et restaurer l'expression des dystrophines cérébrales fonctionnelles dans un modèle murin de DMD.

Mon projet de thèse a porté sur l'étude d'une souris transgénique (mdx52) porteuse d'une mutation dans une région "hot spot" du gène présentant fréquemment des délétions chez les patients DMD (63%). Des mutations dans cette région entraînent la perte de plusieurs dystrophines centrales (Dp427, Dp260 et Dp140) et sont associées à des troubles neurologiques sévères. En utilisant de multiples paradigmes comportementaux, nous avons montré de sévères altérations des réponses émotionnelles et de la peur conditionnée, ainsi que des déficits sensoriels et de mémoire de reconnaissance plus modérés. Ceci consolide nos connaissances des relations génotype-phénotype et valide la souris mdx52 en tant que modèle fiable pour les études précliniques. De plus, la région "hot spot" du gène DMD est éligible aux approches correctives de saut d'exon. Notre équipe a développé des outils moléculaires de pointe (oligonucléotides antisens 'tcDNA' et vecteurs viraux 'AAV-U7') pour étudier le saut d'exon thérapeutique dans le modèle murin mdx52. Les approches de saut d'exon ont déjà démontré leur efficacité pour le traitement de la dystrophie musculaire. Dans la deuxième partie de ce travail, nous avons abordé l'applicabilité de ces outils au système nerveux central (SNC) et déterminé les conditions thérapeutiques adéquates via des injections locales dans le SNC. Nous avons ensuite démontré que ce saut d'exon induit une réexpression partielle de Dp427 qui atténue les troubles émotionnels et améliore les performances de peur conditionnée chez cette souris.

Ces résultats prometteurs ouvrent la voie à de futures études visant à mieux comprendre les troubles centraux dans la DMD et à améliorer leur prise en charge thérapeutiques.

Title: Neurobiology of central defects and therapeutic exon skipping in a mouse model of Duchenne muscular dystrophy

Keywords: DMD, Neurobiology, Exon skipping, Intellectual disability, Neurodevelopmental disorder

Abstract:

Duchenne muscular dystrophy (DMD) is a neuromuscular disease associated with behavioral and cognitive disturbances that can lead to intellectual disability and neuropsychiatric disorders (ASD, ADHD, OCDs). The nature and severity of cognitive dysfunctions and central alterations depend on the position of the mutations within the *DMD* gene. Indeed, this may differentially affect the expression of several brain dystrophins encoded from internal promoters, which have diverse functions in various cell types during development and in the adult brain. This multidisciplinary and collaborative research work is part of the European funded project BIND (Behavioural Involvement In Dystrophinopathies). The first part aimed to clarify the genotype-phenotype relationships of central defects in this disease as well as their molecular and neuroanatomical bases. The second part aimed to develop preclinical therapeutic exon skipping approaches to correct the *dmd* gene and restore the expression of functional brain dystrophins in a mouse model of DMD.

My thesis project focused on the study of a transgenic mouse (*mdx52*) carrying a mutation in a "hot spot" region of the gene frequently presenting deletions in DMD patients (63%). Mutations in this region lead to the loss of several central dystrophins (Dp427, Dp260 and Dp140) and are associated with severe brain disorders. Using multiple behavioral paradigms, we showed severe defects in emotional behavior and fear learning, as well as moderate sensory and recognition memory deficits in this model. This strengthens our knowledge of the genotype-phenotype relationships and validates *mdx52* as a reliable model for preclinical studies. Moreover, the "hot spot" region of the *DMD* gene is eligible for corrective exon skipping approaches. Our team developed state-of-the-art molecular tools ("tcDNA" antisense oligonucleotides and "AAV-U7" viral vectors) to study therapeutic exon skipping in the *mdx52* mouse model. Exon skipping approaches are already effective in treating the muscular dystrophy. In the second part of this work, we addressed the applicability of these tools to central nervous system (CNS) and determined the adequate therapeutic conditions using local injections to the CNS. We then demonstrated that the exon skipping induces partial Dp427 re-expression and alleviates emotional and fear learning deficits in this mouse.

These promising results pave the way for future studies aimed at better understanding the central disorders in DMD and improving their therapeutic management.